Maneb: From synthesis and structure elucidation to toxicological effects in *Caenorhabditis elegans*

Dissertation

Zur Erlangung des Doktorgrades
der Naturwissenschaft (Dr. rer. nat.) in der Fachgruppe Chemie und Biologie
der Mathematisch Naturwissenschaftlichen Fakultät
der Bergischen Universität Wuppertal

vorgelegt von
Laura Kubens
aus Leverkusen

- 2023 -

Dekan:in:	Prof. Dr. Peter Wiesen
Erste:r Gutachter:in:	Prof. Dr. Fabian Mohr
Zweite:r Gutachter:in:	Prof. Dr. Julia Bornhorst
Tag der mündlichen Prüfung:	08.11.2023

Initial comments on the structure of the dissertation

This dissertation follows a semi-cumulative style by integrating two first-author and one co-authorship publications in peer-reviewed journals into chapters 3, 5 and 6. It incorporates the remarks and suggestions of all authors involved in the manuscript preparation, as well as comments from reviewers and journal editors obtained during the peer-reviewing process. Chapters 1 and 2 provide general background information about the multidisciplinary project. Unpublished data on synthesis and structure characterization are presented in chapter 4, whereas further toxicological studies are included in chapter 7. The final chapter 8 concludes with an overview, discussion and future perspectives.

At the beginning of each publication-based chapter, the source of the original publication is mentioned. To ensure clarity and easier understanding, all references, figures and tables were combined using consecutive numbering. Given that the studies were published in different journals, there may be variation in nomenclature, abbreviation and structure. The original formatting has been modified for consistency, but the scientific content remains unchanged.

The following nomenclature was adopted for *Caenorhabditis elegans*-related terminology: Worm strains consist of two capital letters followed by a number (e. g., BY200). Genes are denoted by three or four lowercase letters, a hyphen, and a number (all italicized, e. g., *dat-1*), Proteins are represented by three or four capital letters, a hyphen and a number (not italicized, e. g., DAT-1). The promotor and protein-coding names of fusion proteins are separated by two colons (e. g., DAT-1::GFP).

Table of Contents

Figures and Tables

Figures

Tables

Figures – Appendix

Tables – Appendix

Abbreviations used

Aß	Amyloid beta
ace-1Δ::ace-2Δ	*Caenorhabditis elegans* strain
ACh	Acetylcholine
AChE	Acetylcholine esterase
ACN	Acetonitrile
AD	Alzheimer's disease
ADI	Acceptable daily intake
ADE	Anterior deirids
AI	Adequate intake
ALDH	Aldehyde dehydrogenase
ATP	Adenosine triphosphate
BCA	Bicinchoninic acid
BCR-274	Name for a single cell protein standard
BSA	Bovine serum albumin
BY200	*Caenorhabditis elegans* strain
CAD	Collisionally activated dissociation
cat-2Δ	*Caenorhabditis elegans* strain
C. elegans	*Caenorhabditis elegans*
CEP	Cephalic sensilla
CGC	Caenorhabditis Genetics Center
ChAT	Choline Acetyltransferase
D	Dimensional
DA	Dopamine
DAergic	Dopaminergic
DAT-1	Dopamine transporter 1
DCF	2',7'-Dichlordihydrofluorescein
DCFH-DA	2',7'-Dichlordihydrofluorescein diacetate
DMF	Dimethylformamide
DMSO	Dimethylsulfoxide
DOPAL	3,4-dihydroxyphenylacetaldehyde
DTC	Dithiocarbamate

EBDC	Ethylene bis(dithiocarbamate)
E. coli	*Escherichia coli*
EFSA	European Food Safety Authority
EPA	Environmental Protection Agency
ERA	Environmental risk assessment
ETU	Ethylene thiourea
eq	Equivalents
EXAFS	Extended X-Ray Absorption Fine Structure
FAO	Food and Agriculture Organization of the United Nations
FRAC	Fungicide Resistance Action Committee
GABA	γ-aminobutyric acid
GCS	γ-glutamylcysteine synthase
GFP	Green fluorescent protein
GSH	Glutathione
GSSG	Glutathione disulfide
HPLC	High-performance liquid chromatography
ICP-OES	Inductively coupled plasma-optical emission spectrometry
ISO	International Organization for Standardization
KO	Knock out
L1	First larval stage of *C. elegans*
L4	Fourth larval stage of *C. elegans*
LC	Liquid Chromatography
LC_{50}	Lethal concentration, which causes death by half of a population
LC-MS/MS	Liquid Chromatography – tandem mass spectrometry
LD_{50}	Lethal dose, which causes death by half of a population
L-DOPA	Levodopa
LOD	Limit of detection
LOQ	Limit of quantification
M	Metal
MB	Maneb
MRM	Multiple reaction-monitoring
MS	Mass spectrometry
MZ	Mancozeb or Manzate (Mancozeb formulation)
m/z	Mass-to-charge

n	Number of independent experiments
N2	Wild-type strain of *Caenorhabditis elegans*
NA22	Name of an *E. coli* strain
NB	Nabam
NEM	N-ethylmaleimide
NGM	Nematode growth medium
NMR	Nuclear magnetic resonance spectroscopy
NT	Neurotransmitter
OP50	Name of an *E. coli* strain
8P	Agar medium for *C. elegans* maintain
PD	Parkinson's disease
PDE	Posterior deirids
rcf	Relative centrifugal force
REACH	Registration, Evaluation, Authorization and Restriction of Chemicals
RONS	Reactive oxygen and nitrogen species
ROS	Reactive oxygen species
rpm	Rounds per minute
SD	Standard deviation
SEM	Standard error of the mean
sMRM	Scheduled multiple-reaction monitoring
SRT	Serotonin
THF	Tetrahydrofuran
UPR	Unfolded protein response
WHO	World Health Organization
WT	Wild-type
XANES	X-ray absorption near edge structure
XRD	X-ray diffraction

Summary

Fungicides are important in agriculture and health, but their impact on non-target species and their potential harm are of great concern. Trace element-based dithiocarbamates, introduced in the 1950s, are effective against many plant diseases and are applied in mixtures to prevent resistances due to their diverse mode of action. Exposure to Maneb, a manganese-based ethylene bis(dithiocarbamate) fungicide, has been linked to neurodegeneration in agriculture fieldworker and nearby residents. Despite being essential, excess Mn can accumulate in the brain, affecting the motor system and is associated with Parkinson's disease. The underlying mechanism of Mn toxicity and its impact on Maneb is not fully understood. Surprisingly, even the molecular structure of Maneb is completely unknown. This study aimed to synthesize and characterize these trace element-based fungicides, especially Maneb, and to assess its impact on *Caenorhabditis elegans* (*C. elegans*), a nematode commonly used as an *in vivo* model organism. The hermaphrodite *C. elegans* has emerged as a powerful model organism for diverse scientific investigations such as neurotoxicity and metal homeostasis. Its transparent body, short life-cycle, and many conserved human genes make it a valuable tool to reduce or replace animal experiments.

In contrast to the *in situ* patent synthesis method, an optimized synthesis strategy was developed to obtain trace element-based ethylene bis(dithiocarbamate) fungicides with high yield, purity and consistent microcrystalline quality. The Mn-containing fungicides were subsequently characterized using various analytical techniques. Initially, the structure of Maneb in solution was elucidated via X-ray diffraction. The resulting polymeric Maneb-DMSO coordination adduct demonstrated, for the first time, the polymeric nature of Maneb. Moreover, it represents the actual species utilized in numerous published toxicity studies, and also in this study. Subsequently, approximately 70 years after its market introduction, the solid-state structure of Maneb was successfully determined using electron diffraction.

Following this, the fully characterized Maneb was used to increase the mechanistic understanding of the toxicity associated with metal-based dithiocarbamate fungicides. In contrast to other studies, it has now become possible to investigate pure and defined Maneb directly in comparison with relevant species known as metabolites and degradation products within a living organism.

Therefore, Maneb was investigated in comparison to $MnCl_2$, the main metabolite ethylene thiourea (ETU), and the disodium salt Nabam in terms of lethality, bioavailability and markers of oxidative stress and neurodegeneration. The findings reveal that despite possessing similar Mn bioavailability, Maneb is approximately eight times more toxic than $MnCl_2$ and exhibited significantly higher toxicity than all other species examined. Trough the evaluation of markers associated with oxidative stress, which reflects an imbalance between generation of reactive species and the organism's antioxidant capacity, further insights into underlying mechanisms were gained. It has been found that Maneb significantly influences the antioxidative glutathione (GSH) and glutathione disulfide (GSSG) system by elevating both components. However, reactive oxygen and nitrogen species (RONS) are only induced to a small extent. Mechanisms discussed here involve the reactivity of Maneb towards thiols, as some studies demonstrated similar outcome. The other investigated species showed no such effects.

Finally, the impact of Maneb and its associated species on neurotransmitter levels were examined. For this purpose, a liquid chromatography-tandem mass spectrometry (LC-MS/MS)-based method was developed to simultaneously quantify the neurotransmitters dopamine, serotonin, acetylcholine and γ-aminobutyric acid in *C. elegans*. Exposure to Maneb immediately disrupts neurotransmitter homeostasis of dopamine, acetylcholine, and γ-aminobutyric acid (GABA), by decreasing their levels. Especially the effect on the dopamine system is often discussed as a possible cause of Maneb-induced neurodegeneration. Therefore, the morphology of dopaminergic neurons was examined using the BY200 *C. elegans* strain, expressing a green fluorescent protein (GFP) in the dopamine transporter 1 (DAT-1) protein, allowing to observe specific fluorescence of dopaminergic neurons. Immediately after exposure to Maneb, irregularities in morphology, such as abnormal branching of dendrites reduced cell body size were observed in L1-stage worms. Neurotransmitter levels returned to control level 48 hours after treatment, but the morphological irregularities persisted, indicating a sustained and irreversible effect of Maneb. Unlike other established neurotoxic substances such as 6-hydroxydopamine (6-OHDA), it was observed that a certain type of neurons is more sensitive to Maneb, while other neurons are more sensitive to 6-OHDA. This provides a potential pathway for further investigations into underlying mechanisms. In conclusion, a comprehensive understanding of these mechanisms could enable accurate risk assessments for human health and facilitate the development of targeted therapeutics.

Chapter 1 – Motivation and Scope of the Thesis

Chapter 1 – Motivation and Scope of the Thesis

1.1 Motivation

Fungicides are essential tools in agriculture and industry, designed to control and eliminate fungal diseases in crops and plants. While they play a crucial role in protecting crops and ensuring food safety, concerns about their potential adverse effects on human health and the environment have been raised.[1–3] In the industrial agriculture, the use of crop protection agents is essential to optimize productivity and to prevent significant yield loss and contaminations. Consequently, antifungal agents are intentionally released into the environment. This intentional release can have unintended consequences, as these chemicals may affect non-targeted organisms and accumulate in ecosystems.

Dithiocarbamate fungicides were introduced in the 1950s and have since gained widespread use in agriculture due to their effectiveness against a wide range of plant pathogens.[4,5] Their multi-site mode of action has contributed to the absence of resistances so far, making them very popular and often combined with other active ingredients.[6]

It was already observed in the 1980s that field workers in contact with Maneb, the manganese-containing ethylene bis(dithiocarbamate) (EBDC) fungicide, developed neurological abnormalities.[2] Since then, evidence has been growing that exposure to EBDC fungicides including Maneb can lead to neurodegenerative damage.[7–11] However, the underlying mechanisms, particularly the role of trace elements complexed in dithiocarbamates, are not well understood. Despite Mn being essential for human health, chronic oversupply can result in adverse neurotoxic effects.[12–15]

Given that pesticides typically undergo a stringent approval process, which includes comprehensive characterization of their chemical structure, mode of action and environmental fate, it is surprising that the molecular structure of the Mn-containing representatives is not known. In light of these toxicological concerns and lack of knowledge regarding the molecular structure of Maneb, this dissertation aimed to understand the precise chemical composition for assessing its behavior and potential interactions with non-target organisms. Therefore, Maneb and other trace element-containing dithiocarbamate fungicides were synthesized, characterized and their toxicological effect was assessed in the *in vivo* model organism *Caenorhabditis elegans*.

1.2 Scope of the thesis

- Development of reproducible synthesis methods for metal-based ethylene bis(dithiocarbamates) to obtain products with consistent quality.
- Structure elucidation of the manganese-containing fungicide Maneb using various analytical techniques.
- Studying the species-specific effects in *Caenorhabditis elegans*, comparing Maneb to other relevant compounds in terms of neurotoxicity and oxidative stress.

Chapter 2 – General background information

Chapter 2 – General background information

2.1 Dithiocarbamate Fungicides

2.1.1 Synthesis and Structure

Dithiocarbamates (DTC) are a class of compounds with the general structure shown in Figure 1. The first dithiocarbamates were reported in 1850,[16] while the use of alkyl dithiocarbamate as ligands for transition metals was documented for the first time in 1907.[17] Syntheses of DTC ligands are usually carried out starting from primary or secondary amines reacting with carbon disulfide in the presence of a base. Primary amines yield less stable dithiocarbamates due to their increased susceptibility to hydrolysis owing to the presence of an proton on the nitrogen atom.[18] Therefore, they are often converted *in situ* into the desired product to prevent decomposition. Under acidic conditions, dithiocarbamates derived from primary amines immediately decompose into the free amine and carbon disulfide.[19] DTCs can be described by using resonance structures shown in Figure 1. Due to the double-bound character of the C-N bond, the rotation is limited. (Figure 1).

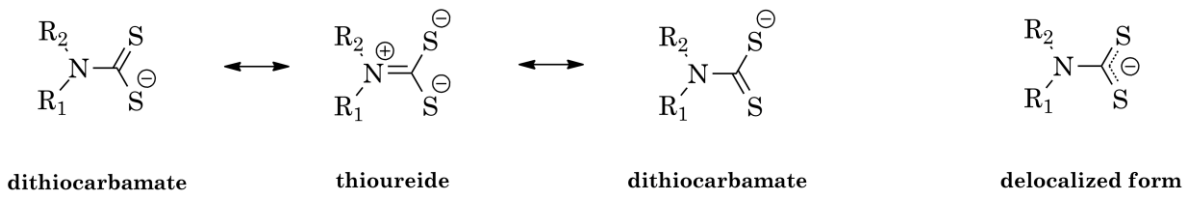

Figure 1: Resonance structures of dithiocarbamate anions.

Dithiocarbamates bind metal ions in up to nine different coordination modes (Figure 2). A monodentate coordination (**A**) occurs when required for steric or electronic reasons or by the possible loss of another ligand. Dithiocarbamates commonly act as bidentate chelate ligands (**B**) with two metal-sulfur bonds of approximately equal length. They form small S-M-S angles in the range of 60-80° and have bond lengths of 2.25 - 2.55 Å, depending on the size of the central atom. In some cases, the S-M bonds are highly asymmetric and have different lengths, described by coordination mode (**C**). Various coordination modes can be found when two or more metals are involved (**D**-**I**). In binding mode (**D**), one of the chelating sulfur atoms is bound to another metal, which results in three metal-sulfur interactions of similar length. In contrast, binding mode (**E**) is not symmetrical. Both are common

coordination modes illustrating the affinity of DTC to build intramolecular polymeric structures. Other coordination modes (**F-I**) are rarely observed (Figure 2).[18]

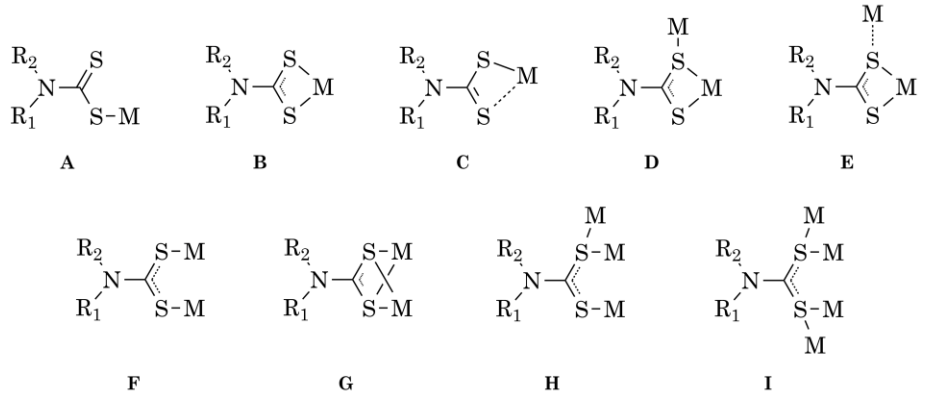

Figure 2: Coordination modes of dithiocarbamates (adapted from [18]).

In coordination chemistry, DTC ligands are considered soft *S*-donor ligands. The "hard and soft (Lewis) acid and base" (HASB) concept is employed to assess the stability of complexes based on their electronic properties and affinity for metal ions. Soft ligands are typically larger, more polarizable and possess lower charge density. As a consequence, they exhibit a preference for coordinating with metal ions of lower positive charge and larger ionic radii such as transition metals. Soft ligand and soft metal interactions between metal ions and ligands are relatively weak, permitting easy exchange and flexibility in coordination geometry.[20]

2.2 Ethylene bis(dithiocarbamate) fungicides

The first dithiocarbamate-containing fungicides were patented by Tisdale and Williams in 1934.[21] In the 1940s, the disodium salt of ethylene bis(dithiocarbamate) (EBDC) was patented as the first broad-spectrum fungicide based on a EBDC ligand and called Nabam (Figure 3).[22] EBDC fungicides are categorized by the Fungicide Resistance Action Committee (FRAC) as fungicides with "multi-site activity", meaning they target multiple sites in the fungal organism, which reduces the risk of resistance developing. These fungicides act in a non-systemic manner on the plant surface and are often used in combination with other fungicides as part of resistance management strategies.[6] As a result, EBDCs are well recognized and widely applied as highly effective components in plant protection. Despite the initial success, Nabam is not considered as an effective fungicide due to its excellent water solubility and instability under environmental conditions. In the 1950s a series of EBDC derivates containing other metals were

introduced as improved alternatives. These derivates were marketed under the brand names Maneb, Zineb, and Mancozeb (Figure 3).[4,23,24] The addition of transition metals to these compounds has a stabilizing effect by forming chelate complexes. As explained in subsequent chapters, dithiocarbamates, especially Maneb and Mancozeb, are the most commonly used fungicides and account for a significant amount of fungicide consumption.[25]

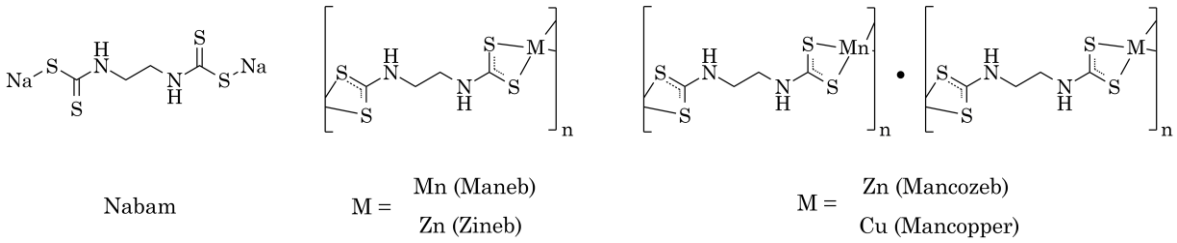

Figure 3: Ethylene bis(dithiocarbamate) fungicides.

2.2.1 Structures and Characteristics

The EBDC complexes based on trace element (TE) are proposed to have a polymeric structure and are insoluble in water and most commonly used solvents. However, Nabam, the disodium EBDC salt, crystallizes as hexahydrate and is soluble in water.[26,27] The Mn-containing EBDC fungicides, Maneb and Mancozeb, are not suitable for analysis using routine nuclear magnetic resonance spectroscopy (NMR) due to the paramagnetic properties of Mn in its +II oxidation state. Even the exact molecular structure of the zinc analog, Zineb, has only recently been elucidated by Lefton *et al.* (2020) using powder diffraction techniques.[28] The structure of Zineb reveals a Zn(II)-ion coordinated by four sulfur atoms from two EBDC ligands, with equal bond lengths of around 2.3 Å - 2.4 Å. Additionally, there is an extra Zn-S bond acting as an intramolecular sulfur bridge with a relatively long bond length of 2.9 Å. Thus, a 2D coordination polymer emerges, build by $Zn_2(\mu S)_2$ trapezoids and *bis*-functional EBDC ligands (Figure 4).

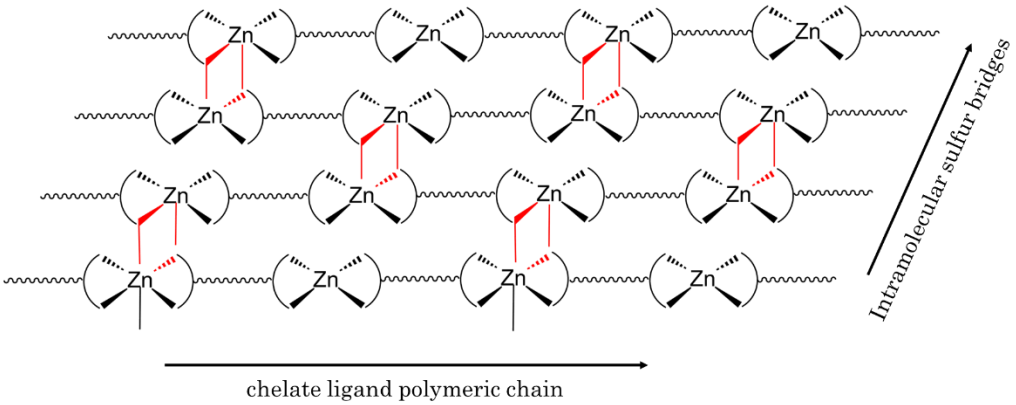

Figure 4: Structure of Zineb. The bridging $Zn_2(\mu S)_2$ trapezoids are highlighted in red. The EBDC ligand is shown as a zig-zag-line for simplification.

The exact chemical structure of Maneb and Mancozeb has remained unknown, despite their extensive agricultural use for over 70 years. Mn(II) contains five unpaired d-electrons ([Ar] $3d^5$ configuration) and typically forms octahedral high-spin complexes.[29] The only dithiocarbamate-related structure with Mn in the +II oxidation state is $[Mn(S_2CNEt_2)_2]_n$, which was published in 1975.[30] In this structure, Mn is coordinated by six sulfur atoms, including two bridging sulfur atoms from neighboring DTC ligands, resulting in a polymeric network. However, Ciampolini *et al.* (1975) described this complex as unstable and extremely air-sensitive. It is important to note that this instability does not apply to Maneb since commercially available pesticide standards can be stored for up to 36 months without degradation.[30] Wang *et al.* (1993) proposed that Maneb might have a structural similarity to the previously reported $[Mn(S_2CNEt_2)_2]_n$ complex, although it is often described as a nona-cyclic monomer.[31,32]

In the case of Mancozeb, the exact chemical structure is more complicated as it involves both Mn(II) and Zn(II) ions. Two different synthetic approaches have been employed for Mancozeb production. The first approach, known as the "co-reacted Mn-metal EBDC" route, involves the reaction of Nabam with varying rations of Mn and Zn.[5] The second synthesis route is based on isolating Maneb, dispersing it in water, and subsequently treating it with solutions of different Zn(II) concentrations.[33] Initially, it was speculated that Mancozeb might be a mixture of Maneb and Zineb. However, analysis of powder diffraction data revealed that Mancozeb possesses distinct patterns, indicating that it is an individual fungicide with its own unique, but unknown chemical structure.[5,33]

2.2.2 Legal status

The approval of Mancozeb, the last EBDC-containing fungicide, expired in January 2021 in the European Union. The non-renewal of its approval as an active substance was due to specific concerns that were raised. In particular, Mancozeb was classified as a category 1B reproductive toxicant, and it was found to possess properties of endocrine disruptors [Implementing Regulation (EC) No. 2020/2087, No. 2016/2035 (Maneb)]. However, EBDC fungicides such as Maneb and Mancozeb continue to be widely used in significant quantities in other agricultural food-producing countries, including the United States (Mancozeb only), Brazil, China, and India. The Food and Agriculture Organization of the United Nations (FAO) estimates that global pesticide usage exceeded 2.5 million tons in 2020. Brazil, in particular, stands as one of the largest consumers of plant protection products, with more than 40 % of all fungicides belonging to the EBDC class, especially Mancozeb.[34,35] EBDC fungicides find application on a wide range of crops, including tomatoes, potatoes, grapes, and bananas, to effectively control around 400 fungal pathogens.[36]

The poor solubility and mostly unknown structures of EBDC fungicides make the analysis of residue levels on agricultural food samples a difficult task. Current residue analyses are based solely on the determination of carbon disulfide content and do not involve the identification/quantification of specific metal species. As a result, it becomes impossible to differentiate between different applied EBDC species and to detect any illegal usage. The enforcement residue definition is "*dithiocarbamates determined and expressed as CS_2, including Maneb, Mancozeb* […]". In crops rich in glucosinolate naturally high background levels of CS_2 occur, making it challenging to distinguish between naturally occurring CS_2 and that arising from fungicide application.[37] This further complicates both laboratory analysis and the legal assessment of residue levels. While a standard maximum residue level (MRL) of 0.01 mg/kg exists for DTC fungicides, there is no specific MRL established for CS_2, even though it is the detected species in residue analysis [Regulation (EC) No. 396/2005]. European Food Safety Authority (EFSA) conducted a comprehensive evaluation of various toxicological studies to assess the hazards and risks associated with EBDC fungicides. The current acceptable daily intake (ADI) varies depending on the species. For Mancozeb, the ADI is set at 0.05 mg/kg body weight per day.[38] In its annual report on pesticide residue for 2020, the EFSA considered different scenarios and calculated the chronic dietary exposure as a percentage of the specific ADI values for each species. This

assessment included all DTC-containing fungicides and their respective toxicological-based ADIs. The chronic dietary exposure expressed as a percentage of the ADI (adjusted as the middle bound) ranged from 9% to 83%. The main contributors to this exposure were apples, pears, and broccoli. In the context of the assessment, the estimated chronic exposure for 176 pesticides was less than 10% of the ADI and for 111 of them it was lower or equal to 1%.[39] Despite EBDC fungicides not being approved for use in the EU, there is growing concern over high residue levels of unapproved pesticides and their metabolites on imported crops. This issue arises due to globalization of agricultural trade, highlighting the importance of monitoring and addressing such concerns in food safety regulations.

The metabolite, degradation product and manufacturing byproduct ethylene thiourea (ETU) was identified as a substance of very high concern (SVHC) in 2013, as per Article 59(3) of Regulation (EC) No. 1907/2006, also known as REACH (Registration, Evaluation, Authorization, and Restriction of Chemicals). This classification was based on the recognized toxicity of ETU. The acceptable daily intake (ADI) for ETU is set at 0.002 mg/kg according to Regulation (EC) No. 1107/2009. In the reference specification for the original approval of Maneb or Mancozeb, considering the toxicological relevance, a maximum allowable impurity level of 0.5% for ETU was defined. This limit was set to mitigate the potential exposure to ETU and its associated toxicity.

2.2.3 Mechanism of action

The emergence of pesticide resistance is a growing concern, and cases of resistance have been documented in all classes of pests, including fungi. Fungal infestations lead to significant losses in commercially important fruits and vegetables worldwide. Similar to the development of multi-drug resistance in human pathogens, the phenomenon of resistance is also becoming more prevalent in plant diseases.[40] According to the definition provided by the Fungicide Resistance Action Committee (FRAC), fungicide resistance refers to the acquired and heritable reduction in sensitivity of a fungus to a specific antifungal agent or fungicide.[41] When a fungus evolves resistance through evolutionary processes, all fungicides that target the same site of action are considered to exhibit "cross-resistance" to each other. In other words, if a fungus develops resistance to one fungicide, it may also demonstrate reduced sensitivity to other fungicides that act on the same target site.[42] Proper rotation of fungicides with different modes of action and the use of integrated pest management practices are key approaches to maintain the efficacy and combat resistance of fungicides.

DTC-based fungicides, such as EBDC fungicides, have not shown any observed resistance since their introduction in the 1950s, mainly due to their "multi-site activity" mode of action.[43] This class of fungicides is effective in controlling a wide range of diseases, including downy mildews, late and blossom blights, leaf spots and others.[6] However, there are certain disadvantages associated with the use of EBDC fungicides. One significant drawback is that high doses are often required to achieve adequate disease protection. Furthermore, they only act preventively and do not possess any curative effect once a plant is infected. They function as surface-acting pesticides and lack systemic properties, which means they need to be applied repeatedly to maintain their efficiency. As a result, repeated application of large quantities leads to increased levels entering the environment.[6]

In contrast to dialkyl dithiocarbamates, EBDC ligands contain two relatively reactive hydrogen atoms bound to the DTC nitrogen, which can initiate intra- and intermolecular reactions. Thus, various degradation products are formed, which could contribute to the fungicidal effect.[44] Although several mechanisms of action have been proposed for EBDC fungicides, their complexity has hindered a comprehensive understanding at the cellular level and none of these mechanisms have been conclusively proven.

One suggested mechanism is that EBDC fungicides interfere with the fungal cell wall by altering cell permeability. This effect is attributed to the enhanced lipophilic nature of the polymeric metal-EBDC chains compared to that of the free metal ions.[45,46] Several studies have reported interactions of DTCs with cellular enzymes in fungi, leading to disruption of critical physiological processes.[11,47] Multiple targets for the mechanism of action are possible. For instance, EBDCs are known to interact with thiols and other sulfur-containing groups, potentially catalyzing irreversible protein cross-links or forming reversible hydrogen bonds. Another proposed mechanism involves the chelation of metal ions through metal-exchange reactions or metabolites. These can affect metal enzyme cofactors within the cellular environment and leads to reduced enzyme activity.[46,48,49]

2.2.4 Toxicity

The non-specific mode of action of EBDC fungicides raises concerns about potential adverse effects not only on fungi but also on non-target organisms, including humans. Numerous studies have demonstrated the toxic effects of these fungicides, their metabolites, and the released metals.[7–11] In the 1980s, Ferraz *et al.* reported a link between occupational exposure to Maneb and the development of neurological deficits in field workers.[2] Since

then, the body of evidence of neurotoxic potential of EBDC fungicides is growing.[50] Several epidemiological studies,[3,51–53] cell culture experiments[9,54,55] or *in vivo* studies[8,32,56] have demonstrated adverse effects including neurodegeneration, oxidative stress and mitochondrial dysfunction. Exposure to Mn-containing fungicides were associated with increased concentrations of Mn in blood and hair, as well as detectable levels of urinary ETU.[51,52] Especially in children living near banana plantations in Costa Rica, where Mancozeb is frequently sprayed aerially, Mn and ETU outcomes have been found to correlate with adverse neurodevelopmental effects.[51] Maneb has been reported to affect dopaminergic neurons and is supposed to increase the risk of Parkinson's disease (PD).[54] Studies using the nematode *Caenorhabditis elegans* (*C. elegans*) have confirmed that neurons expressing dopamine (DA) and γ-amino butyric acid (GABA) are particularly vulnerable and serve as targets for Mn-fungicides-induced toxicity.[32,56,57]

While the adverse effects of EBDC fungicides, including Maneb, are well-documented, the precise molecular toxicity mechanisms are still not fully understood. The subsequent sections will primarily focus on the effects of Maneb and its metabolites, as this work primarily centers on Maneb's synthesis, structure, and toxicity. Figure 5 provides an overview of the proposed mechanisms of Maneb-induced toxicity to illustrate the relatively complex interrelationships.

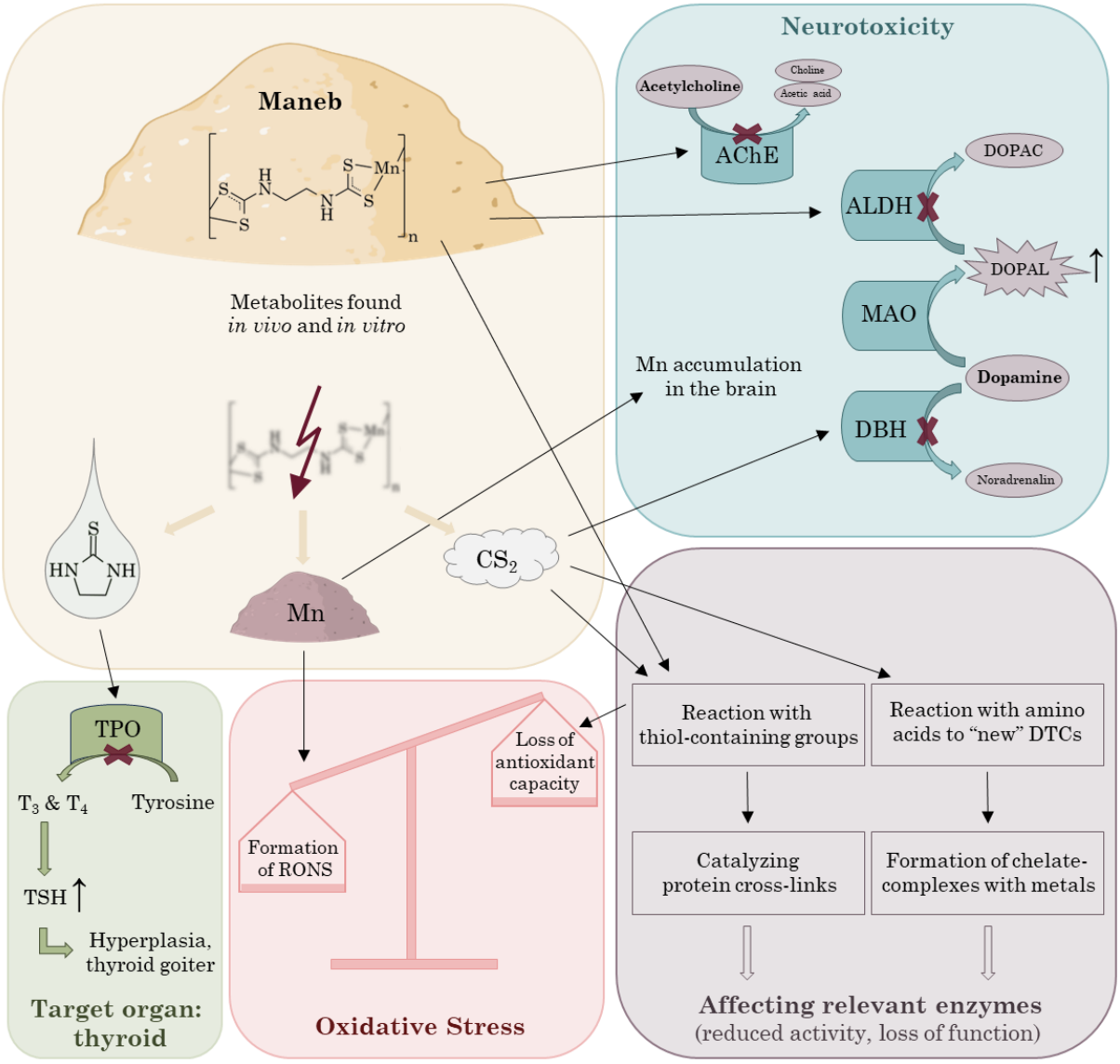

Figure 5: Proposed mechanisms and targets for toxicity of EBDC fungicides and their degradation products using Maneb as an example.[11,32,58–65]

One of the main proposed toxicity mechanisms of Maneb and other polymeric EBDC fungicides is the inhibition of aldehyde dehydrogenase (ALDH) enzymes.[58,59] ALDH enzymes play a crucial role in catalyzing the conversion of aldehydes to carboxylic acids, which is essential for detoxifying both exogenously and endogenously generated aldehydes.[66] Inhibition of ALDH by Maneb and its metabolites can impair the detoxification of 3,4-dihydroxy phenylacetaldehyde (DOPAL), a metabolite of the neurotransmitter dopamine (DA) produced by the monoamine oxidase (MAO), which acts as an endogenous neurotoxicant affecting dopaminergic neurons in physiological concentrations (as shown in Figure 5).[67] The exact mechanism by which ALDH is inhibited

by EBDC fungicides has yet to be confirmed.[59] ALDH inhibition is thought to be associated with the "catechol aldehyde hypothesis," which suggests that ALDH dysfunction is linked to the pathogenesis of Parkinson's disease (PD).[68] PD is characterized by the loss of dopaminergic neurons in the *substantia nigra pars compacta* region of the brain and the formation of protein aggregates referred to as Lewy bodies. Typical symptoms of PD include movement disorders such as bradykinesia (slowness of movement), muscular rigidity, and rest tremor.[69] This has also been proposed for chronic manganese exposure, more details on Mn-induced parkinsonism are given in Chapter 2.4.1. Besides dopaminergic neurons, γ-aminobutyric acid expressing neurons appear to be particularly vulnerable to the neurotoxic effects induced by Mn-containing EBDC fungicide exposure.[32,60]

Another postulated mechanism regarding the neurotoxicity of Maneb is its ability to reversibly inhibit acetylcholinesterase (AChE). *In vitro* studies have demonstrated that AChE inhibitors lead to increased acetylcholine (ACh) levels since ACh is not efficiently split into choline and acetic acid.[61,70] The elevated levels of ACh in the synaptic gap can result in hyperexcitability, leading to subsequent paralysis.[61,71] The inhibition of AChE by Maneb may disrupt the normal balance of ACh in the nervous system, potentially leading to dysregulation of neuronal signaling and subsequent adverse neurological effects. Understanding the precise mechanisms through which Maneb and its metabolites exert their neurotoxic effects, including their impact on ALDH and AChE enzymes, is crucial for unraveling the complex interplay between these fungicides and the nervous system.

In several exposure scenarios it has been observed that Maneb can induce the formation of reactive oxygen and nitrogen species (RONS) and negatively impact the antioxidant system, leading to oxidative stress.[8,10,62,63] In biological systems oxidative stress is reflected by an imbalance between reactive species and the capacity of the antioxidant defense system.[2] When the production of RONS exceeds the normal redox status and the antioxidant protection system is impaired, it can lead to various negative outcomes, including damage to macromolecules such as proteins, lipids, and DNA. Oxidative stress is implicated in the pathogenesis of neurodegenerative diseases including Parkinson's disease and Alzheimer's disease.[72] During normal metabolic activity, small amounts of reactive species are produced, which can be scavenged by the antioxidant system. Glutathione (GSH) is one of the crucial molecules involved in the cellular antioxidant defense system (Figure 6).[72]

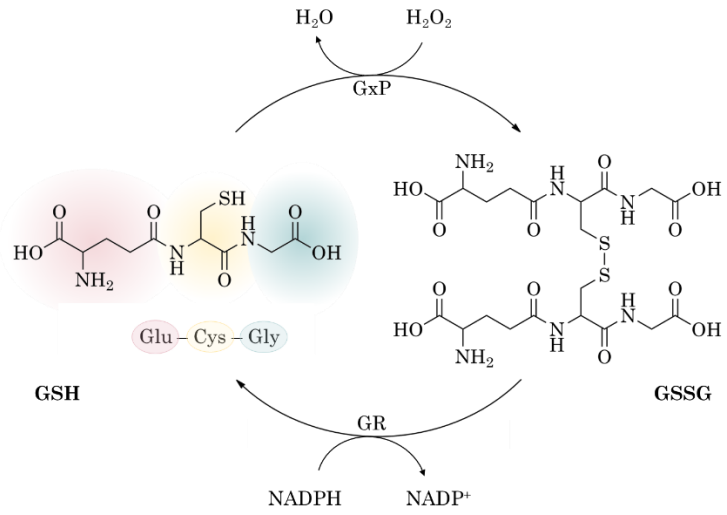

Figure 6: Glutathione (GSH) and its disulfide (GSSG) as part of the antioxidant system. Glutathione peroxidase (GxP) catalyzes the reduction of hydrogen peroxide using GSH as a reducing agent. Glutathione reductase (GR) reduces GSSG back to GSH to ensure a sufficient supply of GSH as an intracellular antioxidant. GSH is a tripeptide composed of three amino acids: glutamic acid, cysteine and glycine. The glutamic acid is bound via the γ-carboxy group.[73]

GSH is the most abundant thiol-containing tripeptide in human cells and its antioxidant properties relies on its oxidation to glutathione disulfide (GSSG) whilst reducing other species (as depicted in Figure 6).[74] Maneb has been reported to interact with thiol-containing molecules like GSH, potentially reducing the capability of the antioxidant system[11,62,75]. This interaction may disrupt the balance of cellular redox status and compromise the ability of cells to counteract oxidative stress. Additionally, the presence of redox-active manganese in Maneb can contribute to the generation of reactive radicals.[76,77] The combination of these properties in Maneb can lead to a shift in the cellular redox balance, contributing to oxidative stress. Furthermore, Maneb is implicated in processes related to mitochondrial dysfunction.[54,78] Mitochondria supply cellular energy and have a critical role since they regulate signaling, cell differentiation, cell death and other key features. Alterations in mitochondrial functions are related to neurodegenerative diseases.[79] Lui *et al.* (2023) documented *in vivo* and *in vitro* the involvement of Maneb in mitochondrial apoptosis pathways.[63] In SH-SY5Y cells exposed to Maneb increased levels of matrix metalloproteinase protease (MMP), a negative regulator of mitochondrial function with zinc-binding motif,[80], were determined. *In vivo* alteration in expression levels of mitochondrial apoptosis related proteins were observed in mice exposed to Maneb.[63]

ETU, which is formed during the intramolecular cyclization of the EBDC backbone under environmental conditions, and as a process contaminant during manufacturing, has been

found to reversibly inhibit the enzyme thyroid peroxidase (TPO). TPO plays a crucial role in the synthesis of the thyroid hormones thyroxine (T_3) and triiodothyronine (T_4).[64] Consequently, the inhibition of TPO by ETU can lead to disruption in the synthesis of both iodine-containing hormones. Therefore, the thyroid gland becomes a target organ for ETU-induced toxicity. A deficiency of T_3 and T_4 triggers a compensatory response in the form of elevated levels of thyroid-stimulating hormone (TSH). Disruption of the hypothalamic-pituitary-thyroid (HPT) axis, characterized by abnormal TSH levels, has been associated with hyperplasia and neoplasia in the thyroid gland in rodent studies.[64] Humans possess a thyroxine-binding globin, which serves as a reserve supply for T_3 and T_4. This protein is absent in rodents, resulting in rapid hormone turnover and rendering them more sensitive to toxins that target the thyroid gland.[36,81] In 1974, the International Agency For Research On Cancer (IARC) classified ETU as possibly cancerogenic to humans..[82] Furthermore, in 2013, ETU was listed as a substance of very high concern (SVHC) by the Registration, Evaluation, Authorization, and Restriction of Chemicals (REACH) regulation. This classification underlines the recognition of ETU's toxicity and potential adverse effects on human health or the environment.

During the formation of ETU carbon disulfide is also generated, which was found in the breathing air of rats after exposure to Zineb.[83] *In vitro* and *in vivo* studies have demonstrated that CS_2 exposure has adverse effects, including thyroid disruption, neurotoxicity, and cardiotoxicity. Due to these effects, CS_2 is often discussed controversially as a possible endocrine disrupter.[65] On cellular level, CS_2 forms intracellular adducts such as dithiocarbamate-species by reacting with amino acids. Many adducts generated *in vivo* have been found in animals and humans after CS_2 exposure.[65] These electrophilic DTC-species can further react with nucleophilic macromolecules such as proteins leading to the formation of protein cross-links, particularly in the neurofilament. On a mechanistic level, CS_2-derived lysine-dithiocarbamates are responsible for protein cross-links by transforming them into dimers.[84,85] Protein cross-linking in neurofilaments has been associated with impaired axonal transport and subsequent neurodegenerative processes.[86] Additionally, CS_2 and its DTC metabolites have an affinity for thiol group-containing biomolecules, including cysteine and glutathione, and can also chelate essential trace elements such as copper and zinc. DTCs are well-suited as chelating ligands, and their interactions with essential trace elements can lead to reduced enzyme activity or loss of function. Furthermore, in contaminated water, CS_2-induced DTC adducts can complex with heavy metals such as lead or mercury, potentially leading to their absorption and

accumulation in the food chain. Chelation or metal exchanges can not only occur by the fungicidal ligands themselves but also by the newly formed CS_2-induced dithiocarbamate adducts. Studies have shown the affinity of DTC ligands to various doubly charged metal ions follows the order Hg > Cu > Ni > Co > Pb = Cd > Zn > Fe > Mn.[87,88] The preference of DTC towards certain metal ions, such as copper raises speculation, that Cu-containing enzymes may be targeted from EBDC-based fungicides. The impairment of crucial enzymes such as the Cu-containing dopamine-ß-hydrolase (DBH) by CS_2 exposure is assumed to contribute to the development of neurotoxicity. DBH is a mono-oxygenase enzyme that converts dopamine (DA) to norepinephrine. Inhibition of DBH by CS_2 exposure can lead to increased DA levels and decreased levels of noradrenaline.[89] Disruption of catecholamine homeostasis, which includes DA, epinephrine (adrenaline), and norepinephrine (noradrenaline) as physiologically occurring catecholamines, may result in catecholamine dysfunction.[90] Noradrenergic neurons, which rely on the proper function of catecholamines, regulate and stimulate the release of thyroid-stimulating hormone TSH[65,91]. CS_2-induced catecholamine dysfunction may lead to neurodegenerative damage and affect the normal functioning of the thyroid.

2.3 Dimethyl dithiocarbamate fungicides

Ziram and Ferbam are two commonly known representatives of the dimethyl dithiocarbamates (Figure 7).

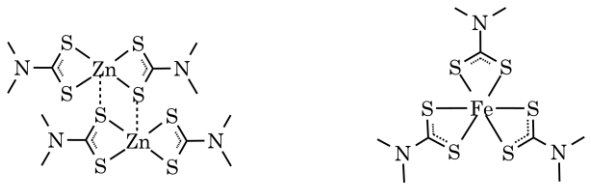

Figure 7: Dimethyl dithiocarbamate-containing fungicides Ziram and Ferbam.

Ziram is a bis(dimethyl dithiocarbamate) (DMDTC) complex containing Zn(II), with the chemical formula $[Zn(S_2CN(CH_3)_2)_2]_2$. In its dimeric form, Ziram consists of two penta-coordinated zinc atoms surrounded by five sulfur atoms. The coordination geometry of Ziram falls between trigonal bipyramidal and tetragonal pyramidal. The Zn-S bonds have a length of approximately 2.3 Å, while the bridging Zn-S interaction is around 2.8 Å. The distance between the zinc atoms in the Zn_2S_2 trapezoids is reported to be approximately 3.97 Å.[92] Ferbam is an iron tris(DMDTC) and the only DTC-based fungicide that contains

a trivalent trace element. Accordingly, three DMDTC ligands coordinate to the Fe(III)-ion, resulting in a distorted octahedral arrangement with a metal-sulfur bond length comparable to that of Ziram.[93]

2.3.1 Legal status

According to the Commission Implementing Regulation (EU) 2023/689 amending Implementing Regulation (EU) No 510/2011, Ziram is approved as a fungicide in the EU until March 2025. The World Health Organization (WHO) published an acceptable daily intake (ADI) for Ziram in 1995, setting it at 0.02 mg/kg body weight.[94] In 2012, Ziram was included in the Community Rolling Action Plan (CoRAP) under REACH Regulation, which involves the reassessment of its effects on human health and the environment. Ziram is not only used as a fungicide but also as an additive in various industrial applications, such as a sulfur vulcanization agent in rubber manufacturing. The registered use amount of Ziram under REACH is reported to be between 100 and 1000 tonnes per annum. On the other hand, Ferbam has not been approved in the EU since 1995 due to missing data for reevaluation. In terms of global use, polymeric fungicides like Maneb and Mancozeb are more commonly preferred over Ferbam and Ziram.[34] As with EBDC-based fungicides, residue analysis involves measuring the CS_2 content, disregarding the specific metal species and the organic backbone of the fungicides.[38]

2.3.2 Mechanism of action

Due to their structural similarity to EBDCs, it is expected that Ziram and Ferbam may have similar mechanisms of action. This includes their affinity to chelate metals from metabolic relevant metalloenzymes[87,88] and the release of CS_2 upon exposure, which has been observed *in vitro* by Magos in 1979.[95] Similar to Maneb and other EBDC-based fungicides, Ziram and Ferbam act as non-systemic contact fungicides with multi-site effects. As a result, they are often used in combination with systemic-acting ingredients to achieve a broader spectrum of protection against fungal pathogens. However, one notable difference between Ferbam, Ziram and EBDC fungicides is that Ferbam and Ziram do not degrade into ethylene thiourea (ETU) as the main degradation product. Instead, they degrade into other products, including tetramethylthiuram and thiram.[96]

2.3.3 Toxicity

Ziram is being investigated as a potential endocrine disruptor with a high-risk characterization ratio (RCR). Available data on Ziram raise concerns regarding its effects on developmental neurotoxicity and its association with Parkinson-related disorders. The European Chemicals Agency (ECHA) has noted in its substance evaluation decision that Ziram acts through multiple modes of action, affecting different targets during development and throughout the lifetime. There have been several epidemiological studies showing an increased risk of neurodegenerative diseases, including Parkinson's disease (PD), associated with chronic pesticide exposure. It has been hypothesized that the inhibition of critical enzymes may play a significant role in the pathogenesis of these diseases.[1]

The CS_2-related actions discussed in Chapter 2.2.4 can be applied to the adverse effects of Ferbam and Ziram as well. In addition, it has been shown that Ziram and also sodium dimethyl dithiocarbamate itself can inhibit the E1 ligase as part of the ubiquitin-proteasome system (UPS) *in vitro*. No inhibitory effects were observed after exposure to related compounds, including $ZnCl_2$ and CS_2.[97] The UPS is an intracellular mechanism responsible for controlling protein degradation in cells. Impaired UPS activities have been reported in the brains of PD patients and mutations in the UPS genes, such as Parkin and UCHL-1, are associated with the genetic form of PD.[98]

Stability constants for trace element-DMDTC complexes have been reported in the order of Mn < Zn << Cu.[99] DTCs are recognized as effective metal chelators, making them valuable for the removal of heavy metals from wastewater.[100] However, it should be noted that upon entering the environment, DTCs may not only chelate heavy metals but also essential trace elements that serve as cofactors for metalloenzymes. As a consequence, the activity of physiologically relevant copper-dependent enzymes such as superoxide dismutase, cytochrome C oxidase or dopamine-ß-hydroxylase may be affected in Ziram- or Ferbam-induced toxicity.[101] Studies involving Ziram exposure have shown increased intracellular concentrations of Zn in rat thymocytes (immune cell), which was correlated with enhanced cell lethality, as reported by Kanemoto-Kataoka *et. al* (2017). Notably, the co-incubation of Zn(II)-chelators resulted in a reduction of cell lethality back to control levels, underlining the role of Zn in Ziram-induced toxicity.[102] Furthermore, in PC12 cells, elevated levels of Ca were observed following exposure to Ziram. Interestingly, the Ziram-induced cell death was found to be mitigated by incubation of Ca-selective chelators or inhibitors of non-selective cation channels.[103]

2.4 Essential trace elements

The human body consists of many elements, with hydrogen, nitrogen, carbon, and oxygen being the most abundant. In addition, there are seven macro elements that are present in high amounts and are required in daily quantities greater than 100 mg: sodium, potassium, calcium, magnesium, chlorine, phosphorus and sulfur.[104] These macro elements make up 99% of the human body. However, there are also many other elements that occur in smaller amounts in tissues. These elements are often referred to as "trace elements" because they were not quantifiable by earlier analytical techniques.[105] Although there is no precise definition of a trace element, quantities of around 50 mg/kg body weight are often used to distinguish trace elements from other macro elements. Several trace elements have been recognized as essential for human health and must be consumed appropriately through food or drinking water. According to the scientific opinion of the EFSA, these include manganese, iron, cobalt, copper, zinc, selenium, molybdenum, and iodine.[106] Except for selenium and iodine, the other elements are d-block elements. Iodine is an essential structural and functional element of the thyroid hormones,[107] and selenium is found mainly in L-selenomethionine and L-selenocysteine as part of 25 selenoproteins in humans.[108] While fluoride,[109] vanadium[110] and chromium[111] have been discussed as essential trace elements, the EFSA panel has not yet confirmed their essentiality. This is because no deficiency has been demonstrated in animal models, and the underlying mechanisms for their essentiality, if any, are not yet fully understood.

In general, transition metals can act in many oxidation states as π-electron acceptors and are present in many metalloproteins and metalloenzymes.[112] Sulfur, nitrogen or oxygen atoms of amino acid side chains of proteins usually coordinate metal ions. Functional groups include imidazole, thiolate and carboxylate groups from histidine, cysteine or aspartate. In addition, organic cofactors serve as ligands such as the tetradentate heme group involved in hemoglobin.[113] According to estimations, approximately half of all identified proteins contain a metal with a catalytic, co-catalytic or structural role.[114] Catalytic active metalloproteins are termed metalloenzymes. Metalloenzymes are engaged in a wide range of physiological processes in the body and play a critical role in metabolism, development and reproduction.[115,116] For evaluating the complex stability, Harry Irving and Robert Williams found in 1948 that almost independently from the participating ligand, the stability of complexes involving divalent first-row transition metal ions exhibits

a rising trend across the period. The stability maximum is reached at copper: Mn(II)<Fe(II)<Co(II) <Ni(II)<Cu(II)>Zn(II).[117]

All essential trace elements occur in humans in a specific homeostatic range. In this context, the term homeostasis was created by *Walter Bradford Cannon*[118] and referred to a state of stable physiological conditions constantly maintained by a living organism. This state is reflected by optimal conditions with many variables to be maintained and regulated within specific predefined limits, the homeostatic range.[118] All regulatory mechanisms, which are required to control the equilibrium, contain a minimum of three independent components for the regulated variable: receptor, control center and effector.[119] Control of metal levels in the body is critical to human health and disease, emphasizing the risk of deficiency and potential overexposure.[115]

For protection against metal-induced toxicity on a cellular level, living organisms have evolved various mechanisms to prevent metal toxicity, including regulation of absorption, distribution, transportation, storage and excretion.[120] The metal uptake can be restricted and their excretion can also be promoted. Many cellular systems with complex interactions play a significant role in the detoxification of metals. According to Fenton's reaction or Fenton-like reactions, redox-active metals (e.g. Fe, Cu, Mn) catalyze and contribute to the formation of reactive oxygen and nitrogen species (RONS).[121] In physiological occurring ranges these are neutralized by antioxidants such as glutathione (GSH). GSH is the most abundant thiol in human cells and protects them by neutralizing RONS through oxidation to glutathione disulfide (GSSG).[122] The ratio of GSH/GSSG is an established marker for assessing the antioxidant capacity concerning oxidative stress. Another function of GSH is directly binding metal ions, allowing the conjugates to be excreted by glutathione transferase (GST). Cysteine-rich metallothioneins (MT) complex metal ions directly but also serve as antioxidants. Furthermore, active ATP binding cassette (ABC) transporters excrete some metal ions and their GSH-conjugates using heat shock proteins (HSP) that bind to metal-protein conjugates for inactivation and prevent aggregation.[122]

Sections 2.4.1 briefly introduce the trace elements, which are found in most commonly used in dithiocarbamate fungicides as Mn, Cu, Zn and Fe. Special attention is given to Mn since the Mn-containing fungicides Maneb and Mancozeb are the fungicides with the most potent fungicidal activity[33] but also appear to be the most toxic.[123]

2.4.1 Manganese

Mn is one of the most abundant elements in the earth's crust and occurs ubiquitously in minerals but usually not in elemental form. Although several isotopes of Mn exist, only ^{55}Mn is stable. Elements with only a single stable isotope are categorized as monoisotopic. Mn can be easily oxidized and is found in many oxidation states; the most common ones being +II, +IV, and +VII. Of physiological relevance are only the oxidation states +II and +III, which are generally most soluble in water.[124] Due to the electron configuration [Ar] $4s^2$, $3d^5$, Mn and its ions feature unpaired electrons resulting in paramagnetic compounds, which may be high-spin or low-spin. Mn offers a wide range of industrial applications, such as batteries and ferromanganese, in the steel production industry, which contains about 80% Mn.[125] In many countries, the organomanganese compound "methylcyclopentadienyl manganese tricarbonyl" (MMT) is added to gasoline as an anti-knock agent.[126] Due to the strongly paramagnetic properties of Mn^{2+}, it was used as one of the first contrast agents for magnetic resonance (MR) based techniques.[127]

In the biology, Mn is required as a cofactor in many enzymes involved in several physiological processes such the amino acid, lipid and carbon metabolism. Due to its ubiquitous occurrence, Mn deficiency is rare in humans, as it is available through food and drinking water.[128] For the general population, the main uptake is via the diet (nuts, legumes, fruits, cholate)[129] and drinking water, with an estimated intake of 2 to 6 mg per day in the EU.[128] The European Food Safety Authority (EFSA) defined an adequate intake (AI) of 3 mg Mn per day for adults and 0.02 – 0.05 mg per day for infants from 7 to 11 months, based on an extrapolation from the adult AI.[128]

The amount of Mn absorbed by the gastrointestinal tract depends on the Mn concentration in the diet and involves both active transport and passive diffusion.[128,130,131] The bioavailability of Mn varies between 2 and 10% and depends on the dietary composition.[132,133] After intestinal absorption, Mn is released into the blood and transported primarily to the liver as a storage organ. The liver, kidney and pancreas generally have the highest amounts of Mn in the human body.[130] Afterwards Mn is transported to other cell tissues, involving several cell-type-specific transporters, which are not Mn-specific.[134] After excretion by the liver into bile, Mn is mainly eliminated *via* the feces.[135]

Although Mn is essential, it can accumulate in the central nervous system when the homeostatic range is exceeded, especially in brain areas rich with dopaminergic neurons.[15]

The phenotype of Mn-induced adverse neurological effects is termed “manganism”. The symptoms are mainly related to those of idiopathic Parkinson's disease (PD), affecting the motor system.[136,137] As early as the nineteenth century, neurological abnormalities were first documented by *James Couper* in workers in manganese dioxide mills.[12–14] In addition, other occupationally exposed individuals, such as agricultural field workers using Mn-fungicides, have also shown neurological deficits due to dust inhalation.[2] High Mn exposure is not limited to those workers; the ubiquitous distribution of Mn in the environment represents a risk for the general population. The European Union (EU) defined in the Directive (EU) 2020/2184 a limit of 50 µg/L for Mn in drinking water. In many other countries Mn levels in drinking water are much higher and associated with adverse effects in children such as impaired manual dexterity, short-time memory and visual identification.[138,139] Other vulnerable risk groups for Mn-induced toxicity include patients, on parenteral (Mn-rich) diet, patients with impaired hepatic function, or fetuses, neonates and children without fully developed liver excretion system,[140] due to the fact that about 98% of dietary Mn is eliminated by the liver.[141]

Both Parkinson's disease and manganism lead to motor deficits like bradykinesia but differ in the expression of postural tremors and balance disturbances.[142] Additionally, both disorders can be differentiated by the affected brain regions.[137] In manganism, Mn is accumulated in the dopamine-rich brain areas responsible for controlling motor skills, known as the *globus pallidus* and *corpus striatum*. In contrast, PD is characterized by progressive loss of the dopaminergic neurons in the *substantia nigra pars compacta*, resulting in acute dopamine deficiency and indirect impairment of the movement control center. Owing to these differences, it can be explained why the drug Levodopa, which is frequently used in Parkinson's therapy, is not effective in the treatment of manganism. Levodopa is an inactive precursor of the tyrosine derivate dopamine. It is supposed to prevent DA deficiency in the brain, as Levodopa is allowed to pass the blood-brain barrier and converted into the active form by decarboxylation.[143]

Many studies have focused on the unknown mechanism for Mn-toxicity in the brain. The proposed mechanism relates to impaired dopaminergic, glutamatergic and GABAergic transmission, mitochondrial dysfunction and oxidative stress.[144–146] In this context, Mn-induced neurotoxicity is mainly discussed as a consequence of oxidative stress due to the formation of RONS in specific Mn-exposed brain regions. Mn ions are generally redox-active, producing RONS in Fenton-like reactions.[147] Furthermore, it has been proposed

that Mn (II) regulates cellular responses by mimicking Ca(II)-ions. Modulation of Ca(II) might disrupt mitochondrial functions, cellular antioxidant defense and other metabolic pathways.[147,148] Overall, the underlying mechanisms of manganism are still not fully understood.

2.4.2 Zinc

Zn is an abundant element in the earth's crust, mainly in the form of sulfur-containing minerals. ^{64}Zn, with its 49% natural abundance, has four additional stable isotopes and usually occurs in oxidation state +II or in its elemental form. Zn is the only metal found in all enzyme classes and, after iron, the most abundant trace element in humans, underlining its ubiquitous distribution. In proteins, the Zn binding sites usually include sulfur, nitrogen or oxygen atoms of several amino acids, mainly building a slightly distorted tetrahedral geometry.[116] In contrast to the other transition metals Fe, Mn or Cu, which are usually redox-active, Zn^{2+} features a completely filled d-orbital and therefore does not participate in redox reactions. Consequently, Zn^{2+} is very stable and well-suited as an electron pair accepting cofactor due to its property as Lewis acid.[116,149] In addition, the role of Zn^{2+} is more of an antioxidant rather than causing RONS.[116]

As an essential trace element, Zn is required in many physiological processes, especially for prenatal and postnatal developmental, metabolism and gene expression.[150] Consequently, a sufficient amount is necessary to maintain the Zn homeostasis. Dietary Zn is absorbed while passing through the small intestine. Zn-rich food sources are fish, meat and eggs but also vegetables. The bioavailability depends on intrinsic luminal and basolateral factors and diet-derived factors such as phytate anions.[151] Phytatic acid in plants functions as phosphor storage and has a strong affinity for metal ions like Zn, inhibiting their absorption from the small intestine. Notable phytate amounts are present in legumes and affect people with plant-based diets more frequently.[150]

In the blood plasma, Zn is mainly bound to albumin, which helps to maintain the Zn concentration relatively constant. EFSA considers in its proposed recommendation an interaction of Zn excretion levels, Zn bioavailability and average daily phytate intake levels (300 to 1200 mg daily) using various published data. The average requirement (AR) to maintain normal Zn concentrations ranges from 6.1 to 10.2 mg/day for women (58 kg) and 7.5 to 12.7 mg/day for men (68 kg).[150] On the cellular level, several transporters such as the Zn importer Zrt- and Irt-like protein (ZIP) and the Zn efflux mediating zinc transporter

(ZnT) are involved in the uptake and export of Zn. No specific organ has been identified for Zn storage; the highest Zn concentrations are in the muscles, bones, kidneys, liver and brain.[150]

In contrast to Mn, Zn deficiency affects many people worldwide, with approximately 20 % of the global population estimated to be at risk.[152,153] Zn deficiency is associated with diverse symptoms that impact the immune system, central nervous system, reproductive system, gastrointestinal tract and skin. Manifestations of Zn deficiency include eczema, impaired wound healing, diarrhea, hair loss and loss of appetite.[154] On the other hand, in the case of a chronic oversupply of Zn, such as through the ingestion of Zn supplements, it has been observed this can lead to oxidative stress and potentially becomes pro-inflammatory and pro-apoptotic.[155] It is suspected that the increase of free Zn-ions, which is normally tightly regulated, leads to an enhanced expression of metallothionein (MT).[156] MT exhibits a high affinity for copper, thus promoting the export of Cu. Consequently, this could lead to symptoms similar to those seen in chronic Cu deficiency.[157] An acute Zn intoxication is rare and typically arising from accidental ingestion of Zn-containing substances like coins or excessive intake of Zn supplements. Symptoms of acute Zn intoxication may involve gastrointestinal disturbances due to high solubility of Zn in the acidic stomach, where it acts as a Lewis acid.[158]

2.4.3 Iron

Iron is a chemical element classified as a transition metal, exhibiting four stable isotopes and ranking among the most geologically abundant elements on earth. This essential and redox-active metal holds critical significance for plants and organisms, including its pivotal role in human health and disease. Fe is commonly found in combination with other elements and forms minerals like hematite (Fe_2O_3), magnetite (Fe_3O_4) and siderite ($FeCO_3$), primarily in oxidation state +II or +III.[159] However, Fe can manifest various oxidation states ranging from -IV to +VII, which facilitates diverse coordination and organometallic chemistry. The human body contains about 4 g Fe, more than other trace elements, highlighting its unique biological role.[160] Fe is present in hemoglobin, myoglobin and in hem and non-hem enzymes, reflecting its multifunctional involvement in oxygen transport, energy metabolism, electron transfer and oxidase activity.[161] Physiologically relevant are mainly oxidation states +II (“ferrous”) and +III (“ferric”), influencing their bioavailability, reactivity and function.[162] Fe bioavailability has been reported to be higher in mixed diets containing predominantly divalent heme iron (14-18%) compared to vegetarian diets (5-

12%) with a higher portion of ferric-bound iron.[163] The absorption in the gastrointestinal tract depends on several factors, including the Fe-species, the individual physiological requirement, storage status and dietary composition. The divalent metal transporter 1 (DMT-1) is mainly involved in Fe(II) absorption in the duodenum and upper jejunum. Hence, it is recommended to include ascorbic acid-rich ingredients in the diet to enable Fe-(III) to be reduced to Fe(II) and also to minimize phytate-related effects by the formation of ascorbic-Fe-complexes.[164] Fe is commonly bound to other substances such as phytates and polyphenols or competitors (e.g. Mn and Zn) that might inhibit absorption.[164]

Human iron requirements depend on different factors such as age (growth) or gender, as premenopausal women excrete more iron *via* blood loss. For men and postmenopausal women, the average requirement (AR) is 6 mg Fe daily, using an absorption rate of 16% to convert physiological needs (1.72 mg/day) into dietary requirements. The population reference intake (PRI) was calculated using the 97.5th percentile and was defined as 11 mg/day. The PRI for premenopausal women was set as 16 mg/day, and for infants and children, 11-13 mg/day, depending on age and gender.[165]

Considering the high nutritional requirements, especially for some vulnerable population groups, and the inefficient absorption of Fe, iron deficiency is the most frequent nutritional deficiency disorder worldwide.[166] Insufficient Fe uptake initially leads to the mobilization of iron stores and then develops into anemia. It is estimated that about 2 billion people worldwide are affected by iron deficiency.[167]

In contrast to other trace elements excreted *via* bile, humans have no actively regulated mechanism for iron excretion. Uptake and homeostasis are strictly controlled to prevent Fe increased accumulation. Although the Fe absorption can be significantly reduced, complete suppression is impossible. Overexposure due to dietary products is marginal with a functional intestine.[168] However, Fe supplementation in children (and adults) to prevent iron deficiency carries the risk of Fe overload, especially if the dosage is not inadequately regulated. There is growing concern that excessive Fe exposure during early ages may be associated with adverse effects later in life.[169] Fe accumulation can be highly toxic to many organs leading to serious diseases such as diabetes mellitus, dysfunctional immune system and diseases affecting the liver, heart and hormones.[170] Abnormal Fe homeostasis and overload in the brain is associated with ageing-related neurodegenerative diseases such as PD and AZ.[171] Postmortem studies of Parkinson's disease (PD) patients have observed Fe accumulation, especially in the *substantia nigra*, a brain region rich in dopamine-producing

neurons.[172] These areas are believed to be involved in the degeneration of dopaminergic neurons, a characteristic feature of PD. Additionally, there is evidence suggesting a role for Fe dysregulation in Alzheimer's disease (AD), as abnormal iron deposition has been detected in brain regions associated with amyloid plaques and neurofibrillary tangles.[173] On mechanistic level, Iron excess is supposed to cause a variety of toxic effects and being responsible for oxidative stress due to the presence of redox-active Fe(II) and Fe(III), which are capable of participating in Fenton-like reactions.[174] Furthermore, Fe is discussed in being involved in a form of non-apoptotic, Fe-dependent cell death, termed as ferroptosis.[175] For more comprehensive information about neurodegenerative diseases, refer to chapter 2.6.

2.4.4 Copper

As one of only a few metals copper can be found as a native metal in its pure metallic form with the characteristic orange-metallic color. Because of its softness and high electrical conductivity, Cu has many applications, including electrical cables, coins and is found in many important alloys such as brass or bronze. Due to its electronic configuration of [Ar]-$3d^{10}$ $4s^2$, the most relevant oxidation states are +I and +II, which also occur under physiological conditions. Cu-related proteins and enzymes are essential for human health since they are important in electron and oxygen transport and neurotransmitter synthesis. For example, Cu-containing enzymes involved in these processes are cytochrome c oxidase and some superoxide dismutases.[176]

Cu is an essential trace element and consequently its uptake is derived mainly from food and drinking water, especially in grain-based products, meat, nuts and fish. However, there is a lack of sensitive or specific Cu-biomarkers in Cu deficiency or excess. Ceruloplasmin, labile copper in serum or activity of cuproenzymes are being discussed as potential biomarkers.[177] EFSA proposes an adequate intake (AI) of 1.6 mg Cu per day for men (women: 1.3 mg Cu/day) based on its bioavailability and absorption rate of approximately 50%.[168] After Cu absorption in the upper small intestine, Cu is released in the blood, mainly bound to albumin and transported to the liver as the Cu storage organ. Once there, Cu is stored in metallothionein or attached to ceruloplasmin. Excess Cu is eliminated through excretion via bile.[178]

Since Cu is crucial for a functioning metabolism, a deficiency can result in various health problems but they occur rarely. A mutation in the gene encoding the copper-transport

protein ATP7A gene causes a lethal multisystemic disorder in Cu metabolism in newborns and is known as Menkes disease.[179] The intake of Zn or Fe supplements in high doses decreases Cu levels, hence interactions between trace elements are of current research interest. Excess Cu does not typically lead to Cu accumulation, since Cu homeostasis is tightly regulated. In certain genetic disorders, such as the rare Wilson's disease, the excretion of Cu is impaired.[180,181] Cu gets accumulated in the liver and consequently over time also heart, kidney, eyes and especially in the brain. Wilson's disease is treated with a low copper diet in combination with chelating agents and Zn supplements.[180] Cu also forms complexes with amyloid-ß-peptides in the brain, which can contribute to the formation of amyloid-plaques, a hallmark of Alzheimer's disease.[182] On cellular level, chronic Cu overexposure is associated with formation of RONS leading to oxidative stress, since Cu is able to cycle between its +I and +II state in cells.[183]

2.5 Species-specific effects in metal-induced toxicity

The influence of the chemical form of a metal, which is often referred as "species" or "metal-speciation", on human toxicokinetics and toxicodynamics was reviewed by Yokel *et al.* (2006).[184] Although many attempts were made, there is no widely accepted definition of metal speciation, but in general it includes attributes such as oxidation state, particle size, associated ligands and the nature of the metal species. All these factors have the ability to change the exposure route and extent of uptake/absorption and thus the toxicodynamic results.[184]

In particular, metal-ligand interactions play a pivotal role in determining toxicity and bioavailability of metals. A classic example of species-specific toxicity is mercury, which is a highly toxic metal that exists in various chemical entity, each with distinct levels of toxicity. The relevant forms are elemental mercury, inorganic mercury salts and organomercury compounds such as the methylmercury cation. However, the diversity in species-specific effects is not exclusive to mercury; this phenomenon extends to many other metal species.[185]

Within the sphere of biologically active substances, the utilization and modification of specific structure analogs are used enhance their activity. Not only in drug development, also in toxicology, the combination between a metal and a ligand plays as a crucial role. It is hypothesized that Mn (II) complexed with ethylene bis(dithiocarbamate) (EBDC) ligands exhibits increased lipophilicity, potentially facilitating its distribution across diverse cellular compartments.[186] The understanding of metal-ligand-related effect in terms of

toxicity is rather poor, therefore this work aimed to shed more light into the species-specific effects of Mn.

2.6 Neurotoxicity as a consequence of environmental contaminants

Neurotoxicity is defined as any reversible or permanent impairment of the structure or function of the central or peripheral nervous system caused by a biological, chemical or physical agent.[187] Hence, neurotoxicity is considered one of the leading contributors to neurodegenerative disorders. The underlying mechanisms are diverse and include exposure to environmental agents like pesticides or metals, abuse of drugs and certain naturally occurring substances.

The human nervous system is highly complex and consists of the central nervous system (CNS) and the peripheral nervous system (PNS). The CNS is located in the brain and spinal cord, which is directly connected to the rest of the body by nerve cells of the PNS. Both nervous tissues are composed of neurons and neuroglial cells. Typical neurons consist of a cell body (the soma), branched dendrites, and an axon reaching up to one meter in length.[188] For inter-cell communication, the signals are transmitted by neurotransmitters from the presynaptic neuron to a target cell via the synaptic gaps and involvement of neurotransmitter receptors. Neurotransmitters are signaling molecules, including dopamine, serotonin, glutamate, glycine, acetylcholine, γ-amino butyric acid and noradrenaline, amongst others. Although the glial cells are not involved in signal transduction, they still constitute half of the neuronal tissue because they stabilize, support and protect the neurons.[189]

Neurodegenerative diseases are characterized by a progressive loss of neuronal function and irreversible neuronal damage, including death of neurons.[79] The progress is referred to as neurodegeneration and is the main pathologic feature in diseases such as Parkinson's disease (PD) and Alzheimer's disease (AD).[190] PD and AD are the most common neurodegenerative disorders, estimated to affect more than 30 million people worldwide.[166,191] The most significant risk factor in developing a neurodegenerative disease is aging. Mitochondria are proposed to play an important role in the pathogenesis of neurodegenerative diseases and aging-related effects by accumulating mitochondrial DNA (mtDNA) mutations and RONS.[79] All early manifestations of the most frequent diseases of this type have been linked to mitochondrial dysfunction and oxidative stress, indicating a role in the pathogenesis.[79]

The main pathological hallmarks of AD are the accumulation of ß-amyloid plaques and τ-protein tangles in the brain.[192] Early symptoms of AD include memory loss and confusion, but as the disease progresses patients experience language problems, disorientation and changes in personality. It is believed, that AD is caused by a combination of genetic, environmental and lifestyle factors. Currently, there is no cure for AD, but treatments aim to manage symptoms and to slow down disease progression.[190]

PD is a neurodegenerative disease affecting the motor system, causing progressive movement disorders. It arises from the degeneration of dopamine-producing neurons in the *substantia nigra*, a brain region responsible for motoric skills control.[193] Primary symptoms of PD involve tremor, bradykinesia and cognitive changes, but non-motor symptoms such as anxiety and depression can also occur. Similar to AD, there is currently no cure for PD but the dopamine precursor Levodopa is in some cases an effective medication for managing PD symptoms.[190]

Neurotoxins or neurotoxicants are synthetic or naturally occurring individual compounds with the potential to disrupt the nervous system *via* direct or indirect consequences.[194] While pesticides can be effective in their intended purpose, there is evidence to suggest that prolonged exposure to certain pesticides can lead to adverse effects on human health, including the development of neurological disorders. Several studies have found a potential link between pesticide exposure and neurological disorders such as PD or AZ but the contributing mechanisms are still investigated. Possible mechanistic explanations include oxidative stress, neuroinflammation, mitochondrial dysfunction or dyshomeostasis of neurotransmitters.[50,52,53,195,196] However, the relationship between pesticide exposure and adverse neurological outcome is complex and influenced by several factors such as pesticide class, duration and intensity of exposure and other environmental factors. Unlike unintentional pesticide exposure through work or residues on food, trace elements are being consumed through food components because of their essentiality. However, trace elements can also provoke neurodegenerative processes in case of excessive chronic exposure. Especially for Mn, Fe, Cu and Zn, the most important information has been summarized in Chapter 2.4.

2.7 *Caenorhabditis elegans* as a model organism

To assess the effects of the metal-based ethylene bis(dithiocarbamates), especially Maneb, in comparison to $MnCl_2$ and its metabolites, the nematode *Caenorhabditis elegans* (*C. elegans*) was used. *C. elegans* represents an alternative *in vivo* model organism in order to **R**educe, **R**eplace and **R**efine animal experiments according to the 3R principle invented by *W. Russel* and *R. Burch*.[197] Animal experiments should be reduced as much as possible by using alternative models.

The free-living worm prefers organic-rich soils in temperate environments. Anatomically, the transparent worm consists of a mouth, pharynx, intestine, gonads and a collagenous cuticle and is unsegmented and bilaterally symmetrical structured. During its lifespan of about three weeks, the self-fertilizing hermaphrodite provides many progenies. In an average population, usually only 0.1 % of the individuals are male.[198] After egg deposition, the worms hatch as L1 larvae, the first of four larval stages of its approximately three-day life cycle (from hatching to adulthood).[199] Under suitable environmental conditions and depending on the temperature, the larvae reach the fourth stage after ca. 48 h at 20 °C.[200] After a further 18 h, the approximately 1 mm long worms are considered as adults (Figure 8). Without food or under unfavorable environmental conditions, the worm can enter the "dauer stage" during the second larval stage. During the dauer stage, the nematode's metabolism is at the lowest possible level, enabling it to survive for many months without food.[201] In this stage, the nematode can be carefully frozen in a glycerol-containing freezing solution and stored at -80 to -196 °C (Figure 8).

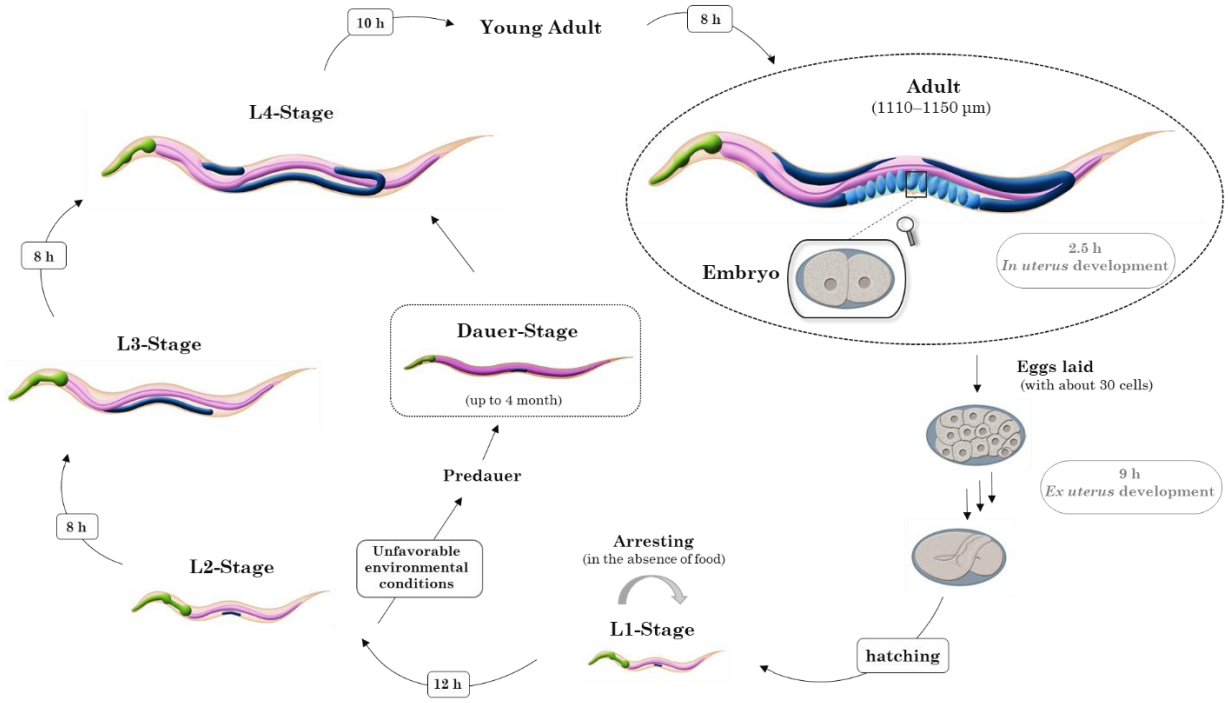

Figure 8: Life cycle of *Caenorhabditis elegans* at 20°C [adapted and modified from [202]].

As an *in vivo* model organism, *C. elegans* is easier to maintain than other multicellular organisms. The worms live on agar plates with *Escherichia coli* (*E. coli*) as food source and are kept at 20 °C with high humidity. Microscopy allows observation of the worms and to study their behavior and appearance. Every adult hermaphrodite always possesses precisely 959 somatic cells, and each adult male has exactly 1033.[203] This phenomenon of cell constancy is referred to as eutely. Despite the worm's small size, about 60-80% of human genes are represented as orthologs.[204] Therefore, the worm is well-suited to investigate metabolic diseases, aging and metal-induced toxicity. In addition, the ability to genetically manipulate the worms enables the generation of disease-associated deletion or knockout mutants, enabling investigation for mechanistic studies. Neurotoxicity can be particularly well studied, since the worms feature a highly conserved nervous system with an absolute number of 302 neurons. The neurons possess dendrites to transmit information to target cells *via* neurotransmitters and use them to form a nerve ring. The nerve ring is a packed bundle of axons consisting of neuron processes located within the head region wrapped around the pharynx. It represents the most synapse-rich segment of the nervous system and is regarded as the "brain" of *C. elegans*.[205] Most processes are located in the ventral or dorsal nerve cord, Two distinct and independent types of nervous systems have been identified: the somatic nervous system with 282 neurons and the pharyngeal nervous system. In signal transduction, *C. elegans* shares many neurotransmitters identical to

humans including dopamine (DA), serotonin (SRT), acetylcholine (ACh), γ-aminobutyric acid (GABA) and glutamate.[206–209] Not only deletion or knockout mutants are available for mechanistic studies but also strains expressing green fluorescent protein (GFP), such as the P_{dat-1}::GFP (BY200) *C. elegans* strain. BY200 expresses GFP in the dopamine transporter (DAT-1), allowing due to the transparency of the worms the observation of a potential dopaminergic neurodegeneration by fluorescence microscopy.[210] Dopaminergic signaling is responsible for locomotion, egg laying and mechanosensory in *C. elegans*. The hermaphrodite possesses four bilaterally symmetric pairs of dopaminergic neurons, that can be divided into three classes. Four cephalic sensilla (CEP) neurons and two anterior deirids (ADE) neurons are located in the head region and two posterior deirids (PDE) neurons in the posterior region of the body.[206,210,211] Each CEP neuron forms dendrites that lead to the mouth of the nematode, visualized for example in the BY200 strain. (Figure 9).

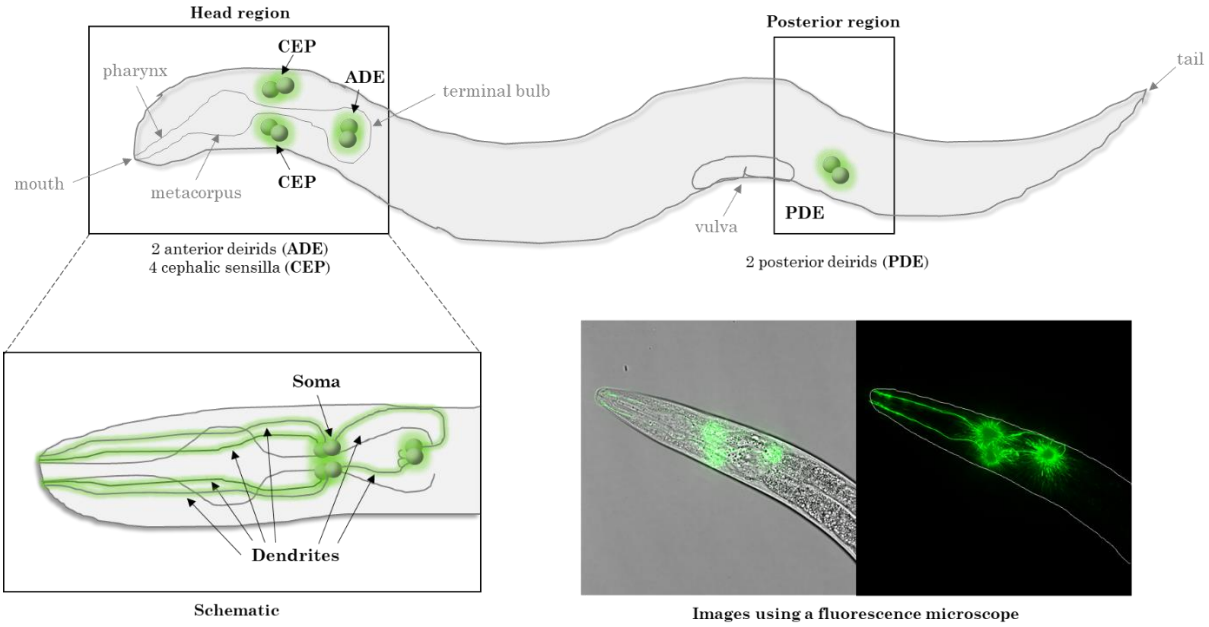

Figure 9: Schematic overview of the eight dopaminergic neurons in *C. elegans* [adapted and modified from [210]]. Images of the BY200 strain were captured using a fluorescence microscope (excitation: 460-500 nm, emission 512-542 nm)

The fact that *C. elegans* is a valuable model organism is reflected in more than 5000 publications per year and several associated Nobel Prizes. Three prizes were awarded, one for the genetic regulation of organ development and programmed cell death (Physiology or Medicine, 2002), one for RNA interference discovery (Physiology or Medicine, 2006), and one for research on green fluorescent protein (Chemistry, 2008). As a milestone, the genome of the nematode with over 100 million base pairs and over 20 k protein-coding genes was the first multicellular organism to be entirely sequenced.[204]

Due to its numerous advantages including its simple anatomy, short lifespan, ease of cultivation, and well-characterized genome, *C. elegans*, like any model organism, has its limitations. These include the fact that the nematode is a relatively simple organism with a limited number of cells and lacks certain organs. Furthermore, due to its small size, most analytical studies are conducted using whole worm homogenates, which makes it challenging to investigate organ- or tissue-specific signaling pathways and gene expression in different cells. Additionally, the behavioral repertoire of *C. elegans* is significantly limited compared to that of mammals. Despite these limitations, *C. elegans* remains a valuable model organism for studying a wide range of biological processes and has made substantial contributions to our understanding of basic biology and human diseases. It also offers the possibility of integration with other model organisms and *in vitro* systems to gain a more comprehensive understanding of biological phenomena.[212]

Abstract:

Maneb is a manganese(II) containing fungicide with a multi-site effect and no resistance, therefore it is widely applied in many parts of the world. There is however mounting evidence for neurotoxic effects with Parkinson-like symptoms (manganism) related to usage of Maneb. Due to its insolubility in most solvents and its paramagnetism, structural elucidation is not trivial and thus its exact molecular structure remains unknown. We report herein a synthesis procedure to prepare Maneb reproducibly in pure form and the use of various analytical techniques including X-ray diffraction, X-ray absorption spectroscopy and electron diffraction to determine the molecular structure of Maneb in the solid state and also in solution.

Chapter 3 – The structure of Maneb: An important manganese-containing bis(dithiocarbamate) fungicide

Based on:

Laura Kubens, Khai-Nghi Truong, Christian W. Lehmann, Dirk Lützenkirchen-Hecht, Julia Bornhorst and Fabian Mohr

Chemistry – A European Journal, **2023**, *29*, 55, e202301721.

DOI: 10.1002/chem.202301721

Chapter 3 – The structure of Maneb: An important manganese-containing bis(dithiocarbamate) fungicide

3.1 Introduction

Fungicides containing ethylenebis(dithiocarbamate) (EBDC) and its salts were patented in the 1940s and have since become one of the most frequently applied class of fungicides in crops including potatoes, tomatoes, soy beans and bananas.[22] In particular, the manganese derivative, known as Maneb, was found to be a highly effective fungicide and has therefore been extensively used.[4] Maneb is, like other EBDC salts, a surface-acting crop protection product, which has to be applied repeatedly to the plant. It is used to prevent fungal diseases but has no curative properties if a plant is infected. Maneb is classified as a fungicide with multi-site activity (group M03) by the Fungicide Resistance Action Committee (FRAC).[213] It is believed that organic degradation products including the main metabolite ethylene thiourea (ETU) formed by decomposition of Maneb under environmental conditions, interferes with thiol groups of fungal enzymes. Due to its non-specific mode of action, it is hardly surprising that it can also have an effect on other living organisms, such as aquatic species and even humans. Maneb itself is non-toxic to the plant,[6,214–216] however, in the 1980s both acute and chronic toxicity affecting the central nervous system was observed in agricultural field workers applying Maneb.[2,217] Indeed, Mn-induced chronic toxicity affecting the nervous system (first termed "manganese madness" and nowadays "manganism") was documented in workers at manganese dioxide mills already in the nineteenth century.[12–14] The neurological symptoms of manganism are similar to those of Parkinson's disease and affects the motor system. The underlying mechanisms of manganism have since been studied in considerable detail and a number of reviews summarize important findings.[60,77,218–228]

Since 2017 Maneb is banned in the European Union, the UK and other countries including the USA, Australia, New Zealand and Canada. However, Maneb is still applied on large scale in Brazil, India and China.[34] Despite its long-time usage and the amassed evidence of its neurotoxic properties, the exact chemical structure of Maneb is still not known. This is also problematic in pesticide residue evaluation, since residue analyses of EBDC fungicides are based on the total CS_2 content, which does not distinguish between approved and banned dithiocarbamate- containing fungicides.[39] Because of its very poor solubility in common solvents and the paramagnetic nature of the Mn^{2+} ion, methods for structural

elucidation are rather limited. There also exist, at times conflicting, reports on the stability of Maneb in both solid-state and in formulations, as determined by powder diffraction or differential thermal analysis.[31,229–231]

As will be detailed below, industrial production methods for Maneb undoubtably result in materials of variable appearance, stability and purity. Even commercial products sold as pesticide reference standards are not uniform in appearance and quality! It is also known that significant amounts of ETU are formed during industrial manufacturing of this class of fungicides.[44] ETU is a well-known thyroid-affecting toxin, classified by the International Agency for Research on Cancer as possibly cancerogenic to humans.[82] Given the relevance of the toxicity of Maneb and its continued large-scale usage, we examined its synthesis and carried out detailed studies of the material in both solid-state and in solution. In addition to X-ray diffraction, we have used X-ray absorption spectroscopy (EXAFS and XANES) as well as electron diffraction to elucidate the solid-state structure of Maneb. The results of our endeavors are reported herein.

3.2 Result and Discussion

In the patent literature Maneb is typically prepared in a one-pot procedure involving a manganese salt, ethylenediamine and CS_2 in the presence of a base (NaOH or KOH) in water.[4] In our hands this method gave products of variable quality as judged by their color (Figure S7) and elemental analysis. Even when the disodium salt of the bis(dithiocarbamate) was isolated and used in the preparation of Maneb, brownish, impure products were obtained in poor yields. In order to reproducibly obtain a defined material, we first isolated the ammonium bis(dithiocarbamate) salt from the reaction of ethylenediamine with two equivalents of carbon disulfide in the presence of methanolic ammonia. Subsequently, the ammonium salt (**1**) was dissolved in water and added to an equimolar amount of manganese chloride in water (Figure 10).

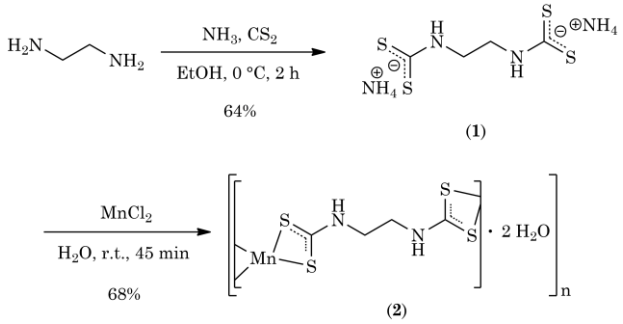

Figure 10: Reaction of ethylenediamine to the corresponding ammonium dithiocarbamate (1), which reacts with an equimolar amount of manganese chloride to Maneb dihydrate (2).

Under these conditions, Maneb precipitates as a yellow solid, which was confirmed by IR spectroscopy (Figure S4), TGA (Figure S6) and elemental analysis and to be the dihydrate of Maneb. This dihydrate can be converted into anhydrous Maneb by drying the solid under vacuum at room temperature overnight. This procedure reproducibly affords Maneb in high-purity and yield. The quality of the products was also assessed by determining their manganese content by EDTA titration.[232] The observed values (20.3% and 18.1% for anhydrous Maneb and Maned dihydrate, respectively) agree well with the expected values. The oxidation state +II of manganese in Maneb and its dihydrate was confirmed by measuring its magnetic moment with a Gouy balance.[233] The observed values of 5.88 and 5.19 B.M. are consistent with the presence of high spin d^5 Mn^{+II} in both compounds. The TGA curves of Maneb and the dihydrate (Figure S6) show similar features: The dihydrate undergoes a weight loss step commencing at 62 °C corresponding to 11.2 % mass loss, consistent with release of two water molecules (calculated mass loss of 11.9 %). In addition, in both the dihydrate and the anhydrous compound, there are two major peaks in the DSC curves, one sharp signal at around 178 °C (dihydrate) and 173 °C (anhydrous), consistent with evolution of CS_2. The residual masses of 27.6 % and 32.1 %, at 1000 °C, correspond to MnS, which is a known thermal decomposition product of manganese dithiocarbamates.[18] This data is consistent with that reported for commercial samples of several bis(dithiocarbamate) fungicides including Maneb.[31,231]

Our anhydrous Maneb is stable in air for months in the solid-state and solutions in DMF or DMSO remain unchanged for a period of at least 10 days. This is somewhat surprising, given that Mn(II) dialkyldithiocarbamates are known to more or less readily oxidize in both in the solid-state and in solution.[30,234] Boschi recently studied the oxidation of yellow Mn(II) bis(diethyldithiocarbamate), which rapidly forms brown oxidation products. Based on mass spectrometry, IR-spectroscopy and its magnetic moment, the final oxidation product was identified as Mn(III) tris(diethyldithiocarbamate), formed via an intermediate Mn(III) superoxide species.[234] It could be, that the brownish products observed in some of our Maneb syntheses using methods from the patent literature are in fact such Mn(III) species as well.

The stability of Maneb towards air may be explained by its polymeric structure (see below), which results in complete coordinative saturation of the six-coordinate manganese center. Maneb is insoluble in common solvents including water, EtOH, MeCN, MeOH, acetone and THF at both room temperature and in the boiling solvents. However, the compound does

slowly (*ca.* 15 min.) dissolve in DMF or DMSO at room temperature. Single crystals formed upon standing 0.5 M solutions in DMF or DMSO for a few days. The crystals rapidly lost crystallinity once removed from solution, even when kept in perfluorinated oil. X-ray diffraction datasets could successfully be collected when the crystals were removed quickly from their mother liquors and directly mounted on the dinitrogen cooled goniometer.

The asymmetric unit of the DMF-complex (Figure 11 top) consists of a manganese atom bound to two sulfur atoms from the chelating bis(dithiocarbamate) ligand as well as two oxygen atoms from the DMF. There are two additional, non-coordinating DMF molecules in the asymmetric unit, which form hydrogen bonds between the oxygen atoms and the NH protons of the bis(dithiocarbamate) ligand. A 1D-coordination polymer results from the second dithiocarbamate group in the ligand *S,S*-chelating to a different manganese atom (Figure 11 bottom). Thus, the overall coordination geometry around the metal can be described as distorted octahedral with the two oxygen atoms being mutually *cis*.

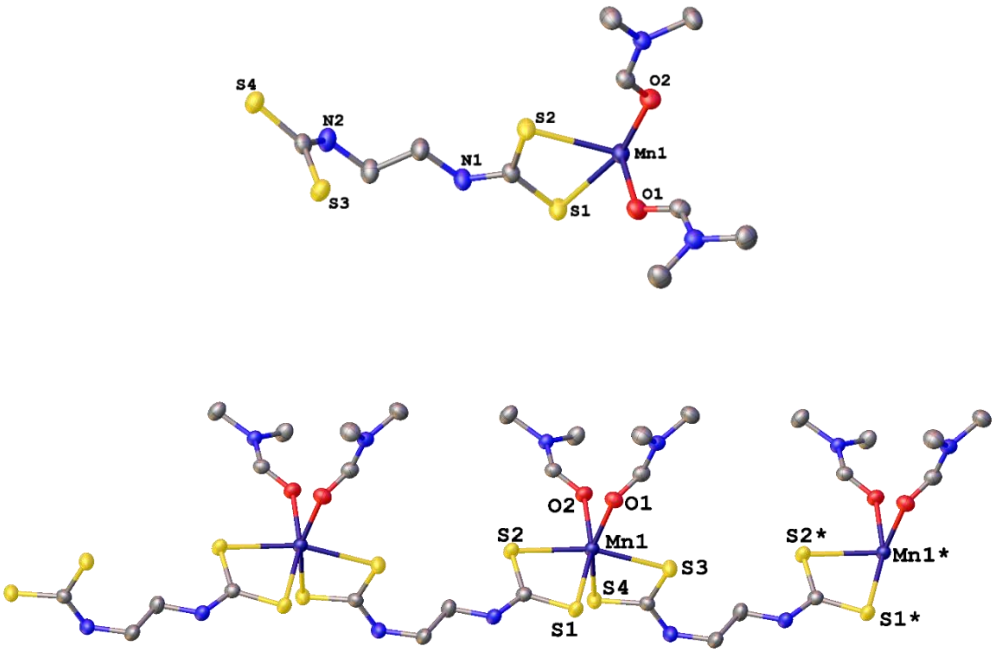

Figure 11: Asymmetric unit of [Maneb·2 DMF] 2 DMF (top). Ellipsoids show 50 % probability levels. Hydrogen atoms as well as the two DMF solvent molecules have been omitted for clarity. The image on the bottom shows the polymer chain. Atoms labelled with an asterisk are generated by symmetry.

In the case of the DMSO complex, the coordination polymer is identical to that described above, except that two DMSO molecules are *O*-bound to the manganese in *cis* positions (Figure 12).

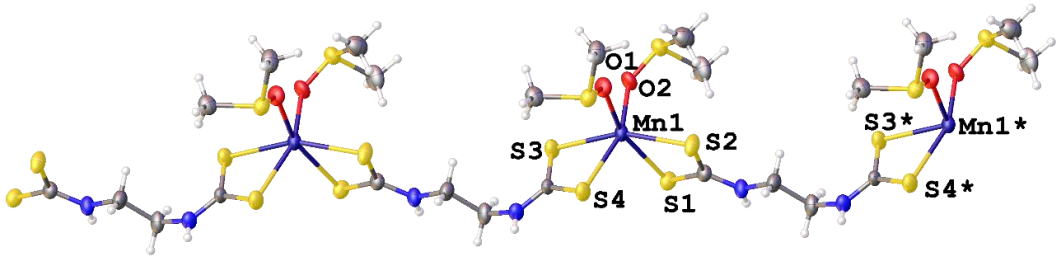

Figure 12: Polymeric structure of [Maneb·2 DMSO] 4 DMSO. Ellipsoids show 50 % probability levels. Hydrogen atoms as well as the DMSO solvent molecules have been omitted for clarity. Atoms labelled with an asterisk are generated by symmetry.

There are four additional, non-coordinating DMSO molecules of solvation in the asymmetric unit, one of which is involved in hydrogen bonding with an NH-proton of the dithiocarbamate. In both complexes the Mn-S bond distances are around 2.59 Å (DMF) and 2.62 Å (DMSO), whilst the respective Mn-O distances are shorter, ranging from 2.16 Å to 2.21 Å. The bite angle of the dithiocarbamate is about 69°, a value typically observed in this class of ligands.[18] The only related structure to those described above is the manganese(II) dithiocarbamate complex $[Mn(S_2CNEt_2)_2]_n$ reported in 1975.[30] In this structure a 1D-polymer is formed by one of the dithiocarbamate sulfur atoms bridging neighboring Mn atoms, forming a $Mn_2(\mu\text{-}S)_2$ trapezoid. This results in short (2.55 Å) and long (2.74 Å) Mn-S bonds for the chelating and bridging-sulfur atoms, respectively.

The structure of our DMSO adduct is of course relevant for all toxicological and biomedical studies involving Maneb, since such *in vivo* or *in vitro* assays are performed using DMSO solutions of the analyte.[8,9,63] Thus, one has to keep in mind, that the species in solution is the *bis*(DMSO) adduct of Maneb. Although the X-ray diffraction data gives us some insight into the structure of Maneb when it is dissolved in a coordinating solvent such as DMF or DMSO, it does not reveal the structure of solvent-free, solid Maneb. We therefore studied both the dihydrate and the anhydrous material using X-ray absorption spectroscopy and EXAFS. Data were collected at 77 K at beamline 10 of the DELTA synchrotron, Dortmund, Germany.[235] Figure S8 shows the XANES spectrum of anhydrous Maneb together with that of several other Mn-containing compounds. From the edge position (inset of Figure S8),

the 2+ oxidation state of Mn in Maneb can be confirmed. EXAFS data of both anhydrous Maneb and the dihydrate was also collected at 77 K (Figure 13).

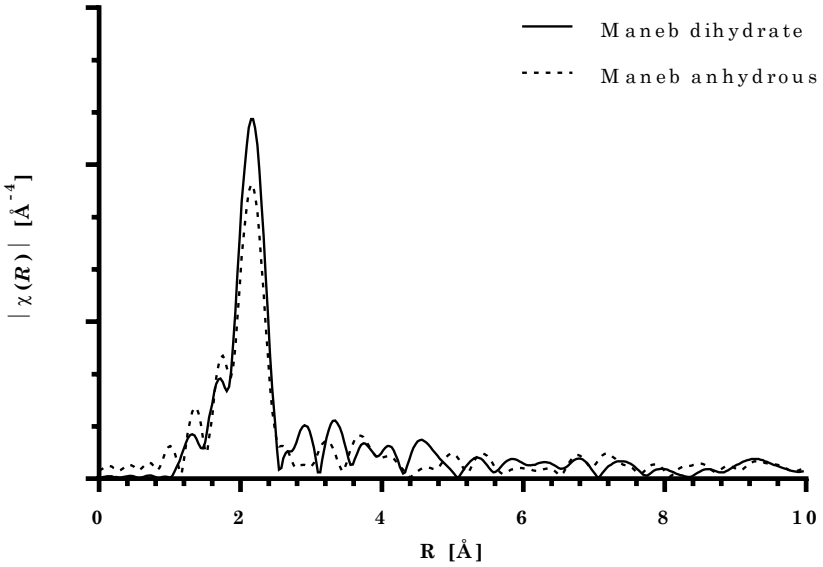

Figure 13: Fourier transform of the k3-weighted EXAFS |(χ(k)*k3)| for Maneb and Maneb dihydrate recorded at 77 K.

This data shows several peaks with radial distances consistent with the presence of Mn-S bonds in the first coordination sphere of the Mn^{2+} ion. Given the similarity of the EXAFS results for the anhydrous Maneb and its dihydrate, the water molecules in the dihydrate appear not to be bound to the manganese atom. The data was thus fitted to a model with two different Mn-S distances in an octahedral arrangement based on the molecular structure of $[Mn(S_2CNEt_2)_2]_n$. The fit results for these bond distances (depicted in Figure S10 in the supporting information) in anhydrous Maneb are $Mn\text{-}S^a$ = 2.59 ± 0.01 Å, $Mn\text{-}S^b$ = 2.74 ± 0.03 Å with an *R*-factor of 1.5 % and $Mn\text{-}S^a$ = 2.570 ± 0.013 Å, $Mn\text{-}S^b$ = 2.696 ± 0.020 Å (*R*-factor 0.7 %) in the dihydrate (see Figure S11). *R*-factors of about one percent can be considered as very good. In general, the distance resolution Δr in an EXAFS measurement is limited by the observed k-space Δk.[236] In our case, this means that a distance resolution of Δr > 0.15 Å between the two Mn-S-shells can be resolved. These Mn-S bond lengths are similar to those observed in the X-ray structures (see above).

Whilst this X-ray absorption data provides important information about the immediate coordination environment of the manganese ion, it does not tell us much about the extended structural arrangement in the structure. Powder diffraction data for both compounds was collected to determine if the solid is microcrystalline. In some cases, structure elucidation

by refinement of powder diffraction data has been successful.[28] However, the observed powder patterns (Figure S12 and S13) were quite broad and unsuitable for further refinement. It did confirm though, that the bulk material was microcrystalline and potentially suitable for an electron diffraction experiment. Indeed, with this technique it was finally possible to completely elucidate the solid-state structure of Maneb and Maneb dihydrate. In both compounds, the asymmetric unit consists of a manganese atom with a chelating dithiocarbamate ligand and, in the case of the dihydrate, two water molecules, which are not bound to the metal (Figure 14 and Figure 15).

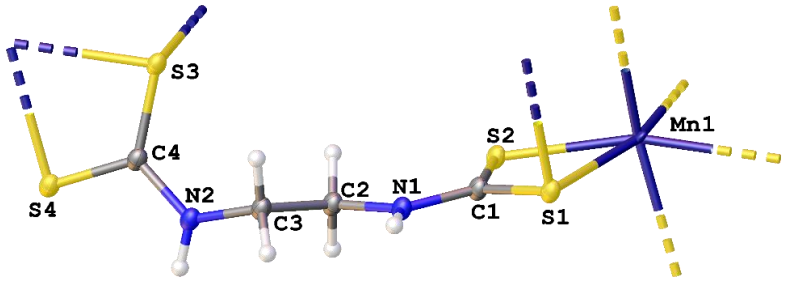

Figure 14: Asymmetric unit of Maneb (anhydrous). Displacement ellipsoids are drawn at the 50% probability level.

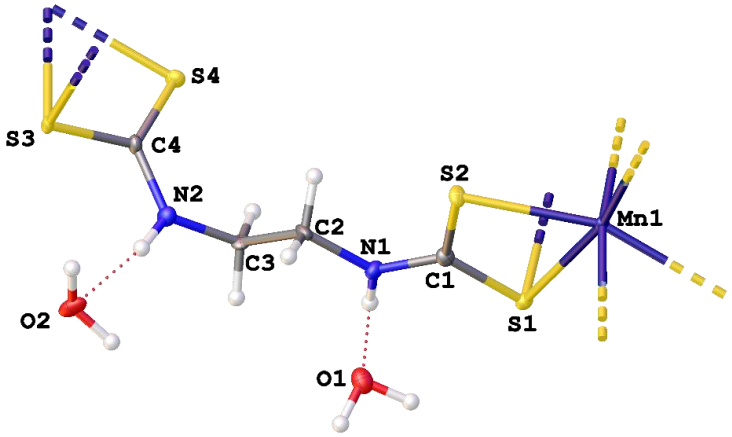

Figure 15: Asymmetric unit of Maneb dihydrate. Displacement ellipsoids are drawn at the 50% probability level.

In anhydrous Maneb there are four short Mn-S distances with an average length of 2.56 Å and two longer ones of 2.68 Å around each distorted octahedral Mn-center. Contrary to our initial assumption and to what is observed in the structure of $[Mn(S_2CNEt_2)_2]_n$, the longer

Mn-S bond distances do not all correspond to the bridging sulfur atoms. Indeed, the long Mn-S bonds are *trans* to each other, with the four shorter bonds in the equatorial positions. The distorted octahedron is evident from the Mn-S angles, which are about 165° for the *trans* S-Mn-S angles. In case of the *cis* S-Mn-S angles, the values are different when the sulfur atom is chelating or bridging, with values of ca. 70° and 100°, respectively. The asymmetric unit of Maneb dihydrate (Figure 15) is similar with average long Mn-S bonds of 2.66 Å and short ones of 2.58 Å. Here too the octahedron is distorted with *trans* S-Mn-S angles ranging from 161° to 170° and *cis* S-Mn-S angles of 97° and 70° for bridging and chelating sulfur atoms. The water molecules are involved in hydrogen bonding with the NH-proton of the dithiocarbamate (dNH···O = 2.92 Å).

In both compounds, these asymmetric units assemble to 2D-coordination polymers, which appear quite similar at first glance. There are however some differences which shall be discussed below. In Maneb there are two different $Mn_2(\mu\text{-}S)_2$ trapezoids formed through intramolecular sulfur bridges with diagonal Mn-Mn distances of 3.97 Å and 3.76 Å. These trapezoids alternate in the polymer in a zig-zag manner, with each trapezoid being rotated by 90° relative to its neighbor (Figure 16).

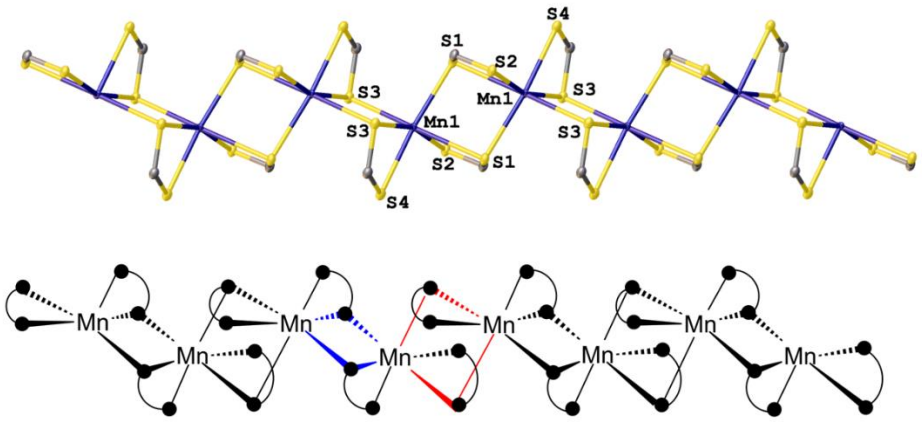

Figure 16: The 2D-coordination polymer of Maneb (top). The image on the bottom depicts the connectivity of Mn and sulfur atoms (solid dots). The two distinct $Mn_2(\mu\text{-}S)_2$ trapezoids are shown in blue and red.

In Maneb dihydrate the 2D-coordination polymer also consists of $Mn_2(\mu\text{-}S)_2$ trapezoids with a Mn-Mn distance of 3.82 Å arranged in a linear layer (Figure 17). In contrast to the structure of the anhydrous compound, there is only one type of $Mn_2(\mu\text{-}S)_2$ trapezoid in the dihydrate. The two ends of the bis(dithiocarbamate) each connect to manganese atoms in

different layers resulting in the polymeric network (Figure 17). In between the manganese-containing layers there is a layer of water molecules formed by a combination of OH···H, NH···O and OH···S hydrogen bonds (Figure S16).

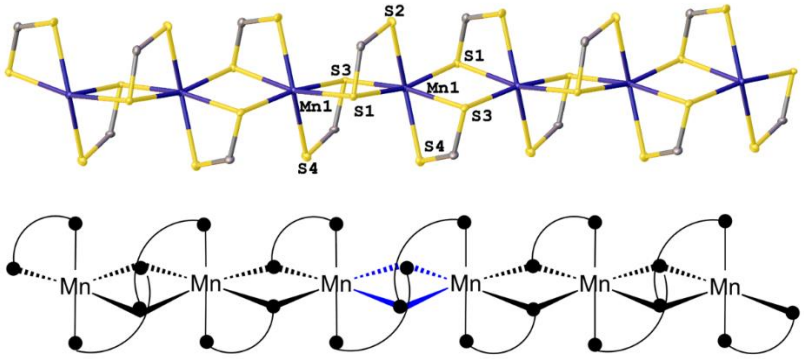

Figure 17: The 2D-coordination polymer of Maneb dihydrate (top). The image on the bottom depicts the connectivity of Mn and sulfur atoms (solid dots). The $Mn_2(\mu\text{-}S)_2$ trapezoid is shown in blue.

A comparison of the EXAFS data and electron diffraction shows that the average Mn-S distances obtained by both methods are comparable: The short Mn-S distances are in both cases with both methods virtually identical within experimental error. EXAFS data seems to slightly overestimate the long Mn-S distances, especially in the case of anhydrous Maneb (2.74 vs. 2.68 Å). It is also worth noting, that powder patterns calculated from the electron diffraction data agree very well with the observed powder patterns of Maneb anhydrous and the dihydrate (Figure S12 and Figure S13). These molecules are further examples for the structural diversity that can be achieved by difunctional dithiocarbamate ligands. A recent review highlights a selection of these with a variety of metals.[237]

3.3 Conclusion

We have developed a reproducible and reliable synthesis method for preparation of high-quality Maneb and have used various techniques to determine its structure. We report the structure of Maneb in solution as DMSO- and DMF-adducts by single crystal diffraction. Especially, the DMSO-adduct is relevant for toxicological testing, since *in vivo* and *in vitro* experiments typically involve Maneb dissolved in DMSO. EXAFS data suggested the presence of distinct Mn-S environments in a polymeric structure. A full understanding of the coordination polymer of Maneb was finally achieved by electron diffraction. Although the overall structures are similar for the anhydrous compound and the dihydrate, there are small differences in the 2D-polymers. Detailed biological studies of the neurotoxic properties of Maneb are currently underway in our groups.

3.4 Experimental Section

All reagents were obtained from commercial suppliers and were used as received. Reactions were carried out under aerobic conditions unless stated otherwise. Following abbreviations for the description of IR band intensities are used: very strong (vs), strong (s), medium (m), weak (w).

Diammonium ethylene bis(dithiocarbamate) (1). A mixture of ethylenediamine (3.3 mL, 50 mmol), methanolic ammonia (14.3 mL, 100 mmol, 2.0 eq.) and carbon disulfide (6.0 mL, 100 mmol, 2.0 eq.) was stirred in ethanol (100 mL) at 0°C for 2 h. The precipitated solid was isolated by filtration, washed with ethanol and dried in vacuum. (8.0 g, 64 % yield.) The material was used directly in subsequent reactions. **^{1}H-NMR** (D_2O, 400 MHz) (δ in ppm) 3.85 (s, 4H, CH_2). **^{13}C-NMR** (D_2O, 100 MHz) (δ in ppm) 213.9 (DTC-C), 48.25 (CH_2).

Manganese ethylene bis(dithiocarbamate) dihydrate - Maneb dihydrate (2). $MnCl_2 \cdot 4\ H_2O$ (2.38 g, 12.0 mmol) was dissolved in water (50 mL) under a nitrogen atmosphere. A solution of diammonium ethylene bis(dithiocarbamate) (2.97 g, 12.0 mmol, 1.0 eq.) in water (30 mL) was added dropwise with vigorously stirring during 45 minutes. A yellow solid precipitated, which was isolated by filtration, washed with a large amount of water and dried at room temperature without vacuo (2.47 g, 68% yield.). **Elemental analysis** calculated for $C_4H_{10}MnN_2O_2S_4$ (330.31 g/mol) Mn, 18.2; C, 15.94; N, 9.40; H, 3.34. Found: Mn, 18.1; C, 15.81; N, 9.22; H, 3.39. **Magnetic moment** calculated for high spin Mn(II) 5.92 B.M. Found: 5.19 B.M. **Infrared spectroscopy** (ATR): 3507 (m) ν(O-H), 3192 (m) ν(N-H), 3008 (w) ν(C-H), 1606 (m), 1524 (s) ν(C-N), 951 (vs) ν(C-S) cm^{-1}.

Manganese ethylene bis(dithiocarbamate) - Maneb anhydrous (3). The anhydrous solid was obtained by drying the dihydrate (**2**) under vacuum at room temperature overnight. **Elemental analysis** calculated for $C_4H_6MnN_2S_4$ (265.31 g/mol) Mn, 20.7; C, 18.11; N, 10.56; H, 2.28. Found: Mn, 20.3; C, 17.84; N, 10.46; H, 3.34. **Magnetic moment** calculated for high-spin Mn(II) 5.92 B.M. Found: 5.88 B.M. **Infrared spectroscopy** (ATR): 3294 (m) ν(N-H), 3149 (m) ν(N-H), 2974 (w) ν(C-H), 1524 (m) ν(C-N), 1505 (s) ν(C-N), 963 (vs) ν(C-S), 945 (vs) ν(C-S) cm^{-1}.

Deposition Number 2177534 (Maneb-DMF), 2177535 (Maneb-DMSO), 2255649 (Maneb anhydrous), 2255650 (Maneb dihydrate) contain the supplementary crystallographic data for this paper. These data are provided free of charge by the joint Cambridge

Crystallographic Data Centre and Fachinformationszentrum Karlsruhe Access Structures service.

3.5 Supporting Information

Details of all analytical methods used as well as copies of spectra (NMR and IR), TGA/DSC traces, additional figures and data relating to EXAFS, X-ray diffraction and ED experiments are provided in the supporting information. The authors have cited additional references within the supporting information.[238–250]

3.6 Acknowledgements

We thank Dr. Björn Beele for carrying out the TGA/DSC measurements. Open Access funding enabled and organized by Projekt DEAL

3.7 Conflicts of Interest

The authors declare no conflict of interests.

3.8 Keywords

Dithiocarbamate • Electron Diffraction • Maneb • Manganese • X-ray Diffraction

Chapter 4 – Synthesis of other trace element-based dithiocarbamate fungicides

Chapter 4 – Synthesis of other trace element-based dithiocarbamate fungicides

4.1 Introduction

Not only was the molecular structure of Maneb unknown until recently, but also the exact molecular structure of the Mn- and Zn-containing EBDC salt Mancozeb is completely unknown. To date, neither the exact Zn content nor the atom connectivity has been determined. In 1965 the U.S. Patent No. 3.210.394[5] documented that so called "co-reacted manganese-metal ethylene (bisdithiocarbamate)" products reveal different X-ray diffraction peaks compared to Maneb or Zineb. For example, a "co-reacted" product results when Nabam reacts with a 90:10 molar ratio of Mn (II)- and Zn (II) salt solutions. These products were compared to a mixture of 90% Maneb and 10% Zineb. At first, it was thought that Mancozeb is simply a mixture of Maneb and Zineb. However, experiments based on X-ray powder analysis showed that the powder diffraction pattern of a mixture of Maneb and Zineb is different from that of the "co-reacted" products. It was therefore concluded that Mancozeb is not merely a mixture but a distinct chemical entity.[5] In 1968, another synthesis route for Mancozeb was documented in U.S. Patent No. 3.379.610.[33] The process involved isolating Maneb and subsequently dispersing it in water and treatment with different equivalents of Zn-(II) solutions. The resulting powder pattern of this Mancozeb was again different compared to that of Maneb/Zineb mixtures. The metal content of Mancozeb varies widely as shown in Table 1. According to a specification of the Food and Agriculture Organization of the United Nations (FAO) the typical Mn and Zn content of Mancozeb is given as 20 % Mn and 2.5% Zn, respectively.[251]

Table 1: Mn and Zn content of different Mancozeb specifications.

	Mn content	**Zn content**	**Year**
Nabam + different Mn/Zn ratios "Co-reacted Mn-Zn EBDC"	8.1 – 18.5 %	2.4 – 14.5 %	1965[5]
Maneb + Zn "Zinc complexed Maneb"	19.2 – 20.7 %	0.1 – 6.6 %	1968[33]
FAO specification for Mancozeb	20 %	2.5 %	1980[251]

4.2 Materials and Methods

4.2.1 General

Instruments. NMR spectra were recorded on a Bruker Avance 400 spectrometer referenced externally to Me_4Si. C, H and N analyses were performed by staff of the in-house elemental analysis facility using an Elementar Vario EL system. TGA/DSC measurements were conducted using a Netzsch STA 449 F5 Jupiter instrument. Experiments were carried out in alumina crucibles, which were closed with alumina lids. Samples were heated from 25°C to 1000 °C with a heating rate of 5 K min^{-1} in a nitrogen atmosphere applying a constant nitrogen flow of 25 ml min^{-1}. IR spectra were recorded on a Thermo Scientific Nicolet iS5 spectrometer equipped with an iD7 diamond ATR unit. Following abbreviations for signal intensity were used: w – weak, m – medium, s – strong, vs – very strong. The magnetic susceptibility was determined using a Sherwood Scientific magnetic susceptibility balance. Calibration against mercury tetrathiocyanato cobaltate (II).

X-ray crystallography. X-ray quality crystals of Ziram and Ferbam were formed by slow evaporation of a mixture of dichloromethane (DCM)/hexane at -20°C within a few days. Crystals of Nabam were formed by slow evaporation of a Nabam solution in D_2O. Diffraction data were collected at 150 K or 100 K using a Rigaku Oxford Diffraction Gemini E Ultra diffractometer, equipped with an EOS CCD area detector and a four-circle kappa goniometer. Diffraction data of Ziram and Ferbam were collected at room temperature on a Rigaku XtaLab Mini diffractometer using Mo-radiation. Data integration, scaling and empirical absorption correction were performed using the CrysAlis Pro program package.[238] All crystal structures were determined using SHELXT and refined using SHELXL.[239,240] The Olex2 graphical user interface was used for all structure manipulations and to generate the graphics.[241]

Inductively coupled plasma-optical emission spectrometry (ICP-OES). Metal content was determined using inductively coupled plasma-optical emission spectrometry (ICP-OES) (Avio 220 Max, Perkin Elmer). The samples were dissolved in a mixture (ratio 1:2) of 0.1 M EDTA and an ammonium/ammonia buffer. The solution was dried at 95 °C and then acid-assisted digested (HNO_3/H_2O_2, 1:1, suprapure® 65% nitric acid, 30% hydrogen peroxide, Merck) overnight at 95 °C. Ashed samples were re-suspended in 1 mL of 2% HNO_3 with Yttrium (100 µg/L, single element ICP standard, Roth) as an internal standard and diluted 1:1000 for ICP-OES measurements. The instrument settings were chosen as follows: plasma power 1500 W, plasma gas flow: 10 L/min, auxiliary gas flow 0.2

L/min, nebulizer gas flow: 0.70 L/min, pump flow rate: 1 mL/min, Wavelength: Mn 257.610 Zn 206.200 nm, Y 371.029 nm. An external calibration was prepared using a multi-element mix (Inorganic Ventures) for evaluation. Recovery of 86% for complexed Mn was determined using the full characterized Maneb as a standard. Recovery of for complexed Zn was not determined since Zineb is not fully soluble in EDTA/buffer solution. In general, metal amounts were validated by measuring acid-assisted certified reference material (BCR-274, single cell protein, Institute for Reference Materials and Measurement of the European Commission, Geek, Belgium) and reference water (SRM-1640a, trace elements in natural water, National Institute of Standards and Technology, Gaithersburg, MD, USA).

4.2.2 Synthesis

Manganese/Zinc ethylenebis(dithiocarbamate) (Mancozeb)

Mancozeb was prepared using two different methods according to U.S. Patent No. 3.210.394 and No. 3.379.610. The co-reacted products were *in situ* synthesized according to "route A" using the ammonium EBDC salt Amobam[252] and different Mn/Zn ratios.[5] In "route B", Maneb was isolated first and then reacted with 0.1, 1.0 or 10 eq. of $ZnSO_4 \cdot 7\ H_2O$ in water.[33] Route A: 1.0 eq. ethylene diamine, 2.0 eq. ammonia and 2.0 eq. CS_2 were added in water and stirred for 3 h at 30 °C. Under a nitrogen atmosphere and with vigorous stirring, the DTC solution was added dropwise to a solution containing "X" eq. $MnCl_2 \cdot 4\ H_2O$ and "X-1" eq. $ZnSO_4 \cdot 7\ H_2O$ in water. The specific values for X, the molar ratios of $MnCl_2$ and $ZnSO_4$, are provided in Table 2. Route B: Maneb was prepared as previously published[252] and dispersed in water. Then, with stirring, a solution of 0.1, 1.0 or 10 eq. $ZnSO_4 \cdot 7\ H_2O$ in water was added dropwise and stirred for 1 h (Table 2).

Table 2: Synthesis parameters for Mancozeb preparation using two different methods.

Route A		Route B
Eq. $MnCl_2$	**Eq. $ZnSO_4$**	**Maneb + $ZnSO_4$**
0.99	0.01	
0.95	0.05	
0.90	0.10	
0.80	0.20	
0.50	0.50	
0.10	0.90	
		0.1 Eq.
		1.0 Eq.
		10 Eq.

Zinc(II) ethylene bis(dithiocarbamate) (Zineb)

4.61 g (9.74 mmol, 1.0 eq.) $ZnSO_4 \cdot 7\ H_2O$ was dissolved in 50 mL water under nitrogen atmosphere. Subsequently, a solution of 2.40 g (9.74 mmol, 1.0 eq.) ammonium ethylenebis (dithiocarbamate) in 50 mL water was added dropwise within 30 min under continuous stirring. The precipitated colorless solid was filtered off and washed with 100 mL cold distilled water and dried in vacuo. 1.95 g (7.08 mmol) product was obtained in a yield of 73%. ^{1}H-NMR (600 MHz, DMSO-d6): δ in ppm = 3.51 (s, 4H), 9.87 (s, NH). ^{13}C-NMR (150 MHz, DMSO-d6) (δ in ppm) 206.11 (DTC-C), 46.77 (CH_2). Elemental analysis calculated for $C_4H_6N_2S_4Zn$ (265.31 g/mol) C, 17.42; N, 10.16; H, 2.19. Found: C, 17.32; N, 10.25; H, 2.29. Infrared spectroscopy (ATR): 3230 (m), 3032 (w), 1532 (vs), 1446 (w), 1378 (s), 1292 (m), 1245 (m), 1047 (s), 975 (vs), 777 (m), 716 (m), 652 (m), 614 (m), 539 (m), 476 (m).

Zinc(II) bis(dimethyl dithiocarbamate) (Ziram)

A solution of 0.806 g (5.00 mmol, 2.00 eq.) sodium dimethyl dithiocarbamate dihydrate in 100 mL water was added to a solution of 0.719 g (2.5 mmol, 1.00 eq.) $ZnSO_4 \cdot 7\ H_2O$ in 100 mL water. During the addition a colorless solid precipitated. The mixture was stirred for 30 min and the resulting colorless solid was filtered off, washed with water and dried in vacuo. The product was obtained in a yield of 69%. (0.532 g, 1.73 mmol). Subsequently, the product was recrystallized from a dichloromethane/hexane mixture. ^{1}H-NMR (600 MHz, DMSO-d6): δ in ppm = 3.38 (s, 4H). ^{13}C-NMR (150 MHz, DMSO-d6) (δ in ppm) 203.75 (DTC-C), 44.58 (CH_2). Elemental analysis calculated for $C_6H_{12}N_2S_4Zn$ (305.81 g/mol) C, 23.56; N, 9.16; H, 3.96. Found: C, 23.47; N, 9.25; H, 3.85. Infrared spectroscopy (ATR): 2924 (w), 1508 (s), 1435 (m), 1380 (s), 1239 (s), 1130 (s), 966 (vs), 562 (s), 442 (vs).

Iron(III) tris(dimethyl dithiocarbamate) (Ferbam)

2.42 g (15.0 mmol, 3.00 eq.) sodium dimethyl dithiocarbamate dihydrate in 100 mL water was added to a solution of 1.94 g (5.0 mmol, 1.00 eq.) $Fe(NO_3)_3 \cdot 9\ H_2O$ in 100 mL water. The mixture was stirred for 30 min and the resulting black solid was filtered off, washed with water and dried in vacuo. The product was obtained in a yield of 75%. (1.57 g, 3.75 mmol). The product was recrystallized from a dichloromethane/hexane mixture. Elemental analysis calculated for $C_9H_{18}FeN_3S_6$ (416.49 g/mol) C, 25.95; N, 10.09; H, 4.36. Found: C, 25.80; N, 10.11; H, 4.29. Infrared spectroscopy (ATR): 3039 (w), 2922 (w), 2656 (w), 1516 (vs), 1385 (vs), 1267 (m), 1246 (s), 1134 (vs), 1048 (s), 970 (vs), 892 (m), 726 (vs), 697 (s). 574 (m), 440 (s).

4.3 Results and Discussion

4.3.1 Synthesis of Zn- and Fe-containing bis(dimethyl dithiocarbamates)

Ziram and Ferbam were synthesized by reacting sodium dimethyl dithiocarbamate salt with 0.33 or 0.5 eq. of a Zn(II)- or Fe(III)-salt solution in water (Figure 18). The products were purified by crystallization in a mixture of dichloromethane (DCM) and hexane overnight. The single crystals were studied at room temperature by X-ray diffraction (XRD) to confirm their molecular structure (Figure 18).

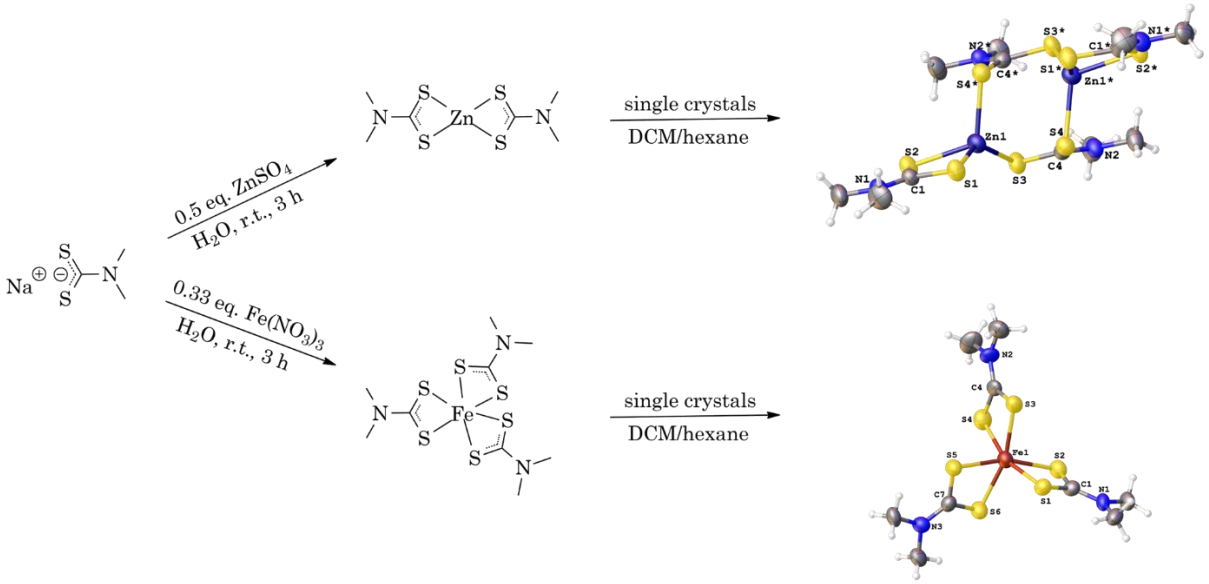

Figure 18: Synthesis of Ziram and Ferbam and molecular structures of both measured via XRD. A co-crystallized dichloromethane solvent molecule was omitted for clarity in the structure of Ferbam.

Ferbam co-crystallized with one DCM molecule, which was subsequently removed by drying in vacuo afterwards. The chelate ligand angles of type S-Fe-S are typical small, around 74°, and contribute to the distorted octahedral arrangement in the iron coordination environment. The S-Fe bond lengths range from 2.36 to 2.39 Å. Crystallographic data of Ferbam without any solvent molecule was published by Albertsson and Oskarsson in 1977.[93]

Ziram crystallizes as a dimer with a distorted tetrahedral coordination geometry. The asymmetric unit consists of two dimethyl dithiocarbamate ligands, with one of them acting as a chelate ligand and the other as a linker to the second tetrahedral Zn atom. This coordination mode of dithiocarbamate is described by Hogarth *et al.,* (2005), but occurs very rarely[18]. Due to the bridging sulfur interactions, a Zn_2S_6-octagon with four different atoms and two identical asymmetric units emerges (Figure 19). The bond angles of the distorted

tetrahedral coordination geometry differ from an ideal tetrahedral angle of 109.5°. In Ziram, the Zn center consists of bond angles between 76.26° (S1-Zn1-S2, chelate ligand) and 136.94° (S1-Zn-S3), but most of them are between 105 to 113°. These findings are in agreement with the published crystal structure of Ziram by Klug in 1966.[92]

The structure of Zineb was determined in 2020 by Lefton *et al.* using a commercially available pesticide standard and powder XRD, since no single crystals of Zineb have been obtained to date.[28] Surprisingly, the coordination environment of Zn in Ziram and Zineb differs, despite both compounds consisting of two dithiocarbamate ligands. In Zineb, Zn is coordinated by five sulfur atoms, four from the chelate DTC ligands and one from an intramolecular sulfur bridge between the polymeric chains.[28] Bonamico *et al.* (1965) observed a penta-coordinated Zn central atom in the dimeric Ziram analog zinc bis(diethyl dithiocarbamate). In this case, one sulfur of the second DTC ligand functions as a chelate ligand as well as a dimeric linker.[253] In Ziram, Zn is coordinated by only four sulfur atoms, resulting in a distorted tetrahedral structure. Latter is the most often observed coordination mode of Zn in metalloenzymes.[116] Pearson (1963) classified Zn as a "borderline" metal, because it is neither considered as a "hard" or "soft" metal according to the HSAB principle.[20] Zn also has no preference in being coordinated by oxygen, nitrogen or sulfur atoms, but in most zinc-binding sites of enzymes, Zn is coordinated by histidine and cysteine.[254] However, it remains unknown what structure Mancozeb exhibits since Mn in Maneb is a hexacoordinated central atom and Zn was observed to be tetra- and penta-coordinated in DTC complexes.

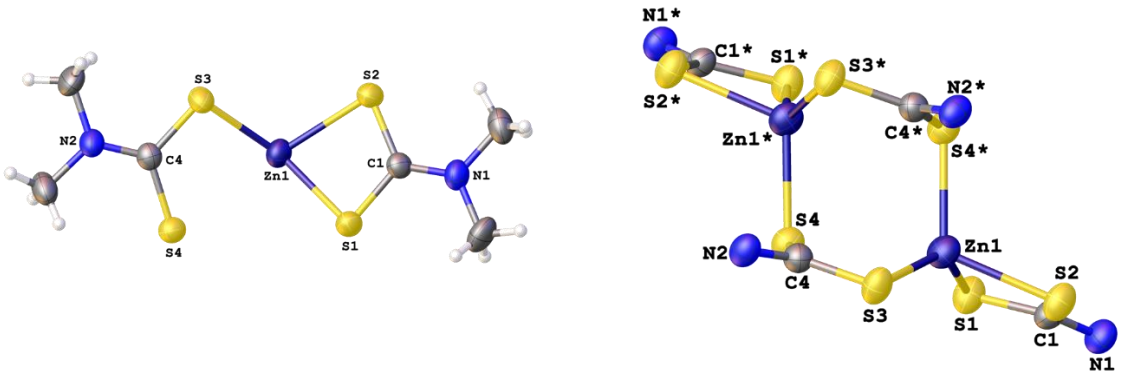

Figure 19: Asymmetric unit of Ziram (left) and the dimeric form shown without the methyl groups (right). One DTC ligand is chelating (via sulfur atoms S1 and S2) and the DTC is linking (via sulfur atom S4) to the other asymmetric monomeric unit.

4.3.2 Synthesis of Mn- and Zn-containing ethylene bis(dithiocarbamates)

Unlike Mn (II), Zn (II) is diamagnetic and consequently amenable for NMR spectroscopy. Therefore, Zineb was prepared as a structural analog to shed more light on the structure and mechanism of action of the Mn-containing ethylene bis(dithiocarbamates). The synthesis of Zineb was similar to the previously published method for Maneb. Zineb was characterized using elemental analysis, thermal gravimetric analysis (TGA) and NMR spectroscopy. Unlike Maneb, Zineb was confirmed to only exist in the anhydrous form. The chemical structure of Zineb was determined in 2020 by Lefton *et al.* using powder X-ray diffraction.[28]

Mancozeb was prepared following the both synthesis routes previously described[5,33] (Figure 20).

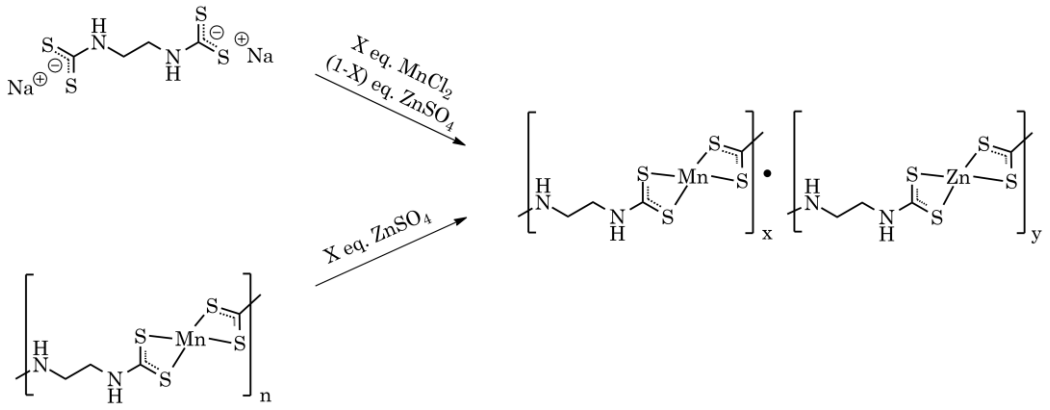

Figure 20: Overview of the two possible synthesis routes.

The metal content of Maneb was confirmed by EDTA titration based on a published method.[232] However, this method only allows for the estimation of the total content of divalent metal ions and cannot distinguish between the two different metals. Initially, an attempt was made to apply the acid-digestion method established for worm homogenates to the solid fungicide compounds. However, a few milligrams of the DTCs reacted violently with the HNO_3/H_2O_2 mixture resulting in an insoluble colorless precipitate (probably ZnO) attached to the plastic tube. Therefore, a new method was developed, combining the solubility of the material in EDTA/buffer mixtures with an acid-assisted digestion. The recovery rate was determined using fully characterized Maneb.[252] Figure 21 illustrates that, different Mn and Zn ratios during EBDC synthesis according to route A results in different products. As the amount of Zn in the ratio increases, the amount of zinc in the product also increased. However, this only applies up to a certain point. For example, at the 50/50 ratio condition, the Mn and Zn content would be expected to be approximately on

the same level, around 10% with respect to the complex. However, experimental results indicate around 3% Mn and 13 % Zn, implying a preferential complexation of Zn, when both metals are equally available. Considering that the total metal sum is equimolar to available EBDC ligand, preference should theoretically not occur. This observation suggests that Zn might somehow induce structural changes, potentially leading to a reduced overall metal binding capacity.

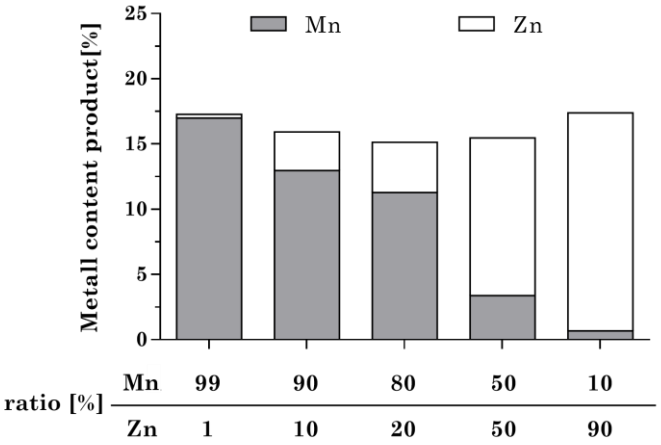

Figure 21: Mn and Zn content in Mn/Zn EBDC complexes using route A and measured via ICP-OES.

When Mancozeb is prepared by reaction of Maneb with Zn solutions of different concentrations (from 0.1 to 10 equivalents), it appears that the same product with about 0.4% Zn is formed regardless of the amount of Zn offered (Route B, Figure 22). Conversely, forcing Zineb to react with a $MnCl_2$ solution using the identical approach did not yield any observable reaction, and subsequent ICP-OES measurements confirmed the absence of Mn.

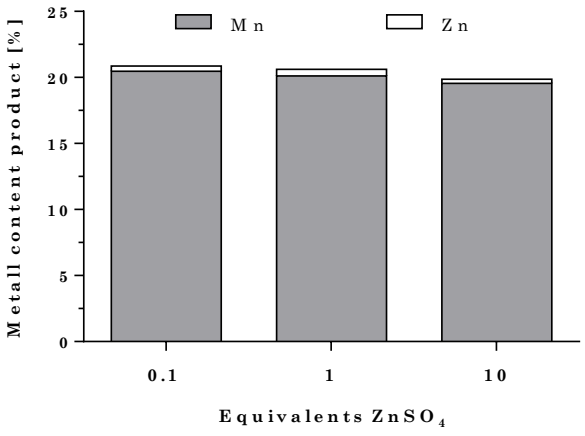

Figure 22: Mn and Zn content in Mn/Zn EBDC complexes using route B and measured via ICP-OES.

4.3.3 Stability of the EBDC complexes

Zineb

For biological experiments, it is important to test the stability of the applied compounds beforehand to ensure that the correct species is being tested. However, this task proved to be very difficult for Maneb, since there are no routine methods to study its fate in solution. IR spectra of Maneb in DMSO solution are dominated by solvent signals. Assuming that Maneb and Zineb have some structural similarity, Zineb was dissolved in deuterated DMSO solution and immediately monitored via NMR spectroscopy over a period of 96 h (Figure 23).

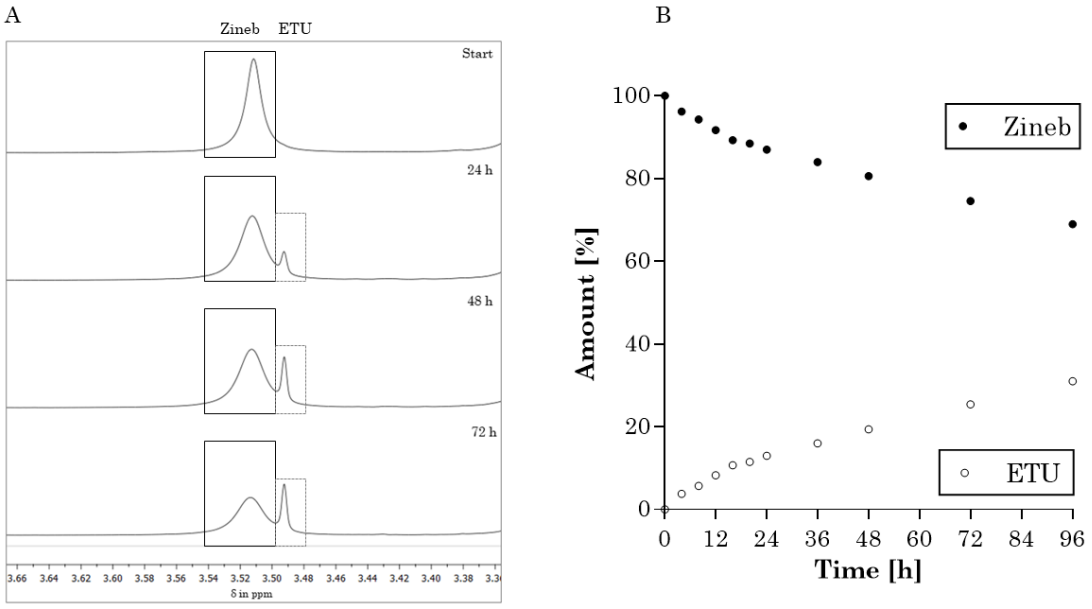

Figure 23: Monitoring a Zineb solution in DMSO using ^{1}H-NMR spectroscopy over time. Stacked NMR spectra show the region containing the resonances of the ethylene groups. **B**: ETU formation over time, displayed as percentage of Zineb and ETU content based on integration of the ^{1}H-NMR signals, starting with 100% Zineb.

Already after 4 h it was observed that Zineb in DMSO solution starts to decompose into ethylene thiourea (ETU). This decomposition product was confirmed by comparing its proton NMR spectrum with that of a commercial sample. Since Maneb seems to be more stable but on the other hand to ensure that the applied species is the DMSO coordination adduct of Maneb, it was concluded that experiments involving model organism *C. elegans* cannot be conducted on agar plates for the usual time intervals, typically ranging from 6 to 48 h. As a result, an exposure interval of 2 h in solution during the L1 larval stage was

chosen to ensure the stability of the testes species and to allow the study of possible developmental effects.

It is important to note that Zineb not only starts to decompose in DMSO solution, as monitored via NMR spectroscopy, but also precipitates a yellow solid within a few days. This is not the case for Maneb, which forms a yellow to brownish solution in DMSO and does not precipitate (except for crystals when saturation is reached). Zineb is highly soluble in DMSO, whereas Maneb only dissolves slowly within about 15 minutes. Consequently, the stability results derived from Zineb may indeed not be applicable to Maneb.

Nabam

The synthesis of Maneb was conducted following the procedure described in the Appendix of Chapter 6, based on a method by Klöpping *et al.* (1951).[255] The purity was verified using NMR spectroscopy and elemental analysis. The presence of a hexahydrate was confirmed through TGA and X-ray Diffraction, which is consistent with literature findings (Figure 24).[27]

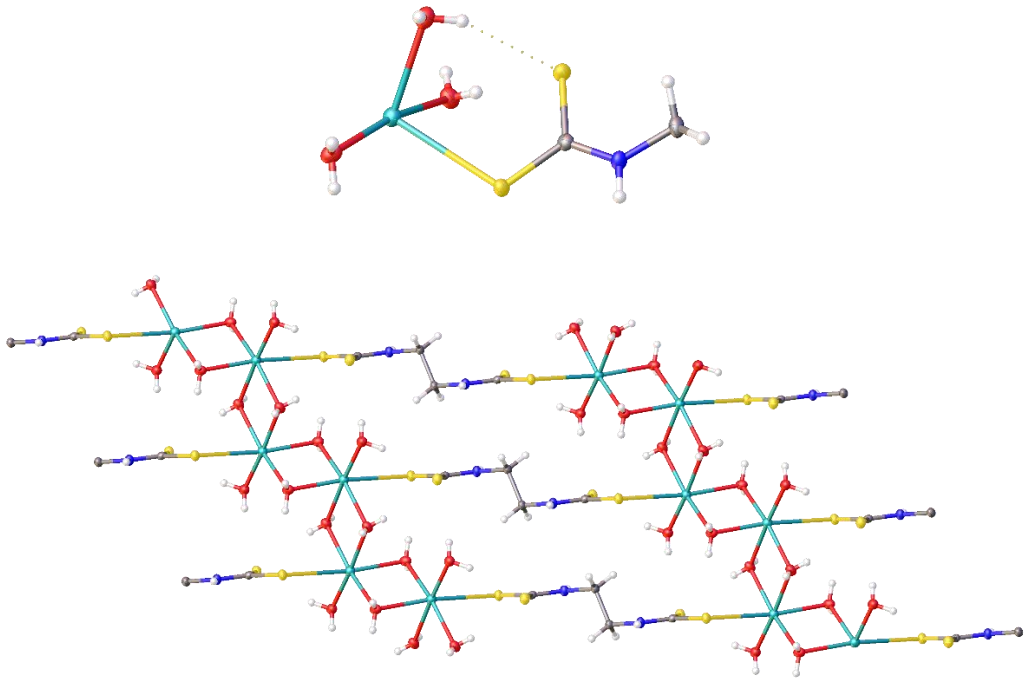

Figure 24: Molecular structure of Nabam hexahydrate. Shown are the asymmetric unit (top)and the 2-dimensional coordination polymer (bottom).

Interestingly, owing to the monovalent sodium cation, Nabam is the only shown complex in which the DTC does not form a chelate complex and binds via a single sulfur atom. Nevertheless, the molecular structure of Nabam in solid state is also a two-dimensional

polymer, as the perfectly symmetrical asymmetric unit (Figure 24 top) assembles into a polymer via sodium-water interactions. In manganese- or zinc-containing chelate complexes, only distorted octahedral structures are found, as the angle of the binding DTC ligand is around 75°. In contrast, Nabam forms a nearly perfect octahedral coordination environment.

Nabam was selected to serve as a structural analogue of Maneb in toxicity studies with *C. elegans*. Due to its water solubility, incubation can be conducted in 85 mM NaCl, analogous to the metal salts. Consequently, NMR spectra were recorded in deuterated water. To investigate Nabam's stability in solution, a spectrum was acquired from the same sample solution after one week. In contrast to Zineb, no ETU formation is observable even after a week (Data not shown). Apart from minor signals, the spectrum remains nearly identical, indicating high stability of Nabam. However, it should be noted that the behavior of Nabam, and indeed Maneb as well, in the presence of a model organism or within a biological system may differs significantly. Thus, reliable conclusions regarding stability during the experimental setup cannot be drawn.

4.4 Conclusions and further perspectives

The synthesis of Mancozeb by adding different metal ratios to an EBDC solution results in compounds with varying amount of the corresponding metals. However, using a 50/50 ratio does not yield a material with equitably composition, suggesting an influence of Zn on the binding capacity of mixed EBDC complexes. When the synthesis involves Maneb reacting with Zn(II)-ions, results indicate the formation of a single product no matter how many equivalents Zn are used.

Overall, the identity and composition of Mancozeb employed in agricultural applications remains unknown, particularly due to the coexistence of two manufacturing protocols. Given that elemental analysis typically includes carbon, nitrogen, and hydrogen content, the differences in these elements in Mancozeb, Maneb and Zineb are minor. Consequently, elemental analysis is unsuitable for distinguishing between Maneb, Zineb, and Mancozeb. Despite that, elemental analysis serves as sole analytical tool in the quality control of commercial pesticide standards!

Abstract:

Neurotransmitters like dopamine (DA), serotonin (SRT), γ-aminobutyric acid (GABA) and acetylcholine (ACh) are messenger molecules that play a pivotal role in transmitting excitation between neurons across chemical synapses, thus enabling complex processes in the central nervous system (CNS). Balance in neurotransmitter homeostasis is essential, and altered neurotransmitter levels are associated with various neurological disorders, e.g., loss of dopaminergic neurons (Parkinson's disease) or altered ACh synthesis (Alzheimer's disease). Therefore, it is crucial to possess adequate tools to assess precise neurotransmitter levels, and to apply targeted therapies. An established *in vivo* model to study neurotoxicity is the model organism *Caenorhabditis elegans* (*C. elegans*), as its neurons have been well characterized and functionally are analogous to mammals. We have developed a liquid chromatography–tandem mass spectrometry (LC-MS/MS) method including a sample preparation assuring neurotransmitter stability, which allows a simultaneous neurotransmitter quantification of DA, SRT, GABA and ACh in *C. elegans*, but can easily be applied to other matrices. LC-MS/MS combined with isotope-labeled standards is the tool of choice, due to its otherwise unattainable sensitivity and specificity. Using *C. elegans* together with our analytically validated and verified method provides a powerful tool to evaluate mechanisms of neurotoxicity, and furthermore to identify possible therapeutic approaches.

Chapter 5 – A Reliable Method Based on Liquid Chromatography-Tandem Mass Spectrometry for the Simultaneous Quantification of Neurotransmitters in *Caenorhabditis elegans*

Based on:

Ann-Kathrin Weishaupt, **Laura Kubens**, Lysann Rücker, Tanja Schwerdtle, Michael Aschner and Julia Bornhorst

Molecules, **2023**, *28*, 5373

DOI: 10.3390/molecules28145373

Chapter 5 – A Reliable Method Based on Liquid Chromatography-Tandem Mass Spectrometry for the Simultaneous Quantification of Neurotransmitters in *Caenorhabditis elegans*

5.1 Introduction

Neurotransmitters are messenger molecules transmitting excitation between neurons across chemical synapses, which enable the brain to sense perceptions and coordinate complex behavior.[256] Here, the most important neurotransmitters, dopamine (DA), serotonin (SRT), γ-aminobutyric acid (GABA) and acetylcholine (ACh) will be discussed, as their dysregulation, among others, is associated with several neurological diseases. DA regulates body movement control, as well as memory function and cognition.[257,258] The most common DA-associated neurodegenerative disorder is Parkinson's disease (PD), which is associated with the progressive loss of dopaminergic neurons in the substantia nigra[259] and is characterized, among other things, by the presence of alpha-synuclein inclusions (Lewy Bodies).[260] SRT acts as a neurohormone controlling the function of several peripheral organs and modulates mood, cognition, sleep, learning and anxiety.[261,262] Hypofunction of serotonergic neurons is associated with depression, and disturbances in SRT levels lead to anxiety disorders.[262] GABA, among other functions, regulates blood pressure and heart rate. In addition, it binds to receptors at inhibitory synapses, thus decreasing neuronal excitability.[263] The balance between excitation and inhibition is a requisite for proper neural function; as a consequence, a disequilibrium contributes to neurodegeneration.[264] The cholinergic system, including in particular the neurotransmitter ACh, is known to be required for a variety of critical physiological activities, such as attention, learning and memory.[265] A decreased activity of choline acetyltransferase (ChAT) and the subsequent altered ACh synthesis are correlated with an increased formation of ß-amyloid (Aß) plaques in the brains of patients with Alzheimer's disease (AD).[266] Furthermore, a deficiency of ChAT, choline uptake and ACh secretion are concomitant symptoms of neuronal loss associated with learning deficits and memory loss.[267] Therefore, the analysis of basal levels of neurotransmitters is an essential tool for neurotoxicity assessment, especially in terms of neurodegenerative diseases such as PD and AD. In addition, neurotransmitter ratios are of great interest, as they interact and depend on each other, and in most neurodegenerative diseases the entire neurotransmitter

system is disturbed.[268,269] In brief, it is crucial to have the ability to determine which neurotransmitter(s) are impaired, in order to apply targeted therapies.

Neurotransmitter quantification in mouse tissue, such as the brain[270] or cerebrospinal fluid,[271] can be employed to assess the neurodegenerative potential of chemical or physical agents that may be harmful, as well as to identify therapeutic strategies. However, animal experiments provoke great ethical debate, requiring novel model organisms to substitute and complement animal experiments for testing neurodegenerative potentials. For this purpose, zebrafish (*Danio rerio*), flies (*Drosophila melanogaster*) and worms are commonly used.[272,273] The nematode *Caenorhabditis elegans* (*C. elegans*) constitutes a distinguished *in vivo* model featuring a well-elucidated nervous system. All neurons are well characterized and mapped over the worm body, and they are structurally and functionally similar to mammals.[274] Furthermore, in *C. elegans,* orthologs are present for 60–80% of human genes related to various diseases, including neurodegenerative disorders.[275] Therefore, *C. elegans* is a well-established model organism in the field of neurotoxicity and neurodegeneration. In addition, worms are easily genetically manipulated, providing a variety of mutants, especially for PD[276,277] and AD.[278,279]

Neurotoxicity in *C. elegans* is predominantly assessed by behavioral assays. Commonly performed assays include that of the basal slowing response, which examines dopamine-dependent behavior in the presence of food,[211] the determination of serotonin-dependent pharyngeal pumping,[280] the synaptic transmission at neuromuscular junctions using the aldicarb-induced paralysis assay,[281] and the assessment of functional changes in locomotion.[211] Additionally, genetically modified worms with fluorescence tags in neurons have been used to study neurodegeneration via fluorescence microscopy.[282,283] However, these techniques have the limitation, among others, of not being able to quantify absolute neurotransmitter levels. Furthermore, the majority of assays, such as that of basal slowing, are focused on a solitary neurotransmitter, in this case, DA. Other assays, namely those of locomotion, are mediated by several neurotransmitters, such as acetylcholine and dopamine; these provide broader outcomes, but can be problematic in interpretation. So far, only Schumacher *et al.* have assessed DA and SRT,[283] but, to date, GABA and ACh have not been quantified in *C. elegans*. Therefore, a method is required for the simultaneous quantification of multiple neurotransmitters in *C. elegans*.

The demands of such a technique are challenging, as the analysis must be specific for the individual neurotransmitters and, on the other hand, requires good sensitivity, as the basal

levels of neurotransmitters are low. In addition, neurotransmitters display poor stability. Methods do already exist to quantify neurotransmitters in a variety of matrices by electrochemical detection,[284,285] fluorescence detection[286,287] or fluorescent dyes.[288–290] However, here, we opted for liquid chromatography–tandem mass spectrometry (LC-MS/MS) as the preferred choice due to its high sensitivity and unmatched specificity, and given its propensity to detect distinctive mass transitions of each analyte, and therefore, its capacity for unequivocal identification. In addition, mass spectrometry allows the use of isotope-labeled standards, which correspond analogously to their respective analyte throughout the entire analytical procedure, from sample preparation to detection. The combination of mass spectrometry and isotope-labeled standards of target analytes is a top-notch technique for the analysis of several biological samples.[291] In recent years, a handful of LC-MS/MS-based methods have been published to quantify neurotransmitters. These refer almost exclusively to mouse[270,271] and rat[292,293] brain tissue and mostly do not provide sufficient LOQs for neurotransmitter quantification in model organisms like *C. elegans*. Only Tufi *et al.* present an LC-MS/MS analysis in zebrafish *Danio rerio*,[294] while Barata *et al.* published a method for neurotransmitter and related metabolites quantification in *Daphnia magna*.[295] A tool for the simultaneous quantification of neurotransmitters, especially GABA and ACh, in *C. elegans* with sufficient sensitivity has yet to be reported.

Here, we aim to present an established and validated LC-MS/MS-based method, which allows the simultaneous quantification of neurotransmitters, specifically DA, SRT, GABA and ACh, in *C. elegans*. A new extraction protocol assured stability and high recovery for all four analytes. The use of isotope-labeled standards and LC-MS/MS analysis in multiple-reaction-monitoring mode provided an unequivocal identification, as well as specificity of all analytes and greater sensitivity compared to other techniques. As method validation parameters, the linear range, limit of detection (LOD), limit of quantification (LOQ), accuracy, recovery and precision were assessed. Further, we analyzed neurotransmitter profiles of transgenic *C. elegans* strains with altered neurotransmitter homeostasis and characterized their synaptic transmission by the aldicarb-induced paralysis assay in order to corroborate the analytical LC-MS/MS data.

5.2 Results

5.2.1 Method Development for Neurotransmitter Quantification via LC-MS/MS

The aim of the chromatography was to establish a baseline-separated elution for all analytes, as well as maximum sensitivity with subsequent mass spectrometric detection. Different solvents (MeOH and ACN) were tested, with ACN demonstrating sharper peaks, lower noise and quicker elution of all analytes when we used the YMC-Triart PFP column. ACN modified with 10 mM FA resulted in a higher response compared to 5 mM FA. For further optimization, the column temperature was varied (20–40 °C), with 30 °C leading to the best result. A gradient of a total of 12 min (including equilibration) was generated with the following retention times for all analytes and their respective deuterated internal standards (used for internal calibration and unambiguous identification): GABA—2.50 min, DA—5.92 min, ACh—7.22 min and SRT—8.38 min. The respective chromatograms of the quantifiers of all analytes and all internal standards in a *C. elegans* matrix (wildtype) are shown in Figure 25.

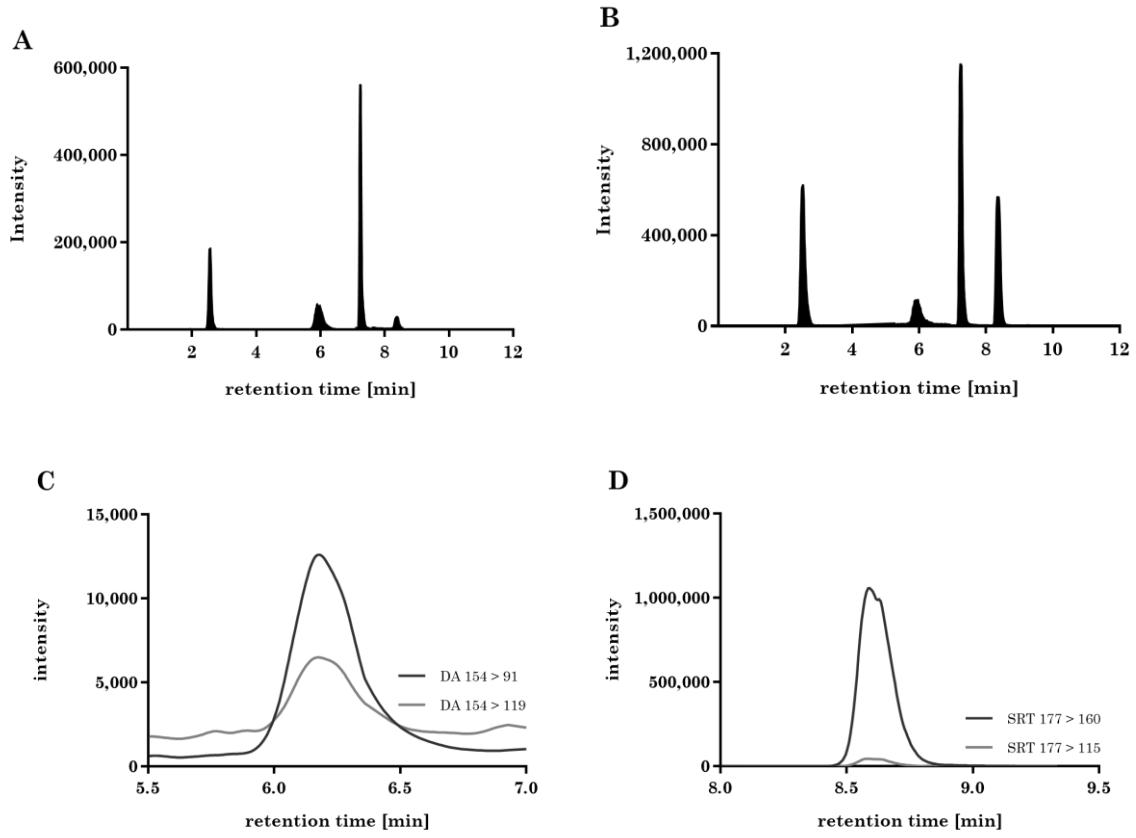

[Figure caption is provided on the subsequent page]

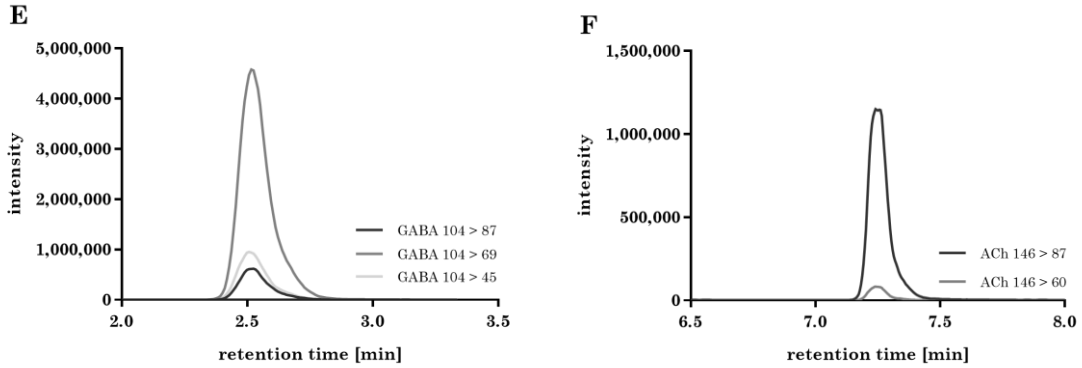

Figure 25: sMRM chromatograms of all analytes (**A**) and their respective deuterated internal standards (**B**) (25 nM of DA_{d4}, 25 mMSRT_{d4}, 500 nM of $GABA_{d6}$ and 25 nM ACh_{d4}) in *C. elegans* worm homogenate (wildtype). (**A**,**B**) only the quantifier mass transitions (Table 3) of DA, SRT, GABA, ACh and the accordant internal standards are presented. The most intensive mass transitions (listed in Table 3) of DA (*m*/*z* 154 > 137 not found in matrix) (**C**), SRT (**D**), GABA (**E**) and ACh (**F**) are displayed in matrix.

Ion source parameters were optimized with standard solutions using the Compound Optimization software wizard of the Sciex Analyst Software (Version 1.7.2); they are listed in the materials and methods Section 2.4. To determine mass-to-charge (*m*/*z*) ratios for the precursor ions, standard solutions of the analytes and deuterated analytes were injected and Q1 scans were performed. Fragment ion scans with varying intensity in collision energy were conducted to determine the *m*/*z* ratios of the respective fragments. The aim was to identify at least two MRM transitions for each analyte with optimal intensity. The following mass transitions revealed the highest responses (Figure 25 C–F) and were therefore used as quantifiers: DA *m*/*z* 154 > 91, DA_{d4} *m*/*z* 158 > 95, SRT *m*/*z* 177 > 160, SRT_{d4} *m*/*z* 181 > 164, GABA *m*/*z* 104 > 69, $GABA_{d6}$ *m*/*z* 110 > 73, ACh *m*/*z* 146 > 87 and ACh_{d4} *m*/*z* 150 > 91. Quantifier precursor and fragment ion structures are stated in Figure 26. Further mass transitions (qualifiers) are listed in Table 3.

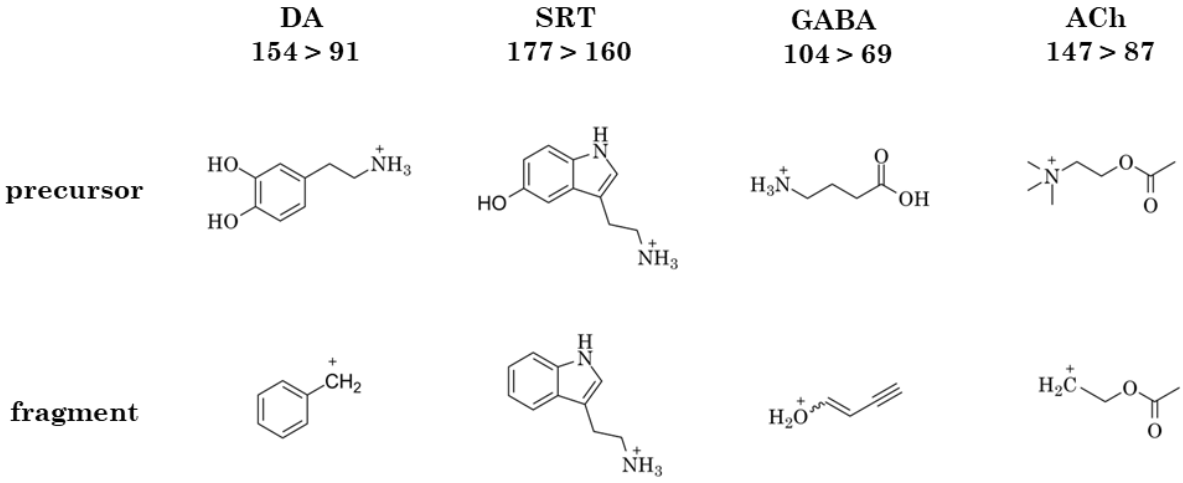

Figure 26: Chemical structures of precursors and their underlying fragment ions $[M + H]^+$ (quantifiers) for DA, SRT, GABA and ACh.

Table 3: sMRM parameters for DA, SRT, GABA, ACh and their respective internal standards. The quantifiers are highlighted in bold. All transitions are single-protonated ions ($[M + H]^+$).

Compound	Q1	Q3	CE	DP	CXP	Retention Time (min)
DA	154	137	15	30	15	5.92
		119	25	30	15	
		91	32	30	15	
DA_{d4}	158	141	15	30	15	
		123	25	30	15	
		95	32	30	15	
SRT	177	**160**	15	15	17	8.38
		115	51	30	41	
SRT_{d4}	181	**164**	15	15	17	
		118	51	30	41	
GABA	104	87	15	17	10	2.50
		69	21	18	10	
		45	28	25	11	
$GABA_{d6}$	110	93	15	17	10	
		73	21	18	10	
		49	28	25	11	
ACh	146	**87**	19	27	13	7.22
		60	16	32	9	
ACh_{d4}	150	**91**	19	27	13	
		60	16	32	9	

5.2.2 Sample Preparation und Neurotransmitter Extraction

Following optimization of the LC-MS/MS conditions, the method was applied to *C. elegans* homogenates. The extraction of neurotransmitters was improved by optimizing the composition of the applied extraction buffer. We tested the pH effect (acidic and neutral) on the stability and recovery of all four analytes. Whereas DA seems to be stable only in acidic pH, GABA shows the highest recovery in neutral pH. In contrast, both SRT and ACh demonstrate no differences in recovery in acidic or neutral pH. In order to identify a suitable compromise, various acids (perchloric acid and formic acid) and pH values (pH = 1–7) were tested. A sufficient response of all four analytes was obtained by adding 2.5 mM perchloric acid (pH = 4). In addition, we analyzed the impact of different amounts (10, 20 and 30%) of organic modifiers (MeOH and ACN) in the extraction buffer. A higher response, especially for GABA, was observed when we modified the buffer with 10% MeOH. The sample extracts were purified by a Spin-X® Centrifuge Tube Filter 0.22 µm (Corning). The recovery of the neurotransmitters as well as the protein content with and without purification steps were determined, and showed statistically indistinguishable results.

5.2.3 Method validation

Samples were spiked with DA, SRT and ACh from 0 to 500 nM and with GABA from 0 to 10 µM. Linearity was observed for all analytes in the indicated range (Figure 3); correlation coefficients are listed in Table 4.

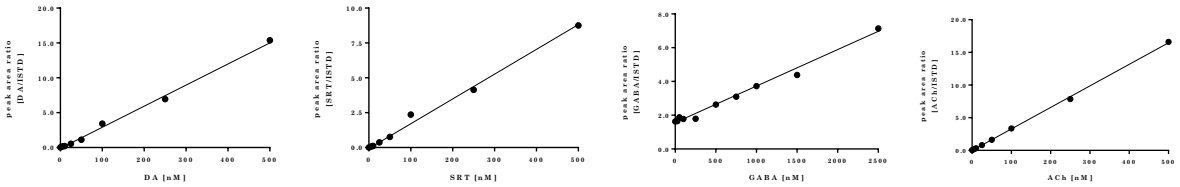

Figure 27: Calibration curves for all four neurotransmitters in the concentration range of up to 500 nM for DA, SRT and ACh and up to 2500 nM for GABA. Correlation coefficients are stated in Table 4.

Table 4: Method validation parameters assessed in *C. elegans* matrix (wildtype). How parameters were assessed is listed in section 5.4.5.

	DA	**SRT**	**GABA**	**ACh**
Concentration in samples #	11.9 nM	2.2 nM	2.6 µM	38.8 nM
Correlation coefficient (R^2)	0.9966	0.9939	0.9873	0.9993
Limit of detection (nM)	0.204	0.097	15.628	0.0009
Limit of quantification (nM)	0.679	0.324	52.094	0.0029
Recovery (%)	103 ± 2.7	64 ± 2.3	80 ± 4.1	56 ± 11.9

analyte concentration of worm homogenates (3000 L4 stage worms in 150 µL extraction buffer) before protein normalization.

The LOD was defined as LOD = $3\times SD_y/b$ (SD_y = standard deviation of analyte concentration in ≥12 blank measurements, b = slope of calibration curve), with 0.204 nM for DA, 0.097 nM for SRT, 15.628 nM for GABA and 0.0009 nM for ACh. The LOQ was defined as LOQ = $10\times SD_y/b$, with 0.679 nM for DA, 0.324 nM for SRT, 52.094 nM for GABA and 0.0029 nM for ACh. Thus, the LOQs were far below the analyte concentrations in *C. elegans* homogenates (3000 L4 stage worms in 150 µL extraction buffer), which were 11.9 nM of DA, 2.2 nM SRT, 2.6 µM GABA and 38.8 nM ACh ($n \geq 20$). The LOQs underline the sensitivity of the method and show that considerably less than 3000 worms can be used for the analysis. The recovery of deuterated standards in matrix amounted to 103 ± 3% for DA, 64 ± 2% SRT, 80 ± 4% for GABA and 56 ± 12% for ACh, compared to deuterated standards in extraction buffer only. This indicates sufficient recovery, as the loss of neurotransmitters during sample preparation and analysis was always balanced by the respective deuterated standards.

Accuracy was determined in samples with low (25 nM), middle (250 nM) and high (2500 nM) concentrations of all analytes and was within ± 20% of the nominal concentration (Table 3). The variation in neurotransmitter quantification from eight samples on the same day was defined as intraday precision and was 3.1% for DA, 6.1% for SRT, 3.4% for GABA and 7.6% for ACh. The variation from eight samples analyzed on different days was defined as interday precision and was 2.6% for DA, 14.0% for SRT, 3.2% for GABA and 1.8% for ACh. Therefore, intra- and interday variations < 15% were considered both reliable and reproducible due to high precision.

Table 5: Method validation parameters: accuracy for low, middle and high analyte concentrations and intraday and interday precision. How parameters were assessed is listed in section 5.4.5.

	Accuracy [%]			Precision [RSD%]	
	Low	**Middle**	**High**	**Intraday**	**Interday**
DA	114.8 ± 8.8	111.1 ± 7.9	112.7 ± 4.1	3.1	2.6
SRT	84.9 ± 1.3	85.6 ± 1.5	81.1 ± 1.8	6.1	14.0
GABA	95.3 ± 8.7	108.2 ± 5.2	116.4 ± 5.4	3.4	3.2
ACh	98.5 ± 4.9	96.6 ± 1.0	99.8 ± 0.6	7.6	1.8

5.2.4 Neurotransmitter Levels in Wildtype Worms and cat-2Δ and ace-1Δ::ace-2Δ Deletion Mutants

By using the validated LC-MS/MS method, we investigated the impact of the genetic background of *C. elegans* strains cat-2Δ and ace-1Δ::ace-2Δ on neurotransmitter levels. The deletion mutant cat-2Δ lacks the enzyme tyrosine hydroxylase, which catalyzes the hydroxylation of tyrosine to L-DOPA (l-3,4-dihydroxyphenylalanine), the precursor of DA.[296] Consequently, DA synthesis in cat-2Δ worms is restricted. *C. elegans* strain ace-1Δ::ace-2Δ displays a loss of acetylcholinesterase (AChE), which is the major enzyme to hydrolyze ACh into acetic acid and choline.[297] As a result, this deletion mutant should not be capable of degrading ACh.

The analysis of dopamine levels (Figure 28A) revealed 2.18 ± 0.19 ng DA per mg protein in wildtype worms and 2.26 ± 0.15 ng DA per mg protein in ace-1Δ::ace-2Δ deletion mutants. cat-2Δ worms displayed 0.11 ± 0.04 ng DA per mg protein or 0.54 nM DA in sample extracts; thus, DA levels were significantly lower compared to wildtype worms. This demonstrates that cat-2Δ worms do not suffer a total loss of DA, but nevertheless present a very low level of DA, which is higher than the LOD, but lower than the LOQ. As a result, cat-2Δ worms exhibited 95% less DA compared to wildtype worms. The quantification of SRT revealed no differences in the deletion mutants used compared to wildtype worms. SRT levels (Figure 4B) amounted to 0.067 ± 0.012 ng SRT per mg protein in wildtype worms, 0.063 ± 0.006 ng SRT per mg protein in cat-2Δ worms and 0.067 ± 0.009 ng SRT per mg protein in ace-1Δ::ace-2Δ worms. Wildtype worms contained 196 ± 30 ng GABA per mg protein (Figure 4C). Interestingly, cat-2Δ worms displayed a significantly lower amount of 121 ± 9 ng GABA per mg protein, whereas the deletion mutant ace-1Δ::ace-2Δ had the lowest amount of 104 ± 4 ng GABA per mg protein, which significantly differed compared to wildtype worms. The next neurotransmitter we quantified was ACh (Figure 28D); 6.24 ± 0.64 ng ACh was contained per mg protein in wildtype worms and 4.97 ng ACh per mg protein in cat-2Δ

worms, representing a slight decrease, although it was statistically indistinguishable from wildtype worms. In contrast, the deletion mutant ace-1Δ::ace-2Δ contained a significantly higher amount of ACh compared to wildtype worms, with 113 ± 9 ng ACh per mg protein. Thus, ace-1Δ::ace-2Δ worms contained 18-fold greater ACh levels compared to wildtype worms.

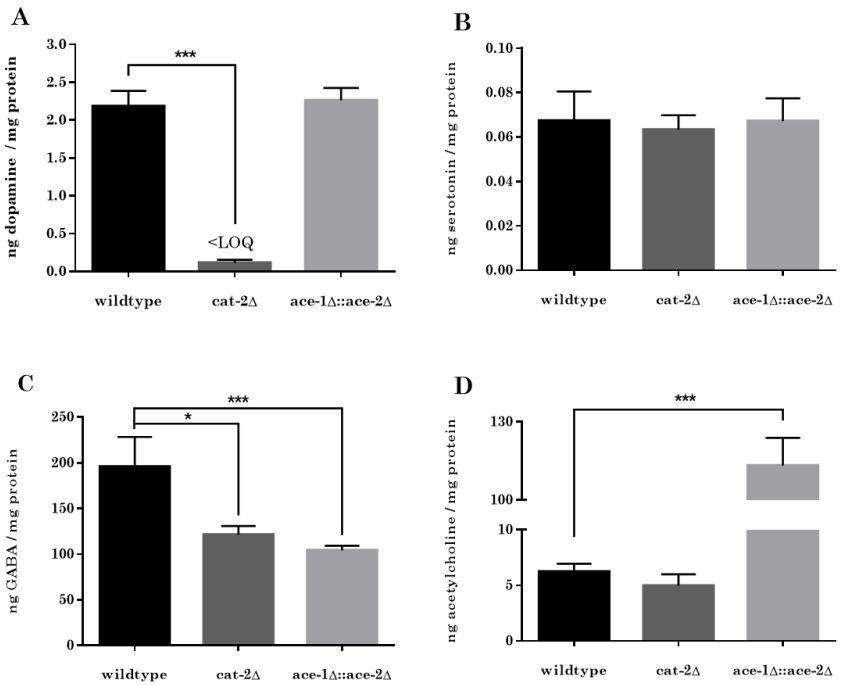

Figure 28: Levels in ng per mg protein of dopamine (A), serotonin (B), GABA (C) and acetylcholine (D) in L4 stage worms (wildtype, cat-2Δ and ace-1Δ::ace-2Δ) quantified via LC-MS/MS. Data presented are mean values of n = 4 independent experiments + SEM. Statistical analysis using unpaired *t*-test. Significance levels with α = 0.05: *: $p \leq 0.05$ and ***: $p \leq 0.001$ compared to wildtype worms

5.2.5 Aldicarb-Induced Paralysis Assay

To investigate the consequences of our findings regarding the neurotransmitter quantification of the two deletion mutants, cat-2Δ and ace-1Δ::ace-2Δ, compared to wildtype worms, a classical applied behavioral assay was performed. Aldicarb is an AChE inhibitor, which leads to an accumulation of ACh, and therefore to a persistent activation of muscles followed by paralysis. The aldicarb-induced paralysis assay examines alterations in the synaptic transmission of *C. elegans*.[298] Aldicarb resistance, compared to wildtype worms, results in decreased synaptic transmission. By implication, aldicarb hypersensitivity leads to increased synaptic transmission.[299]

Results are presented in Figure 29 and demonstrate the paralysis rate in all three tested worm strains over a time span of 240 min. The cat-2Δ strain showed an earlier onset of paralysis compared to wildtype worms, with only 65% ± 14% of worms moving after 60 min (wildtype: 74% ± 7%) and 15% ± 8% after 120 min (wildtype: 22% ± 7%) when exposed to aldicarb, but the difference did not attain statistical significance. ace-1Δ::ace-2Δ worms, in contrast, showed significant aldicarb resistance compared to wildtype worms, with 94% ± 2% of worms moving after 60 min and 45% ± 10% after 120 min of aldicarb exposure. Taken together, these findings establish that the loss of AChE leads to reduced synaptic transmission in *C. elegans* due to aldicarb resistance.

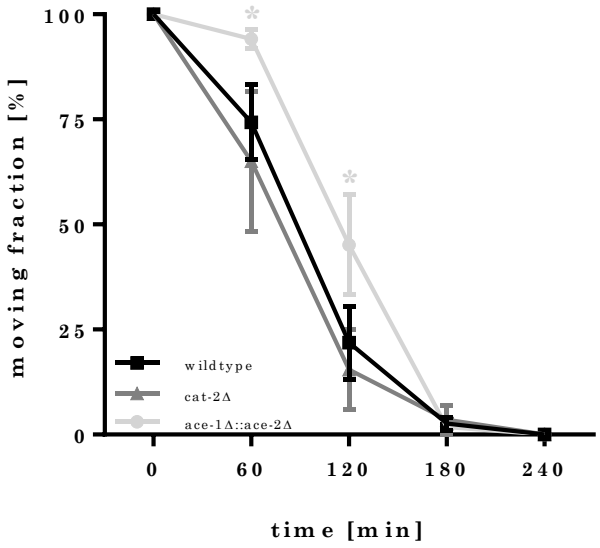

Figure 29: Aldicarb-induced paralysis assays in wildtype worms (black), cat-2Δ (dark grey) and ace-1Δ::ace-2Δ (light grey) deletion mutants. Displayed are fractions of moving worms [%] plotted against assay procedure times [min]. Data presented are mean values of n = 4 independent experiments ± SEM. Statistical analysis using unpaired *t*-test. Significance levels with α = 0.05: *: $p \leq 0.05$ compared to wildtype worms at the same time point.

5.3 Discussion

Tight regulation of the neurotransmitters is required to avoid adverse consequences of deficiency or excess, since various neurological diseases are characterized by a disturbed neurotransmitter homeostasis. Diseases associated with dysregulated neurotransmitters include PD, AD or depression, among others.[300] In this context, it is important to underline that in most clinical disorders, more than a single neurotransmitter is altered in its homeostasis.[301,302] Therefore, we have developed an LC-MS/MS-based method to

simultaneously quantify multiple neurotransmitters within a single sample and run, which allows the quantification of DA, SRT, GABA and ACh, as well as the identification of potential changes in neurotransmitter ratios. It is important to note that this, to our knowledge, is the first method proposed to quantify multiple neurotransmitters, especially GABA and ACh, in *C. elegans*. To verify the optimized and validated method, we took advantage of the fact that *C. elegans* is easily genetically manipulated, and used worms that cannot synthesize DA (cat-2Δ) or degrade ACh (ace-1Δ::ace-2Δ), analyzed their neurotransmitter profiles, and characterized their impacts on synaptic transmission by a further independent assay, which refers to classically performed behavioral assays.

Our method for neurotransmitter quantification distinguishes itself from other published MS-based methods given its advantages. First, only a low quantity of worms is necessary for an analysis. Furthermore, there is only minimal sample preparation required, as the extraction buffer has been optimized regarding pH and organic modifiers for all analytes, so further time-consuming extraction steps are not required. The pH value of the buffer used is particularly important for neurotransmitter extraction, since DA autoxidizes easily at a neutral pH value,[303] and extraction must therefore take place in an acidified milieu. GABA, on the other hand, displayed the best extraction in the neutral to slightly acidic pH range, with the result that we found a good compromise of pH = 4 for maximal extraction, which provides a higher overall sensitivity. The limits of detection for all analytes in matrix are in the very low nM range, which is advantageous compared to other LC-MS-based methods for the quantification of neurotransmitters in other matrices, as well as in standard solutions only.[292,294,304,305] Tufi *et al.* present an LOQ for SRT of 1.7 nM in zebrafish *Danio rerio*, which is roughly comparable to our data, whereas for other neurotransmitters like DA and GABA, two-digit nM quantification limits are displayed.[294] Huang *et al.* and Wang *et al.*'s LOQ for GABA in mice brain tissue is lower than that presented by us at 10 nM; however, their LOQs for DA and SRT are above 1 nM, and thus higher than those demonstrated in our study.[270,304] Olesti *et al.* demonstrate LOQs in the two-digit nM range in rat plasma and brain homogenates,[305] while in Blanco *et al.*'s study, the average values of DA and ACh in mouse cerebrospinal fluid are below the LOQ.[271] However, the sensitivity is increased enough in the presently evaluated method to quantify the four neurotransmitters in a few 100 worms, which would allow high-throughput analyses in order to identify, for example, neurotoxic or neuroprotective substances. The method also offers high accuracy, as we use the respective isotope-labeled standards for each analyte throughout the entire sample preparation to compensate for losses in recovery

and allow for an unequivocal identification of the neurotransmitters. The use of isotope-labeled standards is also a special feature of this method, which is often unconsidered.[270,293,306] Another advantage that underlines the specificity of our method is the use of a tandem mass spectrometer. The fragment pattern, characterized by the m/z ratios of the precursor ion and fragment ions, is as unique as a fingerprint for each molecule[307] and enables us to specifically identify our targeted analytes, rather than using retention times only. Other types of detection, such as quantification by fluorescent dyes,[288–290] are less specific than the method described herein. Neurotransmitter quantification by HPLC with fluorescence detection is also both less specific and less sensitive, since it is necessary to derivatize the analytes into a fluorescent product. In addition, external calibration is commonly necessary.[286,287] In addition, other methods, such as that proposed by Zhang *et al.*, combine precolumn derivatization with LC-MS/MS analysis to increase the specificity and sensitivity.[308] This provides LOQs in the single-digit nM range comparable to those produced by our method, but an additional derivatization step must be performed, which bears a further opportunity for error and takes another 30 min.

The roundworm *C. elegans* has become a prominent model organism and multipurpose tool to study neurotoxicity. Since only very few neurodegenerative diseases are linked to genetic factors, growing evidence strongly implicates environmental factors in their respective etiology. Therefore, the worm, with its existing neurodegenerative disease models (mostly transgenic worms), offers the opportunity for testing potential neurodegenerative substances and treatments, which may reflect or even accelerate the progression of neurodegenerative disorders. The quantification of neurotransmitter levels allows for precise identification of mechanisms that mediate neurotoxicity, and identifies putative targets for efficient therapeutic approaches and neuroprotective strategies. A special feature of *C. elegans* is its short life cycle, which allows a huge sample quantity in a short time period, and in combination with the presented analysis offers an effective high-throughput method. A further advantage of the worm is its completely sequenced genome, allowing its simple genetic manipulation. As a result, especially for neurobehavioral assays, chemicals or toxins are often not used as positive controls; rather, worms with specific mutations are. A commonly used assay is the basal slowing response, which examines dopamine-dependent behavior in the presence of food[211]. cat-2Δ worms are a popular positive control, since they show reduced food sensing due to its deficiency in DA synthesis.[309,310] Mutations of *C. elegans* are also often used to model neurodegenerative

diseases like PD[276] and AD.[278] Despite the extensive use of mutants of this worm in neurobehavioral assays, its neurotransmitter profile has not been characterized, to our knowledge. Despite the usage of behavioral assays and the microscopy of fluorescence-tagged neurons, only a few chromatographic approaches have been carried out in *C. elegans* to quantify DA. Only Schumacher *et al.* displayed a validated LC-MS/MS-based method to analyze DA and SRT in *C. elegans*, but they excluded GABA and ACh,[283] which are, however, essential for the investigation of neurotoxicity.[265,311] Using our method, we were able to determine neurotransmitter profiles in wildtype worms, as well as in cat-2Δ and ace-1Δ::ace-2Δ worms. As suggested in the literature, cat-2Δ worms had lesser DA levels compared to wildtype worms, which was corroborated by our LC-MS/MS method. In addition, we could also identify altered GABA levels. The same applied to ace-1Δ::ace-2Δ worms, wherein we could detect increased ACh levels as expected, but also reduced GABA levels, which underlines the interdependence and homeostatic dependence of different neurotransmitters. Muñoz *et al.* demonstrated interactions between the dopaminergic and serotonergic systems in PD.[312] Qi *et al.* reported how different neurotransmitters modulate neurotransmitter balance, and therefore regulate the function of different brain regions.[268] This emphasizes the importance of simultaneously quantifying multiple neurotransmitters, which has been achieved with this LC-MS/MS-based method. In contrast, behavioral assays do not constitute quantitative methods, but merely provide an insight into the consequences of an eventual neurotransmitter dyshomeostasis. It is noteworthy that the combination of instrumental analytics (especially mass spectrometry) and behavioral assays complement each other remarkably well. Therefore, the worm strains mentioned above were subjected to the aldicarb-induced paralysis assay in addition to neurotransmitter quantification.

Aldicarb, an AChE inhibitor, promotes the accumulation of ACh in locomotor neuromuscular junctions in *C. elegans*.[313] This results in hyperexcitability and excessive muscle contraction, causing paralysis.[71] If a mutant strain displays higher ACh levels, it should undergo paralysis faster. However, it has been shown that not only ACh itself is involved in aldicarb-induced paralysis, but the entire cholinergic system. Upon aldicarb treatment, mutants with impaired cholinergic function accumulate synaptic ACh at a slower rate, resulting in slower paralysis, and therefore aldicarb resistance, compared to wildtype worms.[314]

This is consistent with our data, where ace-1Δ::ace-2Δ mutants showed a slower onset of paralysis, which was also demonstrated by Oppermann and Chang.[315] Hypothetically, it is not an increase in total ACh levels that leads to the onset of paralysis, but increased ACh levels in the neuromuscular junction. Giles *et al.*[314] reported that worms with disrupted inhibitory GABA function had a faster paralysis rate due to a loss of relaxation. Thus, given the GABA deficiency, cat-2Δ worms should paralyze faster in the presence of aldicarb compared to wildtype worms, which does not appear to be the case. It appears that behavior is a not fully understood yet complex construct in *C. elegans*, and further research is required to understand the underlying mechanisms of behavioral assays like the aldicarb-induced paralysis assay. This underscores that the combination of behavioral assays for *C. elegans* and the quantitative and validated methods such as the LC-MS/MS-based method developed herein provide the means for altered functional characterization along with its underpinning mechanisms. It is also noteworthy that the behavioral assays mentioned are species-specific, in this case *C. elegans*-specific. However, our LC-MS/MS method for the quantification of neurotransmitters is universally applicable and can be applied to other model systems and tissues in the future with the eventual adaption of sample preparation.

5.4 Material and Methods

5.4.1 *C. elegans* Handling and Cultivation

C. elegans strains Bristol N2 (wildtype) and deletion mutants (Δ) CB1112 (cat-2Δ) and GG201 (ace-1Δ::ace-2Δ) were obtained from the Caenorhabditis Genetics Center (CGC, Minneapolis, MN, USA), which is funded by the National Institutes of Health Office of Research Infrastructure Programs. Cultivation of *C. elegans* was maintained on 8P agar plates coated with the *Escherichia coli* (*E. coli*) strain NA22 at 20 °C as previously described[316,317]. To generate age-synchronous worm populations, gravid adults were treated with bleach solution (1% NaOCl and 0.5 M NaOH) to release eggs, which were allowed to hatch overnight in M9 buffer. Synchronous L1-stage larvae were placed on nematode growth (NGM) agar plates coated with *E. coli* strain OP50 for 48 h to reach L4 stage.

5.4.2 Neurotransmitter Standard Solution

Dopamine hydrochloride (Alfa Aesar, Kandel, Germany) and 2-(3,4-dihydroxy-phenyl)ethyl-1,1,2,2-d4-amine HCl (DA_{d4}) (CDN Isotopes, Pointe-Claire, Canada) were dissolved in 200 mM $HClO_4$ (Sigma-Aldrich, Steinheim, Germany), whereas γ-aminobutyric

acid (Sigma-Aldrich, Steinheim, Germany) and 4-aminobutyric-2,2,3,3,4,4-d6 acid ($GABA_{d6}$) (EQ Laboratories GmbH, Augsburg, Germany) stock solutions were prepared in 10% methanol (MeOH) (LC-MS grade, Thermo Fisher Scientific, Waltham, MA, USA). Serotonin hydrochloride (Alfa Aesar), serotonin-α,α,β,β-d4 creatinine sulfate complex (SRT_{d4}) (CDN Isotopes, Pointe-Claire, Canada), acetylcholine chloride (Sigma-Aldrich, Steinheim, Germany) and acetylcholine-1,1,2,2-d4 chloride (ACh_{d4}) (EQ Laboratories GmbH, Augsburg, Germany) were dissolved in bidistilled water. The deuterated analogue of the respective neurotransmitter was taken as an internal standard.

5.4.3 Sample Preparation and Neurotransmitter Extraction

Synchronous L4 stage wildtype, cat-2Δ and ace-1Δ::ace-2Δ worms were washed off from NGM agar plates using 85 mM NaCl + 0.01% Tween. The washing procedure was repeated three times to ensure samples were free of *E. coli*. Of each respective strain, 3000 worms were pelletized in 50 µL 85 mM NaCl by centrifugation at 380 g, frozen in liquid nitrogen and stored at −80 °C. Extraction buffer (2 mM sodium thiosulfate, 2.5 mM $HClO_4$, 10% MeOH LC-MS grade, 25 mM DA_{d4}, 25 mM SRT_{d4}, 25 mM ACh_{d4} and 500 mM $GABA_{d6}$) was freshly prepared right before sample preparation. Samples were kept on ice during sample preparation and extracted samples were analyzed immediately by LC-MS/MS. In the first step, worm pellets were defrosted and 100 µL extraction buffer was added, as well as zirconia beads (biolab products, Bebensee, Germany). To homogenize the samples: 4× freeze–thaw cycles (1 min 37 °C, 1 min liquid nitrogen) followed by 4 × 20 sec bead beating by usage of a Bead Ruptor (biolab products, Bebensee, Germany). After centrifugation for 10 min at 16,060 × *g* at 4 °C, 100 µL of the supernatant was transferred to a Spin-X® Centrifuge Tube Filter 0.22 µm (Corning, Amsterdam, The Netherlands) and centrifugation was repeated. An aliquot was transferred to a vial with insert and analyzed via LC-MS/MS, while the rest was used for protein quantification for normalization measured by bicinchoninic acid assay.[318]

5.4.4 LC-MS/MS Parameters

All analyses were conducted using an Agilent 1290 Infinity II liquid chromatography system (Agilent, Waldbronn, Germany) coupled with a Sciex QTRAP 6500+ triple quadrupole mass spectrometer (Sciex, Darmstadt, Germany) interfaced with an electrospray ion source, which operated in positive ion mode. Chromatographic separation was performed using a YMC-Triart PFP (pentafluorophenyl) column (3 µm, 3 × 150 mm)

and an additional precolumn (3 µm, 3 × 10 mm) of the same column material. The elution of neurotransmitters was carried out with bidistilled water + 10 mM formic acid (FA) (LC-MS grade, Thermo Fisher Scientific, Waltham, MA, USA) and acetonitrile (ACN) (LC-MS grade, VWR, Darmstadt, Germany) + 10 mM FA. Three µL of the sample was injected. Analytes were eluted with a flow of 0.425 mL min^{-1} from the column, which was pre-heated to 30 °C. Total run time was 12 min, which was divided in a gradient with 0% ACN for 3 min, 0 to 60% ACN for 6 min, 60 to 100% ACN for 0.5 min, 100% ACN for another 0.5 min, 100 to 0% ACN for 0.5 min and 0% ACN for re-equilibration for 1.5 min. Analysis was carried out in scheduled multiple reaction monitoring (sMRM) mode with detection windows of ±40 sec of the respective retention times (Table 1). Ion source parameters optimization was performed with standard solutions of DA, SRT, GABA and ACh using the *Compound Optimization software wizard* of the Sciex Analyst Software (Version 1.7.2). The following parameters were determined: ion spray voltage = 4000 V, curtain gas (N2) = 40 psi, nebulizer gas = 60 psi, drying gas = 50 psi, collision (CAD) gas = medium, temperature = 600 °C, entrance potential = 10 V. The dwell time for all analytes and deuterated standards was set to 20 ms. Mass transitions for the analytes and internal standards as well as the respective optimized collision energy (CE), declustering potential (DP) and collision cell exit potential (CXP) are listed in Table 3.

5.4.5 Method validation

Method validation was carried out according the "ICH guideline Q2(R2) on validation of analytical procedures" of the European Medicines Agency. Linear range, limit of detection (LOD), limit of quantification (LOQ), recovery, accuracy and intraday and interday precision were assessed for method validation. To investigate linear ranges, LODs and LOQs, solutions with fixed amounts of matrix (wildtype) and deuterated internal standards were added with neurotransmitter standards in a range of 0–500 nM for DA, SRT and ACh and 0–10 µM for GABA, and analyzed twice. Peak areas of the analytes were normalized to the respective internal standards, plotted against the added concentrations and afterwards examined for linear correlation. Signal-to-noise ratios (S/N) were calculated using *Multiquant Software* (Sciex, Version 3.0.3) and plotted against the added concentrations; the slopes were determined subsequently. LOD and LOQ were defined as $LOD = 3 \times SD_y/b$ (SD_y = standard deviation of analyte concentration in ≥12 blank measurements, b = slope of calibration curve) and $LOQ = 10 \times SD_y/b$. To assess the recovery of the deuterated internal standards in matrix, eight samples containing extraction buffer only and eight samples

with worm matrix in extraction buffer were analyzed. Recovery was defined as the ratio of the area of internal standards with to that without matrix. For accuracy, matrix-free samples with low (25 nM), middle (250 nM) and high (2.5 µM) amounts of all neurotransmitters added along with 250 nM of deuterated standards were analyzed twelve times. Accuracy was calculated in percent by how much of the neurotransmitters was actually detected. To determine precision, intraday variation of eight wildtype worm samples pelletized and analyzed on the same day, and interday variation of six wildtype worm samples, each pelletized and analyzed on six different days, were assessed. Samples were normalized for protein content for examination of intraday as well as interday precision. Precision is stated as relative standard deviation in percent (RSD%) of the above-mentioned samples.

5.4.6 Aldicarb-Induced Paralysis Assay

Synchronous L1 stage worms were placed on NGM plates as mentioned above for 72 h until the young adult stage. The assay was performed based on Mahoney *et al.*[281] In brief, a 100 mM aldicarb (Sigma-Aldrich, Steinheim, Germany) stock solution was prepared in 70% ethanol. For plates with 2 mM aldicarb, NGM agar was set up as previously described[295,297] and added with aldicarb for desired concentration. Three mL portions were poured into 3.5 cm petri dishes and stored at 4 °C. The plates were coated at the very beginning of the experiment with 2 µL of *E. coli* strain OP50 to concentrate worms in the middle of the plates. The assay was always performed as a blinded experiment. Of each genotype, 20–25 worms were placed on an aldicarb-containing plate, which were left at room temperature during the assay procedure. Every 60 min, the number of total and paralyzed worms was counted. Worms were defined as paralyzed if they demonstrated no movement after prodding carefully with a platinum wire against head and tail.

5.4.7 Statistics

Statistical analysis was performed using GraphPad Prism 6 (GraphPad Software, La Jolla, CA, USA) via unpaired *t*-test. Significance levels with $\alpha = 0.05$ are depicted as *: $p \leq 0.05$, **: $p \leq 0.01$ and ***: $p \leq 0.001$, compared to wildtype worms.

5.5 Conclusion

In summary, here (1) we developed a novel liquid chromatography–tandem mass spectrometry (LC-MS/MS) method, which enables simultaneous neurotransmitter quantification of dopamine (DA), serotonin (SRT), γ-aminobutyric acid (GABA) and

acetylcholine (ACh) in the nematode, *C. elegans*, an assay (2) which can readily be applied to other matrices. (3) Furthermore, the LC-MS/MS method combined with isotope-labeled standards provides exquisite sensitivity and specificity, (4) providing a validated analytical method for the assessment of altered neurotransmission and neurotoxicity. Our analytical method allows the quantification of neurotransmitters and their ratios as a convenient tool for the identification of mechanisms that mediate neurotoxicity, and it should be helpful in identifying possible putative therapeutic approaches and targets. Neurotoxicity assessment in *C. elegans* is commonly carried out by behavioral assays, which provide a sensitive assay for altered neurological behaviors, but are unable to characterize neurotransmitter levels. Other than *C. elegans* species-specific behavioral assays, our method is equally applicable to other tissues and matrices.

5.6 Author Contributions

Conceptualization, A.-K.W., L.K. and J.B.; methodology, A.-K.W. and L.R.; validation, A.-K.W.; formal analysis, A.-K.W.; investigation, A.-K.W.; data curation, A.-K.W.; writing—original draft preparation, A.-K.W.; writing—review and editing, L.K., T.S., M.A. and J.B.; visualization, A.-K.W.; supervision, J.B.; project administration, J.B.; funding acquisition, J.B. and T.S. All authors have read and agreed to the published version of the manuscript.

5.7 Funding

This work was supported by the DFG Research Unit TraceAge (FOR 2558, BO4103/4-2). M.A. was supported in part by grants from the National Institute of Environmental Health Sciences (NIEHS) R01ES10563 and R01ES07331.

5.8 Keywords

mass spectrometry • liquid chromatography • neurotransmitters • neurodegenerative diseases • *C. elegans*

Abstract:

Maneb is a manganese-containing ethylene bisdithiocarbamate fungicide and is still commonly used as no cases of resistance have been documented. However, studies have shown that Maneb exposure has neurodegenerative potential in mammals, resulting in symptoms affecting the motor system. Despite its extensive use, structural elucidation of Maneb has only recently been accomplished by our group. This study aimed to determine if the toxicity of Maneb is primarily caused by the fungicide itself, the release of manganese ions, the organic backbone, its degradation products, or a combined effect. Therefore, *Caenorhabditis elegans* was used as *in vivo* model for neurotoxicity. Exposure to Maneb did not increase the bioavailability of Mn compared to manganese chloride, although Maneb was about 8 times more toxic with regard to lethality. Maneb generated only mildly reactive oxygen and nitrogen species (RONS) but increased the amount of glutathione and its oxidized form in a dose-dependent manner. Nevertheless, an alteration in the neurotransmitter homeostasis of dopamine, acetylcholine, and gamma butyric acid (GABA) was observed upon Maneb exposure, which underlines the assumption of the neurotoxic potential of Maneb. This study showed that Maneb exhibits effects based on a combined interaction of the ligand and manganese.

Chapter 6 – Exposure to the environmentally relevant fungicide Maneb: Studying toxicity in the soil nematode *Caenorhabditis elegans*

Based on:

Laura Kubens, Ann-Kathrin Weishaupt, Isabelle Rohn, Fabian Mohr and Julia Bornhorst

Submitted to: Environment international

Chapter 6 – Exposure to the environmentally relevant fungicide Maneb: Studying toxicity in the soil nematode *Caenorhabditis elegans*

6.1 Introduction

Polymeric ethylene bisdithiocarbamate (EBDC) containing fungicides and their salts were patented in the 1940s as the first broad-spectrum foliar fungicides.[22] In 1950 the manganese (Mn) containing EBDC fungicide was patented and marketed under the brand name Maneb (MB) [4]. Since then, it has been widely used in over 100 different crops, including potatoes, tomatoes, and bananas.[43,319] Because EBDC-based fungicides have a highly effective multi-site mode of action, they are commonly used in mixtures with other fungicides as part of resistance management strategies.[43] Since this class of fungicides does not act systemically in the plant and is used preventively, they have to be repeatedly applied, which increases the amount of active ingredient entering the environment. Occasionally, exact molecular structures of compounds known for ages remain unknown, this is also true for MB. Its molecular structure was unknown for over 70 years and has only recently been elucidated by our group [252]. Contrary to expectations, MB is very stable towards oxidation in the solid-state due to a two-dimensional polymeric network structure with intramolecular sulfur bridges. In dimethylsulfoxide (DMSO) solution MB forms a coordination polymer with two coordinating DMSO molecules in each unit cell.[252] MB is thus a polymer of unknown length and its insolubility makes it unsuitable for conventional liquid chromatography coupled with mass spectrometry. Therefore, residue analyses of dithiocarbamate (DTC)-containing fungicides in crops are based on carbon disulfide (CS_2) content and do not refer to the specific metal species, which makes it impossible to distinguish between approved and non-approved EBDC fungicides. The European Food Safety Authority (EFSA) published in their annual report on pesticide residues from 2020 that the chronic dietary exposure (expressed in % of the acceptable daily intake (ADI)) was between 9% and 83%, over all DTC-containing fungicides. Most chronic exposures from other pesticides are typically less than 10% or even less than 1% of the ADI. The primary food contributors were apples, pears, and broccoli.[39] Thus, the group of dithiocarbamates repeatedly attracts attention due to cases of increased residue levels. Unlike food samples, environmental samples are collected less frequently. Data on possible ecological accumulation of the metals released from EBDC fungicides, especially in soil or water samples, is somewhat limited, and their fate in the environment has not been identified.

On the one hand, Mn is a necessary cofactor for several enzymes and is involved in different processes, including metabolism, antioxidant defense, development, and reproduction.[130] On the other hand, despite being essential, a chronic over-supply of Mn can lead to neurodegenerative damage with symptoms similar to Parkinson's disease, termed "manganism".[76,137,221]

Various EBDC degradation products are known, including CS_2 and ethylene thiourea (ETU), which is formed by metabolism but also appears as a manufacturing by-product.[44] The proposed mode of action of the fungicidal activity is based on disruption of several metabolic processes in fungi by interactions with amino acids, thiol-containing biomolecules or metals from metalloenzymes.[75,186] Due to the broad mechanism of action, it can be assumed that this class of fungicides acts non-specifically against fungi and may also affect other organisms and humans. In the 1980s, a relationship between MB exposure and the development of neurological symptoms in field workers was observed.[2,3,320] ETU exposure is associated with chronic effects such as thyroid issues and the risk of thyroid cancer.[81,82]

In vivo and *in vitro* studies revealed that MB exposure caused toxic effects similar to ionic Mn(II) overexposure. These include accumulation of Mn,[9,321] neurotoxic effects,[10,54,63,228] and alteration in the glutathione (GSH) antioxidant system[8,54] as a marker for oxidative stress.

Due to the fact that most toxicological studies of MB use the fungicide either as a formulation with various additives or pesticide standards, this study focused on the effect of pure-synthesized MB.[252] However, it has not yet been determined if the toxicity of MB is primarily caused by the fungicide itself, the released ionic Mn, the organic EBDC backbone, its degradation products or a combined effect. Therefore, this study addressed the toxicological effects of MB in comparison to $MnCl_2$, the trace element-free EBDC disodium salt Nabam (NB) and the major EBDC-metabolite ETU using the wild-type nematode *Caenorhabditis elegans (C. elegans)* as an *in vivo* model organism.

C. elegans is a transparent nematode that lives in organic-rich soils in temperate environments and is directly affected by applied pesticides. *C. elegans* has a rapid lifecycle and provides a self-fertilizing hermaphrodite with many offspring using *Escherichia coli* (*E. coli*) as a food source. *C. elegans* also features a fully sequenced genome with many homologs to the mammalian system.[204,317] For example, the nematode features genes involved in trace metal homeostasis and their transporters, allowing investigations into trace metal-induced toxicity.[322,323] Because of its numerous properties, the worm is a

popular model organism for studying neurotoxicity according to the 3 R-principle (refine, reduce, replace).[324,325] *C. elegans* features a nervous system with functionality similar to humans and, for example, also secretes neurotransmitters like dopamine (DA), serotonin (SRT), acetylcholine (ACh), gamma-aminobutyric acid (GABA), glutamate and others.[206–209,323] Thus, *C. elegans* is a popular model for studying neurotoxicity.

In this study, we investigated the acute toxic effects in *C. elegans* of each substance (MB, ionic Mn and the MB derived metabolites) and examined the bioavailability of the individual Mn species. Furthermore, the mechanisms underlying Mn and MB toxicity were examined, specifically focusing on oxidative stress and neurodegeneration.

6.2 Material und Methods

6.2.1 *Caenorhabditis elegans* strain and maintaince.

C. elegans wild-type (WT) N2 Bristol was obtained from the *Caenorhabditis* Genetics Center (CGC) (Minneapolis, MN, USA). Worm populations were cultivated on 8P plates seeded with the *E. coli* strain NA22 at 20 °C, as described by Brenner in 1974.[317] All experiments were performed in synchronized L1 stage larvae. According to standard protocols, age-synchronized worm populations were obtained using a bleach solution (1% sodium hypochlorite, 0.25 M NaOH). The released eggs were purified by centrifugation with a sucrose solution and worms were allowed to hatch overnight in M9 buffer.

6.2.2 Material and synthesis.

Manganese(II) chloride ($MnCl_2 \cdot 4H_2O$, 99.99% trace element basis) was obtained from Sigma-Aldrich. The fungicide MB was synthesized as previously published and characterized *via* elemental analysis, thermal gravimetric analysis, X-ray diffraction, X-ray absorption studies, and electron diffraction.[252] Ethylene thiourea (ETU) was supplied from Sigma Aldrich. Stock solutions of each substance were prepared immediately before each experiment. For $MnCl_2$, a 2 M stock solution in 85 mM NaCl was maintained at 4°C for up to 6 weeks, and the corresponding working solution was diluted fresh daily. The sodium-containing structural analog NB was synthesized as described in the supplementary material.[255]

6.2.3 Acute exposure.

For all experiments 60.000 synchronized L1 larvae were exposed in the absence of *E. coli* for up to 2 h at different concentrations in a volume of 6 mL (resulting in "worm

concentration" 10 k/mL). In the case of the water-insoluble fungicide MB, each concentration contained 2% dimethyl sulfoxide (DMSO, >99.8% p.a., Roth); therefore, a vehicle control with 2% DMSO was included in each experiment. Exposure intervals of 30 min and 2 h were chosen to investigate acute effects on L1 larvae. For some studies, 4.000 exposed L1 worms were transferred on nematode growth medium (NGM) plates coated with the *E. coli* strain OP50, allowing them to reach the L4 larvae stage.

6.2.4 Survival Assay.

Following treatment, nematodes were washed three times with 85 mM NaCl. The lethality of the substances was determined using the survival assay.[146] Approximately 30 to 40 L1 larvae per condition (in triplicate) were pre-counted and transferred to coated NGM plates. 48 h post-exposure, the number of surviving worms was scored as a percentage of the original worm count to evaluate the survival rate.

6.2.5 Measurement of Mn bioavailability.

Mn bioavailability of the species was determined in 60.000 L1 stage worms using inductively coupled plasma-optical emission spectrometry (ICP-OES) (Avio 220 Max, Perkin Elmer). The samples were homogenized on ice to prevent protein denaturation (3x freeze-thaw cycles and sonication (3 x 20 s, 1 cycle, 100% amplitude). After centrifugation (10 min, 10.000 rpm, 4 °C), an aliquot of the supernatant was collected for protein determination. Subsequently, the worm suspension was dried and then acid-assisted digested (HNO_3/H_2O_2, 1:1, suprapure® 65% nitric acid, 30% hydrogen peroxide, Merck) overnight at 95 °C. Ashed samples were re-suspended in 1 mL of 2% HNO_3 with Yttrium (10 µg/L, single element ICP standard, Roth) as internal standard and diluted 1:3 for ICP-OES measurements. The instrument settings were chosen as follows: plasma power 1500 W, plasma gas flow: 10 L/min, auxiliary gas flow 0.2 L/min, nebulizer gas flow: 0.70 L/min, pump flow rate: 1 mL/min, Wavelength: Mn 257.610 nm, Y 371.029 nm. An external calibration was prepared using a multi-element mix (Inorganic Ventures) for evaluation. Mn amounts were validated by measuring acid-assisted digested certified reference material (BCR-274, single cell protein, Institute for Reference Materials and Measurement of the European Commission, Geek, Belgium) and reference water (SRM-1640a, trace elements in natural water, National Institute of Standards and Technology, Gaithersburg, MD, USA).

6.2.6 Protein determination via bicinchoninic acid (BCA) assay.

All analytical data were normalized to protein content, including total Mn bioavailability, neurotransmitter, and GSH/GSSG levels. The protein amount was determined using the bicinchoninic acid (BCA) assay (Sigma Aldrich) with bovine serum albumin (Sigma Aldrich) (100 to 1000 µg/mL) as an external calibration standard. The BCA assay was performed according to standard protocols[326] and absorption was measured at 560 nm using a microplate reader (Infinite M Plex, Tecan).

6.2.7 Neurotransmitter quantification.

Neurotransmitter levels were quantified according to a method using LC-MS/MS and deuterated standards of DA, SRT, ACh, and GABA, which has been previously published.[70] 60.000 L1 worms were exposed to the respective compounds for 2 h and washed three times with 85 mM NaCl solution. 4000 L1 worms of each treatment condition were seeded on OP50 *E. coli*-coated NGM plates and allowed to reach the L4 larvae stage. L1 worms were immediately shock-frozen in liquid nitrogen and L4 stage larvae were pelleted after 48 h resting. Pellets were stored at -80 °C, and sample preparation was performed as described previously.

6.2.8 Carboxy-DCFH-assay for RONS measurement.

The formation of reactive oxygen and nitrogen species (RONS) was determined by a 6-carboxy-2',7'-dichlordihydrofluorescein-diacetate (carboxy-DCFH-DA)-based fluorescence emission assay.[146] A 50 mM carboxy-DCFH-DA stock solution in DMSO was prepared immediately before the experiment. 50.000 synchronized L1 worms were exposed to 500 µM carboxy-DCFH-DA for 1 h in the dark. After treatment, the worms were washed with M9 buffer and three times with 85 mM NaCl. Subsequently, 8000 L1 worms were transferred to each well in a 96-well plate and incubated with 350 µM *tert*-butyl hydroperoxide (*t*-BOOH) as a RONS generating positive control, different MB and $MnCl_2$ concentrations, as well as NB and ETU in triplicate. The cellular oxidation of carboxy-DCFH was monitored immediately (excitation: 485 nm, emission: 520 nm) by a microplate reader (Infinite M Plex, Tecan, Switzerland), and measurements were conducted every 30 min up to 4 h. Data were normalized to carboxy-DCFH-DA treated controls or, in case of MB, to the carboxy-DCFH-DA treated DMSO-vehicle controls.

6.2.9 GSH and GSSG quantification.

The total glutathione (GSH) and glutathione disulfide (GSSG) levels were evaluated according to a previously published method using N-ethylmaleimide (NEM) bound GSH as well as GSSG for external calibration.[327] Exposure of L1 worms was conducted as described in the neurotransmitter quantification section and samples were prepared as described.

6.2.10 Statistical analysis.

All data were analyzed and plotted using GraphPad Prism 6 (GraphPad Software, La Jolla, CA, USA). Data are shown as means with standard error of the mean (SEM). An unpaired *t* test with Welch's correction was used to compare concentrations and species to their respective controls.

6.3 Results and Discussion

6.3.1 Acute Toxicity.

Many studies indicate that MB has a toxic potential, especially its role in neurotoxicity and induction of oxidative stress is discussed.[8,11,63] Mn has also been attributed to cause impaired dopaminergic, glutamatergic, and GABAergic transmission, oxidative stress and mitochondrial dysfunction.[145] However, no direct comparison of MB, ionic Mn and the MB derived metabolites in one model organism were carried out with respect to toxicity. Therefore, as a first step, the toxicity of MB in *C. elegans* after acute exposure was compared with that of $MnCl_2$, NB, and ETU. Since commercially available pesticide standards can vary significantly in quality and the exact molecular structure of MB has just recently been reported, it was synthesized as previously published.[252] Previous studies either used MB in a formulation with other additives or pesticide standards. However, in order to specifically investigate the effect of the active ingredient, the existence of a pure substance is of critical importance. NB was also synthesized and obtained as a hexahydrate.[255]

The dose-response survival curve revealed significant toxic effects induced by MB. It decreased survival rates in a dose-dependent manner, with an LD_{50} (dose which is lethal for 50 % of a tested population) of approximately 0.6 mM after 2 h exposure (Figure 30). Compared to $MnCl_2$ with an LD_{50} of 5 mM, MB appears to be about eight times more toxic (Figure 30). These findings agree with an *in vitro* study comparing MB to several Mn species in PC12 rat pheochromocytoma cells [321].

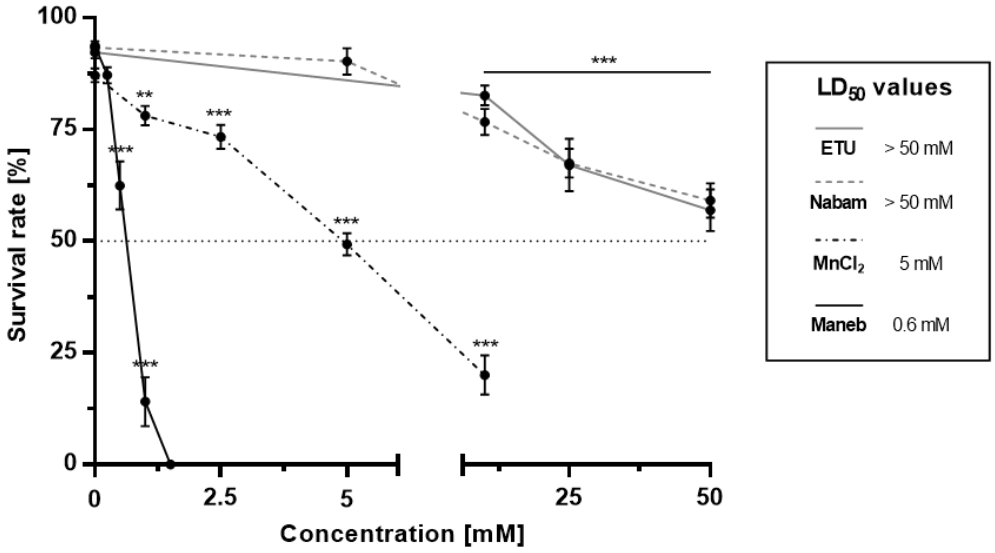

Figure 30: Dose-response curves following acute exposure for Maneb (MB). $MnCl_2$, Nabam (NB), and ETU. In the box the respective LD_{50} values are shown. N2 (wild-type, WT) worms were treated for 2 h at the L1 larvae stage with increasing concentrations of different compounds. Data are expressed as means ± SEM from at least four independent experiments (each experiment with three replicates). An unpaired t test with Welch's correction was used for the statistical analysis. Following p value summary was chosen: **p < 0.01, ***p < 0.001 compared to untreated control.

In contrast, the disodium salt NB and the primary metabolite ETU showed no significant effects in the same concentration range (0 to 5 mM). Both showed increased toxic effects only at concentrations greater than 10 mM, but even at the highest applied dose of 50 mM, a lethality of 50% was not reached. These effects are consistent with cytotoxicity results from the literature.[54,328] Since several studies have shown *in vitro* that MB exposure leads to higher cytotoxicity than NB, ETU, and $MnCl_2$, it was suggested that the complexed Mn in MB might be more bioavailable. Consequently, all subsequent experiments in this study were performed at subtoxic concentrations, including 0.1 mM and 0.25 mM for MB and 0.25 mM and 0.5 mM for $MnCl_2$ and their respective LD_{50} concentrations. In the case of NB and ETU, the subtoxic concentration of 5 mM was chosen as the highest concentration of the Mn-species range (5 mM).

6.3.2 Bioavailability of Mn.

To investigate if the increased lethality of MB might be the result of an increased bioavailability of Mn, the total amount of Mn in L1 stage worms after acute treatment was quantified using inductively coupled plasma-optical emission spectrometry (ICP-OES). Treatment with higher doses for both Mn species increased total Mn time- and concentration-dependent (30 min *vs*. 2 h, Figure 31 (**A**)). A comparison of the total Mn amount after 2 h exposure to a subtoxic concentration showed that the more toxic MB species accumulated to a lower extent than the less harmful $MnCl_2$ (Figure 31 (**B**)). For example, incubating 0.1 mM or 0.25 mM of MB for 2 h resulted in a 1.5-fold lower total Mn level than $MnCl_2$ at the same dose (Table 6). Thus, the data suggest an inverse relationship between toxicity and Mn bioavailability of the species.

Moreover, the total amount of Mn at the LD_{50} concentration was about five times higher in the case of $MnCl_2$ compared to MB. To determine if Mn is still present in the worms while aging, treated and non-treated L1 larvae were placed on NGM plates for 48 h post-exposure. Total Mn content in the L4 animals was also determined *via* ICP-OES but no difference was found compared to untreated control nematodes indicating an elimination of Mn once treatment ended (Figure S4). NB and ETU-treated samples were also quantified, but as expected, Mn levels were not altered (data not shown).

Bioavailability data of $MnCl_2$ are in agreement with data of Peres *et al.*, exposing L1 stage worms for 1 h.[329] Carmona *et al.* also observed an approximately 10-fold higher cytotoxicity of MB *in vitro* in PC12 rat pheochromocytoma cells compared to other Mn species. As in our study, no species-specific differences in Mn bioavailability was found.[321]

Based on the bioavailability results, it was concluded that the higher toxicity of MB may not be caused by overexposure to Mn alone. Therefore, more detailed mechanistic studies were performed.

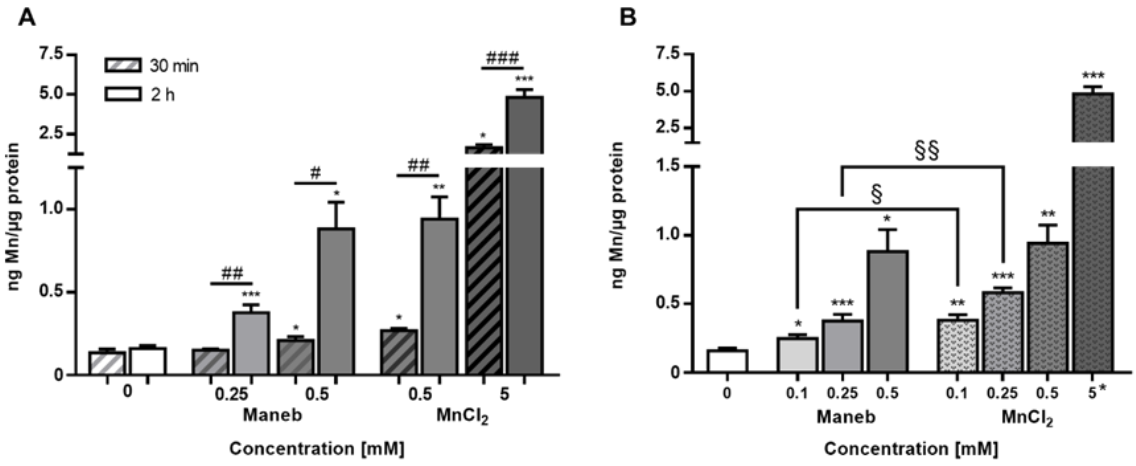

Figure 31: Mn contents following Maneb and $MnCl_2$ exposure (time- and concentration dependent). Total Mn amount (normalized to protein content) of wild-type worms (L1 larvae) following acute Maneb or $MnCl_2$ exposure at two different exposure times. Data are expressed as means ± SEM from at least three (30 min n = 3, 2 h: n = 5) independent experiments. (**B**) Species-specific effects. Total Mn amount (normalized to protein content) of wild-type worms (L1 larvae) following acute Maneb or $MnCl_2$ exposure for 2 h. Data are expressed as means ± SEM from at least five independent experiments. An unpaired t test with Welch's correction was used for the statistical analysis of the total Mn content. Following p value summary was chosen: *p < 0.05, **p < 0.01, ***p < 0.001 compared to untreated control and §p < 0.05, §§p < 0.01, compared to different species and #p < 0.05, ##p < 0.01, ###p < 0.001 compared to different exposure time.

Table 6: Total Mn content of *C. elegans* wild-type L1 worms measured with ICP-OES following 2 h incubation with the respective Mn species. Data are expressed as means ± SEM of at least five independent experiments. The individual LD_{50} dose is printed in bold. For control, a mean (n=26) was built of non-treated worms in 85 mM NaCl and non-treated worms with 2% DMSO as vehicle control.

	Concentration [mM]	**Total Mn ± SEM [ng Mn/µg protein]**	
Control	0	0.15 ± 0.01	x- fold of control
Maneb	0.1	0.25 ± 0.01	1.7 x
	0.25	0.38 ± 0.03	2.6 x
	0.5	**0.88 ± 0.15**	**6.0 x**
$MnCl_2$	0.1	0.38 ± 0.03	2.6 x
	0.25	0.58 ± 0.03	4.0 x
	0.5	0.94 ± 0.12	6.4 x
	5	**4.8 ± 0.4**	**33 x ***

6.3.3 Neurotransmitter quantification.

Neurotransmitters (NT) are essential for proper function of the neural system; even small changes in their homeostasis and equilibrium can significantly impact the signaling cascade. Alterations in NT homeostasis are associated with neurodegenerative diseases including Alzheimer's disease, Parkinson's disease (PD), or Huntington's disease.[330–332] First, no treatment-related changes in NT levels of L1 or L4 larval stage worms were observed at a concentration of 5 mM NB or ETU (Figure 32 **A-D**), Figure S22 **A-D**). An MB concentration of 0.5 mM (LD_{50}) leads to a significant decrease in DA, ACh, and GABA levels in L1 larvae compared to the untreated control (Figure 32 **A-D**). For comparison, exposure to $MnCl_2$ at the LD_{50} concentration (5 mM) did not lead to significant changes in DA, SRT or ACh levels at any concentration or larval stage (Figure 32 **A-C**, Figure S22 **A-D**). GABA levels were significantly decreased at 5 mM $MnCl_2$ in L1 larvae (comparable to the LD_{50} of MB) (Figure 32 **D**). However, after MB exposure the NT level alteration is rather acute since no more long-lasting effects are evident 48 post-treatment in the L4 stage worms (Figure S22 **A-D**).

Epidemiological data prove that MB exposure is associated with a higher risk of Parkinson's disease (PD), especially when exposure occurs at a younger age.[52] Mancozeb (Mn and Zn containing EBDC fungicide) exposure during pregnancy is associated with adverse neurodevelopmental effects in children living near banana plantations in Costa Rica.[51,333] Many assumptions have been made about the loss of dopaminergic neurons for the underlying mechanism of action and the neurotoxic potential of MB. The underlying mechanisms are still poorly understood. Two *in vitro* studies[58,59] demonstrated decreased aldehyde dehydrogenase (ALDH) activities after MB exposure. ALDHs detoxify many reactive aldehydes generated during metabolism or by xenobiotics [334]. The dopamine monoamine oxidase (MAO) metabolite 3,4-dihydroxyphenylacetaldehyde (DOPAL), which is detoxified by ALDH, is even in physiological concentrations known to be selectively neurotoxic in dopaminergic neurons targeting the mitochondria. ALDH dysfunctions are associated with dopaminergic neurodegeneration and the pathogenesis of PD, which is characterized by the loss of dopaminergic neurons in the substantia nigra and the presence of α-synuclein aggregation.[69]

Mesencephalic cells exposed to MB showed decreased cellular uptake of ^{3}H-labeled DA and ^{14}C-labeled GABA in a dose-dependent manner.[54] The underlying principle is based on the fact that irreversible neuronal damage is associated with impaired NT uptake.[335] Domico

et al. also investigated the effect of the other species NB, $MnCl_2$ and ETU. $MnCl_2$ and ETU exposure in the same concentration range did not alter the DA and GABA uptake; only higher $MnCl_2$ concentrations resulted in decreased DA uptake. At higher applied concentrations than MB, NB exposure also leads to reduced uptake of both neurotransmitters [54]. A few studies also investigated the neurotoxic effects of the Mn and Zn-containing EBDC fungicide Mancozeb (MZ) in *C. elegans.*[32] Experiments showed dopaminergic neurons are most vulnerable to MZ toxicity[336] but also GABAergic neurons seem affected by MZ exposure.[56]

Carbamates such as the insecticide aldicarb are known for reversibly inhibiting Acetylcholinesterase (AChE). A similar effect is suspected for dithiocarbamates.[61] AChE inhibitors usually lead to an initial elevation in synaptic ACh levels since it is not enzymatically cleaved into choline and acetate. Elevated ACh levels cause hyperexcitability and paralysis.[71] On the other hand, low ACh levels are associated with Alzheimer's disease due to reduced activity of cholinergic neurons. Here, AChE inhibitors are used to increase ACh levels in the brain and prevent damage to neurons due to loss of ACh.[337]

NB was generally expected to generate similar effects as a structural analog of MB since both species contain the EBDC backbone. NB is *in vivo* partly metabolized to ETU and about 25 % is excreted *via* urine [338]. During EBDCs metabolizing to ETU, other metabolites such as CS_2 or metal sulfides may be produced, but unmetabolized MB and NB are still present. CS_2 exposure displays many adverse effects, including thyroid disruption, neurotoxicity, and cardiotoxicity.[65] However, no alteration was detected in NT levels after NB exposure (Figure 32 **A-D**, Figure S5 **A-D**). One noticeable difference between the disodium EBDC salt NB and MB is the replacement of Mn^{2+}-ion with two Na^{+}-ions. Moreover, the EBDC ligand acts as monodentate ligand toward Na^{+} ions,[27] while EBDCs in the presence of divalent d-block cations, such as Mn^{2+}, act as bidentate chelate ligands.[18] In contrast to MB, which is only soluble in coordinating solvents such as DMSO or dimethylformamide, NB is highly water soluble. Although both EBDC complexes were synthesized in water, the co-crystallizing water molecules of MB are not bound to Mn.[252] Since the Mn ion prefers soft donor ligands one can assume that when MB enters a biological system, it interacts with sulfur functionalities of cellular molecules including proteins or enzymes.[186] Furthermore, MB might be more stable than usually assumed in the literature and therefore the toxicological effects might be more related to intact MB rather than its degradation products.

Due to the significant differences in the toxicity of MB and NB, Mn has a considerable influence on the toxicity of MB. However, this Mn-related impact seems to exist only in combination with the organic backbone. Many studies concluded that the mechanism of action is affected by the ability of the ligand to control the reactivity of the metal.[186] Chronic overexposure of Mn (in the ionic form) can lead to neurodegenerative damage with symptoms similar to Parkinson's disease, termed 'manganism.' The underlying mechanism is not yet fully understood, but it is assumed that Mn accumulates in the brain region substantia nigra and leads to the loss of dopaminergic neurons.[76] However, only GABA levels decreased in L1 worms after $MnCl_2$ treatment (Figure 32 **D**). Mn complexed to EBDC ligands becomes more lipophilic, implying permeability through cellular membranes.[186] In addition, another difference in the mechanism of action of the two Mn species might be a different oxidation state since the Mn(II) ions may be oxidized in the cellular environment. Thus, Mn can act as a redox cycler and induce the formation of reactive oxygen and nitrogen species (RONS), resulting in oxidative stress.[121]

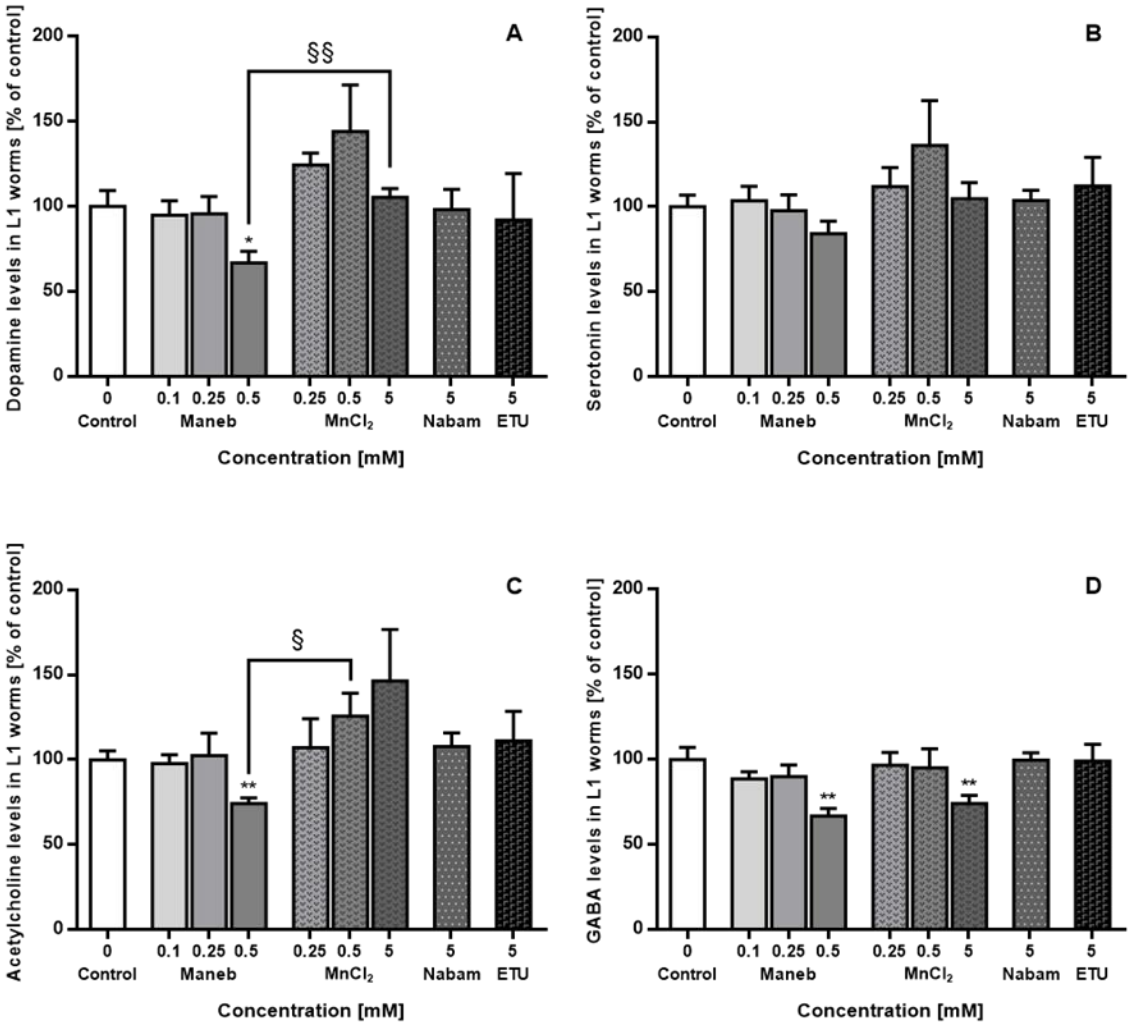

Figure 32: Neurotransmitter levels [dopamine (**A**), serotonin (**B**), acetylcholine (**C**), GABA (**D**)] measured with LC-MS/MS normalized to protein content and normalized to respective control of wild-type worms (L1 larvae) following acute exposure for 2 h. Data are expressed as means ± SEM from at least three independent experiments. An unpaired *t* test with Welch's correction was used for the statistical analysis. The following p-value summary was chosen: *p < 0.05, **p < 0.01 compared to respective untreated control, and §p < 0.05, §§p < 0.01 compared to the same concentration with different species.

6.3.4 Reactive oxygen and nitrogen species (RONS) formation.

Oxidative stress is the imbalance between reactive species generated by metabolic processes and antioxidant capacity.[339] Increased amounts of reactive oxygen and nitrogen species (RONS) are associated with several neurodegenerative diseases. However, it is still unclear if RONS are a primary cause or a consequence in the pathogenesis.[72] Formation of RONS in *C. elegans* was detected during exposure using the fluorescence dye Carboxy-DCFH-DA. RONS exceeding the homeostatic range can cause oxidative stress and cellular damage, especially oxidizing large biomolecules, like lipid membranes, enzymes or desoxyribonucleic acid (DNA).[340] After 30 min exposure MB showed a slightly increased fluorescence emission, corresponding to the induction of RONS at higher MB concentrations. (Figure 33 (**A**)). However, $MnCl_2$ showed no effect at the same concentration (0.5 mM), although bioavailability data revealed similar Mn amounts at concentrations of 0.5 mM compared to both Mn species. After 2 h exposure, the observed trend is identical but except for *t*-BOOH, the level of RONS did not increase compared to the 30 min exposure time (Figure 33 (**B**)). This may be explained by activating an intracellular stress response, resulting in regulation or detoxification processes.

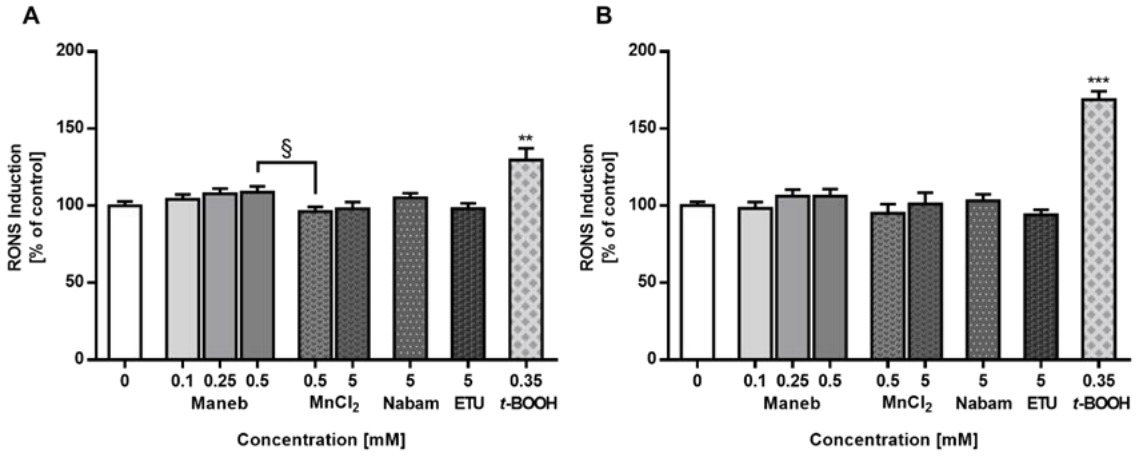

Figure 33 Fluorescence emission intensity normalized to respective control of wild-type worms (L1 larvae) after 30 min acute exposure to the individual species. 0.35 mM *t*-BOOH was used as a positive control. Data are expressed as means ± SEM from at least three independent experiments. **(B)** Fluorescence emission intensity normalized to respective control of wild-type worms (L1 larvae) after 2 h acute exposure. 0.35 mM *t*-BOOH was used as a positive control. Data are expressed as means ± SEM from at least three independent experiments. An unpaired t test with Welch's correction was used for the statistical analysis. The following p-value summary was chosen: *$p < 0.05$, **$p < 0.01$ compared to respective untreated control, and §$p < 0.05 <$ compared to the same concentration with different Mn species.

Other studies indicate that exposure to higher $MnCl_2$ concentrations (> 5 mM) in *C. elegans* leads to slightly increased RONS levels after 2 h in L1 larval stage.[146] For MB no data regarding the formation of RONS are available in *C. elegans*. However, in human neuroblastoma cells[63] MB exposure leads to a concentration-dependent induction of RONS and similar effects were observed after MZ exposure in mesencephalic cells.[55]

6.3.5 GSH and GSSG quantification.

Oxidative stress is a synonym for the imbalance between reactive species produced by the influence of oxygen and the antioxidant protection systems.[339] Since more RONS are generated by MB treatment, the other side of the equilibrium was examined. As a marker for antioxidant capacity the total levels of GSH and GSSG in worm lysates were quantified to determine if MB is affecting the oxidative state as hypothesized. The endogenously synthesized thiol GSH is present in all cells and has many physiological functions, such as its involvement in the antioxidant defense system.[72] MB exposure significantly increased the total GSH levels in L1 stage worms after 2 h exposure in a dose-dependent manner compared to DMSO-treated controls. A maximal increase of total GSH (200%) was observed for the MB LD_{50} concentration (Figure 34 **A**). However, exposure to any other investigated species did not increase GSH levels. Considering the GSSG levels, the effect of MB becomes even more apparent, as a 10-fold increase (0.5 mM Maneb) was observed compared to the DMSO-treated vehicle control (Figure 34 **B**).

MB is thought to interact with thiol groups and might be able to modify protein side chains.[11,75] In a previous *in vitro* study, cells treated with Maneb for 1 h resulted in highly elevated GSSG levels. However, GSH levels were decreased at lower MB concentrations and did not change at a higher MB concentration compared to the control.[62] In contrast, in mesencephalic cells an increased level of GSH after Maneb exposure was found, but no changes in the GSSG levels.[8] No changes in GSSG levels in the study by Barlow *et al.* could be due to the lack of sensitivity of fluorescent dye-based methods for GSSG quantification. In our study, we were able to detect GSSG levels in the picomolar range. Therefore, we could show in this study, that MB is causing oxidative stress, whilst this could not be observed in the other tested species.

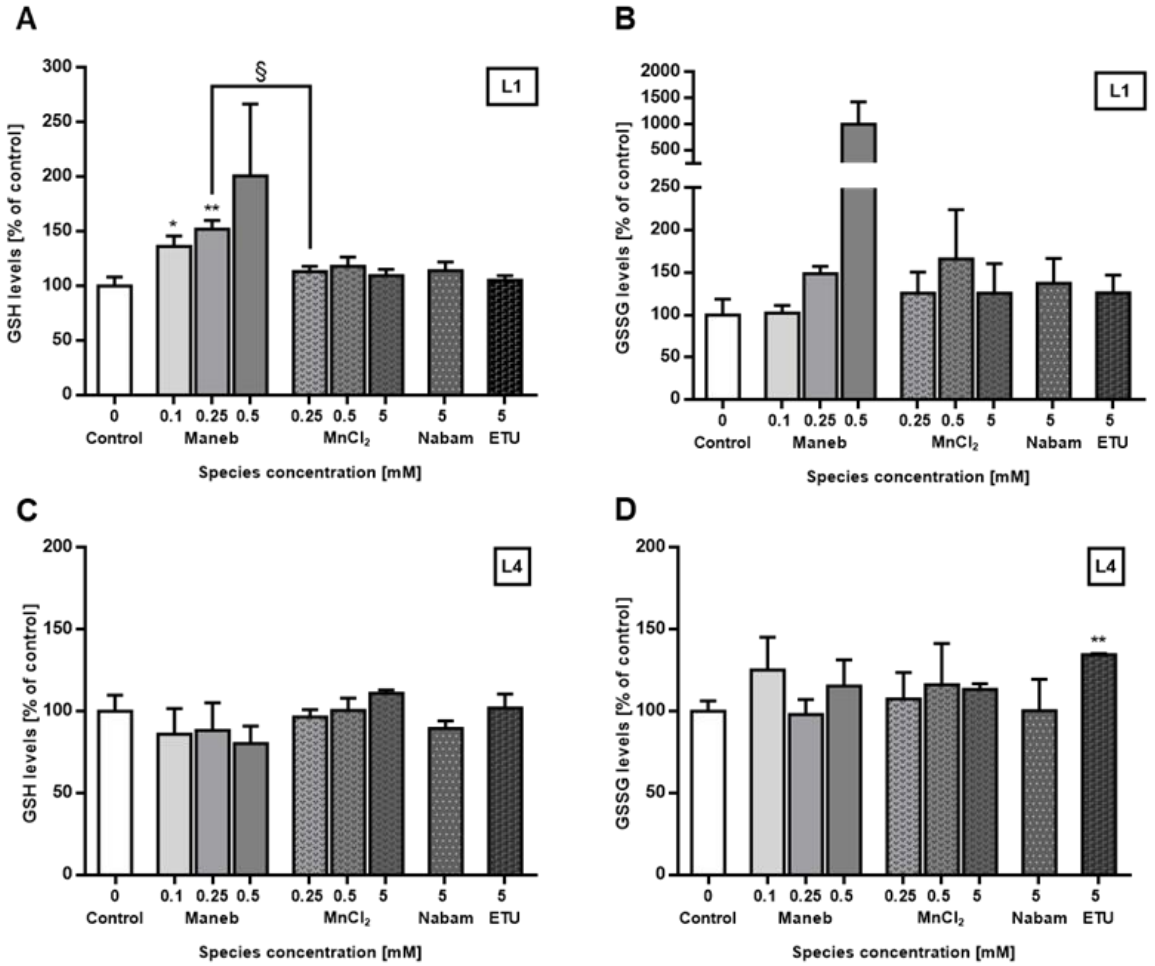

Figure 34: **(A)** GSH amount measured with LC-MS/MS as GSH-NEM adduct normalized to protein content and normalized to respective control of wild-type worms (L1 larvae) following acute exposure for 2 h. **(B)** GSSG amount measured with LC-MS/MS normalized to protein content and normalized to respective control of wild-type worms (L1 larvae) following acute exposure for 2 h. **(C)** GSH amount normalized to protein content and normalized to respective control of wild-type worms (L4 larvae) following acute exposure for 2 h in L1 larvae stage and 48 h rest on NGM plates. **(D)** GSSG amount normalized to protein content and normalized to respective control of wild-type worms (L4 larvae) following acute exposure for 2 h in L1 larvae stage and 48 h rest on NGM plates. Data are expressed as means ± SEM from at least three independent experiments. An unpaired *t* test with Welch's correction was used for the statistical analysis. The following p-value summary was chosen: *$p < 0.05$, **$p < 0.01$ compared to respective untreated control, and §$p < 0.05$ compared to the same concentration with different species.

6.4 Conclusion

Maneb is often used as a part of resistance management strategies and is widely applied in Brazil, India, and China as a multi-site fungicide. However, epidemiological studies indicate an increased risk of neurodegenerative diseases associated with fungicide

exposure, including Maneb. Since Maneb is postulated to degrade into several products under physiological conditions, this study aimed to learn more about the underlying mechanism through a direct comparison of the different species in one organism. By using batches of our in-house synthesized pure Maneb, we could ensure that the effects of the fungicide were not caused by any impurities or additives which may be present in commercial products. This study showed that although Mn in Maneb is slightly less bioavailable than in $MnCl_2$, Maneb is about eight times more toxic in *Caenorhabditis elegans*. For Maneb as underlying mechanisms of toxicity, oxidative stress and neurotoxicity could be identified. Neither $MnCl_2$ nor the metabolites of Maneb such as ETU could be identified as being responsible for Maneb toxicity. The structural analog of Maneb, the disodium salt Nabam, was significantly less toxic and caused no changes in glutathione or neurotransmitter levels. The ligand-controlled metal reactivity plays a critical role in the mechanism of neurotoxicity. Thus, the toxicity appears to be a combined effect of the organic backbone and the coordinated Mn ion.

6.5 Funding

This work was supported by the DFG Research Unit TraceAge (FOR 2558, BO4103/4-2).

6.6 Acknowledgements

We thank the Caenorhabditis Genetics Center (CGC), funded by the NIH Office of Research Infrastructure Programs (P40 OD010440), for providing the *C. elegans* wild-type strain used in this work.

6.7 CRediT author statement

Laura Kubens: conceptualization, methodology, formal analysis, investigation, data curation, writing – original draft, visualization. **Ann-Kathrin Weishaupt:** conceptualization, writing – review & editing. **Isabelle Rohn**: writing – review & editing. **Fabian Mohr**: conceptualization, writing – review & editing, supervision. **Julia Bornhorst:** conceptualization, writing – review & editing, supervision, project administration, funding acquisition. All authors have read and agreed to the published version of the manuscript.

Chapter 7 – Further Studies using the model organism *Caenorhabditis elegans*

Chapter 7 – Further Studies using the model organism *Caenorhabditis elegans*

7.1 Introduction

For conducting toxicity studies using *C. elegans*, it is crucial to ensure the availability of the target species in a suitable form for the nematodes. Common methods for toxicity assessment using the worm involve either incubation on plates or in solution. During plate incubation, inactivated *E. coli* is typically enriched with the target species and spread onto agar plates. The worms are then exposed to the tested species for up to 48 hours. The *E. coli* should be inactivated (heat treatment), to prevent the metabolism of the species being studied. During incubation in solution, the worms are exposed for shorter periods, usually in the absence of food. The established exposure setup for Maneb and its limitation will be explained in the following section.

Insights derived from the data presented in Chapter 6 indicate that the mechanism behind Maneb-induced toxicity involves both the ligand and Mn, as neither Mn-ions alone nor Nabam or ETU exhibit comparable effects. Children living near banana plantations in Costa Rica, which are subjected to aerial Mancozeb spraying, exhibit neurological abnormalities in development. These observed effects correlate with elevated Mn levels in hair or blood and ETU levels in urine.[51,52] Given that Mn and ETU are primary metabolites and degradation products of Maneb, investigating the impact of a combined Mn and ETU exposure becomes crucial in determining whether this combination contributes to enhanced toxicity of Maneb compared to the other species. Furthermore, to investigate the influence of the trace elements within the dithiocarbamates, the zinc-containing EBDC Zineb was examined in comparison to zinc sulfate. Zineb is reported to be less toxic than Maneb.[341,342]

The neurotoxic potential of Maneb has been demonstrated in many studies.[9,54,55] Maneb exposure in *C. elegans* results among others in decreased neurotransmitter levels as shown in Chapter 6. However, this effect is observed only in L1 larvae, immediately after exposure. However, at 48 h post-exposure neurotransmitter levels in L4-stage worms returned to untreated control level, implying a reversibly impact on the neurotransmitter homeostasis. Thus, the *C. elegans* mutant strain BY200 was selected to determine the morphology of dopaminergic neurons in L1- and L4-stage. To identify neurodegenerative characteristics and to validate the assay, a positive control using the LD_{50} concentration of 6-hydroxydopamine (6-OHDA) was included.

7.2 Materials and Methods

7.2.1 *C. elegans* strains and maintaince.

The *C. elegans* wild-type (WT) and BY200 strain (vtls1 [Pdat-1::GFP; rol-6], roller phenotype rarely detectable) were obtained from the *Caenorhabditis* Genetics Center (CGC) (Minneapolis, MN, USA). Handling and maintenance of the worm population was conducted as described in Chapter 6.

7.2.2 Materials.

Manganese chloride ($MnCl_2 \cdot 4H_2O$, 99.99% trace element basis) and Zinc sulfate ($ZnSO_4 \cdot 7H_2O$, 99.99% trace element basis) were obtained from Sigma-Aldrich. The fungicides Maneb and Zineb were synthesized as previously published[252] or described in Chapter 4. Ethylene thiourea (ETU) was supplied from Sigma Aldrich. Stock solutions of each substance were prepared immediately before each experiment. A 2 M $MnCl_2$ and a 1 M $ZnSO_4$ stock solution in 85 mM NaCl was maintained at 4°C. The corresponding working solution were diluted fresh daily. 6-hydroxydopamine was obtained from Sigma-Aldrich.

7.2.3 Exposure.

The exposure was conducted as described in Chapter 6. During the development of the "upscaling" exposure, experiments were carried out using 50,000 L1-stage worms in a volume of 0.5 mL (=100,000/mL).

7.2.4 Survival Assay and Bioavailability.

Survival assay and bioavailability measurements via ICP-OES were also performed as previously described in Chapter 6.

7.2.5 Fluorescence microscopy.

The BY200 strain was exposed for 2 h during L1 larval stage according to the described exposure procedure. For imaging both larval stages (L1 and L4-stage), worms were carefully transferred onto 4% agarose pads and anesthetized with 5 mM Levamisole. Therefore, 10 µL of a 5 mM Levamisole solution and 2-5 µL of a L1 worm suspension or 30-40 L4-stage worms were applied on an agarose pad.

Images were acquired using a Leica DM6 B Fluorescence Microscope equipped with a x63 magnification objective. Fluorescence images were captured with excitation at 460-500 nm and an emission range of 512-542 nm. The following parameters were selected: For L1 worms using the 63x magnification objective: 500 ms exposure time for both modes. For L4 worms using the 63x objective: 750 ms brightfield, 275 ms fluorescence. A series of z-stacked (20 steps) was obtained by optical sectioning at approximately 0.5 µm intervals. Images were processed and edited using the thunder function (small volume computational cleaning, adaptive strategy (water)) of the LAS X (Leica) software. This procedure aimed to obtain blur-free detailed overlays. For evaluation following scoring system was chosen: 1 = no alterations visible, 2 = irregular dendrites (kinks, bends), 3 = blebbing[343] ("beads on a string"), 4 = loss of dendrites or/and shrunken soma, 5 = loss of dendrites or/and loss of soma.

7.3 Results and Discussion

7.3.1 Establishment of an exposure setup for fungicides and metals

$MnCl_2$ incubation in L1-stage worms was conducted as described in the literature.[146,223] Data obtained from 30 min exposure to Mn(II) are in agreement with published lethal doses.[146] While this method is generally suitable for water-soluble compounds, its implementation encountered difficulties when dealing with Maneb. The EBDC-based fungicides Maneb and Zineb are exclusively soluble in DMSO, but the nematode can only tolerate up to 2% dimethyl sulfoxide (DMSO) in 85 mM NaCl without having adverse effects.[344] However, Maneb becomes insoluble and precipitates in water containing 2% DMSO at concentrations exceeding 2.5 mM. 30 min exposure to Maneb resulted in an LD_{50} in L1-stage worms of approximately 2.5 mM. Given that this concentration nears the solubility limit of Maneb and therefore may interfere ICP-OES measurements, the exposure interval was extended from 30 min to 2 h for all experiments in this study.

The bioavailability data presented in Chapter 6 demonstrated a time-dependent Mn concentration in L1-worms, quantified using ICP-OES (Figure 31). Not only the Mn bioavailability was shown to be time-dependent, also the lethality was increased from the LD_{50} concentration 10 mM (30 min) to 5 mM (2 h) (Figure 35).

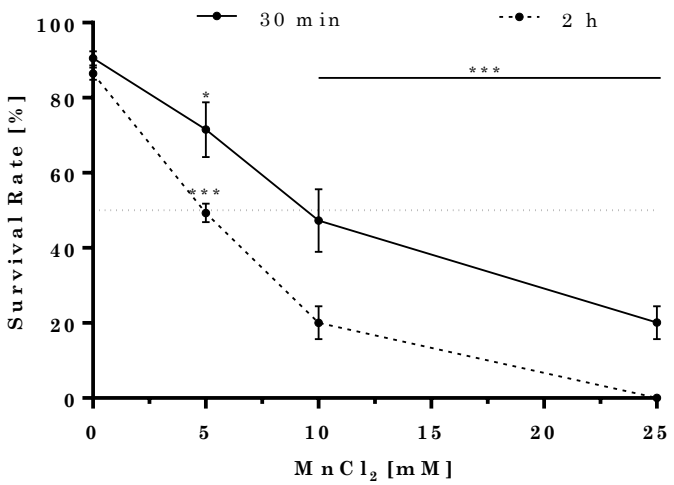

Figure 35: Time-dependency of the dose-response curve of *C. elegans* wild-type exposed to $MnCl_2$ for 30 min or 2 h. Data are expressed as means ± SEM from at least three independent experiments. An unpaired t test with Welch's correction was used for statistical analysis. Following p value summary was chosen: * < 0.05, *** < 0.001 compared to untreated control.

The survival assay was conducted using 5,000 worms per 0.5 mL tube (equivalent to 10,000/mL). However, for assessing the bioavailability, larger number of worms are required due to the ICP-OES and BCA-assay detection limits. To accommodate this requirement, 50,000 worms were treated within a final volume of 0.5 mL (resulting in a concentration of 100,000 worms/mL). However, incubating 50,000 worms in the same volume as before yielded a reproducible shift in the LD_{50} concentration of $MnCl_2$, observed in the survival assay (Figure 36 left). Conversely, incubating the identical worm number in 5 mL (= 10,000 worms/mL) for 30 minutes, resulted in outcomes consistent with the preceding observations.

There is no explanation for this phenomenon yet, since the $MnCl_2$ concentration remained constant. The only factors that underwent alteration were the quantity of available Mn per worm and the "density" of worms. To determine whether the worms exhibit a reduced Mn uptake, the total Mn amount was measured via ICP-OES. Interestingly, there were no differences in the total Mn amount of the two different worm counts (10k vs.100k/mL). To put that in context, worms with lower toxic response exhibit a similar total Mn content per µg protein (Figure 36).

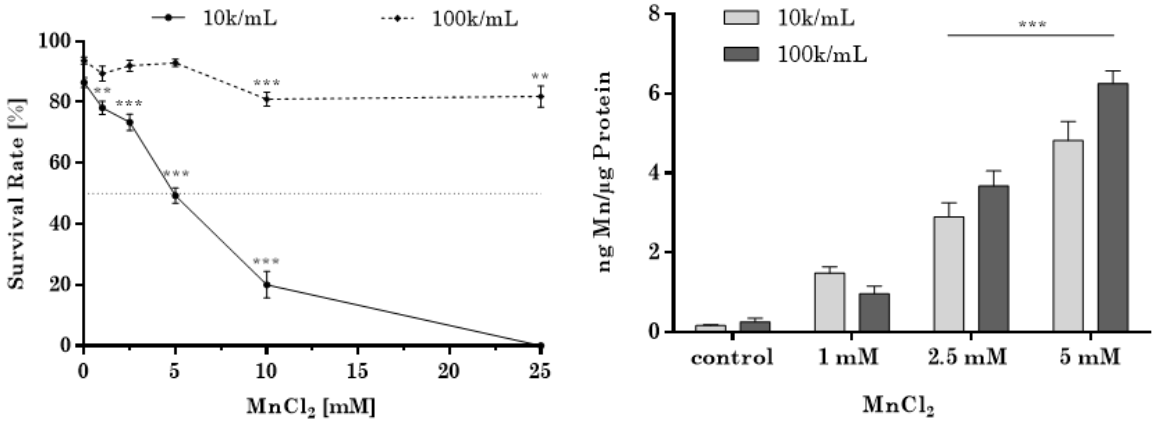

Figure 36: Effect of the worm-to-volume-ratio on the lethality and total Mn amount in L1 worms. *C. elegans* wild-type L1-stage worms were treated for 2h. Data are expressed as means ± SEM from at least three independent experiments. An unpaired t test with Welch's correction was used for statistical analysis. Following p value summary was chosen: ** < 0.01, *** < 0.001 compared to untreated control.

However, subsequent to the fluorescence measurement during the carboxy-DCFH assay, the exposed worms were assessed for any abnormalities under the microscope in the 96-well plate. L1-worms exposed to 5 mM $MnCl_2$ displayed a tendency to aggregate, exhibiting an "attachment to particles" behavior. The carboxy-DCFH assay was performed using 8.000 worms in a final volume of 100 µL (80,000/mL) per well, making the experimental setup comparable to the high worm-to-volume ratio. One plausible hypothesis is that Mn(II) might undergo metabolic transformations, potentially involving oxidation processes, resulting in species that may precipitate. Consequently, the bioavailability assessment of the 100,000 worms/mL samples could potentially yield false-positive outcomes due to the measurement of attached Mn on the worm cuticle. This could also account for the reduced Mn toxicity, as precipitated Mn species might have limited bioavailability. In general, Mn is predominantly found in biological systems in oxidation states +II and +III.[124] In the +III oxidation state, Mn is encountered in forms such as Mn-citrate or bound to transferrin. On the other hand, Mn(III) is also known for undergoing disproportionation to Mn(II) and Mn(IV), while Mn(IV) typically forms precipitates like oxides.[345] However, the analytical characterization of Mn species is challenging due to their instability and low quantities. Michalke *et al.* has found eleven distinct Mn species in liver extracts using various combined analytical techniques.[345] This underlines the complexity of the nature of Mn species and their excretion. It's important to emphasize that this "particles-attaching-phenomenon" was only observed at the high worm-to-volume ratio (100k/mL) and not at

lower worm numbers (10k/mL) or in the absence of worms. All subsequent assays were therefore performed by exposing 60,000 worms in 6 mL.

7.3.2 Influence of the metal on the toxicity of EBDC fungicides

In this study Zineb serves as a structural analog of Maneb. Distinct from the water-soluble disodium salt Nabam, Zineb shares the characteristic of insolubility in water and contains the trace element Zn, integrated within a polymeric network. However, the published structures of Maneb[252] and Zineb[28] have already demonstrated differences in their coordination modes. Despite these structural variances, the aim was to focus on the impact of the contained trace element on the toxicity of EBDC fungicides. Several studies indicated that Zineb demonstrates relatively lower toxicity compared to Maneb.[341,342]

To investigate if these findings can be confirmed in *C. elegans*, L1-stage wildtype worms were exposed to Zineb and $ZnSO_4$. The LD_{50} for Zn(II) is approximately 1 mM (Figure 37), which is fivefold lower than that of Mn(II). Setting aside species-specific effects, this observation implies Zineb to be more toxic than Maneb. However, Zineb in 2% DMSO/ NaCl solution begins to precipitate even at concentrations as low as 0.5 mM. Despite this, concentrations ranging up to 5 mM were examined, but no lethality was evident (Figure 37). This lack of effect might be attributed to the inaccessibility of the precipitates for L1-stage worms. Concentrations below the solubility threshold were tested in small steps (inlet of Figure 37) to avoid any precipitations, but also exhibited no toxicity. Consequently, determining the LD_{50} of Zineb using the experimental framework designed for Maneb was not successful. However, a direct extrapolation between Mn(II)- and Zn(II)-salts to the corresponding fungicides is not possible. Otherwise, Zineb-induced lethality should have emerged at concentrations above 0.1 mM (Maneb LD_{50}, 2 h, L1-worms 0.5 mM).

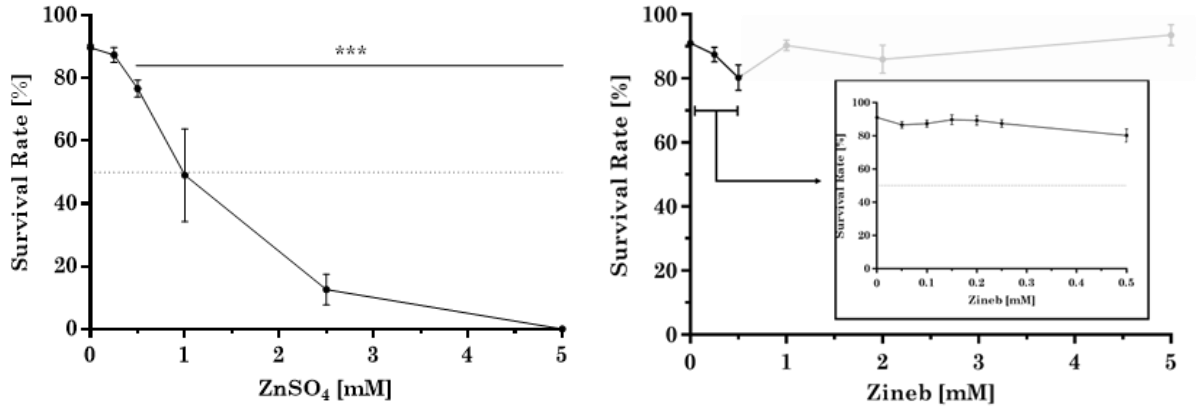

Figure 37: Dose-response curves following acute exposure to $ZnSO_4$ (left) and Zineb (right). *C. elegans* wild-type L1 worms were treated for 2h. Since Zineb starts to precipitate at concentrations above 0.5 mM, concentration below 0.5 mM were also tested. Data are expressed as means ± SEM from at least three independent experiments. An unpaired t test with Welch's correction was used for statistical analysis. Following p value summary was chosen: *** < 0.001 compared to untreated control.

One approach to address the solubility limitation of Zineb could involve extending the exposure interval. The L1-stage worm can be incubated for up to 4 hours without any consequences.[346] However, considering the stability results of Zineb in section 4.3.3, after 4 hours in DMSO, ETU is already formed as a sign of degradation. Given that this study aimed to investigate the species-specific effects, this approach was not continued, but should be addressed in future studies.

7.3.3 Dopaminergic neuron morphology in Maneb-induced neurotoxicity

Neurotoxic effects of Mn-containing dithiocarbamate fungicides have been observed *in vivo*[8], *in vitro*[9,54,55] and in humans.[3,51,52] The immediate impact of Maneb on neurotransmitter levels of DA, SRT and GABA in *C. elegans* upon incubation in the L1-larval stage was demonstrated in Chapter 6. However, no differences in neurotransmitter levels were observed compared to the untreated control after a resting period of 48 h to reach the L4-stage. Therefore, this study aimed to explore potential persisted morphological changes in dopaminergic neurons in both larval stages following Maneb exposure in L1-stage.

For this purpose, the *C. elegans* BY200 strain was used, allowing the visualization of all three classes of dopaminergic neurons (CEP, ADE, PDE) in the hermaphrodite, due to GFP-expression in DAT-1.[206,347] The dopamine transporter (DAT) is a protein responsible for reuptake of the neurotransmitter dopamine from the synaptic cleft into the cytosol of a nerve cell. This process is sodium-dependent, leading to the transport of two sodium ions and one chloride ion alongside each dopamine molecule, which is why the dopamine reuptake is controlled by a sodium/potassium ATPase.[348] In human DATs are prominently expressed in dopamine rich brain areas such as the *substantia nigra*, particularly within the axonal membranes of the nigrostriatal dopaminergic neurons.[349] Analogously, in *C. elegans*, there is a highly DAT-1 expression within the CEP dendrites, which enables to study not exclusively the cell body (soma) but also the morphology of their processes, the dendrites.[210] Dendrites are extensions of neurons that provide a large surface area for receiving, processing, and transmitting signals to the cell body, while axons are sending signals to other cells.[350,351]

To ensure the identification of any morphological changes, a positive control was also included. 6-hydroxydopamine (6-OHDA) was used as a proven neurotoxicant due to its structural similarity to dopamine.[210] 6-OHDA is also of particular interest because it was discovered in brain and urine samples of Parkinson's disease (PD) patients, suggesting its role as endogenous factor in the pathogenesis of PD.[352,353] Nass *et al.* (2002) demonstrated that 6-OHDA specifically targets dopaminergic neurons.[210]

Figure 38 displays L1-stage worms immediately after treatment, showing exemplary distinctive features observed during microscopic analysis. In L1-stage worms, the anterior deirids (ADE) processes (dendrites) and the posterior deirids (PDE) are not yet observable, as they develop between the first and second larval stage.[206] In Figure 38 **A** all four cephalic sensilla (CEP) dendrites of the untreated control worm are visibly intact. The ADE neurons are well observable, while the four CEP neurons are less distinguishable due to their emission intensity. However, overexposure of the soma is required, as the fine dendrites would otherwise not be observable, especially in neurodegenerative processes. Figure 38 **B** represents a L1-stage worm treated with 0.5 mM Maneb. Here only one of four CEP dendrites is visible, and all four CEP neurons emit less intense compared to the untreated control. The worm exposed to 5 mM 6-OHDA (Figure 38 **C**) serves as a positive control and displays also frequently occurring abnormalities which were classified in different groups and summarized in Figure 39. One of the dendrites shows the so called “blebbing”

phenomenon, which can be described as "beads on a string"[343] (Figure 38 **C**). Blebbing is a characteristic of dendrite degeneration.[354] However, this process is not always irreversible, as dendrites can also regenerate up to a certain threshold.[355] Bijwadia *et al.* (2021) introduced system for evaluating the progression of neurodegeneration with focus on all four CEP dendrites.[356] The scale categories abnormalities and ranges from no damage, through kinks, blebs to complete dendrite breakage and removal. Upon microscopic examination, it was observed that not only the dendrites experienced adverse effects, but also the cell bodies displayed indications of neurodegeneration, for example a reduced soma size. Due to these findings, a modified scoring system for evaluation of morphological abnormalities in dopaminergic neurons of L1- and L4-stage worms was developed and took different published methodologies into account.[357]

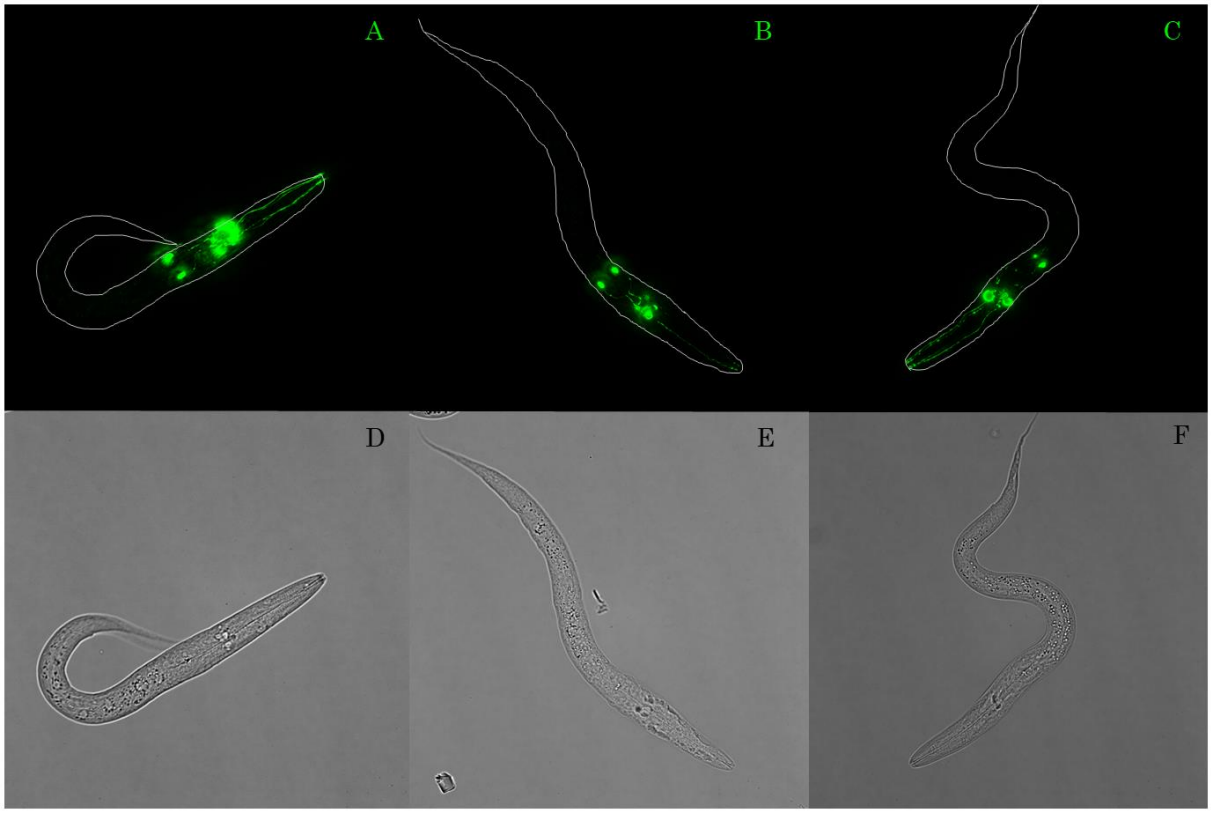

Figure 38: Visualization of the six dopaminergic neurons (CEP and ADE), which are already developed in the L1 worm using the BY200 (pDAT-1::GFP) *C. elegans* strain. Worms were exposed for 2 h in L1-stage to evaluate the morphology of dopaminergic neurons. Shown are combined z-stacked (20 steps) fluorescence images of different conditions: untreated control (**A**), treatment with 0.5 mM Maneb (**B**) a positive control using 6-OHDA (**C**) and their respective brightfield images (**D-F**).

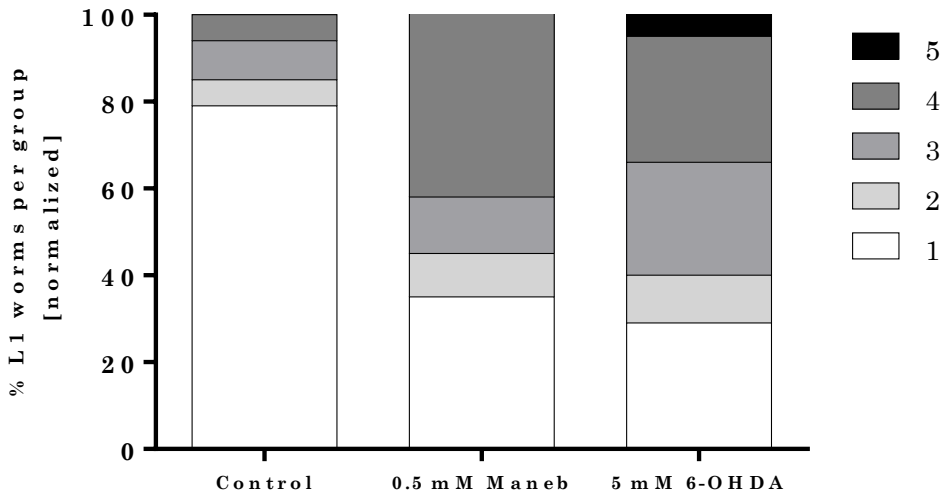

Figure 39: Percentage distribution of L1 worms allocated to individual groups (1-5), with each condition normalized to the corresponding total worm count (approximately 30 worms were evaluated for each condition). *C. elegans* BY200 strain was exposed to the species for 2 h in L1-stage. The definition of each group was chosen as follows: 1 = no alterations, 2 = irregular dendrites (kinks, bends), 3 = blebbing, 4 = loss of dendrites or/and shrunken soma, 5 = loss of dendrites or/and loss of soma.

The expression level of DAT-1 differs in each type of neuron, the highest expression occurs in CEP neurons, followed by ADE neurons and the PDE neurons show the lowest expression levels.[358] Expression levels are directly comparable to the GFP fluorescence intensity as evidenced in Figure 40, representing an untreated L4 stage worm. Considering the cylindrical body shape of the nematode and its common orientation on its side, usually only one of the two cell bodies of the respective neuron pair is visible in the overlaying z-stack images (Figure 40).

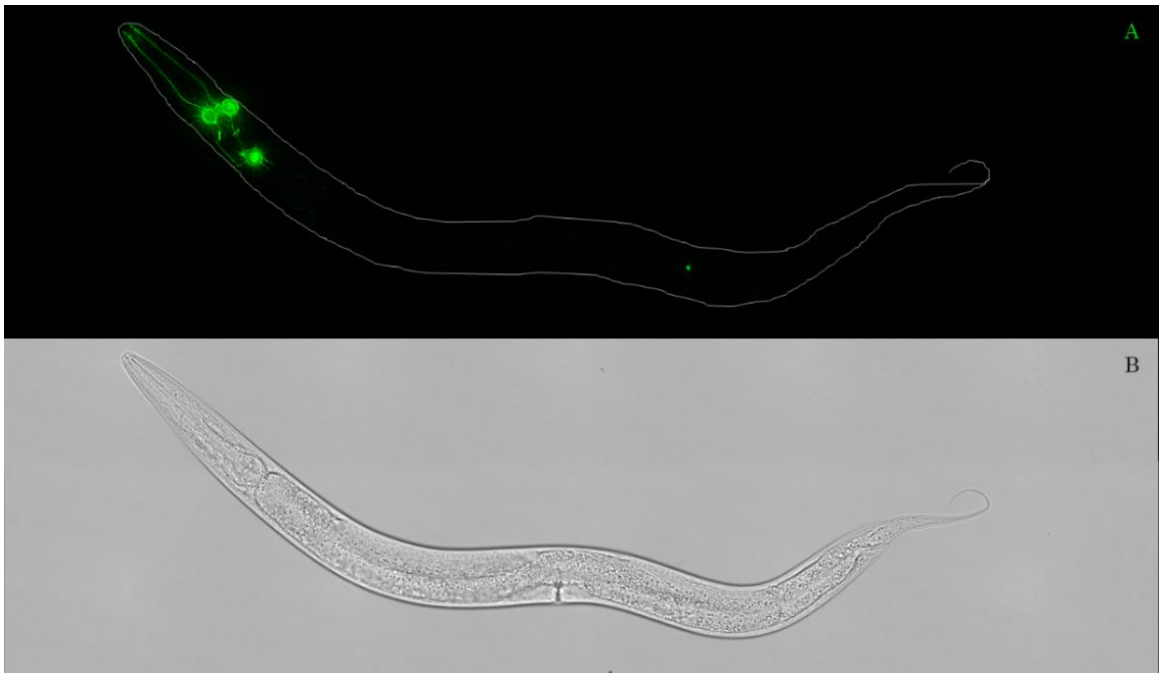

Figure 40: Visualization of the eight dopaminergic neurons (CEP, ADE and PDE) in the L4-stage worm using the DAT-1::GFP transcriptional fusion in the BY200 *C. elegans* strain. Worms were exposed for 2 h in L1 larval stage to evaluate the morphology of GFP expressing dopaminergic neurons after 48 h post-treatment. Shown are a combined tile scan fluorescence image with a combined z-stacked (20 steps) (**A**) of an untreated control and the respective brightfield image (**B**).

Figure 41 displays exemplary images of L4-stage worms at 48 h post-exposure. In the control group, all four CEP dendrites were visible and exhibited no irregularities. Depending on the orientation of the worm, the z-stack captured all four CEP dendrites or layered two on top of each other, as depicted in Figure 41 (**A**). The worm in Figure 41 (**B**) was treated with 0.5 mM Maneb. All four CEP dendrites were present, but several evaluated worms displayed irregular bends and kinks in their dendrites. Additionally, the fluorescence intensity of the ADE neurons was decreased to the extent that both ADE neurons were distinctly visible despite the worm laying in a side position. The positive control (shown in Figure 41 **C**) treated with 6-OHDA exhibited the most pronounced effects across all examined worms. In some cases, all four CEP dendrites were either completely absent or only visible as blebs. Furthermore, many worms exhibited a reduced CEP cell body size, as demonstrated in Figure 41(**C**). These findings are in agreement with Nass *et al.* (2002), who reported that all three neuron classes respond with different sensitivity to 6-OHDA (CEP>ADE>>PDE).[210] However, after Maneb exposure, the dopaminergic ADE neurons seem to be the most sensitive neurons, indicated by the fact that most CEP dendrites are intact or have irregularities, but no blebs (Figure 41 **B**).

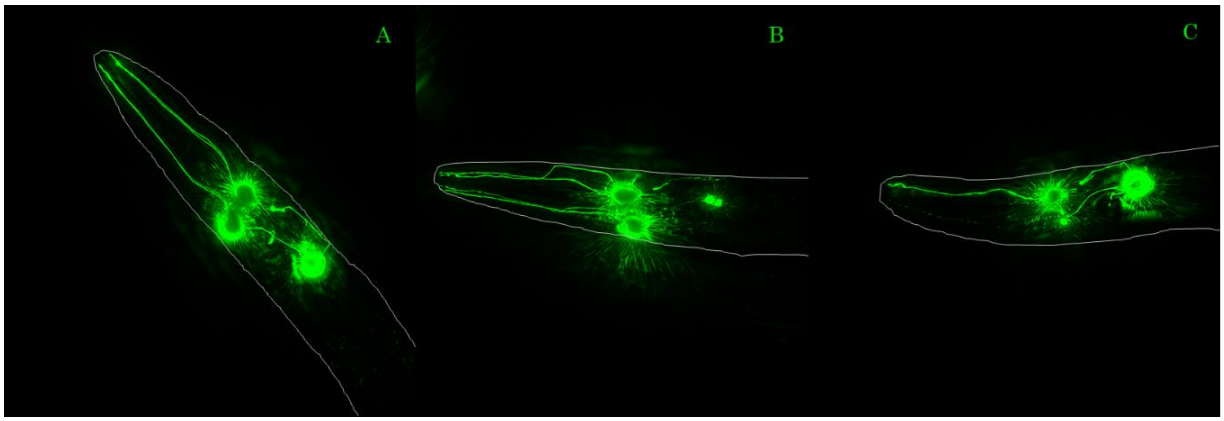

Figure 41: Visualization of the six dopaminergic neurons (CEP and ADE) in the head (anterior) region in the L4-stage worm using the BY200 *C. elegans* strain. Worms were exposed for 2 h in L1-larval stage and the morphology of GFP expressing dopaminergic neurons was evaluated in L4-stage 48 h post-treatment. Shown are combined z-stacked (20 steps) fluorescence images of different conditions: untreated control (**A**), treatment with 0.5 mM Maneb (**B**) and a positive control using 6-OHDA (**C**).

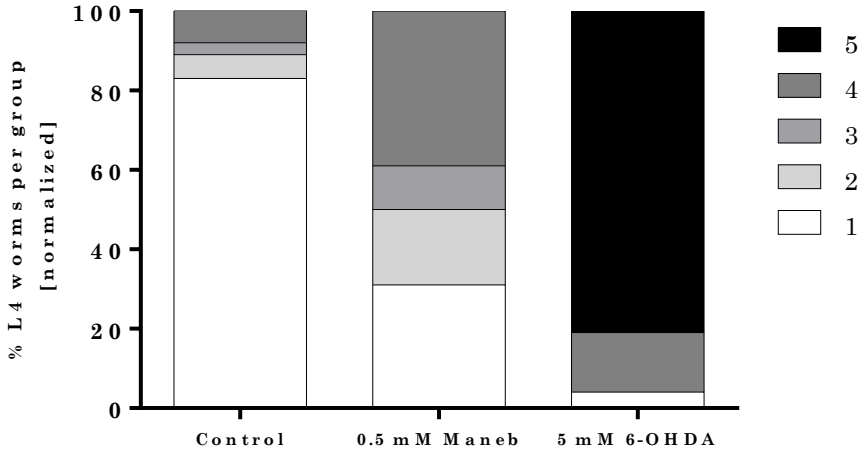

Figure 42: Percentage distribution of L4 worms assigned to each group (1-5), with each condition normalized to the respective total worm count (approximately 30 worms for each condition were evaluated). *C. elegans* BY200 strain was exposed to the respective species for 2 h in L1-larval stage and analyzed via fluorescence microscopy in L4-stage 48 h post-treatment. The definition of each value can was chosen as follows: 1 = no alterations, 2 = irregular dendrites (kinks, bends), 3 = blebbing, 4 = loss of dendrites or/and shrunken soma, 5 = loss of dendrites or/and loss of soma.

Since this is the first study, which exposed the BY200 strain to Maneb, there is a lack of date for comparing the diverse sensitivities of individual dopaminergic neurons. Furthermore, it would be of great interest to investigate whether the neurotoxic dopamine metabolite DOPAL follows a similar pattern in affecting ADE neurons. Maneb is reported to inhibit the aldehyde dehydrogenase (ALDH), which may lead to an accumulation of DOPAL and causes neurodegenerative effects on dopaminergic neurons.[58,59]

7.3.4 Co-Incubation of $MnCl_2$ and ETU

As shown in Chapter 6, the mechanism of toxicity induced by Maneb appears to involve a combination of Mn and the EBDC backbone. Given that EBDC predominantly decomposes into ETU, the lethality of a co-incubation of $MnCl_2$ and ETU was assessed. This experiment aimed to determine whether the same concentration of both species leads to comparable toxicity levels as observed with Maneb.

Indeed, the combination of Mn and ETU was more toxic than $MnCl_2$ alone (Figure 43). The LD_{50} of the combination is approximately 2.5 mM, making it twice as toxic as $MnCl_2$ alone (LD_{50} 5 mM). ETU was not lethal at concentrations below 25 mM (Figure 30), while Maneb is still five times more toxic than the combination of Mn/ETU. However, during the formation of ETU, one equivalent of carbon disulfide is also produced, which could significantly contribute to the overall toxicity. Therefore, in all experiments was Nabam used as a possible CS_2-releasing structure analog.

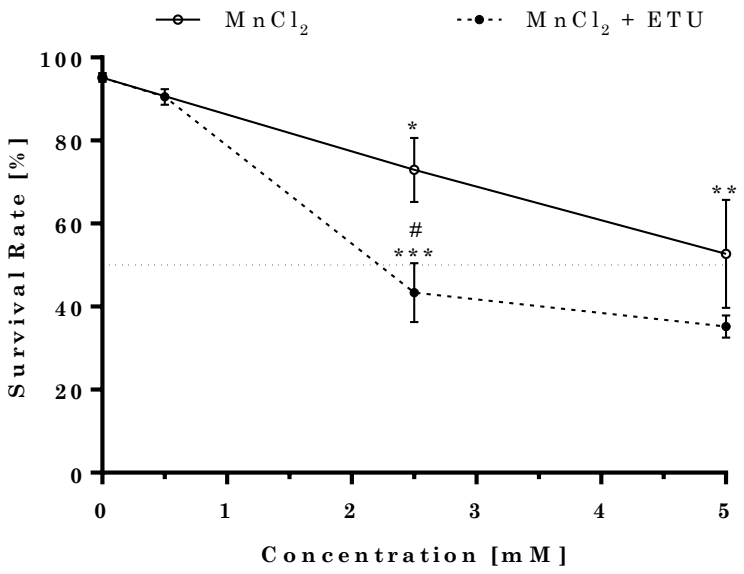

Figure 43: Dose-response curves following acute exposure to $MnCl_2$ and a combination of $MnCl_2$ and ETU. *C. elegans* wild-type L1 worms were treated for 2h. Data are expressed as means ± SEM from at least three independent experiments. An unpaired t test with Welch's correction was used for statistical analysis. Following p value summary was chosen: * < 0.05, ** < 0.01 *** < 0.001 compared to untreated control and # < 0.05 compared between species at the same concentration.

7.4 Conclusions

To assess the toxicity of Maneb, a suitable exposure method was established and applied to other relevant species including $MnCl_2$, ETU, and Nabam. However, due to the distinctive solubility characteristics of Zineb, this method is unsuitable for its evaluation, although investigation of the role of the metal in EBDC-induced toxicity is important. Adjustments of the incubation conditions would be required, potentially involving extended exposure times and the inclusion of a control with the specific ETU concentration, expected to form after Zineb being DMSO solution for 4 h according to NMR spectroscopy (Figure 23).

Dose-response curves from co-incubation experiments indicate that the combination of ETU and Mn enhances toxicity, but not to the extent that it can exclusively account for the toxic effects of Maneb. Zinc sulfate, selected for comparison with Zineb as an inorganic species, exhibited an LD_{50} approximately five times lower than that of $MnCl_2$ (1 mM Zn(II) vs. 5 mM Mn(II)). Other studies involving the nematode also emphasize that Zn(II) displays increased effects on the lifespan compared to Mn(II).[357,359] Mechanisms underlying zinc-induced toxicity are still not fully understood but is hypothesized that labile Zn-ions might play a crucial role[360] and overexposure is associated to PD.[361]

By using the BY200 strain and its GFP-expressing dopaminergic neurons, enabled the identification of effects that remained unclear considering the neurotransmitter levels alone. These findings confirm that Maneb not only acutely disrupts the neurotransmitter homeostasis but induces morphological abnormalities in the dopaminergic neurons of *C. elegans*. The observed morphological changes in L1-stage worms exhibit a similar intensity to those induced by 6-OHDA at concentration of 5 mM (compared to 0.5 mM Maneb). At 48 h post-treatment, neurotransmitter levels of Maneb-treated L4-stage worms returned to control levels, but the morphological irregularities are persisted, implying a sustained and irreversible effect of Maneb. Especially the ADE neurons appeared to be more affected since ADE processes were partially lost and ADE cell body sizes were reduced. However, in the case of 6-OHDA-treated worms, CEP-dendrites and CEP somas were partially lost, consistent with published data that highlight the sensitivity of CEP neurons.[210] The varying sensitivity of the dopaminergic neurons in the anterior region implies the involvement of different mechanisms of dopaminergic neurodegeneration and provides a potential starting point for further studies.

Chapter 8 – Final discussion and Future Perspectives

Chapter 8 – Final Discussion and Future Perspectives

The use of preventive acting fungicides has become increasingly importance due to the growing global population, aiming to counteract crop loss and mycotoxin contamination. However, these agents have the potential to impact not only intended target organism but can also affect non-target organisms and humans by entering the environment. The higher the specificity in the action of active ingredients, the greater the probability of resistance development in target species. In contrast, dithiocarbamate fungicides, known for their non-specific "multi-site" effect, are often combined with other pesticides to combat fungal resistance – an increasing concern due to extensive usage in the industrial agriculture.

Since the 1950s, ethylene bis(dithiocarbamate) fungicides, particularly those containing Mn, have been extensively applied across 100 agricultural crops.[22] Curiously, despite stringent pesticide approval processes, their molecular structure has remained unknown. The undetermined structure, accompanied by challenging residue analysis, raises additional concerns about Maneb-induced neurodegeneration. Occupational exposure of field workers to Maneb has shown neurological abnormalities and residents, especially children, living near areas where aerial Mancozeb spraying is conducted, have displayed adverse neurological effects. These effects correlate with elevated levels of Mn in hair and blood and urinary metabolite (ETU) concentrations.[2,3,51,52] These findings have been confirmed by cell culture experiments and i*n vivo* studies.[32,54–56] Nevertheless, the precise mechanism of toxicity remains unknown, as well as the role of the trace elements complexed in the fungicides. Excess of essential trace elements like Mn, Fe, Cu, Zn are associated with adverse effects and are discussed in the pathology of neurodegenerative diseases.

Hence, this study aimed to establish a reproducible synthesis method for obtaining trace element-containing EBDC fungicides of high purity and consistent quality. The resulting Mn-containing fungicides were characterized using various analytical techniques to elucidate their molecular structure after decades of widespread use. Subsequently, the impact of Maneb on inducing neurodegenerative processes and oxidative stress was assessed in comparison to other relevant species using the *in vivo* model organism *Caenorhabditis elegans*.

8.1 Synthesis and structure characterization

Various strategies for Maneb synthesis were employed including the patent method, using *in situ* generated sodium ethylenebis(dithiocarbamate salts) and carbon disulfide, which yielded byproducts such as ETU,[31] and other possible Mn-derived oxidation-sensitive impurities.[234] Therefore, the ammonium EBDC salt was isolated first and reacted with $MnCl_2$ to Maneb. Initially, the Maneb dihydrate was obtained from water, and transformed into the anhydrous from through vacuum drying. The purity was determined using standard techniques such as elemental analysis and thermal gravimetric analysis. The magnetic moment of Maneb was measured using a Gouy balance, confirming the presence of Mn in the +II oxidation state in a high spin octahedral complex.

Generally, Mn(II)-containing dithiocarbamates are considered to be extremely unstable and sensitive to oxidation.[30,234] Until recently, only one Mn(II)-DTC molecular structure had been reported by Ciampolini *et al.* (1975) using the diethyl dithiocarbamate.[30] However, these unstable properties do not apply to Maneb, which is stored at room temperature for at least several months and is exposed to oxygen. Maneb exhibits insolubility in most commonly used solvents and exclusively dissolves in aprotic solvents such as DMF and DMSO, capable of coordinating via nitrogen or oxygen. Even in solution, there are no indications of the formation of manganese dioxide or any other insoluble oxidation products. In fact, the opposite was observed, whereby single crystals were obtained from a DMSO solution (similar with DMF), which were immediately subjected to low-temperature X-ray diffraction (XRD) analysis. As a result, the Maneb-DMSO species, which has been applied in numerous toxicity studies[9,54,55] as well as in chapter 6 and 7, was successful structural characterized. The molecular structure reveals a polymeric coordination product of Maneb and DMSO, with DMSO coordinating in the *cis* position. Consequently, Mn(II) is hexacoordinated, and due to the relatively small chelate angles of approximately 75°, it adopts a distorted octahedral geometry. These insights were of particular significance, as it opened up new possibilities to develop a fit model for X-ray absorptions studies.

However, the molecular structure of Maneb in solid-state was still unknown. Due to the occurrence of a *cis*-configuration, it was assumed that the *trans*-position in Maneb may be sterically hindered, possibly due to sulfur bridges which are frequently observed in dithiocarbamates (depicted in Figure 2, coordination mode **D, E**). These sulfur bridges were also observed by Ciampolini *et al.* (1975) in the Mn(II) bis(diethyl dithiocarbamate)

complex.[30] Powder XRD indicated that Maneb and its dihydrate are microcrystalline, but the obtained powder patterns were too broad for any structural refinement. In the case of Zineb, a zinc-containing structure, this method of structural elucidation was successful by Lefton *et al.* (2020).[28] To determine the closer coordination environment of Mn in Maneb in solid state, X-ray absorption spectroscopy emerged as the preferred method as it can characterize the surrounding atoms of Mn using synchrotron radiation at the Mn absorption edge. A fitting model defined by 4 shorter and 2 longer Mn-S bonds confirmed that Maneb adopts a hexacoordinated octahedral geometry. It was also confirmed that both water molecules in the dihydrate do not bound to Mn, as expected since they are easily removeable in vacuum.

The exact molecular structure of Maneb in solid state was finally determined using electron diffraction (ED). In contrast to X-ray crystallography, MircoED uses a beam of electrons to obtain diffraction patterns, enabling the determination of structures from crystals in the sub-micron size.[362] The microcrystalline samples with particle sizes in the range of a few 100 nm were measured at low temperature in vacuum, to prevent beam damaging of crystals. To prevent the potential loss of the co-crystallized solvent, the cryo-transfer method was used to freeze the crystals beforehand for a successful structural analysis.

Characterizing Mancozeb, an EBDC fungicide containing Mn and Zn proved to be challenging. The goal was not only to prevent byproduct formation during synthesis but also to manage varying product outcomes from different. The initial patent[5] synthesis of Mancozeb involved reacting an EBDC salt with solutions of varying Mn/Zn ratios while maintaining an equimolar total metal concentration. However, different metal ratios such as 90:10 or 10:90 (Mn:Zn) yielded distinct products, as characterized by ICP-OES. Interestingly, attempts to prepare Mancozeb with equal amounts of Mn(II) and Zn(II) (50:50 ratio) resulted in a product containing more Zn than Mn (Figure 21). Explanations might be that Zn modifies the product structure, making it less accessible for Mn(II) to form two sulfur bridges for stabilizing it oxidation state. Maneb and Zineb themselves exhibit different coordination structures (hexacoordinated vs. pentacoordinated). Consequently, the redox-active Mn(II) might become more sensitive to oxidation processes in solution.[345] Furthermore, it was demonstrated that Zineb does not react with Mn-ions, supporting the hypothesis of inaccessibility of sulfur bridge formation. On the other hand, Maneb reacts with Zn-ions to yield Mancozeb,[33] but reaches saturation with ca. 0.4% Zn. Both observa-

tions align with Irving-Williams theory,[117] which proposes that divalent Mn complexes have lower stability compared to other transition metals in the first transition series.

8.2 Stability of EBDC containing Fungicides

The stability characterization of Maneb in solution is challenging due to its limited compatibility with routine NMR spectroscopy. Therefore, structurally analogous compounds, namely Nabam and Zineb, were subjected to NMR spectroscopy analysis, exhibiting contrasting behaviors. Nabam maintained its stability for more than a week, while the formation of ETU was observed within 4 h in a Zineb-DMSO solution, and after 4 days 30% ETU formation occurred. The ability of Nabam to crystallizes as a hexahydrate in presence of water may contribute to its stability (Figure 24). Despite Maneb being successfully characterized in DMSO solution (Figure 12), Zineb did not yield any crystals, likely due to its degradation and precipitation. A phenomenon which was not observed with Maneb.

The stability of Nabam in aqueous solution appears to be good; however, based on this experiment, only limited conclusions can be drawn concerning stability and the degradation to ETU, CS_2 or other compounds in a model organism like *C. elegans*, especially considering factors such as pH changes. In general, it was shown that dithiocarbamates, particularly those derived from primary amines, degrade rapidly under acidic conditions.[19] Hence, the uptake of dithiocarbamate fungicides via the gastrointestinal tract, such as the consumption of crops containing DTC residues, may cause acidic degradation within the stomach, where the pH ranges from 1 to 4.[363] Consequently, Zineb might be suitable for being a structural analogue for studying the metal-derived effects, since after oral exposure ethylene bis(dithiocarbamates) will degrade anyway.

One further approach to study the stability of Maneb itself in solution could involve electron paramagnetic resonance (EPR) spectroscopy. In this technique, unlike nuclear magnetic resonance (NMR) spectroscopy where atomic nuclei are excited, electrons are excited instead, making it particularly suitable for paramagnetic materials with unpaired electrons. EPR identifies changes within the electron environment such as oxidation state or coordination partners.[364]

In addition, *in vivo* studies[83] have shown that the degradation of EBDC fungicides not only releases the metal and ETU but also CS_2. The release of highly volatile CS_2 was also observed in the TGA analysis (Figure S6). Therefore, monitoring a Maneb-DMSO solution

using head-space gas chromatography to detect CS_2 formation could be a promising method for characterizing the stability of Maneb in solution.

A notable positive aspect is that the specific incubated species from experiments involving *C. elegans* was precisely identified due to the XRD structure of Maneb in DMSO solution. Due to the fact that Maneb is freshly dissolved in DMSO before each experiment and crystals were formed within 17 hours the Maneb-DMSO adduct should be stable during the 2 h worm, regardless of any metabolic pathways within the biological system.

8.3 Toxicity of Maneb in comparison to other relevant species

8.3.1 Lethality

Maneb is significantly more toxic than all other associated species ($MnCl_2$, ETU, Nabam) in the nematode *C. elegans*. Based on the formation of sulfur bridges in solid state and the occurrence of polymeric DMSO-coordination adducts (and crystals) in solution, Maneb might be more stable than previously expected. The polymeric nature of Maneb, may enhance its lipophilic character,[45,46] and enables it to enter different compartments within cells where it eventually undergo metabolism. In animal studies, metabolites like Mn, ETU, and CS_2 have been detected after EBDC fungicide exposure and epidemiological studies have shown that humans exposed to Mancozeb, exhibited higher levels of Mn in hair and blood, as well as detectable levels of ETU in urine.[51,52]

To determine if the toxicity induced by Maneb is attributed to the combination of Mn(II)-ions and ETU, both compounds were co-incubated. The results indicated that when $MnCl_2$ and ETU were co-incubated, the LD_{50} value was 2.5 mM, which is twice as toxic as $MnCl_2$ alone (5 mM) but still five times less toxic than Maneb itself. However, each Maneb molecule, does not only release ETU and Mn, but also releases CS_2, a highly toxic and volatile compound. To avoid the handling of CS_2 in a *C. elegans* laboratory, Nabam and Zineb served as potential CS_2 releasers and structural analog compounds. Nabam and ETU demonstrated similar low toxicity in the examined concentration range up to 5 mM (LD_{50} > 25 mM). Zineb did not display any toxic effects in the concentration range compared to Maneb, likely due to its precipitation at concentrations as low as 0.5 mM. Thus, Zineb was not suitable as a model for EBDC-induced CS_2 release using this specific exposure setup. Despite this, existing literature, reported that Zineb is the comparatively less toxic fungicide species.[11,341,342]

Domico *et al*. (2006) investigated the effect of all relevant species on mesencephalic neuronal cells. Their findings revealed, that Maneb and Mancozeb are significant more toxic than ETU, Nabam and $MnCl_2$, assessed by cell viability measurements. In case Nabam and $MnCl_2$ were co-incubated to mimic Maneb, a comparable level of toxicity compared to that of Maneb alone was observed. It was concluded that the combination of the backbone and metal plays a pivotal role in causing toxicity.[54] However, it is uncertain whether the combination truly mimics Maneb or if both compounds react to generate Maneb within the cell culture medium. It is plausible that the applied species might be actually Maneb itself. Therefore, it might be worth to consider experiments with pre-incubation of Mn and subsequently incubation with Nabam, and *vice versa* to see if Maneb is formed *in vitro*.

8.3.2 Bioavailability

The bioavailability of Mn in L1-stage was assessed via inductively coupled plasma with optical emission spectrometry (ICP-OES) following exposure to Maneb and $MnCl_2$, and revealed a time- and concentration-dependent uptake. However, no species-specific effects were observed. These findings are in agreement with Carmona *et al*., showing a 10-fold increased toxicity of Maneb compared to $MnCl_2$, but no differences in bioavailability in PC12 cells.[321] In summary, the toxicity of Maneb appears to be based on a mechanism distinct from elevated Mn levels. At 48 h post-treatment, the total Mn amount in L4-stage worms returned in both species to untreated control level.

Nevertheless, the method utilizes a worm lysate, making it impossible to localize Mn within the body. It is plausible that Mn(II) ions are transported differently than Mn(II) complexed with ligands, especially polymeric ones like in Maneb, which potentially undergo passive transport processes due to their lipophilic character. Therefore, experiments using metal imaging methods within the worm would be of great interest to localize essential trace element storage after exposure to different Mn species.[365] A method using laser-ablation (LA) coupled with inductively coupled plasma-mass spectrometry (ICP-MS) is already established for imaging Mn uptake in *C. elegans* L1-stage worms with resolutions usually between 4 and 20 µm.[366] An alternative method for element imaging in *C. elegans* is based on synchrotron X-ray fluorescence microscopy (XFM). Due to its higher resolution, the distribution of metals can be investigated even within a single cell and at a subcellular

level. In contrast to ICP-based methods, this technique also preserves structural information and oxidation states.[365] Considering the complexity of Maneb-induced toxicity, species-specific information as well as their storage and distribution could yield more insights and provides a more comprehensive understanding of the underlying mechanisms driving its toxic effects.

Initial results of the effect of Maneb or $MnCl_2$ showed a decreasing trend in the total Cu content in L1 worms. When using 60,000 L1 worms to measure the metal content, Cu levels in untreated control worms were near the LOQ. Exposure of Maneb and $MnCl_2$ appeared to reduce Cu levels below the LOQ. The decrease in Cu levels could be explained by the high Cu-affinity of dithiocarbamte ligands as well as potential CS_2-derived biological dithiocarbamates.[87,88] This mechanism is proposed to underlie both antifungal and toxic effects.[89] It is possible that the elimination of copper-containing complexes is facilitated, leading to observable effects of Cu deficiency. To further investigate this, future experiments should involve increasing the worm count to at least 80,000 (in an 8 mL exposure volume) to enable accurate quantification even at reduced copper levels.

8.3.3 Oxidative Stress

C. elegans L1-stage worms, exposed to Maneb exhibited significant effects on the antioxidative glutathione (GSH) and glutathione disulfide (GSSG) system. The ratio of GSH/GSSG is typically employed to assess the oxidative status of an organism. During oxidative stress conditions, more GSH is converted to GSSG by reducing reactive species, leading to a shift in the ratio towards GSSG.[8,73] However, after Maneb exposure, GSSG levels extremely increases, but also the GSH levels were elevated more than expected (Figure 34). Consequently, it is expected that an excess of reactive oxygen and nitrogen species (RONS) is the reason behind the shifting GSH/GSSG ratio. However, data obtained from RONS detection using the carboxy-DCFH assay revealed only slight effects (Figure 33). In summary, Maneb induces significant alterations in the GSH/GSSG-related antioxidant capacity but impacts cellular RONS formation only mildly. Explanations for the observed effects are discussed below.

Barlow *et al.* (2005) have reported that Maneb elevates the levels of both GSH and GSSG in PC12 cells. This effect is supported by increased activity of glutamate-cysteine ligase (GCL), an enzyme involved in producing the immediate precursor of GSH. Despite this, the

activity of glutathione peroxidase (GPx), the enzyme responsible for catalyzing the conversion of GSH to GSSG, remains unaffected following Maneb treatment.[8] Moreover, two other studies documented that Maneb substantially shifts the GSH/GSSG ratio in three cell lines.[9,62] Roede and Jones (2014) observed that Maneb appears to elevate cellular GSH levels without evident signs of oxidative stress.[75] Taken together, these findings imply a non-enzymatic conversion of GSH to GSSG, potentially arising from a direct interaction of GSH with Mn itself due to its metal-binding affinity.[73] On the other hand, Maneb is proposed to have a high reactivity towards thiol-containing molecules such as cysteine side chains of proteins or GSH.[7,11,75] Roede and Jones (2014) reported that Maneb causes stochiometric loss in protein thiols, leads to reversibly dimerizing them and inhibits enzyme activities using recombinant thioredoxin-1 (Trx-1) as a model protein.[75] Anderson *et al.* (2021) have demonstrated significant alterations in mitochondrial respiration, proliferation, glycolysis and the thiol redox status, assessed by the mitochondrial antioxidant enzyme peroxiredoxin 3 (Prx3).[11] Both studies underline the thiol reactivity of Maneb, which is also implicated in its anti-fungal activity and may be linked to the release of CS_2.[86]

However, other studies demonstrated that Maneb exposure also leads to the formation of RONS.[62,63,367] The observation of only slight effects in our study might be attributed to the fact that the carboxy-DCFH assay is known to detect cellular RONS, especially hydrogen peroxide, hydroxyl radicals, and peroxyl radicals, but not mitochondria-derived RONS.[340] Bailey *et al.* (2016) exposed *C. elegans* to a commercially available Mancozeb-containing fungicide formulation (MZ) and assessed the impact on RONS formation using different detection techniques.[60] It has been reported that hydrogen peroxide, but not the superoxide or hydroxyl radical levels were increased. Increased H_2O_2 levels with the same fluorescence dye were also observed after Mancozeb exposure by Domico *et al.* (2007) in mesencephalic cells.[55] Since exogenous H_2O_2 is able to up-regulate the glutathione-*S*-transferase (GST)[368] a GST:GFP transgenic worm strain was used to reveal an increase of GST expression by elevated GFP intensity after MZ exposure.[60] GST catalyzes the conjugation of GSH to electrophile substrates for detoxification.[369] Since the assay used in our study should detect hydrogen peroxide generation as well, it might be that increased of fluorescence emission (Figure 33) is referred to hydrogen peroxide generation. The increased GST-expression[60] and the non-affected GPx activity[8] supports the hypothesis that GSH is non-enzymatically converted to GSSG for example by binding to redox active Mn or reacting with Maneb or

other species itself. The elevated GSH level may due to increased activity of the γ-glutamylcysteine synthase (GCS).[8]

Furthermore, Bailey *et al.* (2016) and Domico *et al.* (2007) reported inhibitions of mitochondrial functions after Mancozeb exposure.[55,60] Mitochondria have a central role in supplying ATP as cellular energy and are recognized as the primary source of essential reactive species.[370] Consequently, mitochondria become susceptible to oxidative stress-related impairments due to an excess of RONS. While there is no precise definition for mitochondrial dysfunction existent, any abnormalities in mitochondria-related functions, such as oxidative phosphorylation for ATP production, generation/detoxification of RONS, or involvement in apoptosis, can be categorized as dysfunction.[371]

To further investigate the impact of Maneb on oxidative stress, particularly within the mitochondria, the fluorescent dye MitoTracker™ may be a suitable tool. This dye has the ability to passively diffuse across plasma membranes and accumulate within the mitochondria. When the dye undergoes oxidation by RONS, it emits fluorescence.[372] To explore further in which cell compartment Mn might accumulate after Maneb exposure, the isolation of mitochondria and subsequent metal quantification would be promising. Here, it is important that the isolated mitochondria are intact to ensure that the metal is still inside, but functionality is of less importance.[373]

8.3.4 Neurotoxicity

To investigate the impact of Maneb on neurodegenerative processes, a liquid chromatography – tandem mass spectrometry (LC-MS/MS)-based method was developed to simultaneously quantify levels of dopamine, serotonin, acetylcholine, and GABA within *C. elegans* lysates. Special attention was given to achieving low detection limits in the low nM range and optimizing the sample preparation due to the individual properties among the analytes.[70]

Exposure to Maneb resulted in several significant decreased neurotransmitter levels, specifically dopamine (DA), acetylcholine (ACh) and γ-aminobutyric acid (GABA) in L1-stage worms immediately after treatment (Figure 32). However, at 48 h post-treatment in L4-stage, neurotransmitter levels had returned on control level. This raises the question of whether the effects induced by Maneb are more acute or reversible. It may be possible that neurotransmitter levels have normalized as an adaptive response, although the neurons

are still affected. Given that Maneb-induced toxicity predominantly affects the dopamine system and the most pronounced reduction was observed in dopamine levels, the following study was included.

To assess any morphological abnormalities of dopaminergic neurons after Maneb treatment, the in DAT-1 GFP-expressing BY200 strain was used. L1-larvae after Maneb exposure showed reduced soma sizes and loss of dendrites (Figure 38 **B**) similar to the included reference positive control treated with 6-hydroxydopamine (Figure 38 **C**), a neurotoxicant specifically targeting dopaminergic neurons. Interestingly, following Maneb exposure, the anterior deirids (ADE) neurons appeared sensitive, whereas 6-OHDA primarily affected the cephalic sensilla (CEP) neurons.[210] In contrast to the neurotransmitter levels, alteration in the morphology of dopaminergic neurons were evident in L4-worms at 48 h post-treatment. Certain CEP dendrites exhibited irregular bends, while numerous ADE neuron somas were visibly smaller and displayed reduced fluorescence compared to the control group. The positive control group treated with 6-OHDA exhibited strong effects in all types of dopaminergic neuron, including complete loss of CEP dendrites and CEP cell bodies. Although the effects induced by Maneb are not as pronounced as those caused by 6-OHDA, it has been demonstrated that even single exposures to Maneb can lead to lasting consequences in terms of neurodegeneration. Furthermore, the specific sensitivity of ADE neurons, which differs from the response seen with 6-OHDA, suggests possibilities for further mechanistic exploration.

Case-control studies,[2,3] epidemiological studies[51–53], *in vivo* studies[8,336,374] and cell culture experiments[9,54,55] have demonstrated the neurotoxic properties of Mn-containing EBDC fungicides. Mechanistically, it is believed that they inhibit crucial enzymes for neurotransmitter homeostasis, including the aldehyde dehydrogenase (ALDH)[58,375] and acetylcholine esterase AChE.[376] Given that Maneb is thought to undergo metabolism involving degradation products such as Mn, ETU and CS_2, it is important to note that no changes in neurotransmitter levels were observed after exposure to ETU or Nabam. These findings are in agreement with Domico *et al*. (2006) studying *in vitro* the uptake of ^{3}H- and ^{13}C-labled dopamine and GABA after treatment with Maneb, Mancozeb, Nabam, $MnCl_2$ and ETU followed by a 72 h long resting period in mesencephalic neuronal cells.[54] ETU, $MnCl_2$ and Nabam did not affect the cell viability in the observed concentration range (0-125 µM), while Maneb and Mancozeb showed EC_{50} values of approximately 60 µM. However, Nabam exposure at the highest sub-toxic concentration (125 µM) decreased

uptake of dopamine and GABA by about 50%, but not to the extent of Maneb at the same concentration which resulted in a decrease of over 80%.[54] Negga *et al.* (2012) exposed two transgenic *C. elegans* strains, expressing GFP in GABAergic (EG1285) and dopaminergic (BZ555) neuronal cells, to a Mancozeb-containing fungicide. Both strains revealed after treatment decreased pixel number, implying neurodegenerative effects in both dopaminergic and GABAergic neurons.[56] A previous study by Negga *et al.* (2011) was conducted with the NW1229 *C. elegans* strain, which expresses GFP in all neurons. Here, the Mancozeb-containing fungicide decreased pixel numbers in a higher extent at lower concentrations.[32] Consequently, it is assumed that not only the dopaminergic and GABAergic neurons are affected but also glutamatergic, serotonergic and cholinergic neurons.[56] These hypothesis is in agreement with the neurotransmitter levels after Maneb exposure in L1-stage worms (Figure 32), as dopamine, GABA and acetylcholine levels were decreased.

In contrast to that, an *in vivo* study of Zhang *et al.* (2003) revealed that Maneb selectively induces neurodegenerative effects in dopaminergic neurons and does not affect the GABAergic neurons.[78] Potentially, the route of uptake (oral, intravenous) might influence the toxicity, as the stomach has an acidic pH[363] where dithiocarbamates are typically acid hydrolyzed.[19] In the study of Zhang *et al.* (2003) Maneb was administered intraventricularly, directly into the brain of rats. This is particularly interesting given that the data from Chapter 6 demonstrated an effect of $MnCl_2$ on decreasing GABA levels, and Mn could also be released through acid hydrolysis of Maneb in the stomach. Therefore, it might be possible that the varying sensitivity of neurons is attributed to the presence of either Maneb or its metabolites.

Chronic overexposure of Mn can lead to Mn accumulation in the brain and result in symptoms affecting the motor system (manganism) with symptoms similar to those of Parkinson's disease. Although this is pathological distinct from PD, Mn is reported to induce the aggregation of α- synuclein, a hallmark of PD and possible risk for developing PD.[76,141] Both disease affect the *basal ganglia*, and both are characterized by a loss of dopaminergic neurons. However, initial symptoms of manganism involve the GABA-rich area *globus pallidus*, while PD is characterized by dopaminergic degeneration in the *substantia nigra pars compacta*.[377] Consequently, the decreased GABA levels after $MnCl_2$ exposure (Figure 32) in L1-stage worms may be explained by initial effects of Mn accumulation. However, reports of GABA concentrations following Mn exposure are

inconsistent und appear to be highly dependent on the Mn concentration as well as the brain region under investigation.[378] GABA levels in *C. elegans* have not been quantified so far, mainly due to the fact that the developed LC-MS/MS method[70] is currently the only one that quantifies GABA simultaneously to dopamine, acetylcholine, and serotonin.

Carbon disulfide is a metabolite product, formed by degradation of Maneb to ETU and was detected after EBDC fungicide exposure in the breathing air of rats. Consequently, an oral uptake of Maneb may lead to a breakdown in the acidic stomach and releases highly volatile CS_2. Proposed mechanisms for CS_2-induced neurotoxicity are the inhibition of dopamine-ß-hydrolase (DBH)[379] and the chelation of copper.[380] Both may induce neurodegenerative effects, possibly enhanced by combination with other compounds such as Mn, ETU or Maneb.

For further investigations regarding the neurotoxic effect of Maneb and to assess whether the observed alterations in neurotransmitter levels correlates with permanent morphological changes in neurons, it would be of great interest to examine worm strains expressing GFP in specific neurons upon Maneb exposure. For or instance, utilizing the LX929 *C. elegans* strain, which features GFP expression in cholinergic neurons, or the EG1285 *C. elegans* strain, with GFP expression in GABAergic neurons, could provide valuable insights.

To verify further whether the changes in neurotransmitter levels and morphological abnormalities, correlate with progressive functional impairments of neurons, *C. elegans* is particularly suitable for conducting behavior assays in this regard. The functionality of the dopaminergic system can be assessed by the basal slowing response (BSR).[211] In the presence of bacteria, wild-type worms display a decreased movement speed compared to their movement in the absence of bacteria. The sensing of bacteria is mediated by dopamine-containing neural circuits. Consequently, a reduced movement slowing on food is observed when there is a loss of functionality in dopaminergic neurons. Therefore, the worms are observed under the microscope both in the absence and presence of bacteria. During this observation, the number of body movements in the anterior region ("head trashes") is counted within a 20-second interval.[211,325] Other locomotor behaviors of *C. elegans*, to assess the nervous system are body bends, pharyngeal pumping and thermotaxis, which were reviewed by Soares *et al.* (2023) and should be addressed in further experiments.[325]

In summary, Maneb is significantly more toxic than $MnCl_2$ alone, but not due to increased total Mn levels in L1-stage worms. However, Maneb or its metabolites might be possibly located in other cellular organelles, such as mitochondria. The formation of RONS, possibly occurring within mitochondria and not accurately detected by the DCFH-DA assay, may lead to oxidative imbalances. This would explain the significant impact of Maneb on the GSH/GSSG system. Nevertheless, this effect could also be attributed to the reactivity of Maneb and its metabolites, particularly towards thiols. Overall, it is still unclear whether oxidative stress causes neurodegenerative effects or is more a consequence. In this context, Maneb exposure resulted into altered neurotransmitter levels and persistently affected the morphology of dopaminergic neurons in L4-stage worms after one exposure in L1 stage.

A comprehensive understanding of the underlying mechanisms of Maneb could lead to a more accurate assessment of the risks to human health and the environment. Furthermore, this knowledge could facilitate the development of targeted therapeutic strategies aimed to prevent neurodegenerative effects or to slow down their progression. While this work conducted here has been successfully elucidated the molecular structure of Maneb and demonstrated several fundamental principles of Maneb-induced toxicity, further studies are necessary to gain a deeper understanding of the specific effects and their interrelationships.

Appendix – Supplementary Material

Appendix – Supplementary Material

Supplementary Material for Chapter 3
The structure of Maneb: An important manganese-containing bis(dithiocarbamate) fungicide

Experimental Details

Instruments. NMR spectra were recorded on a Bruker Avance 400 spectrometer referenced externally to Me_4Si. C, H and N analyses were performed by staff of the in-house elemental analysis facility using an Elementar Vario EL system. TGA/DSC measurements were conducted using a Netzsch STA 449 F5 Jupiter instrument. Experiments were carried out in alumina crucibles, which were closed with alumina lids. Samples were heated from 25°C to 1000 °C with a heating rate of 5 K min^{-1} in a nitrogen atmosphere applying a constant nitrogen flow of 25 ml min^{-1}. IR spectra were recorded on a Thermo Scientific Nicolet iS5 spectrometer equipped with an iD7 diamond ATR unit. The magnetic susceptibility was determined using a Sherwood Scientific magnetic susceptibility balance. Calibration against mercury tetrathiocyanato cobaltate (II).

X-ray crystallography X-ray quality crystals formed by slow evaporation of a 0.5 M Maneb solution in dimethylsulfoxide (DMSO) (complex 4) or dimethylformamide (DMF) (complex **5**) within a few days. Diffraction data were collected at 150 K or 100 K (complex **4**) using a Rigaku Oxford Diffraction Gemini E Ultra diffractometer, equipped with an EOS CCD area detector and a four-circle kappa goniometer. Data integration, scaling and empirical absorption correction were performed using the CrysAlis Pro program package[238]. All crystal structures were determined using SHELXT and refined using SHELXL[239,240]. The Olex2 graphical user interface was used for all structure manipulations and to generate the graphics[241]. Crystallographic and refinement details for both complexes are listed in Table S1. The structure of the DMSO complex had high residual electron density, which was consistent with the presence of two additional, highly disordered DMSO molecules. No satisfactory model for the disorder could be developed so that the data was subjected to the solvent mask routine as implemented in Olex2.

X-ray absorption studies X-ray absorption experiments at the Mn K-edge (6539 eV) were performed at beamline 10 of the DELTA synchrotron facility (Dortmund, Germany)[235]. A Si(111) channel-cut monochromator was employed, and gas-filled ionization chambers were

used to determine the intensities of the incident and the transmitted X-ray beam with a size of typically 0.4 mm x 4 mm (v x h). A Mn metal foil was regularly measured to calibrate the energy scale of the spectra, however no substantial changes were observed from scan to scan. Energy scans contained a pre-edge region of 200 eV below the Mn K-edge to 20 eV below the edge with a larger step size of about 5 eV, while the edge region (-20 eV to +40 eV above the edge) was acquired with a step size of 0.3 eV to allow a precise determination of the edge position and small pre-edge peaks. The step size above the edge successively increases with increasing energy, so that a full spectrum comprised an energy range to about 650 eV above the edge, with in total 470 data points. Several scans, each of about 25 minutes acquisition time, were averaged to improve the signal to noise ration of the data. The samples were prepared by homogeneously dispersing the Maneb powders on self-adhesive tape, and several tapes were stacked in order to obtain an absorption suited for XANES and EXAFS experiments. A bath cryostat filled with liquid nitrogen (77 K) was used to cool the samples to a temperature of around 80 K. The samples were investigated at room temperature as well as after cool-down to 80 K. For comparison, reference spectra of several Mn-containing compounds of different chemical valence such as zero-valent Mn-metal, MnO (Mn^{2+}), Mn_3O_4 (Mn^{2+}/Mn^{3+}), Mn_2O_3 (Mn^{3+}) and MnO_2 (Mn^{4+}) as well as MnS (Mn2+) were collected. EXAFS data reduction was performed employing the Athena/Artemis software package[242], and quantitative fits used amplitudes and phases calculated by FEFF 8.0[243].

X-ray powder diffraction Powder diffraction was carried out on a Bruker D8 Advance instrument fitted with a Lynx Eye detector using Cu *k*α radiation (λ = 1.5483 Å). Data acquisition and processing was done using the DIFRAC plus XRD Commander software[244].

Electron Diffraction Electron diffraction measurements for Maneb anhydrous and Maneb dihydrate were collected using the Rigaku XtaLAB Synergy-ED, equipped with a Rigaku HyPix-ED detector optimized for operation in the continuous rotation 3D-ED experimental setup[245]. Data acquisition was performed at 100 K under high vacuum with an electron wavelength of 0.0251 Å (200 keV). The instrument was operated and the diffraction data were processed in the program CrysAlis Pro[246]. A multi-scan absorption correction was performed using spherical harmonics implemented in SCALE3 ABSPACK scaling algorithm in CrysAlis Pro. The structure was solved using SHELXT[240], and subsequently, refined with kinematical approximation using SHELXL[239] in the crystallographic program suite Olex2[241,247]. By merging data of several individual

grains/datasets, a completeness of 99.9% up to a resolution of 0.80 Å was achieved. Non-hydrogen atoms were assigned anisotropic displacement parameters unless stated otherwise. The hydrogen atoms bonded to nitrogen atoms as well as hydrogens bonded to oxygen atoms were located from Fourier difference maps. Other hydrogen atoms were placed in idealized positions and included as riding. Isotropic displacement parameters for all H atoms were constrained to multiples of the equivalent displacement parameters of their parent atoms with U_{iso}(H) = 1.2 U_{eq}(parent atom). Enhanced rigid bond restraints[248],[249] with standard uncertainties of 0.001 Å2 were applied. The experimental and refinement details are given below. CCDC 2255649 (Maneb anhydrous) and 2255650 (Maneb dihydrate) contain the supplementary crystallographic data for this publication. These data can be obtained free of charge via www.ccdc.cam.ac.uk/data_request/cif, or by emailing data_request@ccdc.cam.ac.uk, or by contacting The Cambridge Crystallographic Data Centre, 12 Union Road, Cambridge CB2 1EZ, UK; fax: +44 1223 336033. Microcrystalline powder of Maneb anhydrous was spread on a standard TEM grid. Yellowish plate-like crystals with approximately 100 nm thickness were selected for measurements. Microcrystalline powder of Maneb dihydrate was spread on a standard TEM grid. Yellowish plate-like crystals with approximately 100 nm thickness were selected for measurements. Cryo-transfer, i.e. freezing of samples prior to introduction to vacuum, at 100 K using a Gatan ELSA (Model 698) specimen holder was applied. As electron diffraction requires samples to be studied under high vacuum, the cryo-transfer technique is essential for many sensitive compounds. Solvated crystals, such as Maneb dihydrate, lose the weakly bound solvent molecules, and hence loses its crystallinity, when no cryo-transfer is applied. Stabilization of samples in vacuo, reducing beam damage, improving resolution and reducing disorder are typical benefits using the combination of cryo-transfer and low temperature measurement. A crystal-to-crystal transformation from Maneb dihydrate to Maneb anhydrous is observed when first cryo-transfer is applied followed by heating the samples slowly from 100 K to approximately 230 K.

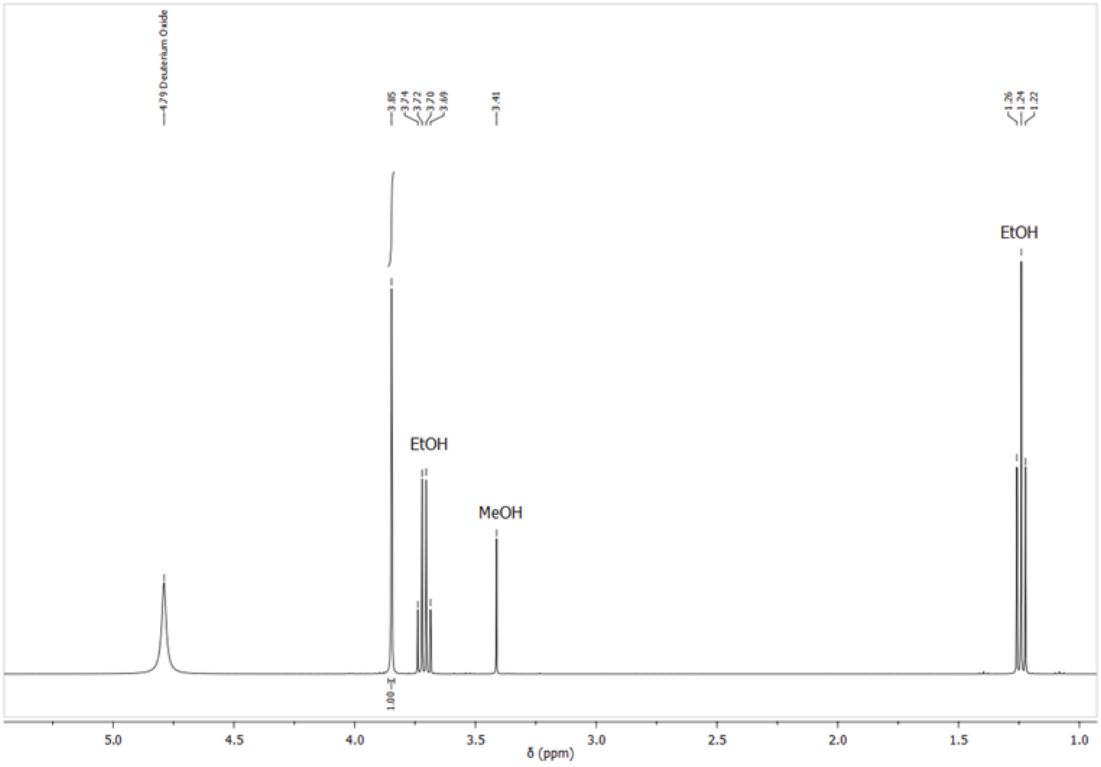

Figure S1: ^{1}H-NMR spectrum of compound 1.

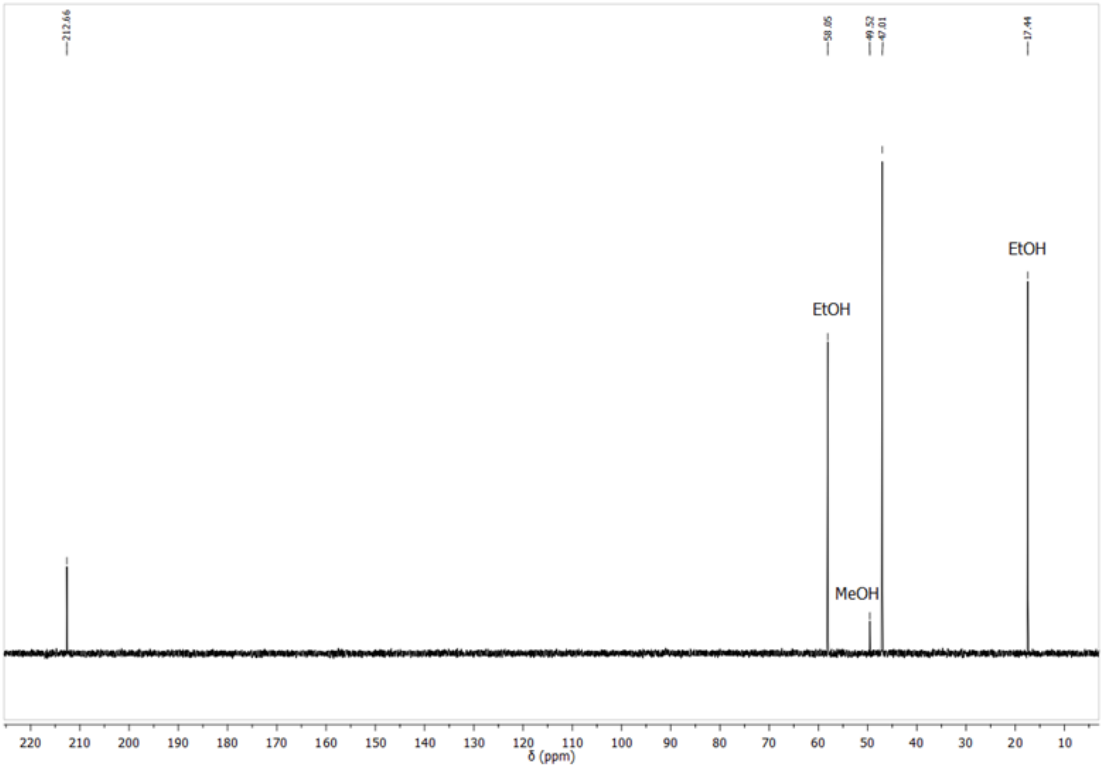

Figure S2: ^{13}C-NMR spectrum of compound 1.

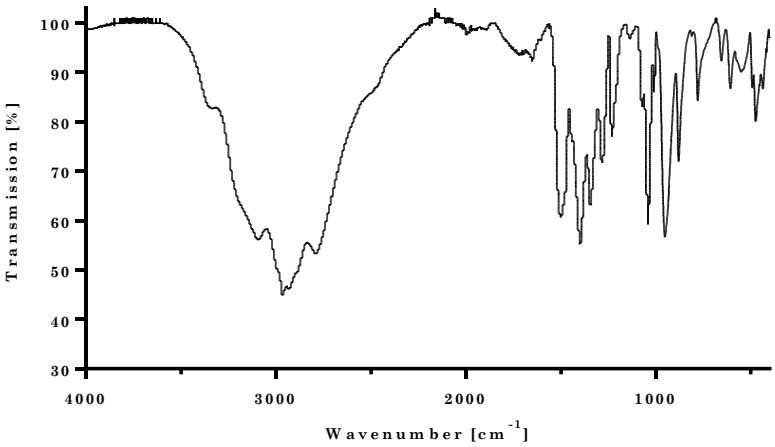

Figure S3: IR-spectrum of compound 1.

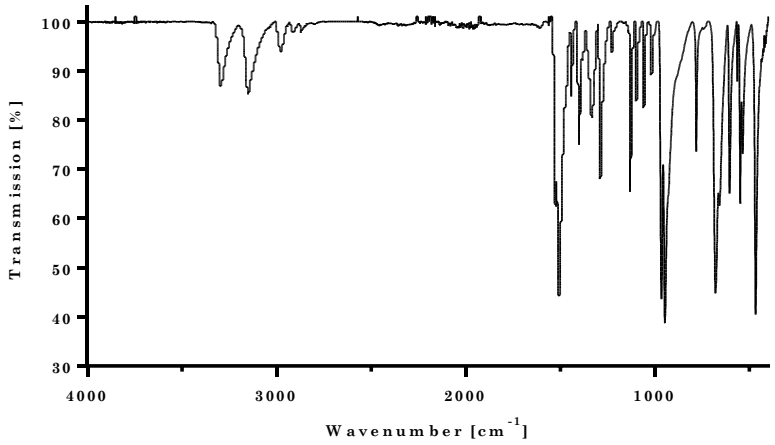

Figure S4: IR-spectrum of Maneb dihydrate (2)

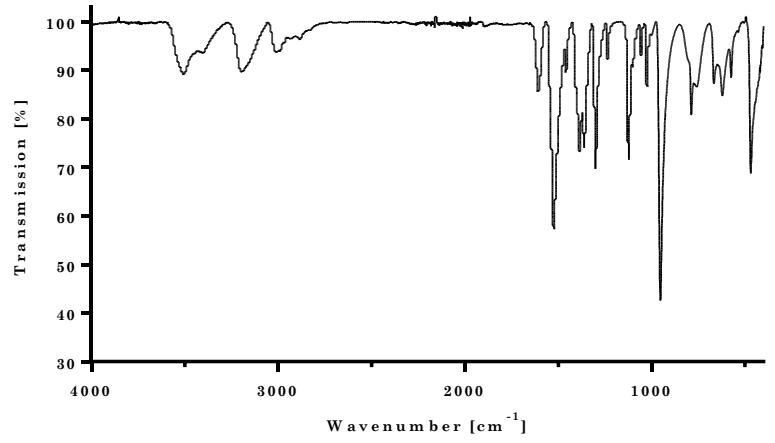

Figure S5: IR-spectrum of anhydrous Maneb (3).

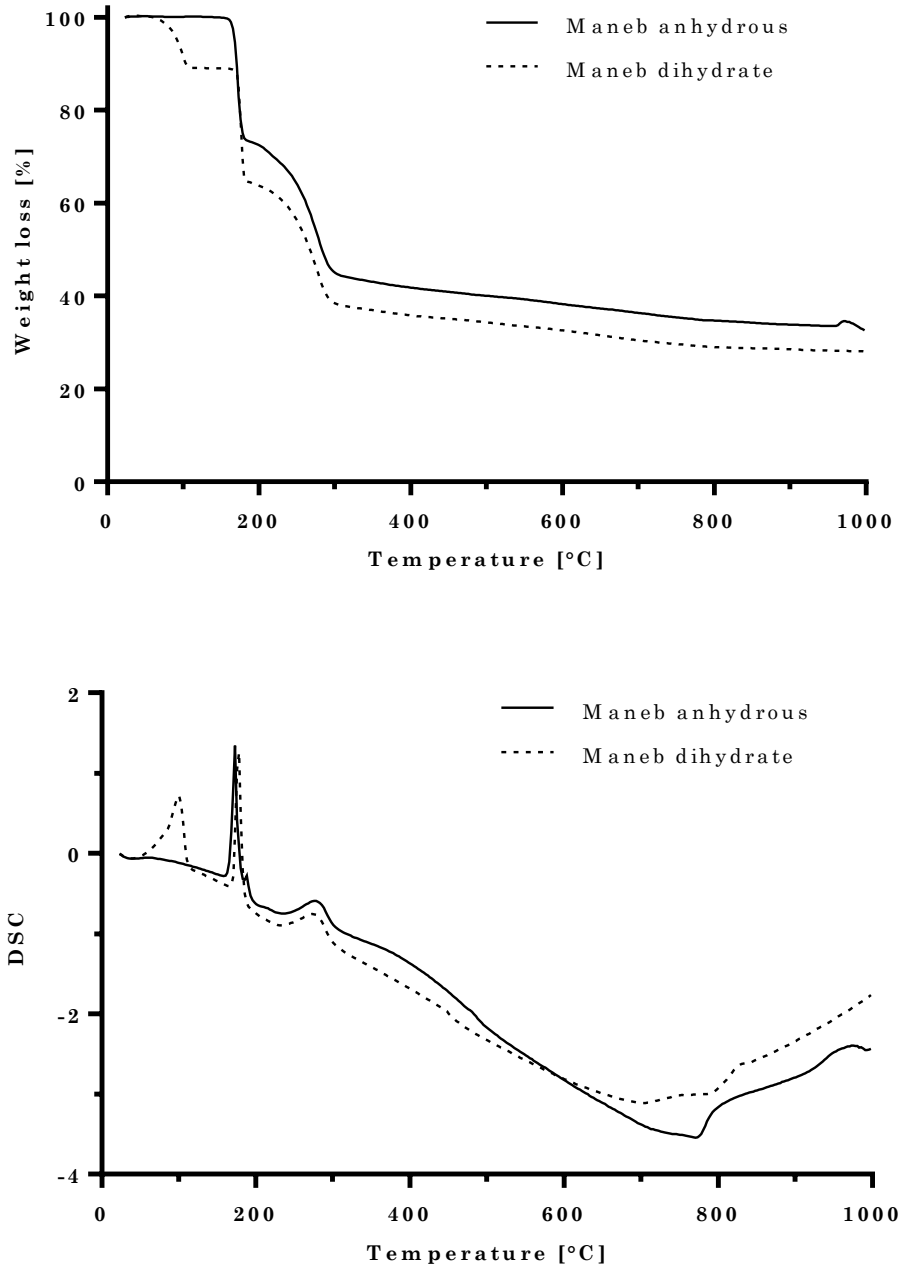

Figure S6: Thermal gravimetric analysis (TGA) curves (top) and differential scanning calorimetry (DSC) curves (bottom)of Maneb dihydrate (dashed line) and anhydrous Maneb (solid line).

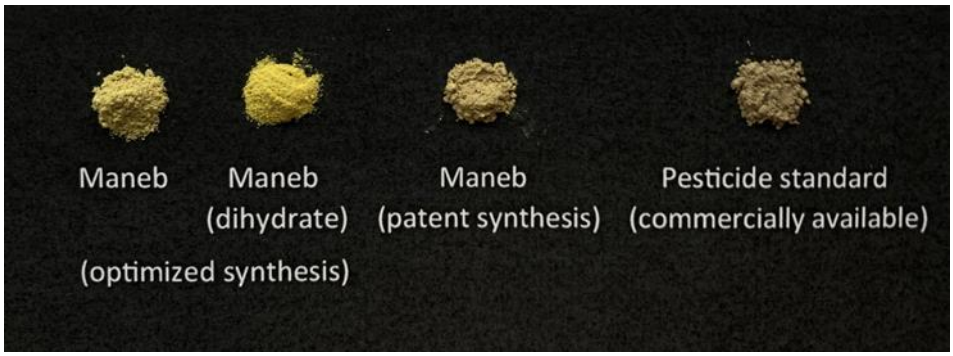

Figure S7: Photographs of products obtained by our optimized synthesis route, the patent method and the commercially available pesticide standard.

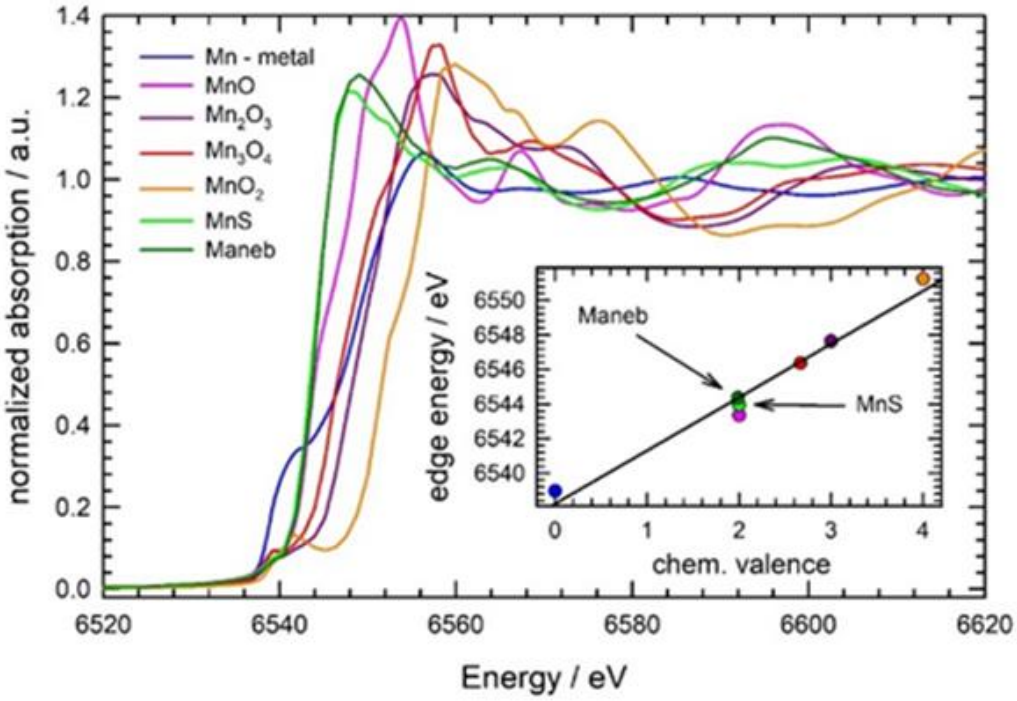

Figure S8: X-ray absorption near-edge spectra (XANES) of the Mn-O reference materials Mn-metal, MnO, Mn_3O_4, Mn_2O_3, and MnO_2 as indicated, (all measurements at room temperature). A clear shift to higher X-ray energies is observed depending on the chemical valence of Mn, and the inset shows a linear relationship between both quantities with a shift of about 3.1 eV per formal valence. The edge location of divalent MnS fits very well with these data (light green data point / spectrum). Anhydrous Maneb (dark green) agrees well with MnS in edge position and in the shape of the near edge.

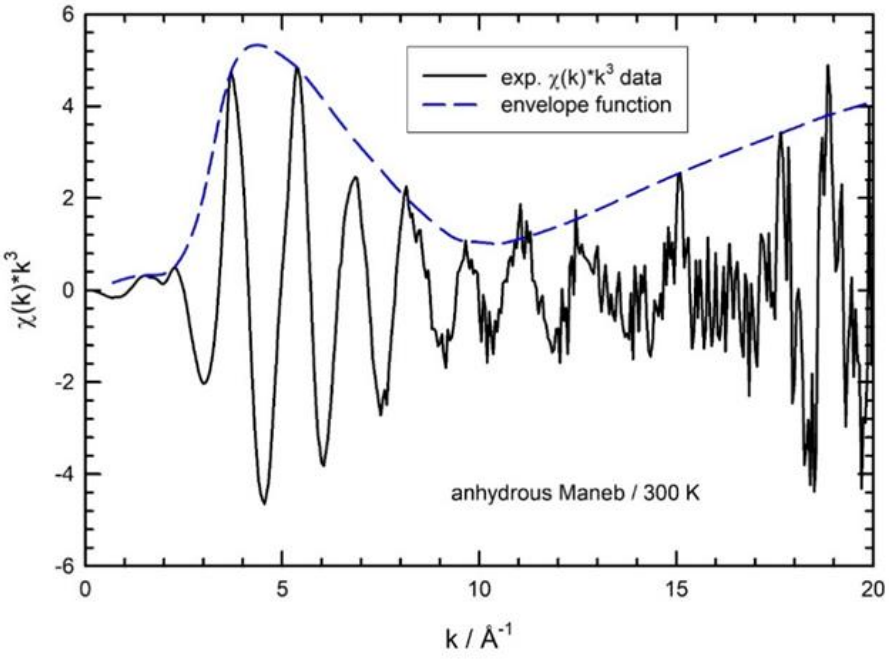

Figure S9: Room temperature k3-weighted extended X-ray absorption fine structure χ (k)*k3 obtained from anhydrous Maneb over an extended range in k and E. The envelope of the experimental EXAFS function is given as a dashed blue line. As can be seen, a beat node, i.e. a minimum, is observed for $k_{bn} \approx 10.3$ Å^{-1}.

In Figure S9 the k^3-weighted X-ray absorption fine structure (χ(k)*k^3) of anhydrous Maneb at room temperature is presented over an extended photoelectron wave vector (k) range. As can be seen, the amplitude of the χ(k)*k^3 first increases to about 5 Å^{-1} and decreases for increasing values of k. However, for further increasing values of k (i.e. k > 15 Å^{-1}), a substantial increase of the χ(k)*k^3 amplitude is again observed. In order to guide the eye, the envelope function is also provided in Figure S9. The observed minimum in the envelope function ("beat node") can easily be related to the superposition of the two Mn-S shells with slightly different bond length, and from the k-value of the beat node (k_{bn}), the difference in the bond distance of the two Mn-S shells (ΔR) can easily be estimated using $\Delta R = n*\pi/2\ k_{bn}$, see Martens *et al.*, 1977[250]. As can be seen from Figure S9, the beat node in the k^3-weigthed EXAFS function of the anhydrous Maneb (dashed envelope line of the EXAFS function) occurs at ca. 10.3 Å^{-1}, so that, employing n=1, ΔR results to 0.152 Å, well in accordance with the quantitative fits of the EXAFS function (Figure 3 in the main text).

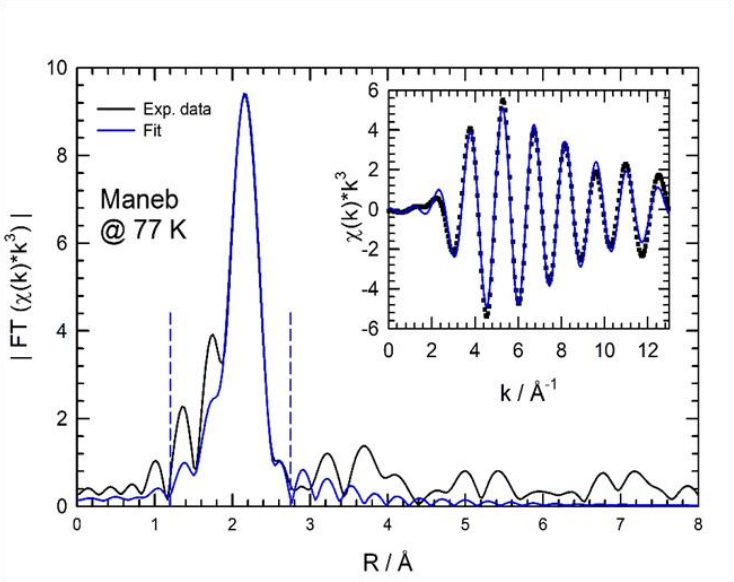

Figure S10: Magnitude of the Fourier transform of the k3-weighted EXAFS fine structure | FT (χ(R) | for the anhydrous Maneb sample at the Mn K-edge measured at 77 K. Both the raw data and a fit to a model structure comprised of 4 short and 2 long Mn-S bonds are shown. The inset depicts the back transform (χ(k)*k^3 data R_{max} = 2.75 Å (dashed vertical blue lines) for the data and the fits. More details are provided in the text (k-range for the Fourier transform: k_{min} = 1.98 Å^{-1} to k_{max}= 12.94 Å^{-1}) of the Fourier transform in the range from R_{min} = 1.2 Å to).

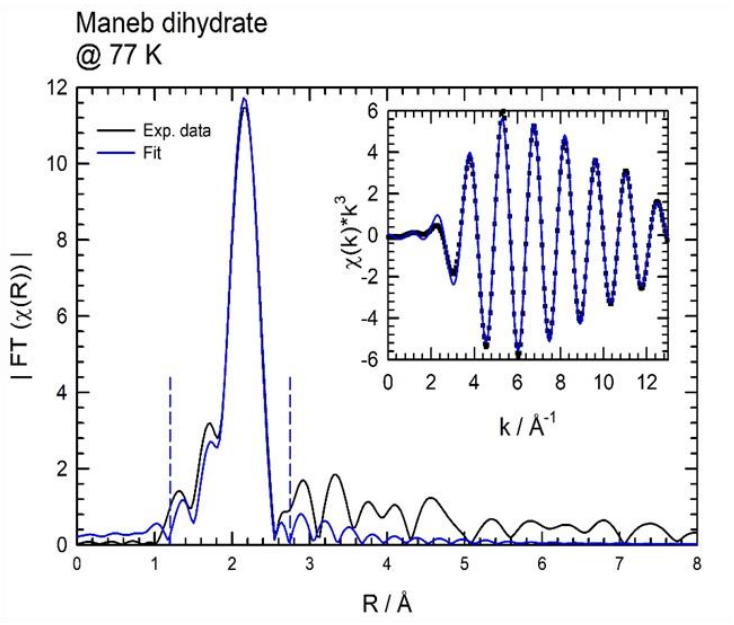

Figure S11: Magnitude of the Fourier transform of the k3-weighted EXAFS fine structure | FT (χ(R) | for the Maneb dihydrate sample at the Mn K-edge measured at 77 K. Both the raw data and a fit to a model structure comprised of 4 short and 2 long Mn-S bonds are shown. The inset depicts the back transform (χ(k)*k^3 data) of the Fourier transform in the range from R_{min} = 1.2 Å to R_{max} = 2.75 Å (dashed vertical blue lines) for the data and the fits. More details are provided in the text (k-rangefor the Fourier transform: k_{min} = 1.98 Å^{-1} to k_{max}= 12.94 Å^{-1}).

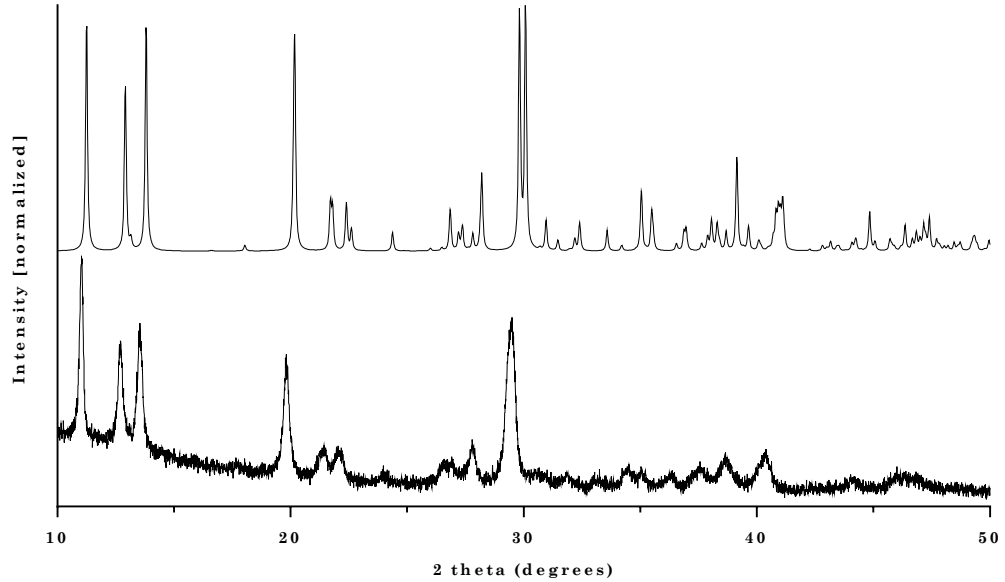

Figure S12: X-ray powder pattern of Maneb dihydrate (bottom). The calculated powder pattern of Maneb dihydrate (top) was obtained using Mercury from electron diffraction data. The small shift of the experimental data towards lower 2θ values can explained by the temperature. Calculated data is based on low temperature ED data, whilst powder diffraction data were collected at room temperature.

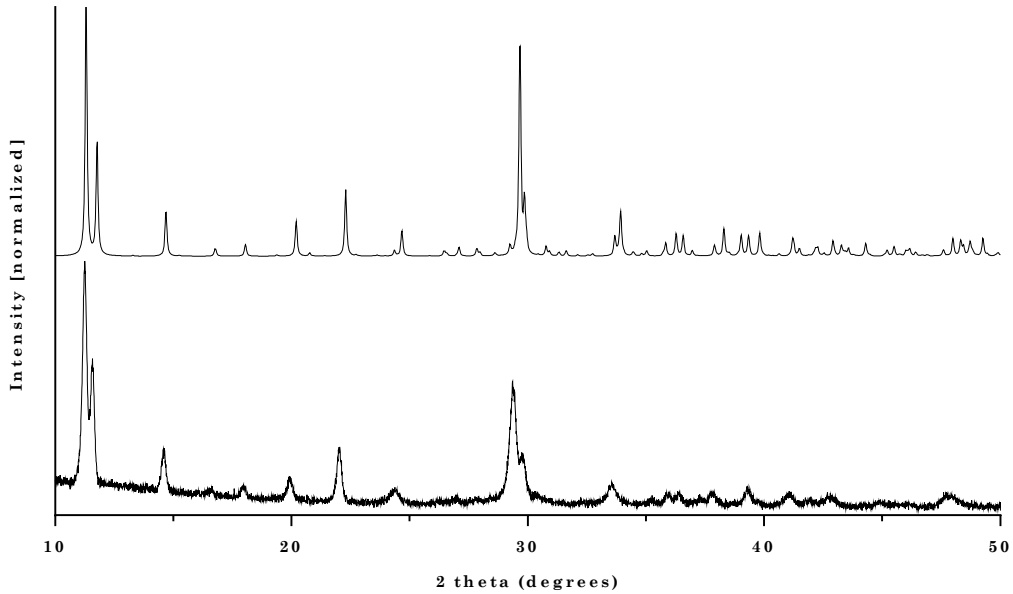

Figure S13: X-ray powder pattern of Maneb anhydrous (bottom). The calculated powder pattern Maneb anhydrous (top) was obtained using Mercury from electron diffraction data. The small shift of the experimental data towards lower 2θ values can explained by the temperature. Calculated data is based on low temperature ED data, whilst powder diffraction data were collected at room temperature.

Table S1: Crystal data and structure refinement for Maneb DMF.

CCDC code	2177534
Empirical Formular	$C_{16}H_{34}MnN_6O_4S_4$
Formular weight	557.67
Temperature/K	150
Crystal System	monoclinic
Space Group	$P2_1/n$
a/Å	17.0330(5)
b/Å	10.4373(2)
c/Å	17.1213(6)
α/°	90
ß/°	118.727(4)
γ/°	90
Volume/Å^3	2669.17(6)
Z	4
P_{calc}/g/cm^3	1.388
μ/mm^{-1}	0.839
F(000)	1172.0
Crystal size/mm^3	0.1 x 0.07 x 0.03
Radiation	Mo Kα (λ = 0.71073)
2θ range for data collection	4.754 to 58.562
Index ranges	$-22 \leq h \leq 23$, $-13 \leq k \leq 14$, $-12 \leq l \leq 23$
Reflection collected	16426
Independent reflections	6127 [R_{int} = 0.0317, R_{sigma} = 0.0345]
Data/restraints/parameters	6127/0/288
Goodness-of-fit on F^2	1.044
Final R indexes [I>=2σ(I)]	R_1 = 0.0345. WR_2 = 0.0837
Final R indexes [all data]	R_1 = 0.0456. WR_2 = 0.0903
Largest diff. peak/hole/e Å^3	0.43/-0.27

Table S2: Crystal data and structure refinement for Maneb DMSO.

CCDC code	2177535
Empirical Formular	$C_{12}H_{30}MnN_2O_4S_8$
Formular weight	577.80
Temperature/K	100
Crystal System	orthorhombic
Space Group	$Pca2_1$
a/Å	35.4838(6)
b/Å	10.81153(14)
c/Å	7.5204(3)
α/°	90
β/°	90
γ/°	90
Volume/Å^3	6721.42(18)
Z	8
P_{calc}/g/cm^3	1.142
μ/mm^{-1}	0.905
F(000)	2408.0
Crystal size/mm^3	0.15 x 0.1 x 0.08
Radiation	Mo Kα (λ = 0.71073)
2θ range for data collection	4.988 to 59.092
Index ranges	$-46 \leq h \leq 36$, $-13 \leq k \leq 14$, $-15 \leq l \leq 23$
Reflection collected	27989
Independent reflections	12001 [R_{int} = 0.0253, R_{sigma} = 0.0409]
Data/restraints/parameters	12001/1/504
Goodness-of-fit on F^2	1.036
Final R indexes [I>=2σ(I)]	R_1 = 0.0459. WR_2 = 0.1102
Final R indexes [all data]	R_1 = 0.0508. WR_2 = 0.1133
Largest diff. peak/hole/e Å^3	0.54/-0.39
Flack parameter	0.42(2)

Crystal data for Maneb anhydrous: CCDC 2255649, yellow plate, $C_4H_6MnN_2S_4$, M_r = 265.29 gmol^{-1}, triclinic, space group *P*-1 (No. 2), a = 7.2027(9) Å, b = 7.3452(10) Å, c = 8.8355(13) Å, α = 108.216(13)°, β = 108.011(12)°, γ = 94.327(10)°, V = 414.53(11) Å^3, Z = 2, Z' = 1, T = 100 K, m(transmission electron microscope) = 0.000, 8137 total reflections, 1538 with $I_0 > 2\sigma(I_0)$, R_{int} = 0.1240, 1757 data, 101 parameters, 121 restraints, GoF = 1.146, R_1 = 0.1934 and wR_2 = 0.4426 [$I_0 > 2\sigma(I_0)$], R_1 = 0.2100 and wR_2 = 0.4541 (all reflections), 0.324 < dΔρ < -0.318.

Table S3: Data collection parameter overview for Maneb anhydrous

Dataset (grain)	Number of frames	Scan range [°]	Scan width [°]	Exposure time [s]	Total time [min]
944	480	-60 to +60	0.25	0.25	02:08
945	480	-60 to +60	0.25	0.25	02:07
947	492	-63 to +60	0.25	0.50	04:13
948	480	-60 to +60	0.25	0.25	02:08
949	480	-60 to +60	0.25	0.50	04:07
				Total:	14:43

Table S4: Data quality statistics overview for all single data collections as well as merged data. All datasets were processed up to a resolution of 0.80 Å. Point group symmetry: *P*-1.

Dataset (grain)	Data	Compl. [%]	Redund.	$\langle F^2 \rangle$	$\langle F^2/\sigma(F^2) \rangle$	R_{int}	R_{rim}	R_{pim}	CC*
944	2246	65.4	2.0	75.13	22.80	0.111	0.156	0.111	0.991
945	2272	66.6	1.9	44.42	16.43	0.097	0.137	0.097	0.996
947	2272	66.2	2.0	36.26	18.78	0.082	0.117	0.082	0.998
948	2281	66.8	2.0	31.78	13.78	0.106	0.150	0.106	0.996
949	2238	65.3	1.9	23.88	15.30	0.080	0.114	0.080	0.998
merged	7781	99.9	4.6	29.69	21.81	0.121	0.137	0.066	0.997

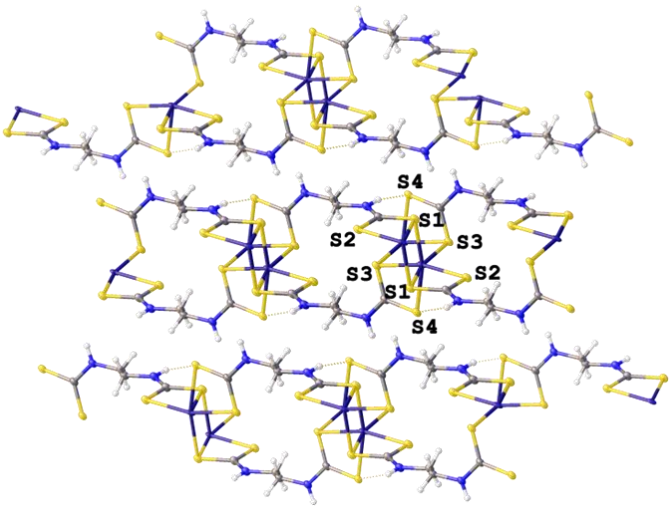

Figure S14: Crystal packing viewing along principal lattice axis : [1 0 0]. Maneb anhydrous forms a two-dimensional coordination polymer. Hydrogen atoms have been omitted for clarity.

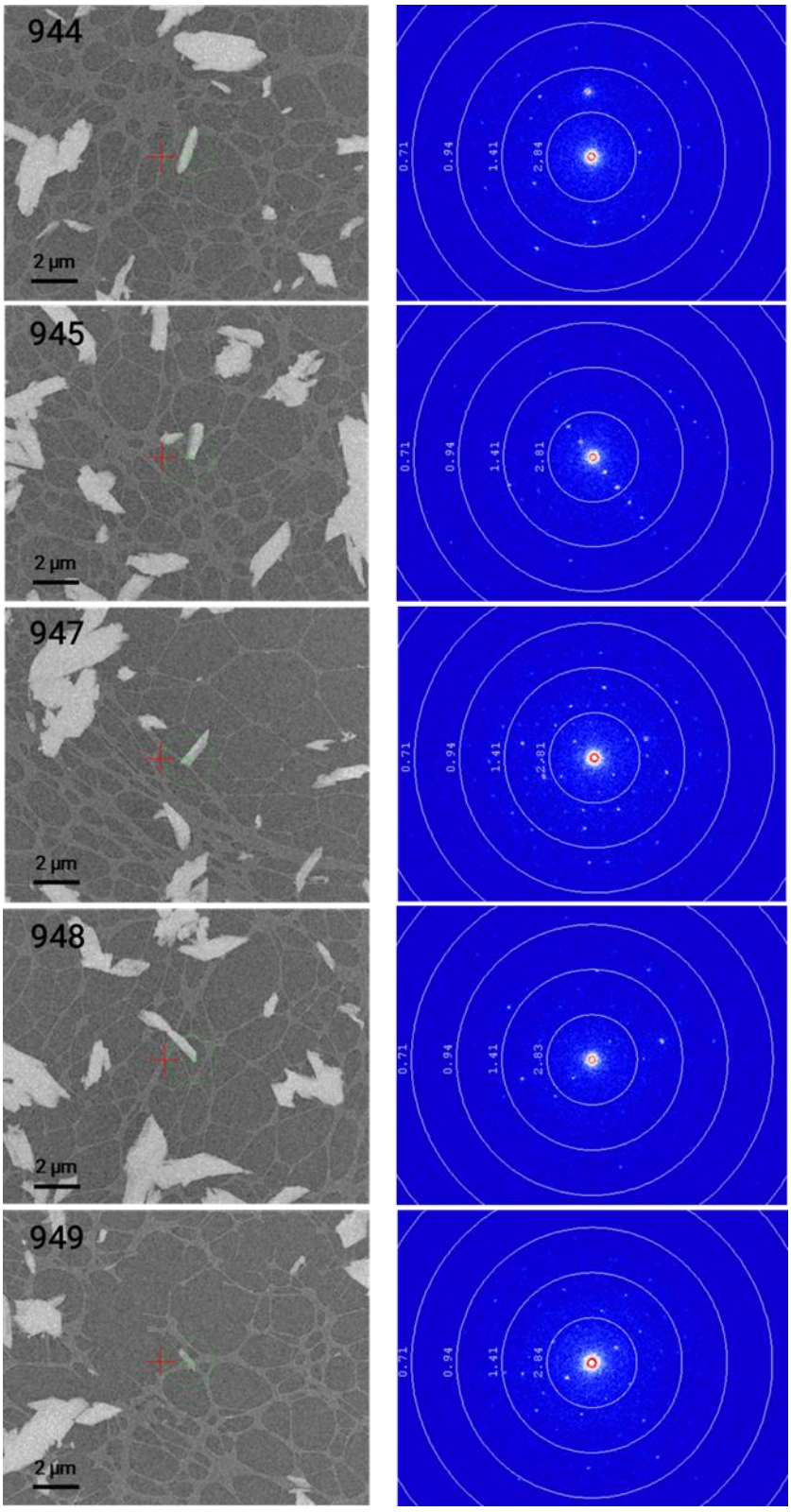

Figure S15: Grain snapshots and diffraction images for all selected measurements of Maneb anhydrous.

Crystal data for Maneb dihydrate: CCDC 2255650, yellow plate, C4H10MnN2O2S4, Mr = 301.32 gmol-1, monoclinic, space group P21/c (No. 14), a = 9.42(9) Å, b = 15.02(12) Å, c = 7.64(8) Å, α = 90°, ß = 103.7(4)°, γ = 90°, V = 1050(17) Å3, Z = 4, Z' = 1, T = 100 K, m(transmission electron microscope) = 0.000, 19363 total reflections, 2443 with I0 > 2σ(I0), Rint = 0.1879, 3209 data, 119 parameters, 122 restraints, GoF = 1.120, R1 = 0.1796 and wR2 = 0.4273 [I0 > 2σ(I0)], R1 = 0.2130 and wR2 = 0.4472 (all reflections), 0.291 < dΔρ < -0.487.

Table S5: Data collection parameter overview for Maneb dihydrate.

Dataset (grain)	Number of frames	Scan range [°]	Scan width [°]	Exposure time [s]	Total time [min]
951	480	-60 to +60	0.25	0.25	02:08
952	400	-60 to +40	0.25	0.25	01:47
953	480	-60 to +60	0.25	0.25	02:08
				Total:	06:03

Table S6: Data quality statistics overview for all single data collections and merged data. All datasets were processed up to a resolution of 0.70 Å. Point group symmetry: *P*2/*m*.

Dataset (grain)	Data	Compl. [%]	Redund.	$<F^2>$	$<F^2/\sigma(F^2)>$	R_{int}	R_{rim}	R_{pim}	CC*
951#	7051	71.5	3.0	28.68	12.33	0.131	0.169	0.097	0.997
952	6212	61.6	3.0	14.41	9.58	0.150	0.192	0.106	0.996
953	7703	95.1	2.4	8.52	7.44	0.186	0.256	0.162	0.991
merged	19876	99.8	6.0	11.72	13.05	0.186	0.220	0.087	0.995

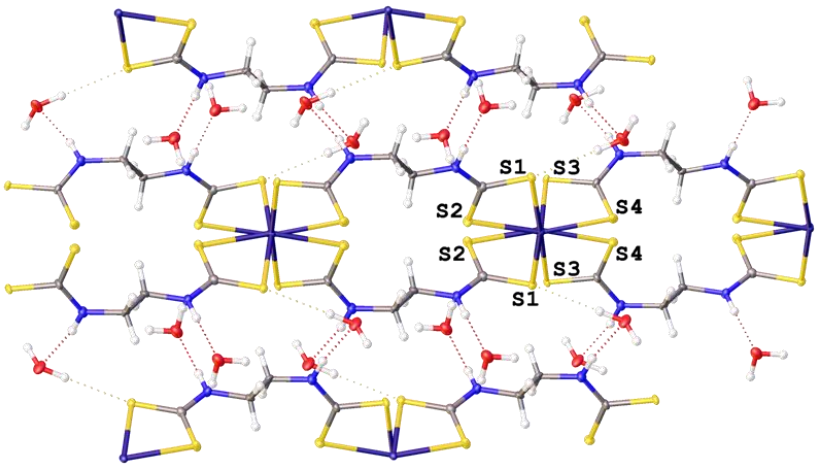

Figure S16: Crystal packing viewing along principal lattice axis: [0 0 1]. Maneb dihydrate forms a two-dimensional coordination polymer with co-crystallized water molecules located in-between the polymer layers stabilizing the structure via hydrogen bonds.

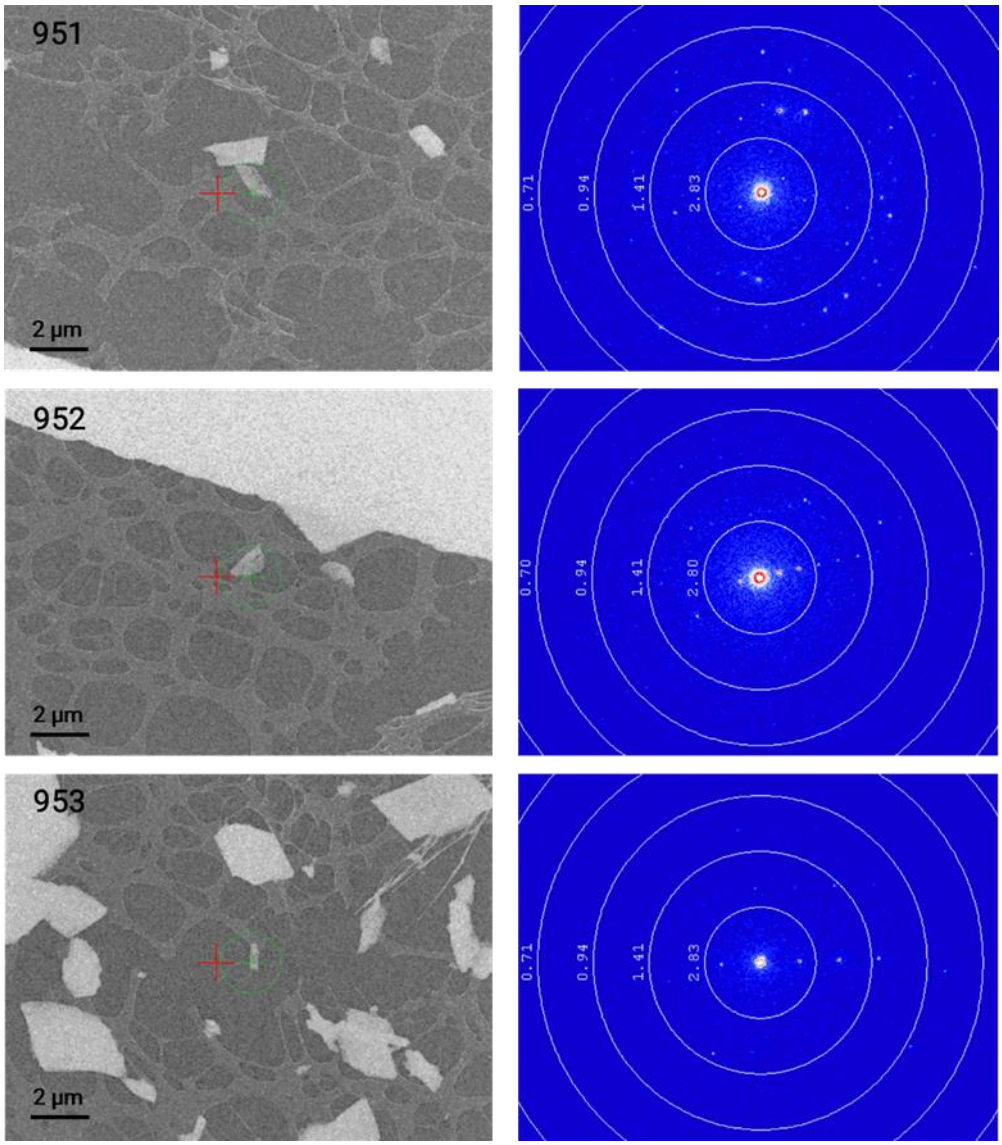

Figure S17: Grain snapshots and diffraction images for all selected measurements of Maneb dihydrate.

Author Contributions

LK: formal analysis (lead), investigation (lead), validation (equal), writing of original draft (lead); **KNT**: data curation (equal), formal analysis (supporting), investigation (supporting); **CWL**: data curation (equal), formal analysis (supporting), investigation (supporting); **DLH**: data curation (equal), formal analysis (equal), investigation (equal), validation (supporting), writing of original draft (equal); **JB**: formal analysis (supporting), validation (supporting), writing of original draft (supporting); **FM**: formal analysis (equal), project administration (lead), writing of original draft (equal)

Supplementary Material for Chapter 6
Exposure to the environmentally relevant fungicide Maneb: Studying toxicity in the soil nematode *Caenorhabditis elegans*

Experimental Procedures

Material.

All reagents were obtained from commercial suppliers and were used as received.

Instruments.

NMR spectra were recorded on a Bruker Avance 400 spectrometer and signals were referenced externally to Me_4Si. Thermal gravimetric analysis experiments were conducted using a Netzsch STA 449 F5 Jupiter instrument. Measurements were carried out in alumina crucibles, which were closed with alumina lids. Samples were heated from 25°C to 400 °C with a heating rate of 5 K min^{-1} in a nitrogen atmosphere applying a constant nitrogen flow of 25 ml min^{-1}. IR spectra were recorded on a Thermo Scientific Nicolet iS5 spectrometer equipped with an iD7 diamond ATR unit.

Syntheses

Nabam (Disodium ethylene bisdithiocarbamate hexahydrate).

Nabam was synthesized according to a published synthesis route[255]. 1.6 g (40 mmol, 2.0 eq.) sodium hydroxide was dissolved in 7.5 mL water and then 1.34 mL (20 mmol, 1.0 eq.) ethylenediamine was added. The solution was cooled to 0 °C and 3.00 mL (50 mmol, 2.5 eq.) carbon disulfide was added. The mixture was then stirred for 3 h at room temperature. To the mixture was added 100 mL of acetone, forming a colorless precipitate. This was isolated by filtration, washed with acetone and dried. Subsequently, the colorless precipitate was re-dissolved in 10 mL of water and precipitated by using 150 mL of acetone. The precipitate obtained was again filtered, washed with acetone and dried in vacuo. 4.2 g (12 mmol, 57%) of a colorless solid was be obtained. Single crystal X-ray diffraction, thermal gravimetric analysis and elemental analysis confirmed the product to be the hexahydrate of disodium ethylene bisdithiocarbamate. ^{1}H-NMR (400 MHz, D_2O): δ in ppm = 3.87 (s, 4H). ^{13}C-NMR (400 MHz, D_2O): δ in ppm = 213.9, 48.3. IR (ATR) $\tilde{\upsilon}$ [cm^{-1}] = 3330, 3284, 1606, 1489, 1429, 1345, 1282, 1239, 1044, 945, 761, 743. Elemental analysis, calculated for $C_4H_{18}N_2Na_2O_6S_4$: C, 13.16; H, 4.98; N, 7.69. Found: C, 13.04; 4.89; N, 7.56. Thermal gravimetric analysis: -

28.5 % mass loss below 100 °C corresponds to - 6 H_2O (Figure S20). Data agree with the calculated mass loss of - 30 % for six water molecules.

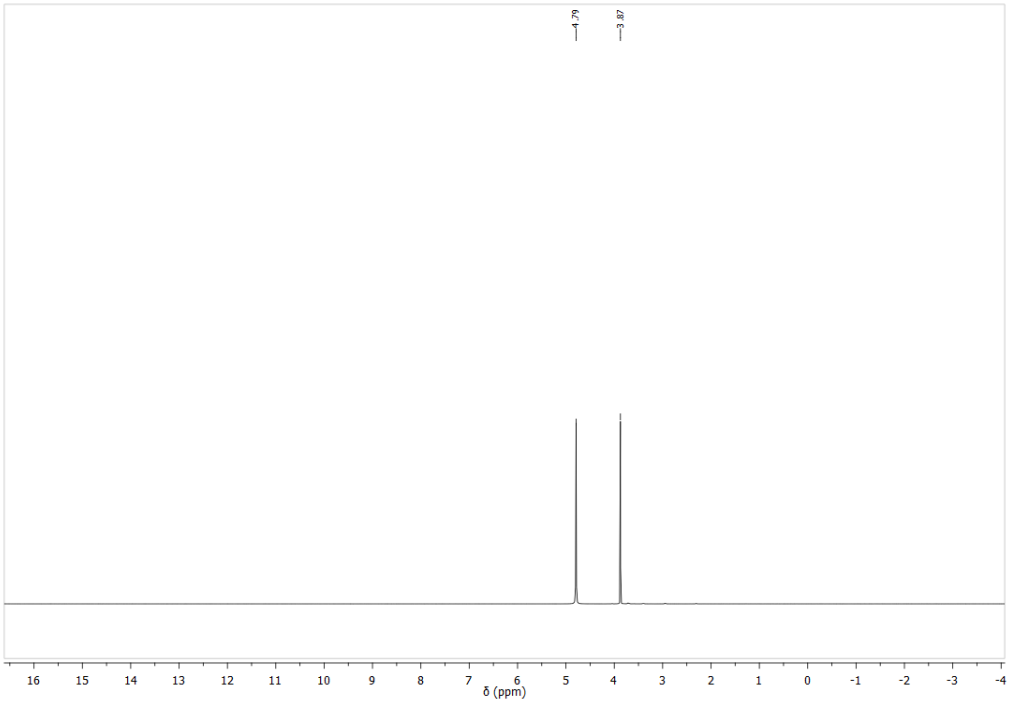

Figure S18: ^{1}H-NMR-spectrum of Nabam.

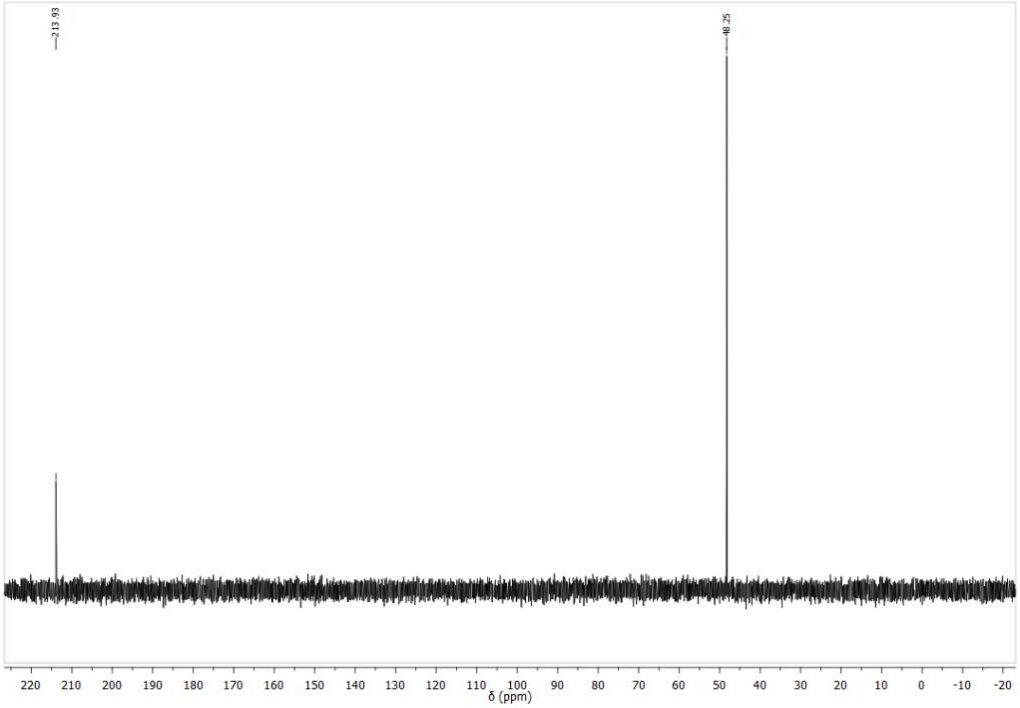

Figure S19: ^{13}C-NMR-spectrum of Nabam.

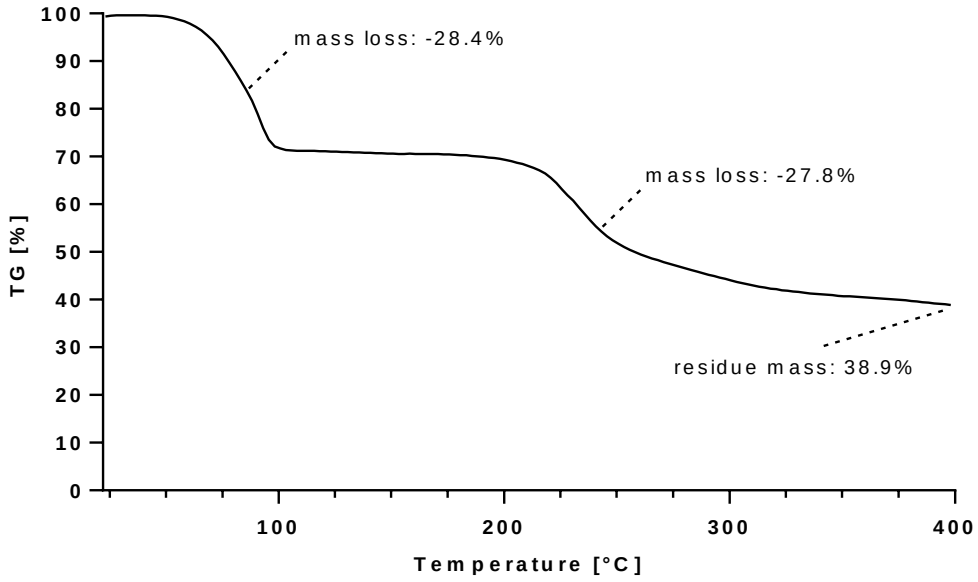

Figure S20: Thermal gravimetric analysis (TGA) curve of Nabam.

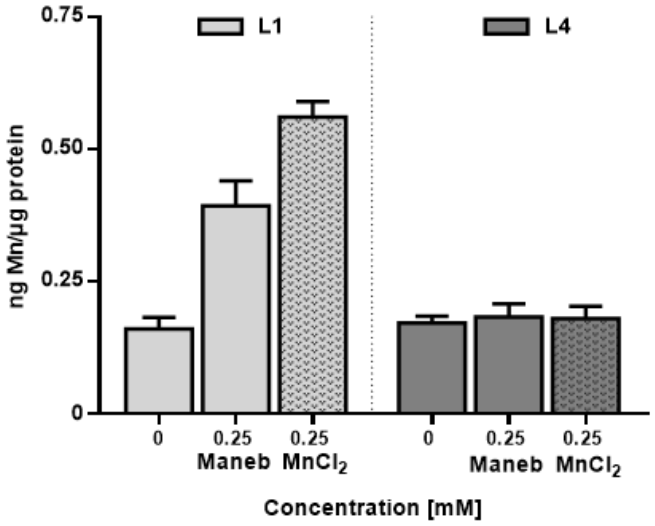

Figure S21: Total Mn amount (normalized to protein content) of L4 larval stage wild-type worms 48 h post-treatment after acute Maneb or $MnCl_2$ exposure for 2 h in L1 stage worms. Data are expressed as means ± SEM from at least three independent experiments.

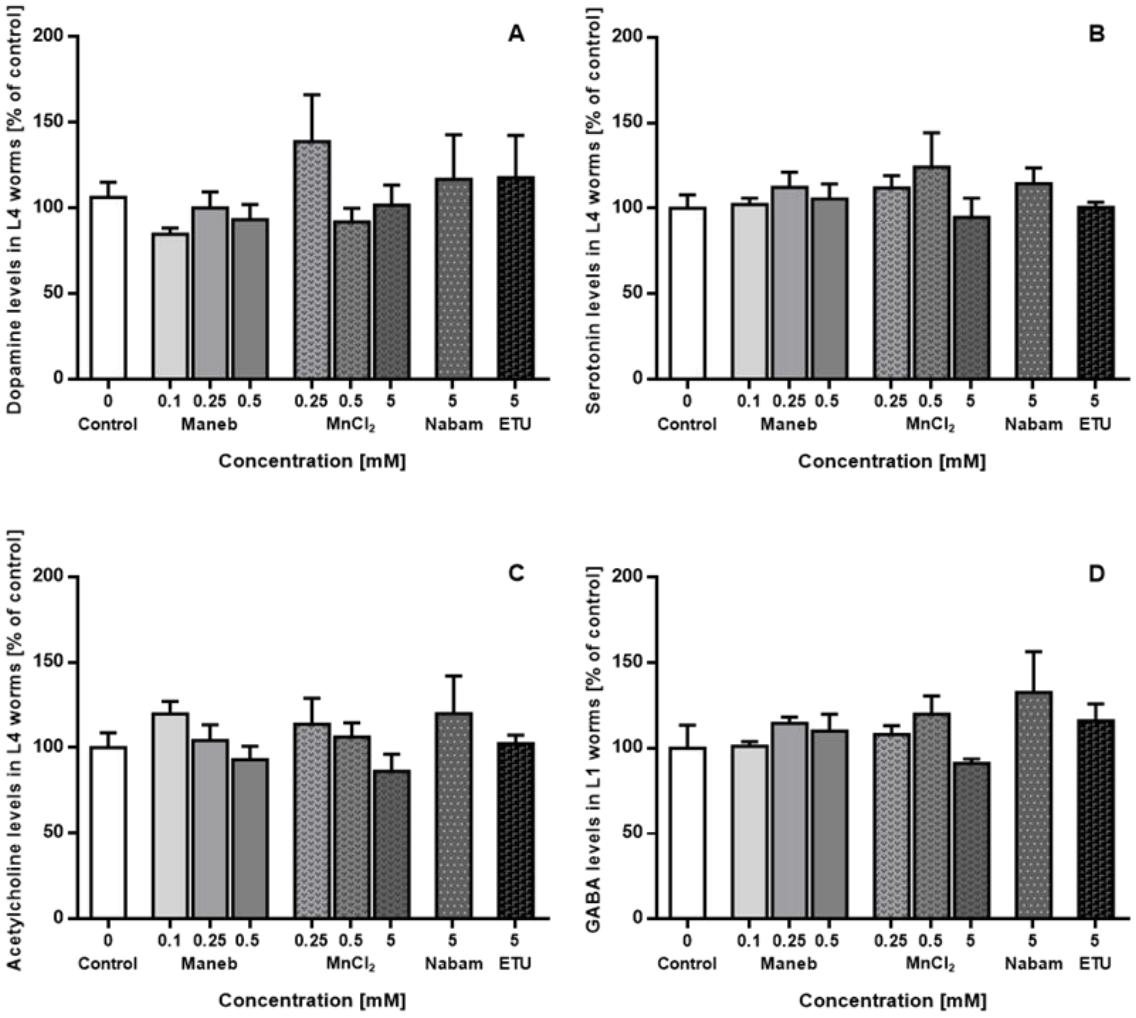

Figure S22: Neurotransmitter levels (dopamine **(A)**, serotonin **(B)**, acetylcholine **(C)**, GABA **(D)**) measured with LC-MS/MS normalized to protein content and normalized to respective control of wild-type worms (L4 larvae) following acute exposure for 2 h and resting 48 h to reach the L4 larval stage. Data are expressed as means ± SEM from at least three independent experiments. An unpaired *t* test with Welch's correction was used for the statistical analysis.

References

[1] D. G. Le Couteur, A. J. McLean, M. C. Taylor, B. L. Woodham, P. G. Board, *Biomed. Pharmacother.* **1999**, *53*, 122.

[2] H. B. Ferraz, P. H. Bertolucci, J. S. Pereira, J. G. Lima, L. A. Andrade, *Neurology* **1988**, *38*, 550.

[3] G. Meco, V. Bonifati, N. Vanacore, E. Fabrizio, *Scand. J. Work. Environ. Health* **1994**, *20*, 301.

[4] A. L. Flenner, US-2504404. (E. I. du Pont de Nemours and Company), **1950**.

[5] J. W. Nemec, V. H. Unger, W. Grove, C. B. Lyon, GB-1000137A. (Rohm & Haas Company), **1965**.

[6] M. L. Gullino, F. Tinivella, A. Garibaldi, G. M. Kemmitt, L. Bacci, B. Sheppard, *Plant disease* **2010**, *94*, 1076.

[7] C. C. Anderson, J. O. Marentette, D. S. Backos, J. R. Roede, *Adv. Red. Res.* **2021**, *2*, 100008.

[8] B. K. Barlow, D. W. Lee, D. A. Cory-Slechta, L. A. Opanashuk, *NeuroToxicology* **2005**, *26*, 63.

[9] L. Hoffman, L. Trombetta, D. Hardej, *Environ. Toxicol. Pharmacol.* **2016**, *41*, 78.

[10] D. M. Kurzatkowski, L. D. Trombetta, *Environ. Toxicol. Pharmacol.* **2013**, *36*, 427.

[11] C. C. Anderson, J. O. Marentette, A. K. Rauniyar, K. M. Prutton, M. Khatri, C. Matheson, J. A. Reisz, P. Reigan, A. D'Alessandro, J. R. Roede, *Free Radic. Biol. Med.* **2016**, *162*, 65.

[12] J. Couper, *Br. Ann. Med. Pharm. Vital Stat. Gen. Sci.* **1837**, *1*, 41.

[13] H. Embden, *Dtsch. Med. Wochenschr.* **1901**, *27*, 795.

[14] L. Casamajor, *JAMA* **1913**, *60*, 646.

[15] D. S. Avila, R. L. Puntel, M. Aschner, *Manganese in Health and Disease*. In: Sigel, A., Sigel, H., Sigel R. Interrelations between Essential Metal Ions and Human Diseases. Metal Ions in Life Science. Vol. 13, Springer, Dordrecht, **2013**.

[16] H. Debus, *Ann. Chem. Pharm* **1850**, 26.

[17] G. Hogarth, *Mini-Rev. Med. Chem.* **2012**, *12*, 1202.

[18] G. Hogarth, *Transition Metal Dithiocarbamates: 1978-2003*. Progress in Inorganic Chemistry (Ed. Kenneth D. Karlin), Wiley-VCH Verlag GmbH & Co, Weinheim, **2005**.

[19] G. Li, H. Tajima, T. Ohtani, *J. Org. Chem.* **1997**, *62*, 4539.

[20] R. G. Pearson, *J. Am. Chem. Soc.* **1963**, *85*, 3533.

[21] W. H. Tisdale, I. Williams, US-1972961. (E. I. du Pont de Nemours and Company), **1934**.

[22] W. F. Hester, D. Hill, US-2317765. (Röhm & Haas Company), **1943**.

[23] Channing Bruce Lyon, Abington, Jospeh W. Nemec, Rydal, Victor H, Unger, Willow Grove, US-3379610. (Rohm & Haas Company, **1968**.

[24] John W. Heuberger, US-2457674. (Röhm & Haas Company), **1948**.

[25] F. Müller, P. Ackermann, P. Margot in *Ullmann's encyclopedia of industrial chemistry*, Wiley, Chichester, **2010**.

[26] T. C. W. Mak, K. S. Jasim, C. Chieh, *Can. J. Chem.* **1984**, *62*, 808.

[27] V. Vrábel, Š. Gergely, J. Lokaj, E. Kellö, J. Garaj, *Acta Cryst. C* **1987**, *43*, 2293.

[28] J. B. Lefton, K. B. Pekar, T. Runcevski, *Cryst. Growth Des.* **2020**, *20*, 851.

[29] B. Trzaskowski, A. Les, L. Adamowicz, *Int. J. Mol. Sci.* **2003**, *4*, 503.

[30] M. Ciampolini, C. Mengozzi, P. Orioli, *J. Chem. Soc.* **1975**, 2051.

[31] G. J. Wang, C. M. Yin, Y. Wang, Y. H. Kong, G. H. Wang, C. Y. Wu, L. F. Zhang, Z. R. Liu, *Thermochim. Acta* **1993**, *220*, 213.

[32] R. Negga, D. A. Rudd, N. S. Davis, A. N. Justice, H. E. Hatfield, A. L. Valente, A. S. Fields, V. A. Fitsanakis, *NeuroToxicology* **2011**, *32*, 331.

[33] C. B. Lyon, Abington, J. W. Nemec, Rydal, V. H. Unger, W. Grove, US-3379610. (Rohm & Haas Company), **1968**.

[34] V. R. R. Lemes, H. A. Martins-Júnior, S. V. C. de Souza, S. Colacioppo, *Food Control* **2014**, *42*, 321.

[35] A. N. Jardim, E. D. Caldas, *Food Control* **2012**, *25*, 607.

[36] S. Hurt, J. Ollinger, G. Arce, Q. Bui, A. J. Tobia, B. van Ravenswaay in *Hayes' handbook of pesticide toxicology* (Ed.: R. I. Krieger), Academic Press, London, **2010**, pp. 1689–1710.

[37] M. Anastassiadou, G. Bernasconi, A. Brancato, L. Carrasco Cabrera, L. Greco, S. Jarrah, A. Kazocina, R. Leuschner, J. O. Magrans, I. Miron, S. Nave, R. Pedersen, H. Reich, A. Rojas, A. Sacchi, M. Santos, A. Stanek, A. Theobald, B. Vagenende, A. Verani, *EFS2* **2020**, *18*, e06108.

[38] H. Abdourahime, M. Anastassiadou, M. Arena, D. Auteri, S. Barmaz, A. Brancato, L. Bura, L. Carrasco Cabrera, E. Chaideftou, A. Chiusolo, D. Court Marques, F. Crivellente, C. de Lentdecker, M. Egsmose, G. Fait, L. Ferreira, V. Gatto, L. Greco, A. Ippolito, F. Istace, S. Jarrah, D. Kardassi, R. Leuschner, A. Lostia, C. Lythgo, S. Messinetti, I. Miron, T. Molnar, L. Padovani, J. M. Parra Morte, *EFS2* **2020**, *18*, e05755.

[39] L. Carrasco Cabrera, P. Medina Pastor, *EFS2* **2022**, *20*.

[40] M. Kretschmer, M. Leroch, A. Mosbach, A.-S. Walker, S. Fillinger, D. Mernke, H.-J. Schoonbeek, J.-M. Pradier, P. Leroux, M. A. de Waard, M. Hahn, *PLoS pathogens* **2009**, *5*, e1000696.

[41] Fungicide Resistance Action Committee (FRAC), "Background Information: How does a Fungicide Resistance evolve?", can be found under https://www.frac.info/fungicide-resistance-management/background.

[42] J.-L. Genet, G. Jaworska, *Pest. Manag. Sci.* **2009**, *65*, 878.

[43] T. S. Thind, D. W. Hollomon, *Pest Manag. Sci.* **2018**, *74*, 1547.

[44] I. Camoni, A. Di Muccio, D. Pontecorvo, P. Citti, *Ecotoxicol. Environ. l Saf.* **1988**, *16*, 176.

[45] F. Shaheen, Zia-ur-Rehman, S. Ali, A. Meetsma, *Polyhedron* **2012**, *31*, 697.

[46] G. Manoussakis, C. Bolos, L. Ecateriniadou, C. Sarris, *Eur. J. Med. Chem.* **1987**, *22*, 421.

[47] H. Rattba, W. Schnaak, *Archiv für Pflanzenschutz* **1971**, *7*, 427.

[48] S. B. Kalia, G. Kaushal, M. Kumar, S. S. Cameotra, A. Sharma, M. L. Verma, S. S. Kanwar, *Braz. J. Microbiol.* **2009**, *40*, 916.

[49] V. Vukosanovic, Z. Leka, N. Terzic, *Fresensius Environ. Bull.* **2013**, *22*, 3803.

[50] J. R. Richardson, V. Fitsanakis, R. H. S. Westerink, A. G. Kanthasamy, *Acta Neuropathol.* **2019**, *138*, 343.

[51] A. M. Mora, L. Córdoba, J. C. Cano, D. Hernandez-Bonilla, L. Pardo, L. Schnaas, D. R. Smith, J. A. Menezes-Filho, D. Mergler, C. H. Lindh, B. Eskenazi, B. van Wendel de Joode, *Environ. Health Perspect.* **2018**, *126*, 57007.

[52] S. Costello, M. Cockburn, J. Bronstein, X. Zhang, B. Ritz, *Am. J. Epidemiol.* **2009**, *169*, 919.

[53] A. Wang, S. Costello, M. Cockburn, X. Zhang, J. Bronstein, B. Ritz, *Eur. J. Epidemiol.* **2011**, *26*, 547.

[54] L. M. Domico, G. D. Zeevalk, L. P. Bernard, K. R. Cooper, *NeuroToxicology* **2006**, *27*, 816.

[55] L. M. Domico, K. R. Cooper, L. P. Bernard, G. D. Zeevalk, *NeuroToxicology* **2007**, *28*, 1079.

[56] R. Negga, J. A. Stuart, M. L. Machen, J. Salva, A. J. Lizek, S. J. Richardson, A. S. Osborne, O. Mirallas, K. A. McVey, V. A. Fitsanakis, *Neurotox. Res.* **2012**, *21*, 281.

[57] K. Montgomery, C. Corona, R. Frye, R. Barnett, A. Bailey, V. A. Fitsanakis, *Neurotoxicol. Teratol.* **2018**, *68*, 66.

[58] A. G. Fitzmaurice, S. L. Rhodes, M. Cockburn, B. Ritz, J. M. Bronstein, *Neurology* **2014**, *82*, 419.

[59] L. J. Leiphon, M. J. Picklo, *NeuroToxicology* **2007**, *28*, 143.

[60] D. C. Bailey, C. E. Todt, S. E. Orfield, R. D. Denney, I. B. Snapp, R. Negga, K. M. Montgomery, A. C. Bailey, A. S. Pressley, W. L. Traynor, V. A. Fitsanakis, *NeuroToxicology* **2016**, *56*, 170.

[61] M. B. Colović, D. Z. Krstić, T. D. Lazarević-Pašti, A. M. Bondžić, V. M. Vasić, *Curr. Neuropharmacol.* **2013**, *11*, 315.

[62] E. Grosicka-Maciąg, D. Kurpios-Piec, M. Szumiło, T. Grzela, I. Rahden-Staroń, *Food Chem. Toxicol.* **2011**, *49*, 1020.

[63] C. Liu, Z. Liu, Y. Fang, Z. Liao, Z. Zhang, X. Yuan, T. Yu, Y. Yang, M. Xiong, X. Zhang, G. Zhang, L. Meng, Z. Zhang, *Environ. Int.* **2023**, *171*, 107696.

[64] R. N. Hill, L. S. Erdreich, O. E. Paynter, P. A. Roberts, S. L. Rosenthal, C. F. Wilkinson, *Toxicol Sci* **1989**, *12*, 629.

[65] N. Printemps, B. Le Magueresse-Battistoni, S. Mhaouty-Kodja, C. Viguié, C. Michel, *Int. J. Mol. Sci.* **2022**, *23*.

[66] S. A. Marchitti, C. Brocker, D. Stagos, V. Vasiliou, *Expert Opin. Drug Metab. Toxicol.* **2008**, *4*, 697.

[67] W. M. Panneton, V. B. Kumar, Q. Gan, W. J. Burke, J. E. Galvin, *PloS One.* **2010**, *5*, e15251.

[68] J. Kopin, Y. Sharabi, *J. Neurochem.* **2013**, *126*, 591.

[69] L. V. Kalia, A. E. Lang, *Lancet* **2015**, *386*, 896.

[70] A.-K. Weishaupt, L. Kubens, L. Ruecker, T. Schwerdtle, M. Aschner, J. Bornhorst, *Molecules* **2023**, *28*.

[71] N. Suthakaran, T. Brock, A. Naraine, P. Gonzalez-Lerma, C. Hopkins, K. Dawson-Scully, *microPubl. Biol.* **2022**, *2022*.

[72] J. K. Andersen, *Nat. Med.* **2004**, *10*, 18-25.

[73] M. Jozefczak, T. Remans, J. Vangronsveld, A. Cuypers, *Int. J. Mol. Sci.* **2012**, *13*, 3145.

[74] A. Meister, M. E. Anderson, *Annu. Rev. Biochem.* **1983**, *52*, 711.

[75] J. R. Roede, D. P. Jones, *Redox Biol.* **2014**, *2*, 651.

[76] M. Aschner, K. M. Erikson, E. Herrero Hernández, R. Tjalkens, *Neuromolecular Med.* **2009**, *11*, 252.

[77] P. Chen, S. Chakraborty, T. V. Peres, A. B. Bowman, M. Aschner, *Toxicol. Res.* **2015**, *4*, 191.

[78] J. Zhang, V. A. Fitsanakis, G. Gu, D. Jing, M. Ao, V. Amarnath, T. J. Montine, *J. Neurochem.* **2003**, *84*, 336.

[79] M. T. Lin, M. F. Beal, *Nature* **2006**, *443*, 787.

[80] S. Löffek, O. Schilling, C.-W. Franzke, *Eur. Respir. J.* **2011**, *38*, 191.

[81] P. M. Hurley, *Environ. Health Perspect.* **1998**, *106*, 437.

[82] International Agency for Research on Cancer, *Some Anti-Thyroid and Related Substances, Nitrofurans and Industrial Chemicals. Supplement 7 p. 207-208*, **1974**.

[83] R. Truhaut, M. Fujita, Nguyen-Phu-Lich, M. Chaigneau, *C. R. Acad. Sci. Paris* **1973**, *276*, 229.

[84] A. W. DeMartino, D. F. Zigler, J. M. Fukuto, P. C. Ford, *Chem. Soc. Rev.* **2017**, *46*, 21.

[85] J. C. Erve, V. Amarnath, D. G. Graham, R. C. Sills, A. L. Morgan, W. M. Valentine, *Chem. Res. Toxicol.* **1998**, *11*, 544.

[86] W. M. Valentine, V. Amarnath, D. G. Graham, D. L. Morgan, R. C. Sills, *Toxicol. Appl. Pharmacol.* **1997**, *142*, 95.

[87] J. Sachinidis, M. W. Grant, *Aust. J. Chem.* **1981**, *34*, 2195.

[88] J. Laubda, Skatulokova M., M. Nemeth, S. Gergely, *Chem. Papers* **1984**, *38*, 597.

[89] S. Caroldi, J. Jarvis, L. Magos, *Br. J. Pharmacol.* **1985**, *84*, 357.

[90] P. B. Molinoff, J. Axelrod, *Annu. Rev. Biochem.* **1971**, *40*, 465.

[91] T. Füzesi, G. Wittmann, R. M. Lechan, Z. Liposits, C. Fekete, *Brain Res.* **2009**, *1294*, 38.

[92] H. Klug, *Acta Cryst.* **1966**, *21*, 536.

[93] J. Albertsson, Å. Oskarsson, *Acta Cryst. B* **1977**, *33*, 1871.

[94] F. C. Lu, *Regul. Toxicol. Pharmacol.* **1995**, *21*, 352.

[95] L. Magos, *Br. J. Ind. Med.* **1972**, *29*, 90.

[96] Y. Wang, H. Zhang, X. Wu, C. Xue, Y. Hu, A. Khan, F. Liu, L. Cai, *Sci. Total Environ.* **2020**, *720*, 137666.

[97] A. P. Chou, N. Maidment, R. Klintenberg, J. E. Casida, S. Li, A. G. Fitzmaurice, P.-O. Fernagut, F. Mortazavi, M.-F. Chesselet, J. M. Bronstein, *J. Biol. Chem.* **2008**, *283*, 34696.

[98] C. Y. Kim, R. N. Alcalay, *Semin. Neurol.* **2017**, *37*, 135.

[99] K. W. Weissmahr, D. L. Sedlak, *Environ. Toxicol. Chem.* **2000**, *19*, 820.

[100] T. O. Ajiboye, T. T. Ajiboye, R. Marzouki, D. C. Onwudiwe, *Int. J. Mol. Sci.* **2022**, *23*.

[101] A. Gupta, S. Lutsenko, *Future Med. Chem.* **2009**, *1*, 1125.

[102] Y. Kanemoto-Kataoka, T. M. Oyama, H. Ishibashi, Y. Oyama, *Toxicol. Res.* **2017**, *6*, 499.

[103] M. Sook Han, K. J. Shin, Y. H. Kim, S. H. Kim, T. Lee, E. Kim, S. Ho Ryu, P. G. Suh, *NeuroToxicology* **2003**, *24*, 425.

[104] M. A. Zoroddu, J. Aaseth, G. Crisponi, S. Medici, M. Peana, V. M. Nurchi, *J. Inorg. Biochem.* **2019**, *195*, 120.

[105] E. Underwood, *Trace Elements in Human and Animal Nutrition*, Elsevier Science, Amsterdam, **2014**.

[106] European Food Safety Authority (EFSA), *EFSA support. publ.* **2017**, *14*.

[107] C. Agostoni, R. Berni Canani, S. S Fairweather-Tait, M. Heinonen, H. Korhonen, S. La Vieille, R. Marchelli, A. Martin, A. Naska, M. Neuhäuser-Berthold, G. Nowicka, Y. Sanz, A. Siani, A. Sjödin, M. Stern, S. J. J. Strain, I. Tetens, D. Tomé, D. Turck, H. Verhagen, *EFS2* **2014**, *12*, 3660.

[108] C. Agostoni, R. Berni Canani, S. S Fairweather-Tait, M. Heinonen, H. Korhonen, S. La Vieille, R. Marchelli, A. Martin, A. Naska, M. Neuhäuser-Berthold, G. Nowicka, Y. Sanz, A. Siani, A. Sjödin, M. Stern, S. J. J. Strain, I. Tetens, D. Tomé, D. Turck, H. Verhagen, *EFSA Journal* **2014**, *12*, 3846.

[109] C. Agostoni, R. Berni Canani, S. S Fairweather-Tait, M. Heinonen, H. Korhonen, S. La Vieille, R. Marchelli, A. Martin, A. Naska, M. Neuhäuser-Berthold, G. Nowicka, Y. Sanz, A. Siani, A. Sjödin, M. Stern, S. J. J. Strain, I. Tetens, D. Tomé, D. Turck, H. Verhagen, *EFSA Journal* **2013**, *11*, 3332.

[110] W. Becker, D. Brasseur, J. L. Bresson, A. Flynn, A. A. Jackson, P. Lagiou, G. Mingrone, B. Moseley, A. Paloi, H. Przyrembel, S. Salminen, S. Strobel, H. van Loveren, *EFS2* **2004**, *2*, 33.

[111] C. Agostoni, R. Berni Canani, S. S Fairweather-Tait, M. Heinonen, H. Korhonen, S. La Vieille, R. Marchelli, A. Martin, A. Naska, M. Neuhäuser-Berthold, G. Nowicka, Y. Sanz, A. Siani, A. Sjödin, M. Stern, S. J. J. Strain, I. Tetens, D. Tomé, D. Turck, H. Verhagen, *EFSA Journal* **2014**, *12*, 3845.

[112] L. Banci, I. Bertini, *Met Ions Life Sci.* **2013**, *12*, 1.

[113] B. L. Vallee, R. J. Williams, *Proc. Natl. Acad. Sci. U.S.A.* **1968**, *59*, 498.

[114] A. J. Thomson, H. B. Gray, *Curr. Opin. Chem. Biol.* **1998**, *2*, 155.

[115] R. Hänsch, R. R. Mendel, *Curr. Opin. Plant Biol.* **2009**, *12*, 259.

[116] K. A. McCall, C. Huang, C. A. Fierke, *J. Nutr.* **2000**, *130*, 1437–46.

[117] H. Irving, R. J. P. Williams, *Nature* **1948**, *162*, 746.

[118] W. B. Cannon, *Physiol. Rev.* **1929**, *9*, 399.

[119] H. Modell, W. Cliff, J. Michael, J. McFarland, M. P. Wenderoth, A. Wright, *Adv. Physiol. Educ.* **2015**, *39*, 259.

[120] M. J. Tamas, E. Martinoia, *Molecular Biology of Metal Homeostasis and Detoxification*, Springer, Berlin, Heidelberg, **2006**.

[121] P. Chen, J. Bornhorst, M. Diana Neely, D. S. Avila, *Oxid. Med. Cell. Longev.* **2018**, *2018*, 7612172.

[122] D. A. Dickinson, H. J. Forman, *Ann. N. Y. Acad. Sci.* **2002**, *973*, 488.

[123] J. R. Hodgson, C. C. Lee, *Toxicol. Appl. Pharmacol.* **1977**, *40*, 19.

[124] M. Farina, D. S. Avila, J. B. T. Da Rocha, M. Aschner, *Neurochem. Int.* **2013**, *62*, 575.

[125] G. Volkert, K.-D. Frank *Metallurgie der Ferrolegierungen*, Springer, Berlin, Heidelberg, **1972**.

[126] H. Frumkin, G. Solomon, *Am. J. Ind. Med.* **1997**, *31*, 107.

[127] S. Lacerda, D. Ndiaye, É. Tóth in *Metal Ions in Bio-Imaging Techniques* (Eds.: A. Sigel, E. Freisinger, R. K. Sigel), De Gruyter, **2021**, pp. 71–100.

[128] C. Agostoni, R. Berni Canani, S. S Fairweather-Tait, M. Heinonen, H. Korhonen, S. La Vieille, R. Marchelli, A. Martin, A. Naska, M. Neuhäuser-Berthold, G.

Nowicka, Y. Sanz, A. Siani, A. Sjödin, M. Stern, S. J. J. Strain, I. Tetens, D. Tomé, D. Turck, H. Verhagen, *EFS2* **2013**, *11*.

[129] M. Rose, M. Baxter, N. Brereton, C. Baskaran, *Food Addit. Contam.* **2010**, *27*, 1380.

[130] J. L. Aschner, M. Aschner, *Mol. Aspects Med.* **2005**, *26*, 353.

[131] J. A. Garcia-Aranda, R. A. Wapnir, F. Lifshitz, *J. Nutr.* **1983**, *113*, 2601.

[132] P. E. Johnson, G. I. Lykken, E. D. Korynta, *J. Nutr.* **1991**, *121*, 711.

[133] L. Davidsson, A. Cederblad, B. Lönnerdal, B. Sandström, *Am. J. Clin. Nutr.* **1991**, *54*, 1065.

[134] P. Chen, S. Chakraborty, S. Mukhopadhyay, E. Lee, M. M. B. Paoliello, A. B. Bowman, M. Aschner, *J. Neurochem.* **2015**, *134*, 601.

[135] R. F. Butterworth, *Metab. Brain Dis.* **2013**, *28*, 261.

[136] L. Spahr, R. F. Butterworth, S. Fontaine, L. Bui, G. Therrien, P. C. Milette, L. H. Lebrun, J. Zayed, A. Leblanc, G. Pomier-Layrargues, *Hepatology* **1996**, *24*, 1116.

[137] D. B. Calne, N. S. Chu, C. C. Huang, C. S. Lu, W. Olanow, *Neurology* **1994**, *44*, 1583.

[138] M. Bouchard, F. Laforest, L. Vandelac, D. Bellinger, D. Mergler, *Environ. Health Perspect.* **2007**, *115*, 122.

[139] M. F. Bouchard, S. Sauvé, B. Barbeau, M. Legrand, M.-È. Brodeur, T. Bouffard, E. Limoges, D. C. Bellinger, D. Mergler, *Environ. Health Perspect.* **2011**, *119*, 138.

[140] J. L. Aschner, A. Anderson, J. C. Slaughter, M. Aschner, S. Steele, A. Beller, A. Mouvery, H. M. Furlong, N. L. Maitre, *Am. J. Clin. Nutr.* **2015**, *102*, 1482.

[141] D. P. Perl, C. W. Olanow, *J. Neuropathol. Exp. Neurol.* **2007**, *66*, 675.

[142] D. G. Ellingsen, G. Shvartsman, R. Bast-Pettersen, M. Chashchin, Y. Thomassen, V. Chashchin, *Int. Arch. Occup. Environ. Health.* **2019**, *92*, 383.

[143] C. S. Lu, C. C. Huang, N. S. Chu, D. B. Calne, *Neurology* **1994**, *44*, 1600.

[144] M. Lin, L. M. Colon-Perez, D. O. Sambo, D. R. Miller, J. J. Lebowitz, F. Jimenez-Rondan, R. J. Cousins, N. Horenstein, T. B. Aydemir, M. Febo, H. Khoshbouei, *J. Neurosci.* **2020**, *40*, 5871.

[145] K. Tuschl, P. B. Mills, P. T. Clayton, *Int. Rev. Neurobiol.* **2013**, *110*, 277.

[146] J. Bornhorst, S. Chakraborty, S. Meyer, H. Lohren, S. G. Brinkhaus, A. L. Knight, K. A. Caldwell, G. A. Caldwell, U. Karst, T. Schwerdtle, A. Bowman, M. Aschner, *Metallomics* **2014**, *6*, 476.

[147] E. J. Martinez-Finley, C. E. Gavin, M. Aschner, T. E. Gunter, *Free Radic. Biol. Med.* **2013**, *62*, 65.

[148] R. B. Tjalkens, M. J. Zoran, B. Mohl, R. Barhoumi, *Brain Res.* **2006**, *1113*, 210.

[149] R. Williams, *Polyhedron* **1987**, *6*, 61.

[150] C. Agostoni, R. Berni Canani, S. S Fairweather-Tait, M. Heinonen, H. Korhonen, S. La Vieille, R. Marchelli, A. Martin, A. Naska, M. Neuhäuser-Berthold, G.

Nowicka, Y. Sanz, A. Siani, A. Sjödin, M. Stern, S. J. J. Strain, I. Tetens, D. Tomé, D. Turck, H. Verhagen, *EFSA Journal* **2014**, *12*, 3844.

[151] M. Maares, H. Haase, *Nutrients* **2020**, *12*.

[152] A. V. Skalny, M. Aschner, A. A. Tinkov, *Adv. Food Nutr. Res.* **2021**, *96*, 251.

[153] S. E. Wuehler, J. M. Peerson, K. H. Brown, *Public Health Nutr.* **2005**, *8*, 812.

[154] A. S. Prasad, *J. Am. Coll. Nutr.* **2009**, *28*, 257.

[155] D. d. N. Marreiro, K. J. C. Cruz, J. B. S. Morais, J. B. Beserra, J. S. Severo, A. R. S. de Oliveira, *Antioxidants* **2017**, *6*.

[156] W. Maret, *Exp. Gerontol.* **2008**, *43*, 363.

[157] L. M. Plum, L. Rink, H. Haase, *Int. J. Environ. Res. Public Health.* **2010**, *7*, 1342.

[158] D. N. Bothwell, E. A. Mair, B. B. Cable, *Pediatrics* **2003**, *111*, 689.

[159] C. Colombo, G. Palumbo, J.-Z. He, R. Pinton, S. Cesco, *J. Soils Sediments* **2014**, *14*, 538.

[160] G. Papanikolaou, K. Pantopoulos, *Toxicol. Appl. Pharmcol.* **2005**, *202*, 199.

[161] N. Abbaspour, R. Hurrell, R. Kelishadi, *J. Res. Med. Sci.* **2014**, *19*, 164.

[162] E. R. Monsen, *J. Am. Diet. Assoc.* **1988**, *88*, 786.

[163] M. Layrisse, J. D. Cook, C. Martinez, M Roche, I. N. Kuhn, R. B. Walker, C. A. Finch, *Blood* **1969**, *33*, 430.

[164] R. Hurrell, I. Egli, *Am. J. Clin. Nutr.* **2010**, *91*, 1461.

[165] J. L. Bresson, B. Burlingame, T. Dean, S. Fairweather-Tait, M. Heinonen, K. I. Hirsch-Ernst, I. Mangelsdorf, H. McArdle, A. Naska, M. Neuhäuser-Berthold, G. Nowicka, K. Pentieva, Y. Sanz, A. Siani, A. Sjödin, M. Stern, D. Tomé, D. Turck, H. van Loveren, M. Vinceti, P. Willatts, *EFSA Journal* **2015**, *13*, 4254.

[166] GBD 2015 Disease and Injury Incidence and Prevalence Collaborators, *Lancet* **2016**, *388*, 1545.

[167] M. B. Zimmermann, R. F. Hurrell, *Lancet* **2007**, *370*, 511.

[168] J. L. Bresson, B. Burlingame, T. Dean, S. Fairweather-Tait, M. Heinonen, K. I. Hirsch-Ernst, I. Mangelsdorf, H. McArdle, A. Naska, M. Neuhäuser-Berthold, G. Nowicka, K. Pentieva, Y. Sanz, A. Siani, A. Sjödin, M. Stern, D. Tomé, D. Turck, H. van Loveren, M. Vinceti, P. Willatts, *EFSA Journal* **2015**, *13*, 4253.

[169] D. J. Hare, B. R. Cardoso, E. A. Szymlek-Gay, B.-A. Biggs, *Lancet Child Adolesc.* **2018**, *2*, 144.

[170] J. O. Kang, *Clin. Lab.* **2001**, *14*, 209-19.

[171] R. J. Ward, F. A. Zucca, J. H. Duyn, R. R. Crichton, L. Zecca, *Lancet Neurol.* **2014**, *13*, 1045.

[172] J.-Y. Wang, Q.-Q. Zhuang, L.-B. Zhu, H. Zhu, T. Li, R. Li, S.-F. Chen, C.-P. Huang, X. Zhang, J.-H. Zhu, *Sci. Rep.* **2016**, *6*, 36669.

[173] H. Jiang, J. Wang, J. Rogers, J. Xie, *Mol. Neurobiol.* **2017**, *54*, 3078.

[174] D. Touati, *Arch. Biochem. Biophys.* **2000**, *373*, 1.

[175] S. J. Dixon, K. M. Lemberg, M. R. Lamprecht, R. Skouta, E. M. Zaitsev, C. E. Gleason, D. N. Patel, A. J. Bauer, A. M. Cantley, W. S. Yang, B. Morrison, B. R. Stockwell, *Cell* **2012**, *149*, 1060.

[176] A. Messerschmidt, *Copper Metalloenzymes*. Comprehensive Natural Products II: Chemistry and Biology, Elsevier, Amsterdam, **2010**.

[177] M. Olivares, M. A. Méndez, P. A. Astudillo, F. Pizarro, *Am. J. Clin. Nutr.* **2008**, *88*, 859S-62S.

[178] J. Chen, Y. Jiang, H. Shi, Y. Peng, X. Fan, C. Li, *Pflügers Arch.* **2020**, *472*, 1415.

[179] Z. Tümer, L. B. Møller, *Eur. J. Hum. Genet.* **2010**, *18*, 511.

[180] R. E. Tanzi, K. Petrukhin, I. Chernov, J. L. Pellequer, W. Wasco, B. Ross, D. M. Romano, E. Parano, L. Pavone, L. M. Brzustowicz, *Nat. Genet.* **1993**, *5*, 344.

[181] T. Y. Tao, F. Liu, L. Klomp, C. Wijmenga, J. D. Gitlin, *J. Biol. Chem.* **2003**, *278*, 41593.

[182] C. S. Atwood, R. D. Moir, X. Huang, R. C. Scarpa, N. M. Bacarra, D. M. Romano, M. A. Hartshorn, R. E. Tanzi, A. I. Bush, *J. Biol. Chem* **1998**, *273*, 12817.

[183] H. Liu, H. Guo, Z. Jian, H. Cui, J. Fang, Z. Zuo, J. Deng, Y. Li, X. Wang, L. Zhao, *Oxid. Med. Cell. Longev.* **2020**, *2020*, 1359164.

[184] R. A. Yokel, S. M. Lasley, D. C. Dorman, *J. Toxicol. Environ. Health - B: Crit.* **2006**, *9*, 63.

[185] R. A. Bernhoft, *J. Environ. Public Health* **2012**, *2012*, 460508.

[186] J. O. Adeyemi, D. C. Onwudiwe, *Inorg. Chim. Acta* **2020**, *511*, 119809.

[187] S. Mohammad Ahmadi Soleimani, H. Ekhtiari, J. L. Cadet, *Prog. Brain Res.* **2016**, *223*, 19.

[188] R. Nieuwenhuys, J. Voogd, C. van Huijzen, *The Human Central Nervous System. A Synopsis and Atlas*, Steinkopff, Heidelberg, **2008**.

[189] P. B. Baltes, N. J. Smelser, *International encyclopedia of the social & behavioral sciences*, Elsevier, Amsterdam, **2001**.

[190] R. L. Nussbaum, C. E. Ellis, *N. Engl. J. Med.* **2003**, *348*, 1356.

[191] Z. Han, R. Tian, P. Ren, W. Zhou, P. Wang, M. Luo, S. Jin, Q. Jiang, *BMC Med. Genet.* **2018**, *19*, 215.

[192] P. Scheltens, B. de Strooper, M. Kivipelto, H. Holstege, G. Chételat, C. E. Teunissen, J. Cummings, W. M. van der Flier, *Lancet* **2021**, *397*, 1577.

[193] W. Poewe, K. Seppi, C. M. Tanner, G. M. Halliday, P. Brundin, J. Volkmann, A.-E. Schrag, A. E. Lang, *Nat. Rev. Dis. Primers* **2017**, *3*, 17013.

[194] P. S. Spencer, P. J. Lein in *Encyclopedia of Toxicology*, Elsevier, **2014**, 489.

[195] T. Farkhondeh, O. Mehrpour, F. Forouzanfar, B. Roshanravan, S. Samarghandian, *Environ. Sci. Pollut. Res.* **2020**, *27*, 24799.

[196] B. R. Ritz, A. D. Manthripragada, S. Costello, S. J. Lincoln, M. J. Farrer, M. Cockburn, J. Bronstein, *Environ. Health Perspect.* **2009**, *117*, 964.

[197] Russell W. M. S., R. L. Burch, *Med. Stud. J. Aust.* **1960**, *1*, 500.

[198] J. E. Sulston, D. G. Albertson, J. N. Thomson, *Dev. Biol.* **1980**, *78*, 542.

[199] L. Byerly, R. C. Cassada, R. L. Russell, *Dev. Biol.* **1976**, *51*, 23.

[200] M. R. Klass, *Mech. Ageing Dev.* **1977**, *6*, 413.

[201] D. L. Riddle, M. M. Swanson, P. S. Albert, *Nature* **1981**, *290*, 668.

[202] "Wormatlas - Introduction to C. elegans anatomy", can be found under https://www.wormatlas.org/hermaphrodite/introduction/mainframe.htm.

[203] J. E. Sulston, H. R. Horvitz, *Dev. Biol.* **1977**, *56*, 110.

[204] C. elegans Sequencing Consortium, *Science* **1998**, *282*, 2012.

[205] R. W. Ware, D. Clark, K. Crossland, R. L. Russell, *J. Comp. Neurol.* **1975**, *162*, 71.

[206] J. Sulston, M. Dew, S. Brenner, *J. Comp. Neurol.* **1975**, *163*, 215.

[207] S. L. McIntire, E. Jorgensen, J. Kaplan, H. R. Horvitz, *Nature* **1993**, *364*, 337.

[208] L. Pereira, P. Kratsios, E. Serrano-Saiz, H. Sheftel, A. E. Mayo, D. H. Hall, J. G. White, B. LeBoeuf, L. R. Garcia, U. Alon, O. Hobert, *eLife* **2015**, *4*.

[209] E. Serrano-Saiz, R. J. Poole, T. Felton, F. Zhang, E. D. de La Cruz, O. Hobert, *Cell* **2013**, *155*, 659.

[210] R. Nass, D. H. Hall, D. M. Miller, R. D. Blakely, *Proc. Natl. Acad. Sci. U.S.A.* **2002**, *99*, 3264.

[211] E. R. Sawin, R. Ranganathan, H. R. Horvitz, *Neuron* **2000**, *26*, 619.

[212] H. A. Tissenbaum, *Invertebr. Reprod. Dev.* **2015**, *59*, 59.

[213] The FRAC Code List 2022 and other relevant documents are freely available from www.frac.info.

[214] F. P. Wong, W. F. Wilcox, *Plant disease* **2001**, *85*, 649.

[215] A. K. Sijpesteijn in *Fungicide resistance in crop protection* (Eds.: J. Dekker, S. G. Georgopoulos), Centre for Agricultural Publishing and Documentation, Wageningen, The Netherlands, **1982**, pp. 32–45.

[216] R. A. Ludwig, G. D. Thorn, *Adv. Pest Control Res.* **1960**, *3*, 219.

[217] R. Israeli, M. Sculsky, P. Tiberin, *Scand. J. Work Environ. Health* **1983**, *9*, 47.

[218] D. Mergler, M. Baldwin, *Environ. Res.* **1997**, *73*, 92.

[219] B. S. Levy, W. J. Nassetta, *Int. J. Occup. Environ. Health* **2013**, *9*, 153.

[220] W. Zheng, S. Ren, J. H. Graziano, *Brain Res.* **1998**, *799*, 334.

[221] C. W. Olanow, *Ann. N.Y. Acad. Sci.* **2004**, *1012*, 209.

[222] B. Michalke, K. Fernsebner, *J. Trace Elem. Med. Biol.* **2014**, *28*, 106.

[223] P. Chen, J. Bornhorst, M. Aschner, *Front. Biosci.* **2018**, *23*, 1655.

[224] V. A. Palzes, S. K. Sagiv, J. M. Baker, D. Rojas-Valverde, R. Gutiérrez-Vargas, M. S. Winkler, S. Fuhrimann, P. Staudacher, J. A. Menezes-Filho, A. L. Reiss, B. Eskenazi, A. M. Mora, *Environ. Res.* **2019**, *173*, 539.

[225] D. Gandhi, A. P. Rudrashetti, S. Rajasekaran, *J. Appl. Toxicol.* **2022**, *42*, 103.

[226] A. A. Tinkov, M. M. B. Paoliello, A. N. Mazilina, A. V. Skalny, A. C. Martins, O. N. Voskresenskaya, J. Aaseth, A. Santamaria, S. V. Notova, A. Tsatsakis, E. Lee, A. B. Bowman, M. Aschner, *Int. J. Mol. Sci.* **2021**, *22*.

[227] T. V. Peres, M. R. C. Schettinger, P. Chen, F. Carvalho, D. S. Avila, A. B. Bowman, M. Aschner, *BMC Pharmacol. Toxicol.* **2016**, *17*, 57.

[228] Y. Zhou, F.-S. Shie, P. Piccardo, T. J. Montine, J. Zhang, *Neuroscience* **2004**, *128*, 281.

[229] S. Gergely, J. Garaj, *Chem. Papers* **1988**, 229.

[230] M. Genchev, K. Davarski, *God. Vissh. Khim.* **1978**, *13*, 39.

[231] F. R. Day, D. J. Hamilton, *J. Therm. Anal.* **1984**, *29*, 317.

[232] A. S. Hyman, *Analyst* **1969**, *94*, 152.

[233] R. H. Schuler, *J. Chem. Educ.* **1950**, *27*, 591.

[234] P. Martini, A. Boschi, L. Marvelli, L. Uccelli, S. Carli, G. Cruciani, E. Marzola, A. Fantinati, J. Esposito, A. Duatti, *Molecules* **2021**, *26*.

[235] D. Lützenkirchen-Hecht, R. Wagner, S. Szillat, A. K. Hüsecken, K. Istomin, U. Pietsch, R. Frahm, *J. Synchrotron Radiat.* **2014**, *21*, 819.

[236] G. Bunker, *Introduction to XAFS. A practical guide to X-ray absorption fine structure spectroscopy*, Cambridge University Press, Cambridge, New York, **2010**.

[237] S. M. Lee, E. R. T. Tiekink, *Inorganics* **2021**, *9*, 7.

[238] *CrysAlisPro 41.123a*, Rigaku Oxford Diffraction Ltd, Oxford (U.K.), **2022**.

[239] G. M. Sheldrick, *Acta Cryst.* **2015**, *C71*, 3.

[240] G. M. Sheldrick, *Acta Cryst.* **2015**, *A71*, 3.

[241] O. V. Dolomanov, L. J. Bourhis, R. J. Gildea, J. A. K. Howard, H. Puschmann, *J. Appl. Cryst.* **2009**, *42*, 339.

[242] B. Ravel, M. Newville, *Physica Scripta* **2005**, 1007.

[243] S. I. Zabinsky, J. J. Rehr, A. Ankudinov, R. C. Albers, M. J. Eller, *Phys. Rev. B Condens.* **1995**, *52*, 2995.

[244] *DIFFRAC plus XRD Commander*, **2003**.

[245] S. Ito, F. J. White, E. Okunishi, Y. Aoyama, A. Yamano, H. Sato, J. D. Ferrara, M. Jasnowski, M. Meyer, *Cryst. Eng. Comm.* **2021**, *23*, 8622.

[246] Rigaku Corporation, *CrysAlisPro software system*, Rigaku Oxford Diffraction Ltd, Wroclaw, Poland, **2023**.

[247] Rigaku Corporation, *AutoChem 6 software system in conjunction with OLEX2*, Rigaku Oxford Diffraction Ltd, Wrocław, Poland, **2023**.

[248] F. L. Hirshfeld, *Acta Cryst A* **1976**, *32*, 239.

[249] A. Thorn, B. Dittrich, G. M. Sheldrick, *Acta Cryst A* **2012**, *68*, 448.

[250] G. Martens, P. Rabe, N. Schwentner, A. Werner, *Phys. Rev. Lett.* **1977**, *39*, 1411.

[251] Food and Agriculture Organization of the United Nations, "FAO tentative specifications for plant protection products, Manoczeb, complex of zinc and maneb containing 20% Mn and 2.5% Zn", can be found under https://www.fao.org/fileadmin/templates/agphome/documents/Pests_Pesticides/Specs/Old_specs/Mancozeb.pdf, **1980**.

[252] L. Kubens, K.-N. Truong, C. W. Lehmann, D. Lützenkirchen-Hecht, J. Bornhorst, F. Mohr, *Chem. Eur. J.* **2023**, e202301721.

[253] M. Bonamico, G. Mazzone, A. Vaciago, L. Zambonelli, *Acta Cryst.* **1965**, *19*, 898.

[254] D. S. Gregory, A. C. Martin, J. C. Cheetham, A. R. Rees, *Protein Eng.* **1993**, *6*, 29.

[255] H. L. Klöpping, G. J. M. van der Kerk, *Recl. Trav. Chim. Pays-Bas* **1951**, *70*, 949.

[256] J. Rizo, *Annu. Rev. Biophys.* **2022**, *51*, 377.

[257] S. Latif, M. Jahangeer, D. Maknoon Razia, M. Ashiq, A. Ghaffar, M. Akram, A. El Allam, A. Bouyahya, L. Garipova, M. Ali Shariati, M. Thiruvengadam, M. Azam Ansari, *Clin. Chim. Acta* **2021**, *522*, 114.

[258] M. O. Klein, D. S. Battagello, A. R. Cardoso, D. N. Hauser, J. C. Bittencourt, R. G. Correa, *Cell. Mol. Neurobiol.* **2019**, *39*, 31.

[259] D. Meder, D. M. Herz, J. B. Rowe, S. Lehéricy, H. R. Siebner, *NeuroImage* **2019**, *190*, 79.

[260] A. Masato, N. Plotegher, D. Boassa, L. Bubacco, *Mol. Neurodegener.* **2019**, *14*, 35.

[261] P. de Deurwaerdère, G. Di Giovanni, *Int. J. Mol. Sci.* **2020**, *21*.

[262] M. Pourhamzeh, F. G. Moravej, M. Arabi, E. Shahriari, S. Mehrabi, R. Ward, R. Ahadi, M. T. Joghataei, *Cell. Mol. Neurobiol.* **2022**, *42*, 1671.

[263] S. B. Sarasa, R. Mahendran, G. Muthusamy, B. Thankappan, D. R. F. Selta, J. Angayarkanni, *Curr. Microbiol* **2020**, *77*, 534.

[264] A. Sood, K. Preeti, V. Fernandes, D. K. Khatri, S. B. Singh, *J. Neurosci. Res.* **2021**, *99*, 3148.

[265] T. H. Ferreira-Vieira, I. M. Guimaraes, F. R. Silva, F. M. Ribeiro, *Curr. Neuropharmacol.* **2016**, *14*, 101.

[266] H. Hampel, M.-M. Mesulam, A. C. Cuello, M. R. Farlow, E. Giacobini, G. T. Grossberg, A. S. Khachaturian, A. Vergallo, E. Cavedo, P. J. Snyder, Z. S. Khachaturian, *Brain* **2018**, *141*, 1917.

[267] S. Habtemariam, *Molecules* **2019**, *24*.

[268] Z. Qi, F. Tretter, E. O. Voit, *PloS One.* **2014**, *9*, e92221.

[269] N. Huber, S. Korhonen, D. Hoffmann, S. Leskelä, H. Rostalski, A. M. Remes, P. Honkakoski, E. Solje, A. Haapasalo, *Mol. Psychiatry* **2022**, *27*, 1300.

[270] L.-S. Wang, M.-D. Zhang, X. Tao, Y.-F. Zhou, X.-M. Liu, R.-L. Pan, Y.-H. Liao, Q. Chang, *J. Chromatogr. B: Anal.* **2019**, *1112*, 24.

[271] M. E. Blanco, O. B. Mayo, T. Bandiera, D. de Pietri Tonelli, A. Armirotti, *J. Neurosci. Methods* **2020**, *341*, 108760.

[272] P. Fernandez-Funez, J. Sanchez-Garcia, D. E. Rincon-Limas, *Curr. Opin. Genet.* **2017**, *44*, 141.

[273] C. A. Taylor, K. Tuschl, M. M. Nicolai, J. Bornhorst, P. Gubert, A. M. Varão, M. Aschner, D. R. Smith, S. Mukhopadhyay, *J. Nutr.* **2020**, *150*, 1360.

[274] J. A. Ruszkiewicz, A. Pinkas, M. R. Miah, R. L. Weitz, M. J. A. Lawes, A. J. Akinyemi, O. M. Ijomone, M. Aschner, *Toxicol. Appl. Pharmacol.* **2018**, *354*, 126.

[275] P. R. Hunt, *J Appl Toxicol* **2017**, *37*, 50.

[276] J. F. Cooper, J. M. van Raamsdonk, *J Parkinsons Dis.* **2018**, *8*, 17.

[277] L. Ma, X. Li, C. Liu, W. Yan, J. Ma, R. B. Petersen, A. Peng, K. Huang, *Curr. Pharm. Des.* **2022**, *28*, 3033.

[278] K. A. Caldwell, C. W. Willicott, G. A. Caldwell, *Dis. Model Mech.* **2020**, *13*.

[279] F. J. Naranjo-Galindo, R. Ai, E. F. Fang, H. L. Nilsen, T. SenGupta, *Front. Aging* **2022**, *3*, 916118.

[280] N. F. Trojanowski, D. M. Raizen, C. Fang-Yen, *Sci. Rep.* **2016**, *6*, 22940.

[281] T. R. Mahoney, S. Luo, M. L. Nonet, *Nat. Protoc.* **2006**, *1*, 1772.

[282] Z. Yan, X. Cheng, Y. Li, Z. Su, Y. Zhou, J. Liu, *Front. Mol. Neurosci.* **2021**, *14*, 780396.

[283] F. Schumacher, S. Chakraborty, B. Kleuser, E. Gulbins, T. Schwerdtle, M. Aschner, J. Bornhorst, *Talanta* **2015**, *144*, 71.

[284] B. A. Patel, M. Arundell, K. H. Parker, M. S. Yeoman, D. O'Hare, *J. Chromatogr. B: Anal.* **2005**, *818*, 269.

[285] J. Y. Baek, T. an Trinh, W. Huh, J. H. Song, H. Y. Kim, J. Lim, J. Kim, H. J. Choi, T.-H. Kim, K. S. Kang, *Biomolecules* **2019**, *9*.

[286] H.-X. Zhao, H. Mu, Y.-H. Bai, H. Yu, Y.-M. Hu, *J. Pharm. Anal.* **2011**, *1*, 208.

[287] N. Şanlı, S. E. Tague, C. Lunte, *J. Pharm. Biomed. Anal.* **2015**, *107*, 217.

[288] J. An, M. Chen, N. Hu, Y. Hu, R. Chen, Y. Lyu, W. Guo, L. Li, Y. Liu, *Spectrochim. Acta - A: Mol. Biomol.* **2020**, *243*, 118804.

[289] F. Sun, J. Zeng, M. Jing, J. Zhou, J. Feng, S. F. Owen, Y. Luo, F. Li, H. Wang, T. Yamaguchi, Z. Yong, Y. Gao, W. Peng, L. Wang, S. Zhang, J. Du, D. Lin, M. Xu, A. C. Kreitzer, G. Cui, Y. Li, *Cell* **2018**, *174*, 481-496.e19.

[290] J. Sun, A. Feng, X. Wu, X. Che, W. Zhou, *Talanta* **2021**, *231*, 122334.

[291] J. Wu, R. Wiegand, P. LoRusso, J. Li, *J. Chromatogr. B: Anal.* **2013**, *941*, 100.

[292] F. Carreño, V. E. Helfer, K. J. Staudt, L. B. Olivo, F. Barreto, A. P. Herrmann, S. M. K. Rates, T. Dalla Costa, *J. Chromatogr. B: Anal.* **2020**, *1155*, 122282.

[293] H. Xu, Z. Wang, L. Zhu, Z. Sui, W. Bi, R. Liu, K. Bi, Q. Li, *Molecules* **2018**, *23*.

[294] S. Tufi, P. Leonards, M. Lamoree, J. de Boer, J. Legler, J. Legradi, *Environ. Sci. Technol.* **2016**, *50*, 3222.

[295] I. Fuertes, C. Barata, *Chemosphere* **2021**, *263*, 127814.

[296] S. C. Daubner, T. Le, S. Wang, *Arch. Biochem. Biophys.* **2011**, *508*, 1.

[297] S. F. McHardy, H.-Y. L. Wang, S. V. McCowen, M. C. Valdez, *Exp. Opin. Ther. Pat.* **2017**, *27*, 455.

[298] K. H. Oh, H. Kim, *Bio-protoc.* **2017**, *7*.

[299] James B. Rand, "Wormbook: The Online Review of C. elegans Biology - Acetylcholine", can be found under https://www.ncbi.nlm.nih.gov/books/NBK19736/, **2007**.

[300] S. Bhat, A. El-Kasaby, M. Freissmuth, S. Sucic, *Pharmacol. Ther.* **2021**, *222*, 107785.

[301] G. Rizzi, K. R. Tan, *Front. Neural Circuits* **2017**, *11*, 110.

[302] C. A. Sanchez-Catasus, N. I. Bohnen, N. D'Cruz, M. L. T. M. Müller, *J. Nucl. Med.* **2022**, *63*, 438.

[303] N. Umek, B. Geršak, N. Vintar, M. Šoštarič, J. Mavri, *Front. Mol. Neurosci.* **2018**, *11*, 467.

[304] F. Huang, J. Li, H.-L. Shi, T. Wang, W. Muhtar, M. Du, B. Zhang, H. Wu, Li Yang, Z. Hu, X. Wu, *J. Neurosci. Methods* **2014**, *229*, 8.

[305] E. Olesti, J. Rodríguez-Morató, A. Gomez-Gomez, J. G. Ramaekers, R. de La Torre, O. J. Pozo, *Talanta* **2019**, *192*, 93.

[306] X.-M. Han, Y.-J. Qin, Y. Zhu, X.-L. Zhang, N.-X. Wang, Y. Rang, X.-J. Zhai, Y.-N. Lu, *J. Pharm. Biomed. Anal.* **2019**, *174*, 683.

[307] F. W. McLafferty, F. Turecek, *Interpretation of Mass Spectra*, University Science Books, U.S.A, **1993**.

[308] M. Zhang, C. Fang, G. Smagin, *J. Pharm. Biomed. Anal.* **2014**, *100*, 357.

[309] S. W. Caito, M. Aschner, *Toxicol. Sci.* **2016**, *151*, 139.

[310] O. M. Ijomone, M. R. Miah, G. T. Akingbade, H. Bucinca, M. Aschner, *Neurotox. Res.* **2020**, *37*, 1018.

[311] C. Defaix, A. Solgadi, T. H. Pham, A. M. Gardier, P. Chaminade, L. Tritschler, *J. Pharm. Biomed. Anal.* **2018**, *152*, 31.

[312] A. Muñoz, A. Lopez-Lopez, C. M. Labandeira, J. L. Labandeira-Garcia, *Front. Neuroanat.* **2020**, *14*, 26.

[313] E. G. Govorunova, M. Moussaif, A. Kullyev, K. C. Q. Nguyen, T. V. McDonald, D. H. Hall, J. Y. Sze, *PloS one* **2010**, *5*, e10368.

[314] A. C. Giles, M. Desbois, K. J. Opperman, R. Tavora, M. J. Maroni, B. Grill, *J. Biol. Chem.* **2019**, *294*, 6843.

[315] C. H. Opperman, S. Chang, *J. Nematol.* **1991**, *23*, 20.

[316] R. Nass, I. Hamza, *Curr. Protoc. Toxicol.* **2007**, *1*, Unit 1.9.

[317] S. Brenner, *Genetics* **1974**, *77*, 71.

[318] J. M. Walker in *Springer Protocols Handbooks* (Ed.: J. M. Walker), Humana Press, Totowa, NJ, **2009**, pp. 11–15.

[319] E. D. Caldas, M. C. C. Miranda, M. H. Conceição, L. C. K. R. de Souza, *Food Chem. Toxicol.* **2004**, *42*, 1877.

[320] R. Israeli, M. Sculsky, P. Tiberin, *Arch. Toxicol.* **1983**, *6*, 238.

[321] A. Carmona, S. Roudeau, L. Perrin, G. Veronesi, R. Ortega, *Metallomics* **2014**, *6*, 822.

[322] P. Chen, E. J. Martinez-Finley, J. Bornhorst, S. Chakraborty, M. Aschner, *Front. Aging Neurosci.* **2013**, *5*, 18.

[323] A. C. Martins, P. Gubert, J. Li, T. Ke, M. M. Nicolai, A. V. Moura, J. Bornhorst, A. B. Bowman, M. Aschner, *Biomolecules* **2022**, *12*.

[324] M. C. K. Leung, P. L. Williams, A. Benedetto, C. Au, K. J. Helmcke, M. Aschner, J. N. Meyer, *Toxicol. Sci.* **2008**, *106*, 5.

[325] M. V. Soares, G. P. Viçozzi, E. C. Kuhn, A.-K. Weishaupt, L. Kubens, J. Bornhorst, D. S. Avila *Advances in Neurotoxicology*, *Vol. 9*, Elsevier, **2023**.

[326] P. K. Smith, R. I. Krohn, G. T. Hermanson, A. K. Mallia, F. H. Gartner, M. D. Provenzano, E. K. Fujimoto, N. M. Goeke, B. J. Olson, D. C. Klenk, *Anal. Biochem.* **1985**, *150*, 76.

[327] A. Thiel, A.-K. Weishaupt, M. M. Nicolai, K. Lossow, A. P. Kipp, T. Schwerdtle, J. Bornhorst, *J. Chromatogr. B: Anal.* **2023**, *1225*, 123742.

[328] D. Cova, P. Fumagalli, A. Santagostino, *Altern. Lab. Anim.* **1991**, *19*, 39.

[329] T. V. Peres, L. P. Arantes, M. R. Miah, J. Bornhorst, T. Schwerdtle, A. B. Bowman, R. B. Leal, M. Aschner, *Neurotox. Res.* **2018**, *34*, 584.

[330] P. T. Francis, A. M. Palmer, M. Snape, G. K. Wilcock, *J. Neurol. Neurosurg. Psychiatry* **1999**, *66*, 137.

[331] O. Hornykiewicz in *Parkinson's Disease and Related Disorders*, Springer, Vienna, **2006**, pp. 9–15.

[332] F. O. Walker, *Lancet* **2007**, *369*, 218.

[333] B. van Wendel de Joode, A. M. Mora, C. H. Lindh, D. Hernández-Bonilla, L. Córdoba, C. Wesseling, J. A. Hoppin, D. Mergler, *Cortex* **2016**, *85*, 137.

[334] S. Singh, C. Brocker, V. Koppaka, Y. Chen, B. C. Jackson, A. Matsumoto, D. C. Thompson, V. Vasiliou, *Free Radic. Biol. Med.* **2013**, *56*, 89.

[335] G. D. Zeevalk, E. Derr-Yellin, W. J. Nicklas, *Pharmacol. Exp. Ther.* **1995**, *275*, 1124.

[336] A. Harrison Brody, E. Chou, J. M. Gray, N. J. Pokyrwka, K. M. Raley-Susman, *NeuroToxicology* **2013**, *34*, 74.

[337] H. Hampel, M.-M. Mesulam, A. C. Cuello, M. R. Farlow, E. Giacobini, G. T. Grossberg, A. S. Khachaturian, A. Vergallo, E. Cavedo, P. J. Snyder, Z. S. Khachaturian, *Brain* **2018**, *141*, 1917.

[338] P. Kurttio, K. Savolainen, A. Naukkarinen, V. M. Kosma, L. Tuomisto, I. Penttilä, J. Jolkkonen, *Arch. Toxicol.* **1991**, *65*, 381.

[339] B. Halliwell, *J. Neurochem.* **2006**, *97*, 1634.

[340] A. Gomes, E. Fernandes, J. L. F. C. Lima, *J. Biochem. Biophys. Methods* **2005**, *65*, 45.

[341] R. D. McMullen, *Can. Entomol.* **1964**, *96*, 541.

[342] E. Grosicka-Maciąg, M. Szumiło, H. Czeczot, D. Kurpios-Piec, M. Skrzycki, I. Rahden-Staroń, *Food. Chem. Toxicol.* **2013**, *60*, 130.

[343] S. Chen, S. Tran, A. Sigler, T. H. Murphy, *J. Neurosci. Methods* **2011**, *195*, 222.

[344] A. AlOkda, J. M. van Raamsdonk, *microPublication biology* **2022**, *2022*.

[345] B. Michalke, S. Halbach, V. Nischwitz, *J. Environ. Monit.* **2007**, *9*, 650.

[346] M. Porta-de-la-Riva, L. Fontrodona, A. Villanueva, J. Cerón, *J. Vis. Exp.* **2012**, e4019.

[347] R. Nass, M. K. Hahn, T. Jessen, P. W. McDonald, L. Carvelli, R. D. Blakely, *J. Neurosci.* **2005**, *94*, 774.

[348] B. I. Kanner, *J. Exp. Biol.* **1994**, *196*, 237.

[349] Y.-G. Lee, S. Jeon, K. Baik, S. W. Kang, B. S. Ye, *npj Parkinson's Dis.* **2023**, *9*, 88.

[350] M. M. Shah in *Encyclopedia of the Neurological Sciences*, Elsevier, **2014**, p. 970.

[351] L. Sundararajan, J. Stern, D. M. Miller, *Dev. Biol.* **2019**, *451*, 53.

[352] D. A. Durden, A. A. Boulton in *Experimental Neurochemistry* (Ed.: A. Lajtha), Springer US, Boston, MA, **1982**, pp. 397–428.

[353] R. Andrew, D. G. Watson, S. A. Best, J. M. Midgley, H. Wenlong, R. K. Petty, *Neurochem. Res.* **1993**, *18*, 1175.

[354] A. S. Clark, Z. Kalmanson, K. Morton, J. Hartman, J. Meyer, A. San-Miguel, *bioRxiv* **2023**.

[355] H. K. Brar, S. Dey, S. Bhardwaj, D. Pande, P. Singh, S. Dey, A. Ghosh-Roy, *PLoS genetics* **2022**, *18*, e1010127.

[356] S. R. Bijwadia, K. Morton, J. N. Meyer, *J. Vis. Exp.* **2021**.

[357] J. Baesler, V. Michaelis, M. Stiboller, H. Haase, M. Aschner, T. Schwerdtle, S. R. Sturzenbaum, J. Bornhorst, *Mol. Nutr. Food Res.* **2021**, *65*, e2001176.

[358] P. W. McDonald, S. L. Hardie, T. N. Jessen, L. Carvelli, D. S. Matthies, R. D. Blakely, *J. Neurosci.* **2007**, *27*, 14216.

[359] L. Shen, J. Xiao, H. Ye, D. Wang, *Environ. Toxicol. Pharmacol.* **2009**, *28*, 125.

[360] J. Baesler, J. F. Kopp, G. Pohl, M. Aschner, H. Haase, T. Schwerdtle, J. Bornhorst, *J. Trace Elem. Med. Bio.* **2019**, *55*, 44.

[361] V. Kumar, D. Singh, B. K. Singh, S. Singh, N. Mittra, R. R. Jha, D. K. Patel, C. Singh, *Mol. Cell. Biochem.* **2018**, *444*, 149.

[362] K.-N. Truong, S. Ito, J. M. Wojciechowski, C. R. Göb, C. J. Schürmann, A. Yamano, M. Del Campo, E. Okunishi, Y. Aoyama, T. Mihira, N. Hosogi, J. Benet-Buchholz, E. C. Escudero-Adán, F. J. White, J. D. Ferrara, R. Bücker, *Symmetry* **2023**, *15*, 1555.

[363] T. C. Martinsen, K. Bergh, H. L. Waldum, *Basic Clin. Pharmacol. Toxicol.* **2005**, *96*, 94.

[364] G. H. Reed, M. Cohn, *J. Biol. Chem.* **1970**, *245*, 662.

[365] M. Aschner, C. Palinski, M. Sperling, U. Karst, T. Schwerdtle, J. Bornhorst, *Metallomics* **2017**, *9*, 357.

[366] S. G. Brinkhaus, J. Bornhorst, S. Chakraborty, C. A. Wehe, R. Niehaus, O. Reifschneider, M. Aschner, U. Karst, *Metallomics* **2014**, *6*, 617.

[367] I. Ben Amara, H. Ben Saad, L. Hamdaoui, A. Karray, T. Boudawara, Y. Ben Ali, N. Zeghal, *Environ. Sci. Pollut. Res.* **2015**, *22*, 12309.

[368] H. Gong, Y. Jiao, W. Hu, E. Pua, *Plant Mol. Biol.* **2005**, *57*, 53.

[369] J. D. Hayes, D. J. Pulford, *Crit. Rev. Biochem. Mol. Biol.* **1995**, *30*, 445.

[370] A. Singh, R. Kukreti, L. Saso, S. Kukreti, *Molecules* **2019**, *24*.

[371] M. D. Brand, D. G. Nicholls, *Biochem. J.* **2011**, *435*, 297.

[372] B. Ayuda-Durán, S. González-Manzano, A. M. González-Paramás, C. Santos-Buelga, *Molecules* **2020**, *25*.

[373] L. I. Grad, L. C. Sayles, B. D. Lemire, *Methods Mol. Biol.* **2007**, *372*, 51.

[374] A. Easton, K. Guven, D. I. de Pomerai, *J. Biochem. Mol. Toxicol.* **2001**, *15*, 15.

[375] A. G. Fitzmaurice, S. L. Rhodes, A. Lulla, N. P. Murphy, H. A. Lam, K. C. O'Donnell, L. Barnhill, J. E. Casida, M. Cockburn, A. Sagasti, M. C. Stahl, N. T. Maidment, B. Ritz, J. M. Bronstein, *Proc Natl Acad Sci U S A* **2013**, *110*, 636.

[376] R. Kackar, M. K. Srivastava, R. B. Raizada, *Indian J. Exp. Biol.* **1999**, *37*, 553.

[377] V. A. Fitsanakis, C. Au, K. M. Erikson, M. Aschner, *Neurochem. Int.* **2006**, *48*, 426.

[378] K. M. Erikson, M. Aschner, *Neurochem. Int.* **2003**, *43*, 475.

[379] L. G. Costa, *Toxicology* **1988**, *49*, 359.

[380] C. W. Lam, V. DiStefano, *Toxicol. Appl. Pharmacol.* **1986**, *86*, 235.

List of publications

Peer Review Journals

Laura Kubens, Ann-Kathrin Weishaupt, Isabelle Rohn, Fabian Mohr Julia Bornhorst: Exposure to the environmentally relevant fungicide Maneb: Studying toxicity in the soil nematode *Caenorhabditis elegans*, submitted to: Environment international.

Laura Kubens, Khai-Nghi Truong, Christian W. Lehmann, Dirk Lützenkirchen-Hecht, Julia Bornhorst, Fabian Mohr: The structure of Maneb: An important manganese-containing bis(dithiocarbamate) fungicide, *Chemistry – A European Journal*, **2023**, *29*, 55 e202301721. doi.org/10.1002/chem202301721

Ann-Kathrin Weishaupt, Laura Kubens, Lysann Ruecker, Tanja Schwerdtle, Michael Aschner, Julia Bornhorst: A Reliable Method Based on Liquid Chromatography-Tandem Mass Spectrometry for the Simultaneous Quantification of Neurotransmitter in *Caenorhabditis elegans*, *Molecules*, **2023**, *28*, 5375. doi.org/10.1016/bs.ant.2023.03.00

Book Chapter

Marcell Valandro Soares, Gabriel Pedroso Vicozzi, Eugenia Carla Kuhn, Ann-Kathrin Weishaupt, Laura Kubens, Julia Bornhorst, Daiana Silva Avila: *Neurotoxicology of organic environmental toxicants using Caenorhabditis elegans as a model,* Advances in Neurotoxicology, Vol. 9, **2023**.

Acknowledgements

Zuerst einmal möchte ich mich bei Fabian Mohr und Julia Bornhorst für die Entstehung dieser super spannenden Kooperation vor mittlerweile fast 5 Jahren bedanken! Ihr habt mich so herzlich in Eure Arbeitsgruppen aufgenommen und ich durfte alles machen, was mir schon im Studium und während der Masterarbeit Freude bereitet hat: Synthese, Strukturaufklärung und das Arbeiten mit dem Fadenwurm. Ihr hattet immer ein offenes Ohr für mich, habt euch für meine Ergebnisse begeistert und mir stets Vertrauen geschenkt. Zusätzlich habt ihr es mir ermöglicht, an einer Konferenz in Australien teilzunehmen reisen. Ich bin jeden Tag mit Freude zur Arbeit gekommen und werde die Zeit sehr vermissen.

Ohne meine lieben Kollegen, wäre die Zeit hier jedoch nur halb so schön gewesen. Daher möchte ich Nicole, Julia, Fabi, Ferdi, Max, Lucie, Sanaz und Björn für die wunderschöne Zeit innerhalb und außerhalb der Uni danken.

Als ich dann für meine Laborarbeit die Stockwerke gewechselt habe, konnte ich viele Schritte für mein tägliches Schrittziel sammeln und habe nicht nur tolle neue Kollegen kennengelernt, sondern auch eine ganz besondere Person: nämlich dich, Marco!

Besonders bedanken möchte ich mich bei Anni, Anna, Vivi, Alici, Yemi und Andy für die tolle Aufnahme, eure Unterstützung, die viele gemeinsamen Stunden und die tollen Ausflüge. Vielen lieben Dank auch dafür, dass ihr Korrektur gelesen habt.

Natürlich möchte ich auch die vielen Menschen nicht vergessen, ohne die meine Arbeit gar nicht möglich gewesen wäre. Dazu zählen Isabelle Rohn, die mir das Arbeiten mit dem Fadenwurm in Potsdam im Labor von Tanja Schwerdtle beigebracht hat, Dirk Lützenkirchen-Hecht, mit dem ich im stürmischen Februar 2021 das Synchrotron in Dortmund besucht habe, das analytische Mess-Team der BUW (Andreas Siebert, Ilka Polanz, Simone Bettinger und Friedbert Lücker), Christian Lehmann und das Team von Rigaku, denen ich die abschließende Strukturaufklärung zu verdanken habe. Bei Frau Litz möchte ich mich nicht nur in meinem eigenen Namen, sondern auch im Namen von Bella für die stetige Unterstützung (und die Snacks 🐾) bedanken. Außerdem möchte ich mich nochmal ganz herzlich bei allen Co-Autoren meiner Publikationen bedanken.

Zuletzt möchte ich mich noch bei meiner besten Freundin Christina bedanken, schön, dass du es schon seit der Krabbelgruppe mit mir aushältst! Mein größter Dank gilt aber meiner Mutter, die mich immer unterstützt hat und ohne die ich niemals da sein könnte, wo ich gerade bin!

Danke!

Declaration

The presented semi-cumulative doctoral is composed of eight distinct chapters. Chapter 3 and chapter 5 have been published in international peer-reviewed scientific journals, while chapter 6 has been submitted and is currently undergoing the peer-review process. The published and submitted articles include suggestions from co-authors, editors and reviewers received during the peer-review process. Chapters 4 and 7 are based on unpublished data from further experiments.

As the leading author of the chapters 3, 4, 6 and 7, the studies were conceptualized with my PhD supervisors Fabian Mohr and Julia Bornhorst. I conducted all experiments, performed data analysis and data interpretation myself. The contributions of all co-authors are acknowledged in the "Author Contribution" section at the end of each published or submitted chapter. In Chapter 5, where I am a co-author, I provided intellectual input.

References to published data, methods, statements, and data interpretation of other researchers are properly cited in the relevant articles and across all other chapters of this thesis.

Laura Kubens